



**University of
Nottingham**
UK | CHINA | MALAYSIA

**EVALUATION ON THERMOCHEMICAL PROCESSES FOR
BIOENERGY APPLICATIONS OF BAMBARA GROUNDNUT
SHELL (BGS), SHEA NUTSHELL (SNS), SHEA NUT CHAFF
(SNC), AND SWEET SORGHUM STALK (SSS)**

MUSTAPHA DANLADI IBRAHIM, BEng, MEng.

Department of Chemical and Environmental Engineering

A thesis submitted to the University of Nottingham for the degree
of Doctor of Philosophy

December 2024

Abstract

Fossil fuel dependency, global threat, and energy crisis drive the need for an alternative and renewable energy source, that's cleaner and cost-effective. Alternative energy like biomass is renewable and remarkable with almost a zero-carbon footprint increasingly gaining attention amidst the environmental challenges of coal and fossil fuels. Bambara groundnut shell (BGS), Sweet Sorghum Stalk (SSS), Shea Nut chaff (SNC), and Shea Nut Shells (SNS) are an underutilized crop-biomass waste after cultivation readily available as industrial and agricultural biowaste for energy generation. This study focused on intermediate pyrolysis, catalytic co-pyrolysis and torrefaction. Firstly, the physicochemical and thermogravimetric analysis of the BGS before and after moisture removal at 105 °C for 4 h, coded UT (untreated) and PT (pre-treated), respectively. The coded investigated samples were untreated (UT1, UT2, and UT3) and pre-treated (PT1, PT2, and PT3), with particulate sizes as 1180, 600, and 300 µm, with additional two BG genotypes (BGS-G4 & BGS-G5). The results showed that BGS-UT1 (1180 µm) had the least ash content (AC) of 6.8 ± 0.5 wt. %, with maximum HHV of 18.6 ± 0.5 MJ/kg, activation energy of 21.00 kJ/mol and suitable pyrolysis temperature ≤ 650 °C. The intermediate pyrolysis (IP) of BGS-G1, SSS, and SNS in a vertical tube reactor at 600 °C, with an average heating rate ≥ 33.0 °C/min. The pyrolysis oil and HHV yield

was 38.0 ± 6.4 , 44.2 ± 6 , and 39.7 ± 5.2 wt. % and 23.7 ± 1.8 , 23.8 ± 1.8 , and 26.5 ± 2.0 MJ/kg for BGS-G1 SSS and SNS, respectively. The biochar recorded the highest HHV for SNS at 26.4 ± 1.8 MJ/kg. The effects of N_2 , CO_2 , and N_2/CO_2 (flue gas) in an IP experiment of BGS did not relatively affect the yields of bio-oil, biochar, and syngas, but had optimum gas flowrate at 17.5 min/s and bio-oil pH within 5.2 – 5.8 indicating minimum presence of acids in bio-oil. Their CHNS analysis of both bio-oil and biochar carbon content are within 50.04 – 60.49 wt. %. Intermediate catalytic co-pyrolysis was conducted for SSS and plastic (polypropylene (PP) over amphoteric catalysts (Al_2O_3 , and 25 %Ni/ Al_2O_3), acidic catalysts (ZSM-5 and 25 %Ni/ ZSM-5) ratios. The mixing ratio of SSS to PP (1:1) at 600 °C, forming the least oxygenate from SSS (15.1 wt. %) and the highest oxygenate in PP (25.2 wt. %), respectively. The feed-to-catalyst, 25 %Ni/ Al_2O_3 _0.25 (1:0.25) had the optimum bio-oil and HHV at 49.02 ± 0.26 wt. % and 41.1 ± 0.7 MJ/kg, respectively. The catalytic co-pyrolyzed in the presence of 25 %Ni/ Al_2O_3 yielded optimum of excellent C-H-containing FTIR functional groups and aliphatic hydrocarbon corroborated by GCMS analysis. GC-MS analysis categorized the bio-oils as ketones, furans, phenolics, acids, phenols, and benzene derivatives. Finally, wet torrefaction of Shea Nut Chaff (SNC) had an optimum yield (55.5 wt. %) and the least hydrophobicity at 260°C-W/B5R10 (45 bar), energy yield and HHV

of 89.54 % and 15.81 MJ/kg. The best-fit model of ANOVA (analysis of variance) is 2FI, with p-values < 0.05, and R² of 0.9443. In conclusion, the BGS, SSS, SNS and SNC provided liquid and solid fuels after being subjected to treatments to minimize the impact of global warming.

LIST OF PUBLICATIONS

Journal Papers

- **Ibrahim M.D.**, Gan S., Abakr Y.A., Lee L.Y., Thangalazhy-Gopakumar S., 2023, Physicochemical Analysis of Bambara Groundnut Shell (BGS) for Biofuel Production, Chemical Engineering Transactions, 106, 1249-1254 DOI:10.3303/CET23106209.
- **Ibrahim, M. D.**, & Abakr, Y. A. (2023). Wet torrefaction of shea nut chaff to improve its fuel properties. Asia-Pac J Chem Eng. 2023; -2972, (August), 1–14. <https://doi.org/10.1002/apj.2972>.
- **Ibrahim, M.D.**, Abakr, Y.A., Gan, S., Thangalazhy-Gopakumar, S., 2022. Physicochemical analysis and intermediate pyrolysis of Bambara Groundnut Shell (BGS), Sweet Sorghum Stalk (SSS), and Shea Nutshell (SNS). Environ. Technol. 0, 1–26. <https://doi.org/10.1080/09593330.2022.2156817>
- **Ibrahim, M.D.**, Abakr, Y.A., Gan, S., Lee, L.Y., Thangalazhy-Gopakumar, S., 2022. Intermediate Pyrolysis of Bambara Groundnut Shell (BGS) in Various Inert Gases (N₂, CO₂, and N₂/CO₂) 15, 1–16. <https://doi.org/10.3390/en1522842>

- **MD Ibrahim**, ST Gopakumar, YA Abakr, MI Yakub & SJ Zwalnan, (2020), Technological Challenges & Environmental Mitigation via Bio-oil Production from Biomass Resources, IOP Conference Series: Earth and Environmental doi:10.1088/1755-1315/489/1/012008.

Conference/Symposium/Poster Presentation:

- **Mustapha Danladi Ibrahim**, Suchithra Thangalazhy-Gopakumar, Yousif Abdalla Abakr and Suyin Gan, (2020). The Potentials of Bambara Groundnut Shell (BGS), Sweet Sorghum Stalk (SSS) & Shea Nutshell (SNS) for Bio-Oil Production through Intermediate Pyrolysis, APPLIED PYROLYSIS – Short Oral Presentation and panel discussion, Korea University, Seoul, Korea 11TH – 13^{YH} Dec. 2020.
- **Mustapha Danladi Ibrahim**, Suchithra Thangalazhy Gopakumar, Yousif Abdalla Abakr, & Suyin Gan. (2020) "Physicochemical analysis on Bambara groundnut shell (G1), (G4), & (G5), sweet sorghum stalk (SSS), shea nutshell (SNS) & shea nut chaff (SNC) for biofuel production" **Poster Presentation at the University of Nottingham Postgraduate Week held on June 10, 2020.**
- **Mustapha Danladi Ibrahim**, Suchithra Thangalazhy Gopakumar, Yousif Abdalla Abakr, & Suyin Gan. (2020) "Physicochemical analysis on Bambara groundnut shell ((G1), (G4), & (G5)), sweat

sorghum stalk (SSS), shea nutshell (SNS) & shea nut chaff (SNC) for biofuel production” **Paper Presentation at the University of Nottingham Postgraduate Week held on June 10, 2020.**

- Master of Sustainability and Environmental Sciences (Joint Degree) & Collaborative Education Program for Sustainable Environmental Engineering Network (Cep-Seen) Joint Seminar Organized by UTM (Universiti Teknologi Malaysia), 15-17th February 2021.

Acknowledgement

Firstly, I like to give all gratitude, praises, and adoration to the Almighty God for the gift of sound health, knowledge, wisdom, guidance, and successful completion of this program. The accomplishment is due to Allah (SWT) alone, while the errors in this work are due to my shortcomings. My sincere appreciation goes to my supervisors, Dr Suchithra Thangalazhy Gopakumar, Prof. Yousif Abdalla Abakr and Prof. Gan Suyin, for their immense guidance, patience, optimism, encouragement, immense knowledge contributions throughout my research. I wish to extend and acknowledge the laboratory staff for their assistance throughout the laboratory work. My sincere appreciation goes to the Petroleum Trust Development Fund (PTDF) for the sponsorship to carry out this research, Abubakar Tafawa Balewa University Bauchi and The University of Nottingham Malaysia for the realization of this research project.

My heartfelt love and regards to my parents, Late Alhaji Ibrahim Muhammad Shaba (Rtd) (Santali Raban Nupe) and Hajiya Aishatu Ibrahim Muhammad, for their life-long love, care, support, and prayers. May the Almighty Allah reward them abundantly. Special thanks to all my siblings for their encouragement and prayers. A warm appreciation to my wife, Ruqaiyat Ibrahim Babayagi, and my

children, Ummul-Bashar Mustapha, Humaira' u Mustapha, Afifa Mustapha, Nihal Mustapha, Zarah Mustapha and Khalilullah Mustapha, for their patience, love, understanding, encouragement, and prayers throughout my studies; I love you all. To all my family members, friends too numerous to mention and to the entire Babayaya family, thank you all for your love and motivation.

Table of Contents

Abstract	ii
Acknowledgement	viii
List of Figure	xvi
List of Tables	xix
CHAPTER ONE.....	1
1 Introduction	1
1.1 Problem statement	4
1.2 Scope and limitation	5
1.3 Aim and objectives.	6
1.4 Research novelty	7
1.5 Thesis overview	8
CHAPTER TWO	11
2 Literature review	11
2.1 Biomass/Feedstock materials.....	11
2.2 Biomass and its properties	18
2.3 Thermochemical processes	26
2.3.1 Challenges in bio-fuel production processes.	29
2.3.2 Torrefaction	31
2.3.3 Biomass combustion	34
2.3.4 Pyrolysis	36
2.3.5 Gasification	46
2.3.6 Design-Expert®	49

2.4	Reactor for biomass pyrolysis	51
2.4.1	Bubbling fluidized bed (BFB) reactor	51
2.4.2	Circulating fluidized bed reactor (CFBR)	53
2.4.3	Conical spouted bed reactor (CSBR).	54
2.4.4	Rotating cone-pyrolysis reactor (RCPR)	55
2.4.5	Auger reactor (AUR)	56
2.4.6	Ablative flash-pyrolysis reactor (AFPR)	58
2.4.7	Summary of technological challenges in bio-fuel production	60
2.5	Hydrothermal process	62
2.5.1	Hydrothermal carbonization (HTC)	62
2.5.2	Factors of hydrothermal carbonization	65
2.5.3	Hydrothermal carbonization (HTC) case studies	70
2.5.4	Summary of hydrothermal carbonization	73
2.5.5	Hydrothermal gasification (HTG)	75
2.5.6	Factors of hydrothermal gasification	76
2.5.7	Hydrothermal gasification (HTG) case studies	78
2.5.8	Summary of hydrothermal gasification	81
2.6	Concluding remarks	85
CHAPTER THREE		87
3	Materials and methodology	87
3.1	Introduction	87
3.2	Materials	87
3.2.1	Chemical reagents and equipment	87

3.2.2	Feedstock collection and preparation	88
3.3	Methodology.....	91
3.3.1	Biomass characterization	91
3.3.2	Ultimate analysis.....	92
3.3.3	Proximate analyses.....	92
3.3.4	Thermogravimetric analysis (TGA).....	94
3.3.5	The kinetics rate equation	94
3.3.6	Higher heating value (HHV)	97
3.3.7	Catalyst preparation.	98
3.3.8	Characteristics of catalyst.....	100
3.4	Experimental set-up	101
3.4.1	Intermediate pyrolysis	101
3.4.2	Synergetic effect determination of biomass and PP ...	103
3.4.3	Wet torrefaction experimental set-up (Objective 5). .	104
3.5	Product characterization.....	107
3.5.1	Bio-oil characterization.....	107
3.5.2	GC- MS analysis	107
3.5.3	Fourier transform infrared (FTIR)	108
3.5.4	Biochar characterization	109
3.5.5	Field emission scanning electron microscope/energy dispersive x-ray (FESEM/EDX).....	109
3.6	Statistical experimental design and model development....	109
CHAPTER FOUR.....		112
4	Results and discussion.....	112

4.1	Evaluate the effect of particle size on physicochemical and kinetic properties of BGS for biofuel.....	112
4.1.1	Proximate analysis for BGS-G1.	113
4.1.2	Ultimate analysis and Van Krevelen plot.....	116
4.1.3	TGA analysis and kinetics	120
4.2	The physicochemical analysis and intermediate pyrolysis of BGS-G1, SSS, & SNS.	122
4.2.1	Proximate analysis of BGS-G1, SSS and SNS.....	123
4.2.2	Ultimate analysis of BGS-G1, SSS and SNS	125
4.2.3	Thermochemical analysis of BGS-G1, SSS and SNS. .	126
4.2.4	Pyrolysis of BGS-G1, SSS and SNS product yield.....	131
4.2.5	Physicochemical analysis of BGS-G1, SSS, and SNS bio-oil and biochar	134
4.2.6	Fourier transform infrared (FTIR) of BGS-G1, SSS and SNS	137
4.2.7	Field emission scanning electron microscopy-energy dispersive x-ray (FESEM/EDX).....	146
4.3	The role of various inert gases (N ₂ , CO ₂ , and N ₂ /CO ₂) in intermediate pyrolysis on BGS.	149
4.3.1	Feedstock properties.....	149
4.3.2	Product yields for different inert gases and flow rates. ...	150
4.3.3	Bio-oil energy and pH of bio-oil	154
4.3.4	Thermogravimetric analysis	158

4.3.5 Fourier transform infrared (FT-IR)	161
4.3.6 Field emission scanning electron microscopy - electron dispersive x-ray (FESEM-EDX).....	163
4.3.7 Bio-oil chemical composition via GC-MS analysis	165
4.4 Synergetic effects and intermediate catalytic co-pyrolysis of SSS with polypropylene (PP).	173
4.4.1 Catalyst properties	174
4.4.2 Thermogravimetry Analysis	180
4.4.3 Intermediate co-pyrolysis	187
4.4.4 Intermediate catalytic co-pyrolysis.	189
4.4.5 Physicochemical (ultimate, proximate, and EDX) analysis of SSS/PP products.	193
4.4.6 Van Krevelen analysis	197
4.4.7 Fourier transform infra-red (FTIR) SSS:PP pyrolysis products.	198
4.4.8 GC- MS (Gas chromatography-mass spectrometry) ..	203
4.4.9 Comparison of the Intermediate and catalytic co- pyrolysis.....	207
4.5 Wet torrefaction of SNC under different temperatures and residence times to improve its fuel properties.	209
4.5.1 Hydrothermal process water phase diagram	209
4.5.2 ANOVA statistical model analysis.	212
4.5.3 Proximate analysis of raw and torrefied SNC biomass.	219

4.5.4 Atomic ratio (AR).	222
4.5.5 Thermal analysis of SNC.....	224
4.6 Summary of products analysis of the objectives.	226
CHAPTER FIVE	233
5 Conclusion and recommendation (Future work)	233
5.1 Research summary.....	233
5.2 Conclusion	233
5.3 Recommendation (Future work).....	235
Appendices.....	237
References	239

List of Figure

Figure 2.1: The UNIQUE integration of gasification, hot gas cleaning and conditioning in one reactor vessel [116].....	47
Figure 2.2: (a) The BFB reactor and (b) CFB pyrolizer, adopted and redrawn from [122].....	53
Figure 2.3:(a) Conical spouted bed and (b) Rotary cone reactor (adopted and redrawn from [122] and [137], respectively)	55
Figure 2.4: (a) Auger and (b) Ablative reactor (adopted and redrawn from [122], and [139] respectively).....	58
Figure 3.1: Flowchart for the research activities	90
Figure 3.2: A vertical tubular reactor	102
Figure 4.1: Van Krevelen Diagram of BGS-G1, G4 & G5.	119
Figure 4.2: The (a) TGA and (b) DTG plots of BGS-G1, G4, & BGS-G5.	122
Figure 4.3: TGA plot of BGS-G1, SSS, & SNS.	126
Figure 4.4: DTG plots of BGS-G 1, SSS, & SNS.	127
Figure 4.5: Van Krevelen plot of BGS, SSS, and SNS products.	136
Figure 4.6: The BGS, SSS, & SNS FTIR analysis of (a) bio-oil and (b) biochar.	139
Figure 4.7: SEM-EDX (a) BGS-G1 (1,500X, 50 μm), (b) SSS (3000X, 40 μm) (c) SNS (3000X, 40 μm) image analyses.	147

Figure 4.8: Intermediate pyrolysis products yield at 5, 17.5, and 30 mL/min flow rates for different inert gases (N ₂ , CO ₂ , and N ₂ /CO ₂).	150
Figure 4.9: HHV (MJ/kg) and pH of bio-oils produced at 5, 17.5, and 30 mL/min flow rates for different inert gases (N ₂ , CO ₂ , and N ₂ /CO ₂).	155
Figure 4.10: (a) TGA and (b) DTG graphs for biochar produced in N ₂ , CO ₂ , and N ₂ /CO ₂ inert gases at 17.5 mL/s.	160
Figure 4.11: FTIR (a) Bio-oil and (b) biochar produced in N ₂ , CO ₂ , and N ₂ /CO ₂ inert gases at 17.5 mL/s.	162
Figure 4.12: SEM images for (a) BGS-G1 (biomass) (b) biochar BGS-N ₂ (c) biochar BGS-CO ₂ (d) biochar BGS- N ₂ /CO ₂	165
Figure 4.13: The XRD data for the catalyst analysis.	176
Figure 4.14: FESEM (a) Al ₂ O ₃ (b) 25wt.%Ni/Al ₂ O ₃ (c) ZSM-5 (d) 25wt.%Ni/ZSM-5 catalyst.	179
Figure 4.15: The (a) TGA and (b) DTG graph for PP: SSS and SSS: PP (1:3 to 3:1) ratio.	182
Figure 4.16: The TGA SSS:PP (a) (1:3), (b) (1:1), and (c) (3:1) and DTG SSS:PP (d) (3:1), (e) (1:1), and (f) (1:3) synergetic experimental and theoretical plots.	185
Figure 4.17: The co-pyrolysis oil, char, and gas yields.	188
Figure 4.18: The catalytic co-pyrolysis product (bio-oil, biochar, and biogas) products.	192

Figure 4.19: Van Krevelen of SSS:PP (0:1), SSS:PP (1:1), SSS:PP (1:0), SSS:PP-Al ₂ O ₃ (1:1/4), SSS:PP-Al ₂ O ₃ (1:1/2), SSS:PP-ZSM-5 (1:1/4), SSS:PP-Ni/ZSM-5 (1:1/4), SSS:PP-Ni/ Al ₂ O ₃ (1:1/4) samples.	198
Figure 4.20: FTIR for pyrolysis oil (a) SSS:PP (0:1), SSS:PP (1:1), SSS:PP (1:0) and (b) Feed-Al ₂ O ₃ (1:1/4), Feed- Al ₂ O ₃ (1:1/2), Feed-ZSM-5 (1:1/4), Feed-Ni/ZSM-5 (1:1/4), Feed-Ni/ Al ₂ O ₃ (1:1/4).	199
Figure 4.21: The GCMS classification according to the significant chemicals and area percentage.	205
Figure 4.22: Water phase diagram for a hydrothermal process.	211
Figure 4.23: (a)The 3-D surface standard error of design and (b) model graph parameter interactions for the experimental yield %.	218
Figure 4.24: Van Krevelen diagram for hydrochar 230°C-W/B10R20, 260°C-W/B5R10, 200°C-W/B5R10, 260°C-W/B15R10, 200°C-W/B15R10, and Raw SNC.	223

List of Tables

Table 2.1: Biomasses investigated as bioenergy materials/sources.	12
Table 2.2: Hydrochar comparison with coal fuel properties.	31
Table 2.3: Thermochemical processes and their challenges	60
Table 2.4: Summary of the operating conditions for HTC of Biomass	74
Table 2.5: Summary of the operating conditions for HTG of Biomass	83
Table 3.1: Summary of the samples and the processes.....	90
Table 3.2: Factors of boundary, constraints, levels, and SNC responses.	111
Table 4.1: The BGS-G1, BGS-G4, and BGS-G5 proximate and ultimate analysis results.....	114
Table 4.2: Proximate analysis of some biomass.....	118
Table 4.3: Ultimate, proximate, and EDX analysis of raw BGS-G1, SSS, and SNS.....	123
Table 4.4: The Kinetic and TGA analysis.....	130
Table 4.5: The bio-oil and bio-char proximate and ultimate analysis	132
Table 4. 6: The GCMS classification according to the major chemicals area percentage.	142

Table 4.7: The CHNS of biomass, product yield and their EDX analysis for the inert gases at 17.5 mL/min.	153
Table 4.8: GCMS bio-oil compound produced at 17.5 mL/s.	169
Table 4.9: The intermediate catalytic co-pyrolysis products, HHV and ultimate analysis.....	194
Table 4.10: ANOVA for 2FI model, yield, fit & model summary statistics.	215
Table 4.11: Design of Experiment, report on the actual and predicted responses product yields for SNC	216
Table 4.12: Proximate analysis raw and torrefied SNC result. ..	220
Table 4.13: Electron-dispersive X-ray (EDX) analysis composition.	225
Table 4.14: Summary of products analysis for objectives 2, 3, 4 and 5.....	229

List of Nomenclature

A	Apparent frequency factor
AAK	Acid, aldehyde, ketones
BGS	Bambara groundnut shell
BGS-G	Bambara groundnut shell-genotype
α	Conversion degree
CFF	Crops for the future
CR method	Coats-Redfern method
DAEM	Distributed activation energy model
DTG	Derivative thermogravimetric
E_a	The apparent activation energy (kJ/mole)
EDX	Energy-dispersive X-ray spectrometry
$f(\alpha)$	Function of conversion
FT-IR	Fourier transform-infrared spectrum (1/cm)
$g(\alpha)$	Integrated function of conversion
GC-MS	Gas chromatography-mass spectrometry instrument
HHV	Higher heating value (MJ/kg)
H	Hydrogen
HC	Hydrocarbon
H/C	Hydrogen/carbon ratio
I.C.	Ion Chromatography
N	Nitrogen
O	Oxygen
ICP-AES	Inductively coupled plasma-atomic emission spectrometry
SEM	Scanning electron microscopy
SNC	Shea Nut Chaff
SNS	Shea Nutshell
T	Temperature, °C
TG	Thermogravimetric
TGA	Thermogravimetric Analysis
XRF	X-ray fluorescence
XRD	X-ray diffraction

CHAPTER ONE

1 Introduction

In recent years, there have been different renewable energies on the world map, such as tidal power, geothermal, hydrogen, nuclear waste, hydroelectricity, biofuel, winds, solar thermal, and fusion. Biomass and solar are both eco-friendly energy sources but have their advantages and disadvantages. The weather factors are unpredictable, which is a challenge for both energy systems [1]. Solar energy is from natural sunlight, is smokeless, and it's of high energy generation in tropical regions, but lower during raining seasons. The rainy season increases the biomass yield in marginal soil. Biomass produces more alternative energy with carbon neutral, where the CO₂ emission from the process is easily reabsorbed by the green plants as compared to CO₂ emitted from fossil fuel. Biomass is a promising feedstock option because it is readily available as humans survive on agricultural products and is the only carbon-rich material next to fossils. It is also renewable because they are reproduced yearly, twice, or intermittently depending on the crop or planting season or harvest. Biomasses are relatively cheap resource materials which can be processed via various thermochemical processes such as torrefaction, pyrolysis, and gasification into the various desired products' fuels (solid, liquid, or gaseous) state [2].

The European Union (EU) commission proposal in the 3rd and 4th quarters of 2018 for the new EU directive (RED II) requested a reduction in food-based biofuel from 7 % energy content in 2021 to 3.8 % by 2030 [3]. To meet up with the proposal of the new EU directives the primary biomass conversion processes such as biochemical, physiochemical, and thermochemical processes had to be reconsidered [3]. However, the thermochemical processes are safer, timely, and cost-effective because their products are produced within hour(s) and have less chemical application compared to other technologies or processes such as biochemical, and fermentation [4]. Researchers are focused on thermochemical processes to carry out system upgrades for high efficiency and productivity because reactors have the greatest influence on bio-oil yields [5]. The significant thermochemical pyrolysis technology employed in the advancement of biofuel research is bubbling fluidized beds (BFBs), circulating fluidized beds (CFB), conical spouted beds (CSB), rotating cones (RC), ablative and auger reactors, which could be scaled-up for commercial or industrial purposes.

Two significant challenges faced by countries are climate change and the high demand for fuels associated with fossil fuel consumption. Worldwide energy consumption is estimated to

increase from 575 British thermal units (BTU) to approximately 736 quadrillion BTU from 2015 to 2040 [6], renewable energy as an energy source to supplement fossil fuels, would help reduce the greenhouse gas emissions and global warming impacts. Biomass is an energy source with high carbon material next to coal or fossil fuels. It has become necessary to explore the energy potential of biomass to improve energy generation and production, which consists of carbon, hydrogen, oxygen, and nitrogen, with a negligible amount of sulphur, indicating its potential as bioenergy [7]. The main biomass components are polysaccharides, lignin, oxygenated compounds, and highly polymerized macromolecules. Traditional biomass usage constitutes ~13 % of cooking and heating; nonetheless, it declines in some regions as new energy sources efficiently substitute them. Biofuel provides around 3 % of the world's fuel for transport [8], and the International Energy Agency has set the target of 25 % of diesel used in the vehicle to be obtained from alternative fuels (biofuels) by 2050 to minimize the dependence on petroleum and coal [9]. As more research intensifies on biomass, recent predictions of its energy are likely to make up one-third of the global energy mix and double the global rate of improvement in energy efficiency by 2050 [10]. Biomass appears as an essential fuel role-player in more national and international policies like the European Union or Spain enacting white papers on energy saving. The policies promotion of renewable

in Sweden is stable by the introduction of incentives and carbon tax imposition [11] and the EU food-based biofuel reduction in 2021 from 7 to 3.8 % by 2030 [3]. The future of biomass energy conversion is quite optimistic; agro residues have an enormous scope to produce biofuels, chemicals, and biomaterials to contribute to the global economy.

1.1 Problem statement

The fossil fuel price hike, effect on climate, and its existential threat to plant, animals and human necessitate the quest for alternative energy sources [121]. Alternative clean energy sources are a great contributor to the world energy especially from biomass which is renewable and eco-friendly, with emphasis on non-food and underutilized crop to mitigate the food security crisis. According to Isah et al, 2017 the global share of modern renewable energy is 10.1 % and biomass is ≤ 6.1 % as of 2015 [305]. The total world energy consumption from all the energy sources in the last decades sum up to 80.1 % fossil fuels, 16.7 %, renewable energy, and 2.7 % nuclear energy. In 2016, the global production of biofuel amounted to 82 million tons, with 4 % in transport fuel. The world's biomass resources can cater 66 % of energy demand [306].

Agricultural wastes, forestry residues, industrial wastes, and municipal solid wastes derive cleaner fuels and green chemicals, via biochemical and thermo-chemical processes, compared to fossil fuels [304]. Underutilized crop such as Bambara groundnut shell (BGS), sweet sorghum stalk (SSS), shea nutshell (SNS), and shea nut chaff (SNC) are potential Biomass energy sources. In thermochemical (pyrolysis and intermediate or co-pyrolysis) processes there are little or no research activities on biomass materials (BGS, SSS, SNS, and SNC), which are eco-friendly energy sources.

Due to the little or no research activities on these biomass materials, this research focused on the parameter's evaluation using Design-Expert® to determine the optimum yield, effect of catalyst and co-pyrolysis for bio-oil production.

1.2 Scope and limitation

This study assessed underutilized biomass's physicochemical properties and kinetic behaviour of Bambara groundnut shell, sweet sorghum stalk, shea nutshell, and shea nut chaff. The research covered the thermochemical (intermediate pyrolysis) and hydrothermal (wet torrefaction) processes, in the production of bio-oil, biochar or hydrochar and in the characterization of resulting

products to determine their potential as an energy source (biofuel/transport fuel). It also includes catalyst preparation and the investigation of intermediate catalytic co-pyrolysis of SSS, and PP. This work was to determine the physicochemical analysis of the intermediate pyrolysis and catalytic co-pyrolysis products (bio-oil and char) and analyse their suitability for transport fuel and powering machinery applications. Due to the similarity in the physicochemical properties of SSS with BGS-G1, BGS-G1 was used for inert gas pyrolysis and analysis while SSS was used for catalytic co-pyrolysis in this work. The research work is limited to using the following feedstocks, e.g., BGS, SSS, SNS, SNC, and Polypropylene (PP). The inability to access fresh biomass from farm fields immediately after harvest was added to another limitation.

1.3 Aim and objectives.

This research aims to explore the energy potential of Bambara groundnut shell (BGS), Sweet sorghum Stalks (SSS), Shear nutshell (SNS), and Shear nut chaff (SNC) via intermediate pyrolysis, catalytic co-pyrolysis, and wet torrefaction. The objectives to achieve the aim are through the followings:

- 1 To investigate and evaluate the effect of particle size on physicochemical and kinetic analysis of treated and untreated BGS for biofuel production.

- 2 To determine the physicochemical analysis and intermediate pyrolysis of an improved Genotype of BGS-G1, SSS, and SNS to produce bio-oil.
- 3 To evaluate the impact of different inert gases (nitrogen, carbon dioxide, and N₂/CO₂ (75:25) vol. % mixture (flue gas) atmosphere, in a varying flow rate in the intermediate pyrolysis of BGS.
- 4 To examine the synergetic effects of SSS and polypropylene (PP) in an intermediate catalytic co-pyrolysis for bio-oil generation.
- 5 To investigate the wet torrefaction of SNC using a Design-Expert® software with temperatures (180 - 260 °C), biomass-to-water (1:5 - 1:15) ratio and residence times (15 - 30) minutes to improve its fuel properties.

1.4 Research novelty

This research investigated the energy potential of some biomass species (BGS, SSS, SNS and SNC) that have not been studied for intermediate, catalytic co-pyrolysis, and hydrothermal carbonization (wet torrefaction).

The novelties are as follows.

1. The particulate size of 1018 µm improved the BGS HHV to 18.6 ± 0.5 MJ/kg on their particle size physicochemical and kinetics analysis. It also reflected and contributed to the best

bio-oil HHV of 26.5 ± 2.0 MJ/kg for Shea Nutshells (SNS) from an intermediate catalytic co-pyrolysis as compared to Bambara Groundnut Shells (BGS-G1), and Sweet Sorghum Stalk (SSS).

2. The impregnated catalyst 25 %Ni/Al₂O₃ (1:1/4) had optimum bio-oil yield at 49.0 ± 0.26 wt. % and HHV at 41.1 ± 0.7 MJ/kg, with more excellent C-H-containing functional groups aliphatic hydrocarbon in the Intermediate catalytic co-pyrolysis of SSS and PP as compared to the other catalyst developed.
3. Finally, the Shea Nut Chaff (SNC) wet torrefaction recorded high energy yield of 89.54 % and 15.81 MJ/kg HHV. In addition, energy generated from the Shea nut (bio-oil and chaff) only had more than 40 MJ/kg.

1.5 Thesis overview

This thesis is structured as follows:

Chapter One: General Introduction

This chapter provides a background of biomass as an alternative energy source and other benefits of developing biofuels. The chapter includes the importance and technological challenges of thermochemical process conversion for bio-oil production. Fossil fuel's effect on the environment has been the driver of alternative

energy such as green/clean energy. Biomass energy has been used from time immemorial and is presently discovered among the clean energy products to secure the earth. Biomass such as Bambara ground, sweet sorghum, and shea nut waste are underutilized waste, thereby exploring their energy potential into the energy-mix could also save energy integration within the process. Lastly, outline the objectives of the research work.

Chapter Two: Literature Review

Chapter two summarizes the literature review on biomass, and its properties outlines the current challenges in thermochemical technology, biomass reactors, and hydrothermal processes to produce more high-quality products, and the need for further understanding towards producing good quality biofuels.

Chapter Three: Materials and Experimental Methodology

Chapter three provides detailed information on Bambara groundnut, sweet sorghum stalk and shea nutshell biomass, catalyst and chemical reagents used in this study. This chapter summarises the intermediate pyrolysis method, the reactor system details used, and the analytical procedures for the characterization of materials and their products. It also elaborates on the raw materials used for the catalyst production, techniques, and characterizations.

Chapter Four: Intermediate pyrolysis, catalytic co-pyrolysis of BGS, SSS, SNS, hydrothermal process of SNC and product characterization

This chapter discusses the results of the biomass characterization used for this study. It provides detailed information on the results of the intermediate, catalytic co-pyrolysis and hydrothermal product distribution, and their characteristics. It discusses the quality of bio-oil and biochar or hydrochar obtained from the feedstock.

Chapter Five: General Conclusion and Recommendation for Future Studies

Chapter five gives general concluding remarks on the overall project. It highlights challenges encountered and proposes future studies.

CHAPTER TWO

2 Literature review

2.1 Biomass/Feedstock materials

The global energy demand by 2040 was estimated to be about 739 quadrillion of BTU; it has become imperative to explore alternative renewable energy sources [12]. Biomass is a potential source for many organic or green chemicals and carbon-based fuels. The physicochemical characteristics of biomass significantly impact the efficiency of energy conversion technologies. High ash and moisture content impedes the energy generation from biomass, while high carbon and hydrogen content, with low sulphur, and nitrogen yield clean energy and high HHV [13]. The operational parameters of the biomass, such as moisture content, specific gravity, heating value, and fixed carbon-content play significant roles in biofuel generation [14]. According to Bošnjaković., (2020), high moisture content of wood chips produces lower HHV, and results in lower boiler efficiency [15], while improving the specific gravity and viscosity of bio-crude enhances biofuel quality [16]. High carbon content tends to form high-grade biomass fuel [17], and carbon and fixed carbon-content are also a function of HHV. Different types of biomasses have been investigated as energy sources, tabulated in Table 2.1 below.

Table 2.1: Biomasses investigated as bioenergy materials/sources.

S/No	Feedstock (s)	Pre-treatment, process, and conditions	Properties and application of products	Ref.
1	Poplar and willow	<ul style="list-style-type: none"> Willow biomass moisture removal. Continuous gasification process The 104 MW Greenidge pulverized coal power plant demonstrated continuous co-firing of wood at 10 % by heat input for over three years. 	<ul style="list-style-type: none"> Used as heat and energy sources. Environmental and social benefits simultaneously use as solid fuel. 	[18]
2	Treated sawdust	<ul style="list-style-type: none"> The lignocelluloses pretreatment was conducted with NaOH and H₂O₂ Pre-treated sawdust with enzyme was optimized at pH of 5.0, 50 °C, and substrate concentration of 0.5 %. The saccharification process was studied to determine the release of soluble and reducing sugars. 	<ul style="list-style-type: none"> NaOH-treated sawdust can produce cellulase and saccharification on a large scale. The rate of saccharification with crude enzyme of <i>Aspergillus niger</i> cellulase alkali-treated sawdust was found to be maximum (23 %) as against 5.4 % on native sawdust under optimal conditions after 48 h. 	[19]
3	Orange peel waste	<ul style="list-style-type: none"> The pretreatment (moisture content) of orange peel was reduced to 10 %. Fast pyrolysis process to produce bio-oil. 	<ul style="list-style-type: none"> Bio-oil CHNSO (46, 6, 1.52, 0.05 and 46). Bio-oil HHV (18.35 kJ/kg). 6029 tonnes of orange peel yield an estimated 3.01 million litres of bio-oil. 	[20]

4	Real food waste	<ul style="list-style-type: none"> • Thermal process for real food waste treatment. • Temperature within 400 - 700 °C. • Carbon dioxide (CO₂) applied to food waste thermal treatment. 	<ul style="list-style-type: none"> • During the thermal treatment of CO₂ supplied, less condensable compounds but more non-condensable gases such as H₂, CO, and CH₄ were generated at temperatures (400 – 700 °C), while the amount of solid residue was not affected. • The change in product distribution and generation of cyclic compounds was inhibited by applying CO₂ to the thermal treatment. 	[21]
5	Peat moss and miscanthus	<ul style="list-style-type: none"> • Hydrothermal carbonization (HTC) process. • The life cycle assessment (LCA) of HTC of wet biomass environmental performance of the hydrothermally treated and untreated biomass applied for energy and soil amendment. • The decomposition rate of peat moss is dependent on the carbon-nitrogen ratio, the conditions (e.g., temperature, and availability of water) at the place of application, and the state of biomass. 	<ul style="list-style-type: none"> • Miscanthus hydrochar had a lower global warming potential (GWP) compared to peat moss or their blend. • Hydrochar used in soil amendment (S₂, S₄, S₆, S₈) was more environmentally benign than the energy application (S₃, S₅, S₇), but the benefits were dependent on the decomposition rate of biomass. • Life cycle impact is S₁ (-1505.60), S₂ (830.5), S₃ (824.3), S₄ (79.5), S₅ (283.3), S₆ (-320.9), S₇ (-369.8), and S₈ (-830.1) kg-CO₂ eq./t. 	[22]

6	Cork, pine pellet and olive pomace	<ul style="list-style-type: none"> Residues were dried using screw dryers. Hot gases are used from biomass stove chimneys. The drying air flow rate was fixed at 10 m³/h and the average temperature at 180 °C. 	<ul style="list-style-type: none"> Combustion and drying yields are 80 % and 47 % respectively. A boiler and a stove for olive pomace combustion as a clean fuel and exhaust gases were measured and analysed with very low emissions. 	[23]
7	Oil palm frond and, Leucaena Leucocephala	<ul style="list-style-type: none"> Torrefaction pre-treatment process. The heating rate was at 10 °C/min in a Horizontal tube furnace. Temperatures (200, 225, 250, 275 and 300 °C) and holding time of 60 min. 	<ul style="list-style-type: none"> The increasing energy density (higher fixed carbon content, calorific values and reduced hydrogen and oxygen contents) and eliminating problems with raw biomass such as high moisture content. HHV improved from raw biomass (18 MJ/kg) to treated biomass (25 MJ/kg). 	[24]
8	Beech stick and beech bark pellet	<ul style="list-style-type: none"> Pyrolysis process of beech bark pellet and beech stick in a fluidized bed reactor. Temperatures at 450, 650 and 850 °C. Cylindrical wood particles (beech bark pellet: Φ10 x 15 mm and beech stick: Φ6 X 10 mm) 	<ul style="list-style-type: none"> The different chars were prepared at a pyrolysis temperature of 850 °C and their reactivity exhibited a true density close to graphite. 	[25]
9	Wood sawdust	<ul style="list-style-type: none"> Analytical pyrolyzer in a thermogravimetric analyzer and fast pyrolysis conducted in a Py-GC/MS, at a 	<ul style="list-style-type: none"> The production of phenolics, cyclooxigenates and linear hydrocarbons decreased, and non- 	[26]

		fast-heating rate ($\sim 10,000 \text{ }^\circ\text{C s}^{-1}$) <ul style="list-style-type: none"> • Particle sizes (26.5 – 925 μm) • Different heating rates (0.5–100 $^\circ\text{C min}^{-1}$). 	condensable gases like CO, and CO ₂ increased with particle size. High. <ul style="list-style-type: none"> • Intraparticle mass transfer of volatiles and temperature gradients in irregularly shaped particles significantly affect the kinetics of biomass pyrolysis and product composition.
10	Sorghum bagasse biomass	<ul style="list-style-type: none"> • Pyrolysis process of sorghum bagasse biomass into biochar and bio-oil products. • The pyrolysis temperature from 623 - 823 K leads to a decrease in biochar (42.55 - 30.38 %). • While a maximum bio-oil of 15.94 % was obtained at 723 K. The biochar obtained at 673 and 773 K is composed of a highly ordered aromatic carbon structure. 	<ul style="list-style-type: none"> • FTIR analysis of sorghum bagasse biomass composed of highly ordered aromatic carbon structure. [27]

Biomass can be grouped as; (1) agricultural residue and waste: rice husk, rice straw, jute stalk, wheat straw, coconut leaf, groundnut straw, vegetable plant and peels, potato plants, pulse straw, cotton stalks, sugarcane leaf, and tops and bagasse; maize straw leaf, maize husk, animal faces, and poultry droppings. (2) Forest residue:

tree branches, twigs, leaves, wood, and wood residues [28]. Lastly, (3) Industrial wastes: Municipal Solid Waste (MSW), refuse-derived fuel (RDF), plywood, sewage sludge, paper-pulp sludge, railway sleepers, and hospital waste [29].

There are some challenges with biomass being utilized as feedstock for energy, such as particle size, moisture, and ash content which affect the desirability of fuel properties such as higher heating value. The particle size of biomass affects the production process by attrition, poor heat transfer, unstable reaction, more CO₂ production due to high moisture with large particle size, and ineffective product yield [26]. The smaller the biomass particle size, the faster the heat transfer to the centres of the particles, thereby reducing the residence time during pyrolysis [30].

Mainly, biomass feedstock has high moisture content, e.g., birch (18.9 wt. %), food waste (74 – 90 wt. %), paper sludge (70 – 80 wt. %), textile sludge (80 wt. %), leather (10.25 wt. %), Municipal Solid Waste (MSW) (52 – 66 wt. %), wood (20 wt. %), barley straw (30 wt. %) and wheat straw (15 – 16 wt. %) [31]. High moisture content lowers the process temperature, causes incomplete combustion, reduces boiler efficiency, and leads to operational problems [15]. Typically, the moisture content of biomass is in the range of 5 – 35 % [32], but the optimum for biofuel processing is

within 10 - 15 wt. % [33]. To reduce the moisture content, drying of biomass is required. More standardized approaches with cost-effective and high efficiency drying technologies are required. The drying technologies include two distinct techniques, i.e., Dry Torrefaction (DT) and Wet Torrefaction (WT). The DT is a similitude to pyrolysis which occurs at 200 – 300 °C in an inert environment under atmospheric pressure while WT refers to a hydrothermal pretreatment process in subcritical water between 180 – 260 °C, and at about 4.6 MPa within 240 min residence time [34]. The primary biomass pretreatment methods are physical, chemical, biological, and combinatorial. The combined or integrated methods apply physical parameters (temperature, pressure or biological) in combination with chemical treatments, referred to as physicochemical treatment e.g. AFEX or biochemical (Bioorganosolv) pretreatment methods, which are more effective, enhance digestibility, and lead to pretreatment method [35]. The physical pretreatment (dried and reduced particle sizes) of biomass could be harnessed optimally via the most cost-effective thermochemical conversion technology with a high-yield (output) product [36].

Thermochemical conversion processes are employed in the processing or conversion of the treated biomass or raw biomass, which include torrefaction, combustion, liquefaction, pyrolysis,

gasification [37], and hydrothermal, [39] into different biofuels or various energy products.

2.2 Biomass and its properties

Although biomass has inherent energy potential, they have few challenges too. More than three (3) biomass challenges include biomass bulkiness, high moisture content, and CO₂ and SO₂ emissions that militate against its energy recovering. Its heterogeneous nature spans from industrial wastes to wood, agricultural residues, or energy crops. The bulkiness and high moisture content will generate more smoke which is constituting air pollution and inhibit high-quality and clean biofuel. The physicochemical analysis of biomass is highly significant in understanding its energy potential as each has its peculiar properties such as moisture content, lignin, cellulose, and hemicellulose distribution across various biomass. Pollution control and the high efficiency of each of the technological processes would enhance the environmental control measures of air pollution (NO_x and SO_x emissions). However, the established thermochemical processes are robust and flexible in co-firing biomass feedstocks for energy.

Biomass characterization is essential for thermal conversion processes, such as combustion, gasification, and pyrolysis. The chemical properties of fuel aspects are ultimate or elemental analysis (C, H, N, S, and O), proximate analysis (moisture, ash, volatile, and fixed carbon) and higher heating value (HHV). Proximate analysis estimates the feedstock efficiency for power generation and product yield (char, oil and gas) in thermal conversion systems, by the determination of carbon content and its HHV [40]. Proximate properties affect the combustion behaviour and plant design such as low carbon and high ash contents in lowering the energy generation, while residues courses fouling and rusting on the design and operated plant. High moisture values decrease the combustion yield, while high volatile matter/fixed carbon ratios are related to the fuel's reactivity 41, employing significantly elevated temperatures (900 °C), particularly in volatiles determination [40]. On the other hand, ash profoundly influences corrosion, and slag formation, in the reactor and accumulates both facilities and management costs. Analytical studies of fuel types classified biomass fuels as having high volatile matter and moisture content, with mineral matters co-rich in alkali and alkaline earth metals such as potassium and calcium. Ash compositions for a wide range of biomass fuels vary as in woody Biomass (Ca-, K-rich & Si-lean), herbaceous (Si- &, Ca-rich & K-lean), and rapeseed expeller ash (Ca-, K- & P-rich) [42].

Bambara groundnut, one of the underutilized crops, survives in minimum rainfall and generates shells (BGS). Bambara groundnut (*Vigna subterranean*) an indigenous African crop grown from North to South and East to West Africa. Bambara groundnut is a grain legume grown mainly by subsistence farmers in the Sub-Sahara of the African continent. According to Atiku et al. (2004), legume is the third most crucial after groundnut and cowpea as Bambara groundnut is widely grown in Anambra and 50 % of Northern states in Nigeria, with Gombe State (least land area of 17,802 km²) [43]. In Zambia, Bambara groundnut flour is used for baking bread and producing flavoured milk that tastes better than cowpea, pigeon pea, and soybean. They are suitable for food and medicinal purposes in North-eastern Nigeria [43].

The subterranean Bambara groundnut physical properties had hard pods and produced justifiable yields in low fertile farmland. Its seeds are black, dark brown, red, creamy, white, a mixed colour depending on the varieties; approximately 1.5 cm long, slightly oval, often wrinkled at the matured stage, and contain 1-2 seeds. Bambara groundnut (*Vigna subterranean* (L) Verdc) is an underutilized legume seed for consumption in various meals. Its composition of protein, carbohydrate, lipid, fibre, and ash are (16 – 25 %), (42 – 60 %), (5 – 6 %), (4.8 %), and (3.4 %), respectively.

Legumes like Bambara have the capacity for atmospheric N-fixation and climate change mitigation without expensive inorganic Nitrogen-fertilizers, which are also not readily available to local farmers. The potential yields of Bambara groundnut at its cultivation can increase significantly without high agronomic inputs and a leguminous crop for global food security and nutrition.

Notwithstanding, its important nutritional and agroecological profile enriching the world food system is under threat by a lack of financial resources, knowledge limitation, social stigma, and lack of incentive policy. More research would lead to a promising outlook and sustainability to realize its full potential [44]. The growth and development of Bambara groundnut in response to soil moisture and the Bambara groundnut landraces responses reflect their adaptation to the local climates, where mean annual rainfall is between 365 mm and 1390 mm in different continents 45. Bambara groundnut performance with rice husk biochar and Christmas Island Rock Phosphate application was investigated by revealing that farmers could apply rice husk biochar at 10 t/ha to enhance crop performance [46]. In contrast, no trace effect of rock phosphate on nitrogen content and fixation of the crop in the study area [46]. Agriculturists commonly grow them in marginal land across Africa and have broader acceptance in the Asian continent, countries like Indonesia, Philippines, India, Malaysia, and Thailand, while

research is underway to improve their varieties [47]. It survives better than other tropical legumes, e.g., cowpea and groundnut. Bambara groundnut constitutes pod weight which is about 1000 kg/ha, 374 - 896 kg/ha of the total nut weight and approximately 28.6 - 34.2 % of the total pod weight. To curtail pollution and fossil fuel challenges, it could be harnessed for green energy [48].

Valorization of Bambara groundnut shell via intermediate pyrolysis of product distribution and characterization was studied and recorded to recover high-quality fuel precursors and other valuable materials [48]. Recovery of clean energy precursors from Bambara groundnut waste via pyrolysis also emphasized kinetics, product distribution, and optimization using response surface methodology [49]. This study revealed the shell of the Bambara as a potential source of energy precursors to developing a sustainable bioenergy system and biomaterials. Bambara ground nut shells and programme of breeding to improve nitrogen fixation capacity to date [38], not much on biofuel production.

Sorghum is best known as a grain crop; sweet sorghum is like grain sorghum; the juice, grain, and bagasse produce food fodder, ethanol, and electricity [50]. The total global area of marginal land suitable for growing sweet sorghum is 4802.21 million hectares. The maximum annual temperature contributes more than other

variables to the predicted distribution of sweet sorghum, with 40.2 % [51]. It occupies about 45 million hectares, with Africa and India accounting for about 80 % of the global acreage [50]. According to the study by Wang et al., (2014) in China, the pilot base has an area of 267 hm²; simultaneously, the average fresh weight of the sweet sorghum grain was 3.3 t/h the stalk reached 60 t/h [52]. The production of sweet sorghum in South Africa has been about 180,000 tonnes. It has a higher tolerance to salt and drought than sugarcane and maize. It is currently used worldwide for biofuel [53], alkaline soils, and waterlogging of its wide range of prevalence in various world regions [50]. It has a lower cost of cultivation and familiarity with sorghum cultivation; farmers' ability and willingness to adopt sweet sorghum is much easier [50]. It also has high carbohydrate content like sugarcane. Still, its water and fertilizer requirements are much lower than sugarcane, the stalks are waste, and no threat to food security, as potential for biofuel production [53], the stalk is central in this study. Next significant biomass waste material is generated from the shea nut fruit used to produce shea butter.

Shea nut survives in areas with 400 - 800 mm of yearly rainfall. It grows naturally from the west (Senegal) through East Africa (Sudan) to the Ethiopian highlands. About 19 countries on the African continent, e.g., Mali, Ghana, Niger, Senegal, Uganda, Benin, Ivory

Coast, Zaire, Guinea, Serra Leone, Sudan, and Burkina Faso. In Nigeria, the states include Niger, Kwara, Kebbi, Kaduna, and Oyo State; and, the Democratic Republic of Ghana has large acreages of the shea nut tree used in the food industry, soap making, and health care [54]. The shea nut tree bears good-quality sweet fruits after about 15 - 30 years, for up to 30 - 250 years. The shea nut tree has a cylindrical trunk in circumference of 0.5 - 2.5 m and 3 - 4 m in height before branches. The potential number of shea trees in Africa's shea zone ranges from a couple of a billion; Africa produces ≥ 1.76 million metric tons of raw shea nuts annually. The fruit production is oval and resembles small avocado fruits, and harvesting is between May to August. The kernel inside the nut is about 3.2 cm large, 2.3 cm wide \times 0.1 - 2.1 cm thick in size. A pulp covering in each fruit is delicious when the fruit is ripe. The shea fruit consists of a green epicarp, a fleshy mesocarp, and a relatively hard shell (endocarp) that encloses the shea kernel (embryo), sometimes two or more. The fruit weighs from 10 to 57 g, and its annual production is from 15 - 30 kg/tree [55]. Many natural resources extracted from these agricultural resources result in heaps of biomass waste, which are convertible to clean energy through thermochemical processes. Several studies were done on shea nut's nutritional value on shea butter and application. The oil, known as shea butter, is used to manufacture soap, candles, cosmetics, skin care, pharmaceutical products, and butter

substitutes. Investigating the shea nut kernel's physical properties seems to have limited research [56]. According to Itodo., (2011), pyrolysis and kinetic studies determined that shea nutshell activated carbon was suitable for treating textile wastewater to remove organic dyes compared to commercial activated carbon [57]; it is an added value when researching pyrolytic oil production. After the shea butter or oil extraction, the shea nutshell and chaff are waste materials. Discovering the potential in the waste is an added value chain to the process. Agricultural residues and waste produce approximately 168.49 million tonnes (MT), which could generate the energy of about 2.01×10^{-6} Terajoule [TJ] per annual in Nigeria [58]. The Emission Protection Agency (EPA, 2021) reported that a tonne of agricultural residue burnt produces approximately 1400 kg of CO₂, 58 kg of CO, 11 kg of particulate matter, 4.9 kg of NO_x (Nitrogen oxides), and 1.2 kg of SO₂ released into the atmosphere. These pollutants contribute to global warming, increase oxidant levels, acid deposition, and visual impairment, cause nutrient loss, and deteriorate soil fertility [59]. Therefore, it is vital to solve agro-residue disposal and energy recovery issues.

2.3 Thermochemical processes

There are several thermo-chemical processes which include torrefaction, combustion, liquefaction, pyrolysis, gasification [37], and hydrogenation [38]. However, torrefaction, pyrolysis, and gasification are the most used [60] for biomass conversion into different biofuels or various energy products. Torrefaction is a thermal treatment or thermochemical conversion of biomass or wood to improve its properties for long-term storage or HHV of biochar as biofuel [61]. In the absence of oxygen, it's called mild pyrolysis. Dry torrefactions are often carried out in an inert gas atmosphere, while wet torrefaction uses H₂O as a medium of reaction and temperatures between 200 - 300 °C, with char and gaseous fuels as final products. It lowers the oxygen level and increases the carbon content of the char matrix [62]. Pyrolysis reactions are endothermic, which operates within 300 - 700 °C. The processes associated include heat transfer, product diffusion from biomass pores to the gas phase, and reactions in series. It's subdivided into primary and secondary; where the primary pyrolysis temperatures range is 300 - 600 °C in-line with the decomposition of biomass into tar, char, and volatiles. Secondary pyrolysis is noticed beyond 600 °C which constitutes tar cracking to form light hydrocarbons [63]. An improved and new concept of the gasification process is integrating pyrolysis, combustion,

supercritical water gasification, multi-staged gasification and gas cleaning technologies (UNIQUE gasifier) etc. as a unit system [28]. It's a promising technology for biofuel production but hasn't reached full commercial readiness due to technical issues related to the high-scale operation, high gas cleaning costs, biomass availability, biomass market instability, and investment difficulties [64]. Nonetheless, much effort is currently underway to make gasification a mature and feasible biomass conversion route [65]. Many strategies that involve pressurized gasification and biomass handling are highlighted by the International Energy Agency (IEA) and the International Renewable Energy Agency (IRENA) [66]. The gasification converts carbonaceous resources into syngas (H_2 and CO_2) [67]. Biomass gasification mostly relies on its density factor which determines the solid matter to total volume ratio a reactor can handle. The density factor may divide gasification into dense and lean-phase reactors. In the former, feedstock materials occupy the maximum space of the reactor, and the latter is one large reactor chamber for stimulating the reactions of the drying zone, combustion zone, pyrolysis zone, and reduction zone [28]. Research studies on biomass conversion to liquid fuel are rapidly developing via the various thermochemical processes from biomass to liquid (BTL) and have sophisticated technologies for product upgrading [68].

Thermochemical processes are effective energy conversion processes among biofuel production technologies. Heat and catalysts are used to convert biomass into bioenergy and other value-added chemicals through pyrolysis, combustion, and hydrothermal processes. High liquid yields are at high heating rates, reaction temperature of 425 - 600 °C, and low residence time (3 s). Reusing pyrolysis by-products lowers NO_x, and SO₂ emissions, increases energy recovery efficiency and reduces overall costs. Building a pyrolysis technology plant has more financial advantages than gasification, incineration, or combustion technologies [31]. The greenhouse gases' life cycle reduction in pyrolysis is influenced by feedstock, conversion technology, size of the pyrolysis unit, and use of by-products [70]. It's one of the most cost-effective, feasible, and environmentally friendly biomass-to-energy conversion processes [59]. Intermediate pyrolysis differs from fast pyrolysis in heat transfer rate to the feedstock. The typical operating conditions for intermediate-pyrolysis, such as heating rates, reaction temperatures, residence times, feedstock water content, and short residence time are usually ≤ 50 °C/min, 400 - 550 °C, ≤ 10 min, ≤ 10 wt. %, 2 - 4 s respectively. The best opportunity for intermediate pyrolysis technology is to use raw materials with comparatively larger particles and higher vapour residence time than fast pyrolysis. An intermediate pyrolysis plant's construction and operation are more straightforward than other thermochemical processes.

Therefore, a constructed plant can be near the feedstock source and the resulting bio-oil channel to biorefineries for further processing. Bio-oil, the liquid product of pyrolysis, has a complicated composition with primary acids, phenols, and aldehydes, leading to thermal instability and corrosiveness. It also contains nitrogen and oxygen heteroatoms [71]. Since bio-oil is a mixture of many chemicals, it can be used as a source of basic chemicals or refined as a hydrocarbon fuel. As discussed earlier, biomass conversions are mostly through varying processes such as thermochemical, biochemical, or biological processes to produce various essential forms of energy and value-added products. Biomass thermochemical conversion is a feasible route to reduce the dependence on fossil fuels and provide carbon-neutral energy for a sustainable future with higher efficiency [72]. The thermochemical process specifically uses heat and catalysts in some cases to transform biomass into biofuels and other value-added chemicals [73] as discussed in the following subsections 2.3.2-2.3.5.1 below.

2.3.1 Challenges in bio-fuel production processes.

Biomass is a promising energy source and safer in the twenty-first century amidst the energy scenario in the global community as a carbon-neutral fuel. The climate change effect on the ecosystem can be minimized by using renewable energy in the stream of world

energy projects. According to OECD/FAO (2018), global ethanol and biodiesel production is projected between 2017 - 2027 from 120 to 131 and 36 to 39 billion litres, respectively [74]. The elimination of CO₂ emissions requires biofuel-upgraded technology and innovation, notably for the transport and manufacturing sectors [3]. However, these biofuels will go a long way in curtailing the rise in temperature, sea level, and the effect of climate change and adopting the most effective thermochemical technology.

There are several biomass-to-liquid plants across the globe to mention a few. A minimal and sizable number of biomass to liquid (BTL) FT plants, location(s) with their feedstock(s) such as Solena Fuels, Green Sky (Essex, UK)-(Municipal & commercial waste), Red Rock Biofuels (Oregon, USA)-Forest & sawmill waste, Sierra Biofuels, Fulkrum Bio-energy (Nevada, USA) - Municipal solid waste, SYNDIESE CEA (Nevada, USA)-Forest & agricultural waste, CHOREN Sigma Plant (Freiberg, Germany) - 3044 t/d dry biomass, Velocys (Gussing, Austria) - 150 t/d dry Biomass, CUTEC (Germany) - 2.7 t/d dry biomass [75]. However, plants use several technologies in their operations and the most commonly used processes and challenges will be highlighted below.

2.3.2 Torrefaction

Torrefaction is a thermal process that converts biomass into a coal-like material, called torrefied biomass, with fuel characteristics rather than raw biomass. A comparison in Table 2.2 for torrefied biomass and coal fuel properties.

Table 2.2: Hydrochar comparison with coal fuel properties.

S/No	Biomass	Properties	Ref.
1	Wetland plant	18.0 – 27.1 MJ/kg	[76]
2	Lignocellulosic, non-lignocellulosic and ash-rich types	The concentrations of H ₂ and CH ₄ in syngas increased, while the gasified tar from hydro chars reduced to half of its original value from biowastes under similar conditions	[77]
3	MSW-derived hydrochar under	Removal of 90.5 % chlorine of MSW at 220 °C HTC temperature for 30 min. The highest H ₂ yield was in the steam/O ₂ gasification, resulting in the highest H ₂ /CO ratio of 4.58 at 1000 °C gasification temperature.	[78]
4	Wet Torrefaction of Miscanthus	20.099 MJ/kg at 220 °C	[79]
5	Palm shell	12.24 - 22.11 MJ/kg (raw palm shell to hydrochar) produced at 240 °C for 60 min	[80]
6	Lignocellulosic Microalgae Manures Sewage sludge Dried distillers' grains with solubles	36 MJ/kg 32 - 34 MJ/kg 35 MJ/kg 32 MJ/kg 35 MJ/kg	[81]
7	Alstonia congenital wood-dust biomass.	30.58 MJ/kg	[82]
8	Coal (brownish black)	Moisture (0.5-10 %) Volatile Matter (20 - 35 %) Ash (5 - 40 %) Grade A: ≥25.9408 MJ/kg.	[83]

B: 23.4304 MJ/kg.
C: 20.6689 MJ/kg.
D: 17.5728 MJ/kg.
E: 14.0582 MJ/kg.

Torrefaction operations are categorized into stages such as heating, drying, and cooling, based on temperature-time variations [35]. Dry torrefaction converts biomass into biochar ≤ 300 °C, and under atmospheric pressure with inert nitrogen gas [84]. while wet torrefaction is a subcritical water pretreatment process to upgrade biomass of high moisture content into hydro-char solid fuel with high fuel characteristics, avoidance of energy-intensive conventional thermal drying, and high cost [85].

Advantages of torrefied biomass include increased heating value, energy density, carbon content with a reduced atomic ratio (H/C and O/C) and moisture content compared to its raw biomass. These properties distinguish the high fuel content of biomass or fuel material and reduce the cost of a pellet of torrefied biomass. Torrefied pellets cost 4.7 Euro/GJ cheaper than regular pellets at 5.8 Euro/GJ production in Europe while costing \$7.6/GJ for torrefied pellets as compared with \$8.6/GJ for regular Canadian pellets sold in the European market [86]. Wet torrefaction uses lower temperatures and residence time to produce high energy density and hydrochar compared to dry torrefaction [84].

Nevertheless, on a commercial scale, torrefied biomass is in its development stage with few industrial facilities worldwide [87], such as the Blackwood technology plant in Duiven, the Netherlands, Torrefaction plant, Servoda, (Gujarat) India and Airex Energy, Québec H7C 0A5 Canada. The setback of WT is the operating and maintenance cost due to high pressure during the torrefaction process [84]. There is limited information on the performance of the existing plants and also the impact of pretreatment cost until the final delivery of the torrefied materials [88].

Principally, the role of biomass pretreatment is to overcome its recalcitrant nature, modify its structure and make it more flexible for final product conversion. Feedstock becomes imperative to meet the required quality and homogeneity as it is to be applied successfully in the conversion technologies. An affordable pretreatment requires relatively low energy, limited waste streams, and sustainable with an environmentally friendly process [89].

The drying technologies include combustion, gasification, or microwave units depending on the process plant/unit's capacity and operating parameters. Microwave technology (MT) could be scaled up as it demonstrates a niche for biomass pretreatment and upgrades on a pilot scale, with the merit of rapid and efficient heating of the bio The MT reduces the processing time of the

conventional method by 80 %. Integration of microwave technology for biomass pretreatment has become paramount for its improvement and cost minimization [76]. The MT reduces the processing time of the conventional method by 80 %. Integration of microwave technology for biomass pretreatment has become paramount for its improvement and cost minimization [86].

2.3.3 Biomass combustion

The most recent energy technologies for biomass are in various stages of research, test running, development, and commissioning. However, biomass combustion is a well-established electricity generation technology that engages boiler-steam turbine systems.

Biomass combustion consists of various steps: heating, drying, and de-volatilization to produce char and volatiles [1]. The precise modelling of biomass fixed-bed combustion of all aspects is not readily achievable due to the sophistication (i.e., more detailed, biomass-specific chemistry) of solid fuel conversion and fuel bed behaviour to improve burn-out prediction and pollution formed [63]. Its combustion often generates a substantial amount of heat and power for process industries, has low efficiency in energy conversion, elevated gaseous, and particulate pollution, and competes with established coal-based technologies [91].

Biomass combustion produces ash, which is characterized by numerous laboratory techniques, e.g., inductively coupled plasma-atomic emission spectrometry (ICP-AES), X-ray fluorescence (XRF), X-ray diffraction (XRD), scanning electron microscopy (SEM) with energy dispersive X-ray spectrometry (EDX), and ion chromatography (IC) analyse significant elements in fuel materials, including Si, Al, Fe, Ca, Mg, Ti, Na, K, P, Cl, S, Pb and Zn, which cause deposits are determined [92].

The biomass burning emission threshold is 50 mg/m³ (at 11 % O₂). Generally, particulate matter is less than 10 μm (PM₁₀). Environmental protection Agency (EPA) in countries around the globe require new and strict laws on emissions, with the expectation of implementation soon. Currently, there are no common international, national, or even regional emission standards for emission control [1]. Several studies on ash formation and deposition in boilers of biomass species for biomass thermal conversion have been conducted. However, process reactions of the alkali elements, and reaction types before the fly ash contact the heater exchange surface, no practical and cost-effective methods to retard these reactions are entirely known [92].

Generally, biomass fuel properties are categorised as physical, chemical, thermal, and mineral. Biomass combustion properties are sub-classified into two, microscopic and macroscopic. The microscopic include thermal, chemical, kinetics, and mineral, while the macroscopic properties include heating value, ultimate analysis, moisture content, particle size, bulk density, and ash fusion temperature [93]. The aforementioned classification is to highlight the biomass properties and aid in the direction of research or findings for improving lifestyle.

2.3.4 Pyrolysis

"Pyrolysis," a promising thermochemical conversion technology for biomass processing into renewable biofuels, converts biomass to energy and carbon-based chemicals. It's one of the most cost-effective, feasible, and environmentally friendly biomass-to-energy conversion processes, with the major products as bio-oil, biochar, and syngas [94].

2.3.4.1 *Slow and Fast pyrolysis*

A slow pyrolysis process was conducted in a fixed bed reactor at temperatures ranging from 300 - 600 °C and at a 10 °C/min heating rate. The bamboo biochar has good properties as an energy source

and for agricultural applications; with high porosity and after activation as activated carbon [95]. The reduction of greenhouse gases from biomass pyrolysis products may depend on factors such as feedstock or co-products and, processes [70], about 41.02 kg of biochar returned to the field indicates zero net greenhouse gas emission as the whole carbon cycle maybe renewable [96]. Fast pyrolysis is a thermal decomposition process in the absence of oxygen or low oxygen content not resulting in incomplete combustion. In this process, up to 75 % of the biomass energy can be converted to a liquid bio-oil [97]. According to Gong *et al.*, (2014), fast pyrolysis of cellulose was quickly converted into a maximal yield of water-soluble intermediates phase with a heating rate of 100 °C/s, achieving ~21 % carbon at 450 °C and a solid residue of sugar and anhydrous sugar oligomers than other pyrolysis reactors [98]. This pyrolysis processing of biomass is highly effective at breaking down macromolecular structures into smaller organic compounds, the mixture of which has an appearance resembling liquid crude oil (bio-oil) [99]. Depending on the biomass feedstock used, fast pyrolysis bio-oil composition can drastically vary [99].

2.3.4.2 *Intermediate pyrolysis*

Intermediate pyrolysis is the pyrolysis between fast and slow pyrolysis, with the heating rate at around 50 °C/min. The typical operating conditions for intermediate-pyrolysis, such as heating rates, reaction temperatures, the water content of the feedstock, and short residence times, are mostly ≥ 30 °C/min, 400 - 600 °C, ≤ 10 wt.%, and 2 - 4 s respectively. Bio-oil, the liquid product of pyrolysis, has a complicated composition with primary acids, phenols, and aldehydes, leading to thermal instability and corrosiveness, and contains nitrogen and oxygen heteroatoms [71]. Since bio-oil is a mixture of many chemicals, it can be used as a source of basic green chemicals and refined as a hydrocarbon fuel. Reuse of by-products lowers the NO_x (Nitrogen oxides) and SO₂ emissions; increases the process energy recovery efficiency and reduces the overall cost. These additional advantages of pyrolysis led to its adoption in favour of gasification, combustion, or incineration [69].

However, it has high profitability considering the low feedstock costs, excellent product yields, higher value, and scale-up production opportunities [100]. The modular technologies reduce the feedstock logistics (transportation) challenges from sources to the plant site. Technical development of pyrolysis requires integration with a renewable energy policy to expand its renewable

energy production capacity. Nevertheless, the investment in technology should be broader for human needs, sustainability, and sensitivity analysis to control environmental pollution and economic risks [100].

As reported by Waluyo et al., (2018) a 10 g Palm Kernel shell (PKS) was pyrolyzed with a heating rate of 75 °C/min, under N₂, at a constant 200 mL/min. The product yields for bio-oil, water, char, and gaseous at 600 °C were 39, 8, 28, and 25 wt. %, respectively [100]. Another study in a vertical fixed bed at 500 – 600 °C and heating rate of 50 °C/min with a nitrogen flow rate of 5 L/min produced a bio-oil yield of 37.21 wt. % at 600 °C for BGS-Karo compared to the Ex-Sokoto shell with the bio-oil yield of 32.79 wt. % [48]. A study on intermediate pyrolysis of red algal biomass in a fixed-bed tubular reactor at different temperatures (400 - 600 °C) and heating rates of 15, 30, and 50 °C/min, respectively provided the highest bio-oil yield (45.02 wt. %) at 450 °C, with a heating rate of 50 °C/min. In this study, bio-oil had a high percentage of aliphatic functional groups and the presence of phenolic, ketone- and nitrogen-containing groups [101].

2.3.4.3 *Co-pyrolysis*

Co-pyrolysis experiment is to understand the synergetic interactions of biomass-plastics ratio and the product quality and quantity. Several co-pyrolysis of biomass-plastics behaviours are mostly defined based on their energy consumption, and reaction dynamics, which affect their product yields, and composition, but differ in feedstocks, either biomass or plastic. Factors like reaction time, heating rate, energy utilization and char contribute little or no impact on the compositions of bio-oil and gas yield. Co-pyrolysis interactive effects may favour the bio-oil or gas depending on the feed's temperature effect and chemical properties [102]. Plastics are H₂-rich, and co-pyrolysis of biomass and plastics will address the H₂ deficiency of bio-oil from biomass, and the process will produce a stable and higher heating value (biomass-plastic) bio-oil. The plastics are primarily oxygenated-free hydrocarbons and cost-effective feedstock for co-pyrolysis. According to Chiun et al., (2023), biomass and plastic waste are the two main anthropogenic wastes. Plastic waste accounting for 464 million tonnes is yearly generated globally, which only 20 % recycled, 25 % incinerated, and 55 % landfilled. Additionally, biomass from the agriculture and lignocellulosic biomass from forestry generates 140 billion tonnes and 181.5 billion tonnes respectively worldwide, with only 40 % agricultural residues and 4.5 % biomass reuse annually [310]. According to Ncube et al., (2015), the Global plastic waste record

was about 50 %, while food packaging waste alone was quantified over 33.3 % of the world packaging economy. Environmental pollution, greenhouse gas (GHG) emissions and high carbon footprints had a yearly growth of 12 % in the food packaging industry is of great concern. Europe alone generates 23 MT of plastic packaging waste yearly and is projected to 92 MT by 2050. European union directives to campaign on amendments of the recycling of 75 % packaging waste by 2030. Recycling is an approach that can significantly control the environmental threat from plastic and the food packaging industry. Well sustainable schemes of integrated waste management could mitigate waste generation that both threaten the society and environment [103]. Co-pyrolysis process effectively applies plastic waste in end-life plastics as a waste management strategy [104]. Fast microwave-assisted catalytic co-pyrolysis of microalgae and scum on HZSM-5 catalyst optimal ratio was 1:2 as the synergetic effect became significant only when the effective hydrogen index (EHI) of feedstock was larger than 0.7 [105]. Co-pyrolysis of 3 different microalgae spirulina platensis (sp), nannochloropsis sp. (ns), and enteromorpha prolifera (ep) with low-density polyethylene (LDPE) reported co-pyrolysis successfully inhibited the formation of n- and o- compounds which promoted the formation of esters and long-chain alcohols [106]. Co-pyrolysis of microalgae with low-density polyethylene (LDPE) 3:1 ratio for deoxygenation and denitrication

could influence algae components on pyrolytic products and the transformation of nitrogen and oxygen interactions [107], which effectively reduced the nitrogen and oxygen-rich compounds in the products [106].

2.3.4.4 Catalyst co-pyrolysis

Catalytic Co Pyrolysis (CCP) improves the problem of hydrogen deficiency in biomass pyrolysis and raises the yield and characteristics of pyrolysis products [108]. The use of ZSM-5, MgO, and ZSM-5 and MgO catalyst mixtures to upgrade the bio-oil produced from microalgae *Spirulina platensis* (SP), the mixture of the catalysts MgO-ZSM-5 catalyst produced an improved oil yield (37.8-48.6 wt. %) than single catalysts [106]. The upgraded bio-oil was rich in chemicals with a carbon number of C₇ - C₁₈ and minimum oxygenated compounds [106]. Catalyst promotes secondary cracking reactions to form lighter non-condensable compounds, yielding char, and gas and reducing the bio-oil. The biomass (*Jatropha* residues) to catalyst (Ni/HZSM-5) of a 1:2 ratio at 500 °C recorded an aromatic content of 20.9 % [102].

Catalytic co-pyrolysis (CCP) of biomass and plastics is more advantageous than thermal co-pyrolysis in terms of improving product quality. The catalyst can increase the rate of reactions such

as aromatization, and oligomerization facilitating the conversion of more O-containing compounds into hydrocarbons. More profoundly used catalysts are molecular sieves, metal oxides and alkali/alkaline earth metals. The porous support is used to load transition metals on as a catalyst and uses the metal catalytic activity, high surface area, shape, and porous support selection. Bimetallic support catalysts have recorded higher catalytic activity as revealed according to some studies [109].

The catalyst plays a vital role in rapid pyrolysis, increasing the yield and selectivity of aromatics and other products in bio-oil [108]. Its selection depends on the pyrolysis product composition and enhancements and to improve product yield of interest [106]. Application of catalysts in biomass pyrolysis research is intensely happening to produce deoxygenated pyrolysis oil in recent years, to improve the quality of low bio-oil and biochar yields, which are some of the prevalent challenges in the process [110]. Also, hydrogen-deficient leads to rapid char formation and, catalyst deactivation, and water formation during the catalytic deoxygenation process [104]. The common metal oxides used in catalytic pyrolysis are ZnO, Al₂O₃, CaO, MgO, and SrO. In a multi-level porosity and rich active Al₂O₃, metal oxides prepared via digestion precipitation and coupled calcination method used along

with ZSM-5 as a dual-stage of catalysts for pyrolysis reveal the addition of Al_2O_3 promoted the selectivity of toluene (18.3 %) [102].

Zeolite is generally applied in pyrolysis as a solid acid catalyst because it efficiently removes oxygen from biomass, resulting in a final liquid product with low O/C and high H/C ratios. The Brønsted and Lewis acid sites of zeolite convert oxygenated compounds to aromatic hydrocarbons via cracking [111]. Zeolites are ideal catalysts for producing hydrocarbons and aromatics due to their framework and high-acid sites, which make zeolites highly susceptible to coking and deactivation in biomass pyrolysis. The introduction of mesopores into the structure of ZSM-5 by alkali treatment or metal loading can increase the yield of aromatics due to enhanced mass transfer of reactants [112].

Catalyst support is a critical factor of consideration for catalytic performance in pyrolysis. Commonly used molecular sieves and supports are ZSM-5 due to their high catalytic activity. Recent studies elucidating metal loaded on ZSM-5 could promote the formation of monomer aromatic compounds and hydrocarbons [109], more biochar and coke [108], other products and the rapid deactivation of the zeolite catalyst [113]. Upgrading bio-oil requires ex-situ equipment to re-heat and hydrogen purge, but fast catalytic pyrolysis can directly convert pyrolysis vapour with the catalyst.

However, few papers focus on the formation of 'wax', a group of long-chain hydrocarbons that can be produced during the pyrolysis of aliphatic polymers. These by-products attach to the inner wall of the condensers and reduce their efficiency. Additionally, the co-pyrolysis optimum condition, biomass-to-catalyst ratio, and pyrolysis temperature for higher yield of aromatic hydrocarbons and reduced wax formation are not well understood yet [111].

The acidity of catalysts and the hydrogen-to-carbon efficiency (H/C_{eff}) biomass ratio are essential factors affecting the yield and selectivity of catalytic pyrolysis products. Quite several cooperative fracture and free radical reactions occur due to highly complex pyrolysis products. The connecting bonds between the three structural units of biomass (prominently lignin) chemical bonds are either homogeneous or heterolysis reactions that produce unstable intermediates and pass through various competitive reactions to form more stable products, otherwise forming oligomers and then coke. The addition of substances with different and high hydrogen content effectively improves the H/C_{eff} ratio of feedstocks, yield and quality of organic chemicals and reduces coke formation [102]. The hydrogen-to-carbon efficiency H/C_{eff} , the ratio describes an economical conversion of feed into hydrocarbons by applying a zeolite catalyst depending on the amount of oxygen, carbon, and hydrogen present in the feed determined by Eqn. 2.1 [113].

$$\frac{H}{C_{eff}} = \frac{H-20}{C}$$

Eqn. 2.1

where,

H= Hydrogen

C= Carbon

H/C_{eff} = Hydrogen-Carbon efficiency

The feedstocks with < 1 H/C_{eff} ratios are difficult to upgrade to produce premium products over a ZSM-5 catalyst due to the quick ageing and deactivation of the catalyst. The H/C_{eff} ratio of petroleum-derived and biomass feedstocks is between 1 - 2. and 0 - 0.3, respectively [113].

2.3.5 Gasification

Gasification is a thermochemical process that converts carbonaceous resources into syngas (H₂ and CO₂). It is the most adaptable biomass conversion technology into valuable biofuel in energy, which has a cleaner and more sustainable energy future [2]. Waluyo is among the most promising technologies for exploring energy from agricultural products, by-products, and residues [114]. This method is the most adopted method of converting biomass into gaseous-based energy, with a conversion efficiency of more than 50 % 91. In addition, the cleaner biofuel (liquid fuel) would be harnessed through the gasification followed by Fischer Tropsch

synthesis via Selexsol or Rectisol operations. Gasification is the partial oxidation of biomass, converted to a mixture of solid, liquid, and gaseous products, depending on the quality and distribution of feedstock, oxidizing agent, reactor type, and reaction conditions [2]. The processes are robust and flexible and accept a wide range of feedstocks [115].

Figure 2.1 is an improved new concept of the gasification process, an embedded process of pyrolysis, combustion, supercritical water gasification, multi-staged gasification, and a gas cleaning technologies (UNIQUE gasifier) unit process [28]. The gasification relies on the density factor, which divides gasification methods into dense phase and lean phase reactors.

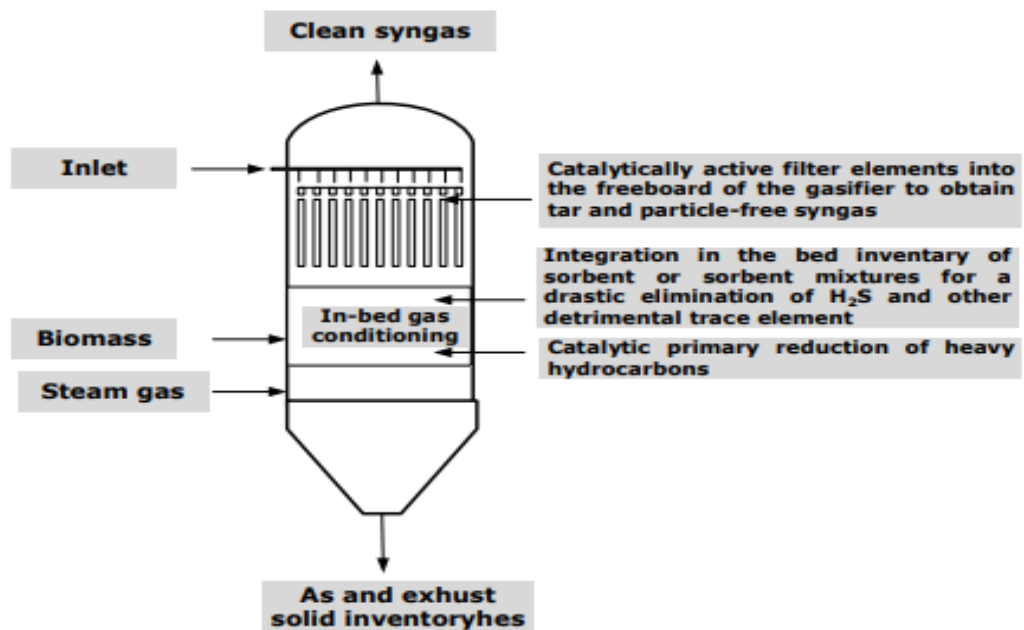


Figure 2.1: The UNIQUE integration of gasification, hot gas cleaning and conditioning in one reactor vessel [116]

The application of gasification as a thermochemical process in conventional syngas production is a well-established practice. The gasifying agent (air) is cost-effective in syngas production, but the syngas produced is severely diluted with N₂ and CO₂ lowering the heating value, while air-enriching oxygen up to 40 % (vol. %) can improve the heating value above 8 MJ/m³ [117]. Steam as a gasification agent increases the heating value above 10 MJ/m³ for a small to medium thermal power output below 20 MW_{th} of a fixed bed gasifier. It is more economical, as the thermal output steam production is reused in gasifiers, bubbling and circulating fluidized bed gasifiers can operate at much higher power scales, but they are more complex, with much higher operating and maintenance costs than fixed bed gasifiers [117].

2.3.5.1 *The Fischer Tropsch Synthesis (FTS)*

The FT process is a well-developed technology on a large scale, with coal and natural gas as feedstock, associated with high capital, operation, and maintenance costs [118]. Biofuel production via biomass gasification and subsequent conversion by FTS is of great interest due to the high quality of fuels produced with no sulphur content and zero carbon dioxide [119]. Additionally, Fischer Tropsch (FT) off-gas is converted through or in a gas turbine for power production [120]. The increased importance of

transportation fuels from renewables is due to environmental impacts, and growing fossil fuel prices necessitate the FT production of liquids, methanol, mixed alcohols, substitute natural gas (SNG), and hydrogen from biomass of high importance [121]. FTS would be a better technology for processing biofuel into liquid as a transportation fuel.

2.3.6 Design-Expert®

Design-Expert® software has different types of designs suitable for various choice of intended experimental goals and objectives. The Standards Designs constitute Factorials (Regular Two-Level Factorial, Minimum-Run Revolution V Characterization, Minimum-Run Resolution IV Screening, Multilevel Categorical, and Optimal (Custom) Design). While others are the Response Surface (Central Composite, Box-Behnken, Optimal Custom and Definitive Screen Design) and Mixture which also contain Custom Designs

The Regular Two-Level Factorial Design, Central Composite Design (CCD), and Box Behnken Design (BBD) are commonly used for design of Experiments to investigate catalyst composition, biomass percentage, and reaction temperature etc depending on the factors to be studied as input variables. According Oyebanji et al., 2023) optimization tools are now playing great roles in thermochemical

operations or processes [307]. According to Khairuddin et al., (2011) a two-level fractional design was carried out, for the thermogravimetry and the optimisation of bio-oil yield from fixed-bed pyrolysis of rice husk using response surface methodology (RSM) of the Design-Expert® Version 7.5.1 (Stat Ease, USA), which the confirmed runs gave 48.30 % and 47.80 % of bio-oil yield compared to 48.10 % of predicted value [308]. According to Witchakorn Charusiri., (2015) the relationship between the independent variables and response variable were unknown but was estimated by using regression analysis program (Design-Expert® Software). As the ANOVA analysis of the experimental data best fit into a quadratic equation, which performed at 95 % level of confidence for the designed experiment. The model terms are significant as the P-Values less than 0.05 indicated [309]. Design-Expert® among the optimisation tools is gaining traction in biomass thermal, pyrolysis decomposition and nanotechnology for the production of bio-oil which contain several functional groups of hydrocarbon compounds with temperature components dependent, but independent of the catalysts used. The effect of process parameters can utilize RSM in nanomaterials in pyrolysis experimental Design in Design-Expert®. Box-Behnken designs are also introduced and developed as a green, cheap, and stable eco-friendly catalyst from agro residue to upgrade bio-oil effectively [307]. The significance of the application of the Design Expert is to

explore all the possibilities in identifying the optimum or best option in applying the research with minimum cost and optimum out in terms of clean energy production.

2.4 Reactor for biomass pyrolysis

Batch, semi-batch, or continuous biomass processing was adopted for biofuel production. Several studies revealed the challenges of batch processes, such as high residence time, product variance, high labour cost, and commercial scale-up complexity [31]. Researchers have shifted their studies toward a semi-batch and continuous pyrolysis technology for commercialization [122]. Continuous Fluidized Bed Reactor (CFBR), Bubbling Fluidized Bed Reactor (BFBR), Conical Spouted Bed Reactor (CSBR), Auger Reactor (AUR), Rotating Cone Pyrolysis Reactors (RCPR) and Ablative Fast Pyrolysis Reactor (AFPR) are the most common thermal pyrolysis reactor technologies among the top six (6) to be discussed [123].

2.4.1 Bubbling fluidized bed (BFB) reactor

BFBR has been used extensively in the chemical industry for its scalability, excellent mass and heat transfer properties, homogeneity among solids and fluids products, uniform catalyst

distribution, and ability to operate continuously. Therefore, many studies investigated biomass pyrolysis in BFB reactors through experimentation, simulation, and commercial scale-up [124]. These reactors are employed widely in pyrolysis for their technological maturity and ability to produce a high yield of bio-oil. They use preheated gas as a heat carrier to the bed creating homogeneity, short residence times, and high heating rates from convection [125]. Dynamotive Energy System Corporation has constructed four installations based on BFBR technology, and the most prominent positioned industry is Guleph, Richmond, British Columbia, Canada, with an operating capacity of 200 t/d [126].

BFB reactors as captured in Figure 2.2 (a) can operate continuously [124], but their shortcomings are sensitivity to hydrodynamic conditions, inability to use bed agglomerated feedstocks, high densities of bed material with high fluidization velocities, and fluidization sweeps gas leads to increased energy input and cost [125]. The uncondensed gas output discharge from the process plant was not mentioned or reported in the work while bio-oil yields are produced under atmospheric (ATM) pressure according to Burton and Wu (2016) and several authors [127].

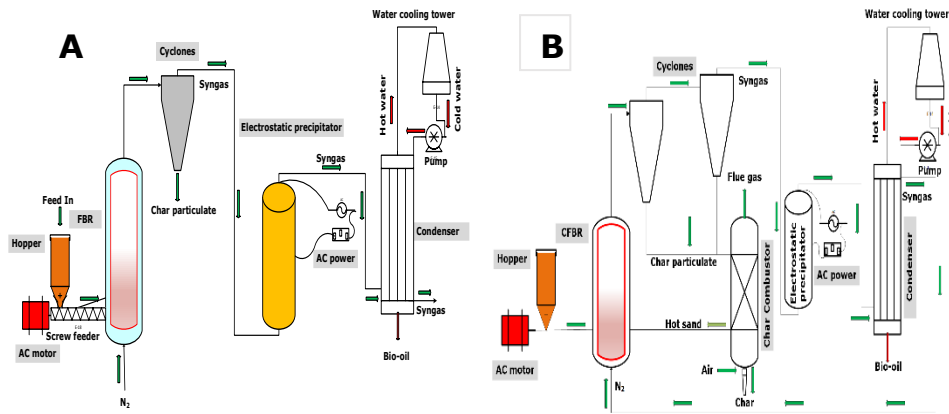


Figure 2.2: (a) The BFB reactor and (b) CFB pyrolyzer, adopted and redrawn from [122]

2.4.2 Circulating fluidized bed reactor (CFBR)

The components of CFBR in Figure 2.2 (b) comprise but are not limited to a riser, a distributor plate, a riser exit, a cyclone, a downcomer, a solid feeder, and a butterfly valve [128]. In a CFBR reactor system, particles circulate in the bed [129], have a high heat transfer rate (uniform effective solids circulation and temperature distribution) [128], effective gas-solids contacting, reduced gas-solid back mixing, allowing high gas flowrate, negligible intra-particle diffusion resistances, efficient solid regeneration capability [130], mild reaction conditions and high catalytic efficiency. Nevertheless, its pressure drops limitations generally affect the design and operation of CFBR units for solid fuel conversions. A dense bubbling bed formed at the bottom of the riser, transforming the CFBR bed to a conventional BFBR has been undermined [131], and the sand and biomass transport dynamics

are aggressively increasing wearing problems. The gas output is recirculated mainly into the process of CFBR, while the bio-oil processes are within 45.2 - 78.07 wt. % according to Treedet & Suntivarakorn (2017) and other literature works [127].

2.4.3 Conical spouted bed reactor (CSBR).

Figure 2.3 (a) CSBR is a fast pyrolysis technology for residual biomass, even with a heterogeneous composition, as an alternative to fluidized beds. It has a short residence time suitable for reducing the catalytic activity of the ashes for high bio-oil yields, even for a high ash content material [132]. CSBR was judged best for valorisation by fast pyrolysis of multiple wastes, such as sewage sludge, lignocellulosic biomass (pinewood sawdust, forest shrub wastes and rice husk) and other materials, such as tyres or plastics. This reactor has also been applied successfully in other thermochemical processes, such as drying, coating, gasification or reforming in CSBR [133].

The merits of CSB reactors are co-pyrolysis, with varying particle densities [124], high ash biomass content and producing high yield bio-oil [132]. The conical spouted-bed design has excellent mixing, operates in continuous mode, has low residence time and continuous removal of char [133]. However, excess gas injected

into the CSBR invariably hikes the processing cost, a scale-up challenge because the ratio of the reactor inlet is 20 - 30 times the average particle diameter [122], and the continuous mode threshold might affect its scalability [133]. The syngas output generally is not accounted for, while the bio-oil yield ranges between 45.4 - 70 wt. % according to several works and pieces of literature including Qureshi *et al.*,(2018) [97].

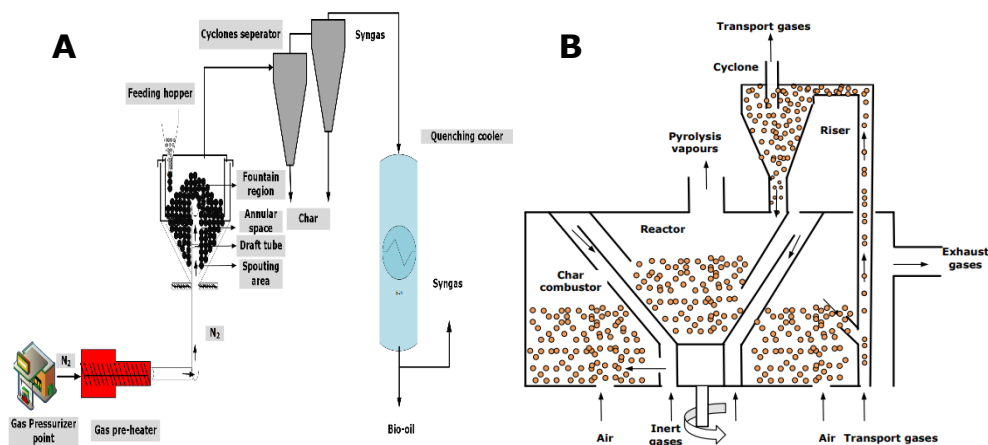


Figure 2.3:(a) Conical spouted bed and (b) Rotary cone reactor (adopted and redrawn from [122] and [137], respectively)

2.4.4 Rotating cone-pyrolysis reactor (RCPR)

Figure 2.3 (b) is an RCP reactor and was realized as a novel reactor type for flash pyrolysis of biomass with negligible char formation, rapid heating and short solids residence time [138]. The pioneering RCPR development was made at Twente University, Netherlands, in the early 90s, with a 200 kg/h biomass capacity. The biomass feed and heat carrier sand are injected into the system, where the solids

are forced by centrifugal force through the cone's walls. Solids move to the centre of the cone, and pyrolysis vapours escape through the outlet of the condenser, while the char and sand in the combustor bottom of the cone, get re-heated are introduced at the cone base with the fresh biomass feed [139].

The merits of the RCPR are around 60 % bio-oil yield, consistently demonstrated design, and ease in product recovery. It is compact in design and does not require a carrier gas for pyrolysis (but for sand transport), which makes bio-oil product recovery easier. The sand and biomass transport dynamics are not as aggressive as in the CFBR process, reducing wearing problems [140]. At the same time, the demerits are its complex integrated process in scale-up, pneumatic transport of sand back to the reactor, lower temperature, and longer residence time might set in after scale-up. The gas output generated is largely not accounted for, while the bio-oil yield is between 14.27 and 51.8 wt. % as reported in several works and according to Treedet and Suntivarakorn [103].

2.4.5 Auger reactor (AUR)

Auger reactor technology is adapted from the Lurgi process for coal gasification [144]. AUR in Figure 2.4 (a) had a main component biomass feeder as an off-the-shelf volumetric screw feeder.

Biomass is conveyed using a screw feeder into the reactor. The auger is calibrated where the feed flow rates are linearly proportional to screw speed [145]. The auger reactor design is suitable for fast pyrolysis processing; the heat carrier provides enough reaction heat and heat transfer. It holds promise for being a robust system capable of continuous processing with minimal carrier gas compared to other designs. Establishing an industrial scale is viable, with minimal operating costs due to minimal gas handling and compression equipment. The auger design may be more compact than other reactor types [144]. The AUR residual carbon increases as high as 20 wt. % of the total char yield and heat carrier attrition of about 7 % mass basis after operation for about 2h. Trade-offs may exist during heat carrier materials selection for biomass pyrolysis in an auger reactor [125]. According to Jahirul et al. (2012) several pyrolysis process plants at different 25 locations across the globe, with production capacities of 1700, 2000, 500, and 400 kg/h for chemicals, char, gas and bio-oil respectively [139]. Similarly, researchers at Air Liquide and Karlsruhe Institute of Technology (KIT), Germany, established a biofuel plant feed capacity of 500 kg/h with an installed twin-screw mixing pyrolysis auger reactor, their organic and aqueous condensate products yield up to 55 % [97].

The merits of auger (AU) reactors are operating at a lower heat transfer rate, the ability to convey robust materials, reduced solid particle entrainment in the effluent stream and minimal requirements of sweep gas [125], and it is operational in forests on-site for bio-oil production [146]. At the same time the demerit is solids residence time ≤ 120 s required for total conversion and mechanical wear [125]. The uncondensed gas produced from the auger processing systems was mostly not recorded, while the bio-oil, since it is the primary focus of the research produces between 21.7 - 56.3 wt. % as reported by Mathew and Muruganandam, (2017) and as reported by several studies [127].

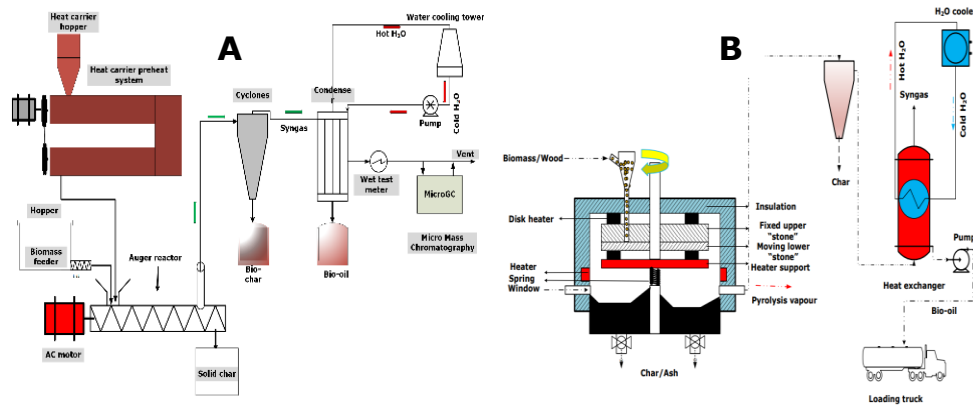


Figure 2.4: (a) Auger and (b) Ablative reactor (adopted and redrawn from [122], and [139] respectively).

2.4.6 Ablative flash-pyrolysis reactor (AFPR)

Ablative fast pyrolysis (AFPR) technology in Figure 2.4 (b) provides an opportunity to use large pieces of wood, which saves grinding

costs [147]. Possible mobility of AFPR unit for a straw upgrade, thereby minimizing transport expenses (almost 80 % of the straw cost are logistic) and also characterized by low construction and operational costs [3].

The difference between ablative reactors uses particle sizes up to 20 mm in contrast to the 2 mm particle in fluidized bed reactors particle size, yield, and composition, yield, and composition. Except for slight differences in yield, HHV, and higher water content resulting from longer vapour residence times in the ablative reactor, which enhances secondary reactions [147]. The merits of the AFPR are, that operating as a vortex reactor with high bio-oil yields [148], characterized by low plant and operational costs [147], uses large biomass particles and saves processing costs 3 and bio-oil yield quantity are similar to those produced from the BFB reactor. However, the AFPR have a complex mechanical design which complicates the scale-up. It requires a "gas ejector" to provide extremely high gas velocities and a low rate of heat to the reactor rather than the rate of heat absorption by the pyrolyzing biomass. The uncondensed gas output values are unrecorded, but the bio-oil production is within 50 - 70 wt. % as confirmed according to Singbua et al. (2017) [145].

2.4.7 Summary of technological challenges in bio-fuel production

The challenge of biomass is the sustainability of the energy crop biomass bulkiness, residues supply, transportation network to a centralized biomass storage facility, biomass densification, and high moisture content. Also, the development of deoxygenated catalysts for aqueous phase bio-oil conversion to organic phase or green chemicals to improve the quality, purity and bio-oil stability.

The challenges of thermo-chemical biomass conversion technologies are complexities in the scale-up of the technologies, The process challenges are classified in Table 2.3 below.

Table 2.3: Thermochemical processes and their challenges

S/no	Thermochemical process	Challenges
1.	BFBR	<ul style="list-style-type: none">• Sensitivity to hydrodynamic conditions.• Inability to use bed agglomerated feedstocks.• High densities of bed material with high fluidization velocities and sweeps gas led to increased energy input and cost.
2.	CFBR	<ul style="list-style-type: none">• Pressure drops limitations affect the design and operation of CFBR units for solid fuel conversions.• A dense bubbling bed at the bottom of the riser transforms the CFBR bed into a conventional BFBR.• The sand and biomass transport dynamics are aggressively increasing wearing problems.

3. CSBR	<ul style="list-style-type: none"> • Excess gas injected into the CSBR invariably hikes the processing cost. • Scale-up challenge because the ratio of the reactor inlet is 20 - 30 times the average particle diameter.
4. CSR	<ul style="list-style-type: none"> • A complex integrated process might affect scale-up. • Pneumatic transport of sand back to the reactor. • lower temperature, and longer residence time
5. AUR	<ul style="list-style-type: none"> • Solids residence time ≤ 120 s, needed for total conversion and, • Mechanical wear.
6. AFPR	<ul style="list-style-type: none"> • Had a complex mechanical design which complicates the scale-up. • It requires a "gas ejector" to provide extremely high gas velocities and • A low heat rate reactor rather than the rate of heat absorption by the pyrolyzing biomass.

The most promising technology is BFBR, with an average yield of 40 – 70 wt. % prospect presently. Continuous BFBR had the best operating parameters for an optimum product are feedstock particle size < 2 mm [139], adjustable electric heater at 10 °C/min and achieving an average yield of 51 - 60 wt. %, 23 wt. % and 12 wt. % for bio-oil, char, and gas respectively. A recommendation of techno-economic analysis of the processes to determine the most cost-effective and, return on investment (ROI) on specified operating capacity [127]. Higher efficiency of the technology and effective operation cost will determine its profitability and sustainability or its life cycle.

2.5 Hydrothermal process

Hydrothermal processes (HTP) are a promising technology platform for processing wet and sludgy biogenic residues; they use water as their principal process medium to convert biomass into materials and fuels at high pressures and temperatures [149]. The HTP of biomass includes hydrothermal liquefaction (HTL), hydrothermal carbonization (HTC), and hydrothermal gasification (HTG) [150], which produce hydrochar, liquid, and gas, in varying quantities depending on their operating conditions [151].

2.5.1 Hydrothermal carbonization (HTC)

According to Wang et al., (2018), Bergius discovered hydrothermal carbonization (HTC) in 1913 to imitate the natural coal formation process that converts cellulose to coal-like properties. The HTC is a thermochemical conversion process that transforms wet Biomass into energy and chemicals without pre-drying [151]. HTC process occurs in hot water (subcritical) and produces gases, liquids, and solids fractions. It is a wet process for a high biomass-H₂O of about 70 - 90 % water content by weight. The main product of HTC (hydrochar) is applied significantly in the agriculture, medical, environment, and energy sectors. However, liquid and gaseous

(mainly CO₂) by-products are produced. The method is practical, eco-friendly, producing high-energy density solid fuels [152], and proven adaptable to different types of biomasses to produce several products, with lower temperatures and mild reactional conditions compared to several thermal conversion processes [73].

Raw biomass is converted into a lignite-like solid product, significantly affected by the medium relatively low temperatures (180 – 250 °C) and under autogenous pressure around (2 - 10MPa) for a specified period [152], which lowers the oxygen and hydrogen content of the feedstock through dehydration and decarboxylation [151]. That process increased the energy density of the hydrochar ranging from 40 – 60 % [152].

Hydrothermal parameters such as residence time and temperature determine the reaction severity and degree of coalification and affect the structural properties of feedstocks due to their complex composition to produce hydrochar. Hydrochar is separated from water quickly due to its high hydrophobicity and homogeneous properties [152]. Hydrochar demonstrates superior performance relative to raw biomass in terms of reduced mass which eases its storage and transportation, and increased energy density, better dewaterability, carbon-rich material, and improved combustion performance with high-value as solid fuel after hydrothermal

treatment that reduces its hydrogen and oxygen content [151]. It also improves the hydrochar for higher energy efficiency, and activated carbon as catalyst support, adsorbent and medical applications [153]. The FTIR analysis determines the surface functional groups of both the biomass and hydrochar product [151].

Hydrochar applications are in various fields of human endeavours, such as solid fuel that is comparable to brown coal, soil amendment, activated carbon for water purification systems and CO₂ sorption, low-cost adsorbent, or permeable reactive barrier for Uranium (VI), carbon material with nanostructure, carbon catalyst to produce fine chemicals, and carbon material for fuel cells efficiency enhancer [152]. The extraordinary properties of hydrochar and its potential applications could be harnessed optimally by exploring the critical process parameters (reaction temperature, feedstock, reaction time, catalyst, and pressure) governing HTC and the mechanisms of the hydrochar formation. Therefore, treatments of such materials are highly needed to control pollution, reduce processing time, and increase product quality [152].

The critical hydrothermal parameters of HTC are temperature, residence time, heating rate, reactant concentration, aqueous quality [151], pressure [12], and catalyst [152]. However, the residence time and temperature govern the reaction severity and

degree of coalification of the raw biomass [125]. Several findings have described the HTC process of biomass materials as stochastically phenomenal but illustrate how to deal with experimental data appropriately [154]. A well-optimized process parameter provides achievements of a well-organized structure, ideal pore size, high BET surface area, high yield, and purity [152].

2.5.2 Factors of hydrothermal carbonization

HTC is a process that treats biomass at an elevated temperature (180 – 260 °C) and pressure in an aqueous medium 4,6–9, producing structured carbon known as fuel-grade hydrochar [4]. The HTC is a thermochemical conversion process of wet biomass waste conversion with low temperatures within 180 – 260 °C conditions and pressure (2 – 6 MPa) during the carbonization [22]. Temperature is a distinctive and critical factor determining the water properties of ionic reactions in the subcritical region to convert high water content biomass to upgrade solid fuels replacing coal. Bond cessation commences in the biomass macromolecular organics. According to Nizamuddin *et al.* (2015), as the temperature goes beyond the activation energy, the hydrochar production temperature was within 180 - 250 °C [152] in sub-critical (180 – 260) °C for 2 h [76], while derived from municipal sewage sludge at 190 – 260 °C [155]. Higher temperatures facilitate the

secondary decomposition leading to a reduction of solid residue, hydrochar densification of energy, and conversion of total organic carbon (TOC) of sugars and organic acids to liquid products [151]. The HTC temperature and reaction time of product composition yield were around 215 - 295 °C and 5 - 60 min, respectively, and hydrochar yield reduced from 69.1 - 50.1 % [156]; the higher the reaction temperature, the lower the mass yield [157].

According to Wang et al., (2018), HTC temperature might go beyond 280 °C, as the two stages process is technically challenging to distinguish. Dissociation of H₂O into H₃O⁺ and OH⁻ is achievable with an increasing temperature below 374 °C, reducing the dielectric constant, weakening water-hydrogen bonds, and producing a high ionization constant. This ionization brings the best medium for the acid-catalysed reaction of organic compounds without adding acid, which sufficiently increases the H⁺ concentration compared to liquid water [151]. Temperatures approaching a certain reaction intensity have a decisive influence on the hydrolysis reaction of biomass, and the higher temperatures can lead to dehydration, decarboxylation, and condensation simultaneously [152]. With temperatures in the HTC process around 230 - 250 °C, the O/C and H/C atomic ratios decrease, and the degree of hydrochar condensation is enhanced. Empty palm fruit bunches at reaction temperatures of 150, 250, and 350 °C recorded a steady reduction of the hydrochar H/O and

O/C atomic ratios [151]. Cellulose and water mixture were heated in a closed vessel at 250 – 310 °C, and the result recorded a lower O/C ratio of hydrochar qualifying HTC as an excellent process to improve fuel properties [152].

2.5.2.1 Compound and residence time

The compound and residence time production of hydrochar of higher condensed carbon was through the removal of H and O in a coalification-like process due to increased hydrothermal severity (i.e., residence time or temperature) [151]. Researchers have developed an amino acids model employed with hydrothermal conditions; the glycine and alanine as model compounds produced were evident at a relatively short residence time. The significant reactions of amino acids were decarboxylation and deamination [151]. The ease and ability to produce hydrochar during HTC are a function of the oxygenated functional group it contains. The production of hydrochar from waste eucalyptus bark gradually decreases the C=O in ketone, amide, and carboxylic groups, as the decarboxylation increases with residence time in the HTC process [151]. Perhaps energy recovery from the HTC process with high moisture content biomass would be unsustainable. According to Zhao et al., (2014) the effect of the HTC temperature and holding time on the biofuel recovering ratio, calorific value and energy

recovery rate was investigated and revealed that HT biofuel production was more cost-effective than other processes [158], the suggested operating conditions for the hydrochar production were 60 min residence time at 300 °C. The energy recovery pattern followed this order corncob > cornstalk > sawdust > rape straw and an SS/corncob blend, while the energy recovery rate was at about 71.60 % [151]. Generally, obtaining more solid products at higher reaction times, and reaction duration defines the product composition as well as overall biomass conversion Under supercritical conditions, the hydrolysis rate and degradation of biomass rate are relatively fast [152].

2.5.2.2 Heating rate and reactant concentration

Generally, a higher heating rate does not favour hydrochar formation. HTC is a similitude to pyrolysis but of better advantage. Pyrolysis produces char, while HTC produces hydrochar of higher heating value (HHV) with a lower heavy metals content than biochar produced via pyrolysis [76]. The heating rate is another factor impacting the HTC process. In the HTC process, the O/C and H/C ratios decrease as the temperature and residence time increase with low heating rates. As a low heating rate favours the degree of carbonization in hydrochar, high heating rates enhance the relatively low HHV of hydrochar. The controlled distribution of the

hydrochar and liquid products is achievable as appropriate heating rate selections are made during the HTC process [151].

HTC in the presence of different initial concentrations of acidic and basic conditions using HCl, H₂SO₄, NaOH, and Ca (OH)₂ affects cellulose degradation. The additives quicken the solid cellulose's dissolution and facilitate glucose conversion as concentrations increase. Carbon dioxide (CO₂) production by the acid additive enhanced decarboxylation of the decomposition of organic acids. Acids enhanced dehydration, resulting in significantly decreased oxygen content in the hydrochar [159],[160]. Additionally, acid virtually has the same outcome on solid recovery; a specific environment remarkably promotes the decomposition pathway of 5-hydroxymethyl-furfural-1-aldehyde (HMF), converted into levulinic or formic acid [151].

The addition of a base showed no effect on the dominant dehydration mechanism. HMF had its minimum content at a pH of 12 and 200 °C but was undetected at 260 °C during fast degradation. HTC process of wheat straw at a feedwater pH (2 – 12) prepared by acetic acid and potassium hydroxide. Low pH conditions lead to fewer sugars, more furfural derivatives, higher surface area and pore volume, and more organic acids. The acid and essential additives significantly impact the processing water, and the

hydrochar composition, coupled with process mechanisms, can be determined by the hydrothermal environment. In particular, adding acid accelerated hydrolysis and decomposition by enhancing the intermediate products, including organic acid production and decarboxylation for CO₂ production. The hydrochar produced from pH 2 feed water had 2.7 times more surface area than that produced at a pH of 12 [151], and with the addition of acid and alkali, the mass yield of hydrochar slightly declined to various degrees compared with neutral conditions [157].

Lower pH feedwater was critical to the pore structure for accelerating the hydrolysis of carbohydrates and enhancing microsphere formation in the early stage of the reaction. A higher adsorptive capacity was observed generally for hydrochar processed with HCl than hydrochar processed with deionized water and NaOH due to differences in ionic strength [151].

2.5.3 Hydrothermal carbonization (HTC) case studies

HTC investigation of phoenix tree leaves studied under different reaction severities, the higher heating value of hydrochar increased from 17.70 – 22.42 MJ/kg but decreased mass yield. The use of microwave-assisted heating reduces more than 50 % time. The highest energy retention rate of hydrochar was at 220 °C, 60 min,

and pH of 7, and about 27.7 % higher heating value than the feedstock. Morphological change analysis showed the surface morphology of hydrochar was partially destroyed, suggesting OH⁻ can effectively promote the destruction of wood structure and make cellulose components in contact with the reaction medium degrade faster [157].

Hydrochar, a substitute for carbonaceous environmental sorbents, is produced by the HTC process of sawdust with a low surface area limitation. A one-pot biomass/metal salt co-hydrothermal synthesis method might improve its sorption properties while retaining its efficient production characteristic. Thus, combining bamboo sawdust and zinc chloride (ZnCl₂) in a hydrothermal reactor at 200 °C for 7 h to modify hydrochar. The carbon-modified hydrochar increased its carbon content from 54 – 64 % compared to non-modified hydrochar, and the surface area increased after acid washing at 30 versus 1.7 m²/g. Nonetheless, the Methylene blue adsorption capacity of the modified hydrochar increased by nearly 90 % and 257 % after rinsing with acid. The modified hydrochar has the potential to be suitable for environmental remediation and water treatment [161].

HTC study of pure cellulose and birchwood samples at temperatures of 160 and 280 °C, 0.5 h residence time, and 1:5 biomass-to-water

ratio to investigate the reactivity of cellulose in lignocellulosic biomass. The dehydration and aromatization reactions occurred at temperatures ≥ 230 °C for pure cellulose samples, while only aromatization of birchwood hydrochar was noticeable at ≥ 260 °C. The acid hydrolysis, TGA, and FTIR suggested that a higher thermal resistance of naturally occurring cellulose in birchwood compared to the pure cellulose sample may result from a 'protecting shield' offered by interlinked lignin in the plant matrix [162].

Wang et al., (2020) determined the hydrochar characteristics of maize straw produced through the HTC process as a solid fuel for blast furnace injection. The HTC studied temperature and time over 220 – 340 °C and 15 – 120 minutes at an increased temperature and time decreased the H/C and O/C values of hydrochar and increased its higher heating value (HHV). The trend is like that of bituminous coal because of dehydration and decarboxylation. The physicochemical properties and structure analyses revealed an increase in the specific surface area, and the C-C, C-O, and aromatic functional groups gradually increased. This process may convert maize straw biomass into a high-quality solid fuel [163].

2.5.4 Summary of hydrothermal carbonization

Table 2.4 is a summary of the HTC process operating parameters of biomass. Depending on the biomass material used, hydrochar has a wide range of applications, from carbon material (adsorbent) for water treatment, soil amendment, permeable catalyst barrier for producing fine chemicals, wastewater treatment, and fuel cell efficiency enhancer. The products are affected by temperature, residence time, concentration, pH, and heating value. However, the temperature ranges between 180 - 340 °C, and the residence time of ≤ 2 hours; the heating rate ranges from 5 - 100 °C/min, and the pH should be below neutral to produce high surface area, the catalyst used as ZnCl_2 , and Ni supported on Al_2O_3 catalysts to fastening the rate of reaction.

Table 2.4: Summary of the operating conditions for HTC of Biomass

S/ No	Reactor	Biomass & ratio	Catalyst /pH	Temp. (°C)	Residence Time (min)	Heating rate (°C/min)	Pressure (MPa)/ HHV (MJ kg ⁻¹)	Product yield (%)	Ref.
1	Microwave- assisted heating	phoenix tree leaves	7	220	60	-	17.70–22.42	61.81	[157]
2	50-mL hydrothermal reactor	Sawdust	ZnCl ₂	200	7 h	-	-	--	[161]
3	50 mL batch reactor	cellulose (CE) and birchwood (BW) (1:5)	-	280	30	-	Autogenous pressure (1– 7), (27.46 & 27.89)	-	[162]
4	High-pressure reactor (Parr 4520)	wetland plants (1: 10)	5.0–7.7	200 260	- 120	3	18.0–27.1	46.0– 46.5 22.8– 29.2.	[76]
5	250 ml, high- pressure batch reactor	maize straw (1:3)	-	220– 340	15–120	-	Autogenic pressure (18.22 29.90)	35.8– 35.3, and 58.5– 57.7.	[163]

2.5.5 Hydrothermal gasification (HTG)

Hydrothermal gasification (HTG) process utilizes sub- or supercritical water (critical properties of water are ($T_c \geq 374$ °C, $P_c \geq 22.1$ MPa) [164] to convert low-quality high-moisture content (industrial wastewater and or biomass) into renewable hydrogen-rich gas [165]. HTG for hydrogen and synthetic natural gas production, which operates at moderately low temperatures, can potentially become a cheaper source of hydrogen compared to electrolysis and conventional gasification. Additionally, with the high potential of CO₂ capture, the technology has increased its effectiveness and overall efficiency, with almost zero net negative carbon [166], and capacity to use various feedstock [165]. Supercritical water gasification (SCWG), among other hydrothermal processes, is a promising technology. Supercritical water has identified physical and chemical properties, such as high diffusion rates, low viscosity, and low dielectric constant [164].

HTG of lignocellulose (microalgae) has several advantages over hydrothermal liquefaction (HTL); the produced fuel is nitrogen-free, from high-protein microalgae. The organic carbon in the water phase is also much lower than that for HTL, which could increase the carbon gasification efficiency [166].

2.5.6 Factors of hydrothermal gasification

Co-gasification processes are affected by several factors which largely include feed mixture proportion, air flow rate, type of gasifier, and temperature [167]. The feed mixture and airflow should be proportionate in the process during co-gasification, while the gasifier (updraft or downdraft) system and temperatures conform with the process-optimized parameters to yield the forecasted product. During hydrogen production in gasification, supercritical water had its main operating conditions as reaction temperature as high above 700 °C [168], feedstock generating unconverted carbon led to low gasification efficiency [168], catalyst type e.g. potassium hydroxide, KO [169], and loading [164].

2.5.6.1 *Biomass-H₂O ratio and Catalyst type*

Using sewage sludge produced during wastewater treatment has gained attention for Hydrogen production. It contains 80 - 98 wt. % water and various organic and inorganic matter. Supercritical water treatment of sewage sludge is a modern approach as a result of the high moisture content. The C-C or C-O bonds will change the reaction route as the catalyst tends to aid in the cleavage of the reactants. The splitting capability of water is also an influential factor in the reactivity of the mixture [165]

The higher conversion rates depend on the operation conditions, feedstock type, catalysts, or reactor design [167]. The alkali catalysts, including KOH, NaOH, K₂CO₃, and Na₂CO₃, are widely applied whenever the reactions are subcritical or supercritical water. The catalyst loading was from 0.1 - 0.5 wt. %, which increased molar fraction and hydrogen from 49.84 - 55.96 % and 9.8 - 15.49 mol/kg, respectively [164].

2.5.6.2 *Residence time, temperature, and pressure*

Reaction time on distillery wastewater gasification generates the highest volume of hydrogen at the extended reaction time [165]. The main critical factor, among others, in terms of thermodynamics and energy efficiency of a system is process temperature. However, HTG is a process that operates at relatively lower temperatures (350 – 500 °C), and water serves as both a reaction medium and a gasifying agent fitting for wet feedstock usage with no additional drying energy-related processes [167]. The high temperature was promising for the gasification efficiency and hydrogen yield [165]. The temperature has been the most important influencing factor in this process, even reactions at either subcritical or supercritical water states. The molar fraction and methane received a minimal yield at temperatures within 480 - 500 °C, swiftly increasing at a

temperature range of 500 – 540 °C [164]. The three main parts of hydrothermal biomass gasification processes proposed are (1) Aqueous phase reforming (APR) of oxygenated Biomass-derived components is gasified to hydrogen at around 215 – 265 °C; (2) near-critical gasification to methane at around 350 °C; (3) Supercritical water gasification (SCWG) to mainly hydrogen and carbon dioxide [167]. The fluidized bed reactor, designed for temperature and pressure up to 650 °C and 30 MPa, respectively, was operated at 540 °C and 25 MPa, achieving its optimum yield. A back pressure regulator with a deviation of ≤ 0.5 was used to control the pressure system [164].

2.5.7 Hydrothermal gasification (HTG) case studies

As the temperature increased above 200 °C, the cellulose product decreased due to improved fragmentation of large molecules by decomposition into components (liquids and incondensable low molecular gas). The gas products were CO, H₂, CH₄, and CO₂, with the largest percentage. As the temperature increased from 250 – 350 °C, the yield of CH₄ and H₂ increased from 1.92 - 4.89 % and approximately 10.6 %, respectively [151]. *Chlorella Vulgaris*, *spirulina platensis*, and *saccharina latissima* under supercritical water gasification conditions at 500 °C, 36 MPa in an Inconel batch

reactor for 30 min in the presence of NaOH and absence of Ni–Al₂O₃ yielded more than double the amount of H₂ in the presence of NaOH than in its absence, and tar yields were reduced by up to 71 %. This carbohydrate-rich macro-alga (Saccharina) gave the highest hydrogen gas yields of 15.1 mol/kg, while the algae tars contained aromatic compounds. During the algae's gasification, 97 % of TOC (Total Organic Carbon) removal in the process waters was achieved. Specific nutrient analyses in the process waters indicated that the process water from Saccharina could potentially be useful for microalgae cultivation [166].

As reported by Seif et al., (2016) the investigation of industrial waste streams (distillery, oil refinery, and petrochemical complex) of three transition metal oxide catalysts (MnO₂, CuO, and Co₃O₄) with various catalyst loadings (20, 40, and 60 wt. %) at various temperatures (300 – 375 °C) and reaction times (15, 30, 45 min). It revealed that distillery wastewater possessed great potential for hydrogen production compared to another wastewater. The catalyst's catalytic activity for hydrogen production was as follows: Co₃O₄ > CuO > MnO₂ and revealed 40 wt. % loading of Co₃O₄ as the best conditions at 375 °C and 45 min optimum reaction time to gain the maximum hydrogen from distillery wastewater. Finally, it concluded that catalyst effectiveness was much more pronounced

at lower temperatures, with longer reaction time, and inhibited char formation [165].

According to Okolie et al., (2019) the gasification study of H₂ production from soybean straw and flax straw in subcritical water at 300 °C and supercritical water at 400 and 500 °C of the non-catalytic process, with a biomass-to-water ratio of 1:5 and 1:10, the particle size of 0.13 and 0.8 mm, within the residence time of 30 – 60 min at a pressure range of 22 – 25 MPa. The result revealed a maximum H₂ yield and total gas yields of 6.62 and 14.91 mol/kg, respectively, at the temperature of 500 °C, feed concentration of 1:10 BTW, particle size of 0.13 mm, and 45 min residence time. However, the KOH catalyst elevates the H₂, CO₂, and CH₄ yields for soybean straw and flax straw. The findings suggested that supercritical water gasification could be an efficient green technology for H₂ production from waste biomass [169].

Gökkaya et al., (2020) conducted an HTG of isolated hemicellulose from white poplar and white poplar sawdust to evaluate the effects of temperatures ranging from 300 to 600 °C and catalyst. In comparison to poplar sawdust, white poplar hemicellulose produced more gaseous residue and left less gasified solid residue. At 600 °C, K₂CO₃ generated the highest H₂ and CH₄ yields; as the liquid and

solid yields decreased, the yield formation of aqueous products occurred in the following order: organic acids > aldehydes and ketones > furfurals > phenols [170].

According to Chen et al., (2013), sewage sludge (SS) gasification in supercritical water was conducted in a fluidized bed reactor, with manipulated variables such as temperature, feedstock concentration, alkali catalysts loading on gaseous products, and carbon distribution. The increased temperature and decreased feedstock were favourable for gasification, and catalyst application enhanced hydrogen formation. As the K_2CO_3 catalyst may enhance gasification efficiency, different catalysts and their catalytic activity for hydrogen production are in the following order: $KOH > K_2CO_3 > NaOH > Na_2CO_3$. The result reveals that the optimum molar fraction and hydrogen yields were 55.96 % and 15.49 mol/kg, respectively, with KOH at 540 °C. The carbon in feedstock primarily exists in gaseous and liquid products, while alkali catalysts promote a water-gas shift reaction rather than steam reforming [164].

2.5.8 Summary of hydrothermal gasification

Table 2.5 shows the summary of HTG parameters and yields. The operating parameters such as temperature, residence time,

autogenous pressure, concentration, and catalyst are fundamental in HTC and HTG. They play a significant role in the generation of gaseous products. Temperatures range from 300 – 540 °C; the residence time is above 30 min; the pressure is within the range of 22-36 MPa; the minimum concentration of biomass-to-water ratio is 1:5, while the pH and catalyst commonly used and most suitable for the reaction pathway are Co_3O_4 , CuO , MnO_2 , NaOH , $\text{Ni- Al}_2\text{CO}_3$, KOH , NaOH , K_2CO_3 and Na_2CO_3 .

Table 2.5: Summary of the operating conditions for HTG of Biomass

S/ No	Reactor		Biomass & ratio	Catalyst/ Loading (wt. %)	Temp. (°C)	Residence Time (min)	Heating rate °C/ min	Pressure (MPa)	Product yield	Ref.
1	Inconel reactor	batch	Chlorella vulgaris, Spirulina platensis & Saccharina latissima	NaOH Ni- Al ₂ CO ₃	500	30		36	H ₂ =15.1 mol/kg CH ₄ = 2x(catalyst)	[166]
2	Stainless 316L batch autoclave	steel	Distillery, refinery & petrochemical complex	oil & MnO ₂ , CuO and Co ₃ O ₄ 20, 40 & 60	300 -375	15 30 45	-	≤ 18	H ₂ =0.75 mol/kg	[165]
3	Stainless 316L	steel	Soybean straw & flax straw 1:5 & 1:10		300 400 & 500	30 - 60	30	22-25	(H ₂ =6.62 & 14.91) mol/kg CH ₄ =1.73 mol/kg CO ₂ =4.61 mol/kg C ₂ - C ₄ =0.38mol/kg	[171]
4	batch autoclave		white poplar & white poplar sawdust (1:12.5)	K ₂ CO ₃ (mass fraction of 10 biomass (0.12g))	300- 600	60	10 -15		H ₂ =37.8 & 38.2 CH ₄ =25.7 & 27.7 mol %	[170]

5	fluidized reactor	bed	Sewage (SS)	sludge	KOH > K ₂ CO ₃ > NaOH > Na ₂ CO ₃ (0.5 wt. %)	540	-	-	25	H=15.49 mol/kg	[164]
6	500 mL stainless steel high-pressure reactor)		sorghum and low rank C (5.0 g)	biomass (5.0 g)	K ₂ CO ₃ (3 %, (w/w)) and CaO	500	90	12.5	22.06	H ₂ /CO ₂ ratio of 88.5.	mol [167]

2.6 Concluding remarks

Energy crops used as biofuel globally have been within 20 – 60 % with estimated energy generation between 130 – 270 EJ/year by 2050 via an energy conversion (thermochemical) process technology, robust and flexible for bio-oil yields. Based on the review, several biomass materials have been utilized for biofuel, but few studies have been carried out on the Bambara Groundnut shell (BGS), Sweet sorghum stalk (SSS), Shea nutshell (SNS) and Shea nut Chaff (SNC). Numerous waste biomass materials in the African continent are largely underutilized as their energy potential is undiscovered. Exploring the potential through the thermochemical and hydrothermal process would improve biofuel in bioenergy production and intermediate pyrolysis, which has not been explored adequately. The scale-up of thermochemical conversion technologies is complicated; the BFB, CFB, RCP, and AFP reactors are promising, with an average yield of 40 - 75 wt. % bio-oil. However, a techno-economic analysis is recommended for the technological processes to determine the most cost-effective return on investment (ROI) with specific operating capacity. In HTC and HTG, temperature, residence time, autogenous pressure, concentration, and catalyst are critical. They play an important role in product generation with a temperature range of 300 - 540 °C; a

residence time (30 - 60) minutes; 22 - 36 MPa pressure; minimum biomass-water ratio of 1:5 concentration, and catalyst commonly used and most suitable for the reaction pathway are commonly metal oxides.

CHAPTER THREE

3 Materials and methodology

3.1 Introduction

This chapter outlines the materials and methodology adopted in the current research. The subsections include the physicochemical analysis of biomass, biochar, bio-oil, and the conversion processes (intermediate pyrolysis, catalytic co-pyrolysis, and wet torrefaction). The statistical analysis and optimization of the process parameters for the experimental data analysis were done using Design-Expert® software.

3.2 Materials

3.2.1 Chemical reagents and equipment

Chemical reagents used were Aluminium Oxide (Al_2O_3) (R&M Chemicals), Nickel (II) nitrate hexahydrate, 98 % (Alfa Aesar), and ZSM-5 catalyst (Alfa Aesar), Methanol (SYSTEM®, Chem AR®), Acetone (R&M Chemicals) and glass wool (Bendosen). The laboratory types of equipment used were a pH meter (PH100 ExStik®pH Meter, China), Hot plate (Cole-Parmer (S/N: C1921100300797), Centrifuge 5430 (V4.4), Carbolite Gero Furnace

(Type:11/6B) with stainless steel tubular reactor, Carbolite Gero Reactor Controller (Type: TVS 12/900), Vacuum pump, High-pressure Autoclave reactor (Model A2335, Amar Equipment Pvt. Ltd). The analytical instruments include X-ray diffraction analysis (Model X'pert Pro), PANalytical, Netherland, Nitrogen adsorption/desorption analysis (ASAP 2020 Micromeritics) Co., USA, Bomb Calorimeter (Parr 6100 Calorimeter), TGA/DSC 02 (Perkin Elmer STA6000 TGA-DSC), GC-FID/GCMS (Perkin Elmer Clarus 680), FTIR (Perkin Elmer Frontier MIR/FIR Spectrometer with PIKE Gladiators) and the CHNS (varioMacrocube SN20146077) elemental analyzer.

3.2.2 Feedstock collection and preparation

The feedstocks used for the study were Bambara Groundnut Shell (BGS), Sweet Sorghum Stalk (SSS), Shea Nutshell (SNS), Shea Nut Chaff (SNC), and Polypropylene (PP) to investigate their biofuel potentials. The BGS was collected from the Crop for The Future Field Research Centre (CFFFRC) in Semenyih, Malaysia. The SSS sample was collected from Ahmadu Bello University Zaria, Kaduna State. SNS and SNC samples were as well collected at the Federal Polytechnic Bida, Niger State - Nigeria. The Polypropylenes (PP) were collected from the researchers' house in Malaysia. Used food takeaway boxes were used as PP. The received biomass samples were sun-dried.

The dried BGS, SSS, SNS, and SNC were ground in a Rotor Beater Mill (model Retsch SM100) and sieved to sizes 1.18 mm, 0.6 μm , and 0.3 μm with a Heavy-Duty Sieve Shaker. The polypropylene food containers were cleaned, dried, and milled to an average particulate size of 2 mm. They were all sealed in a transparent plastic sample holder according to their particle size and stored for further analysis and experiments in the laboratory. The methodology flowchart for the research activities is shown in Figure 3.1 below. It illustrates the sample collection and physicochemical analysis, thermochemical processes (intermediate pyrolysis, catalytic co-pyrolysis, and wet torrefaction) and product (bio-oil, biochar or hydrochar) characterization for their energy potential.

This chapter presents the characterization of feedstocks, methodology, and equipment used in the current project to achieve the objectives shown in Chapter One. Table 3.1 is the summary of the samples, and the processes studied in chapter three (3)

Table 3.1: Summary of the samples and the processes

S/No	Sample identification	Process/Treatment	Remark(s)
1	BGS- G1, G4 & G5	• Physicochemical analysis	BGS-G1: Figure out their HHV
2	BGS-G1, SSS, & SNS	• Physicochemical analysis	Bioenergy potential
3	BGS-G1	• Intermediate pyrolysis • Intermediate pyrolysis with different inert gasses	Effect of different inert gases
4	SNC	• Wet torrefaction	High MC
5	SSS/PP	• Intermediate pyrolysis	SSS/PP waste and energy management

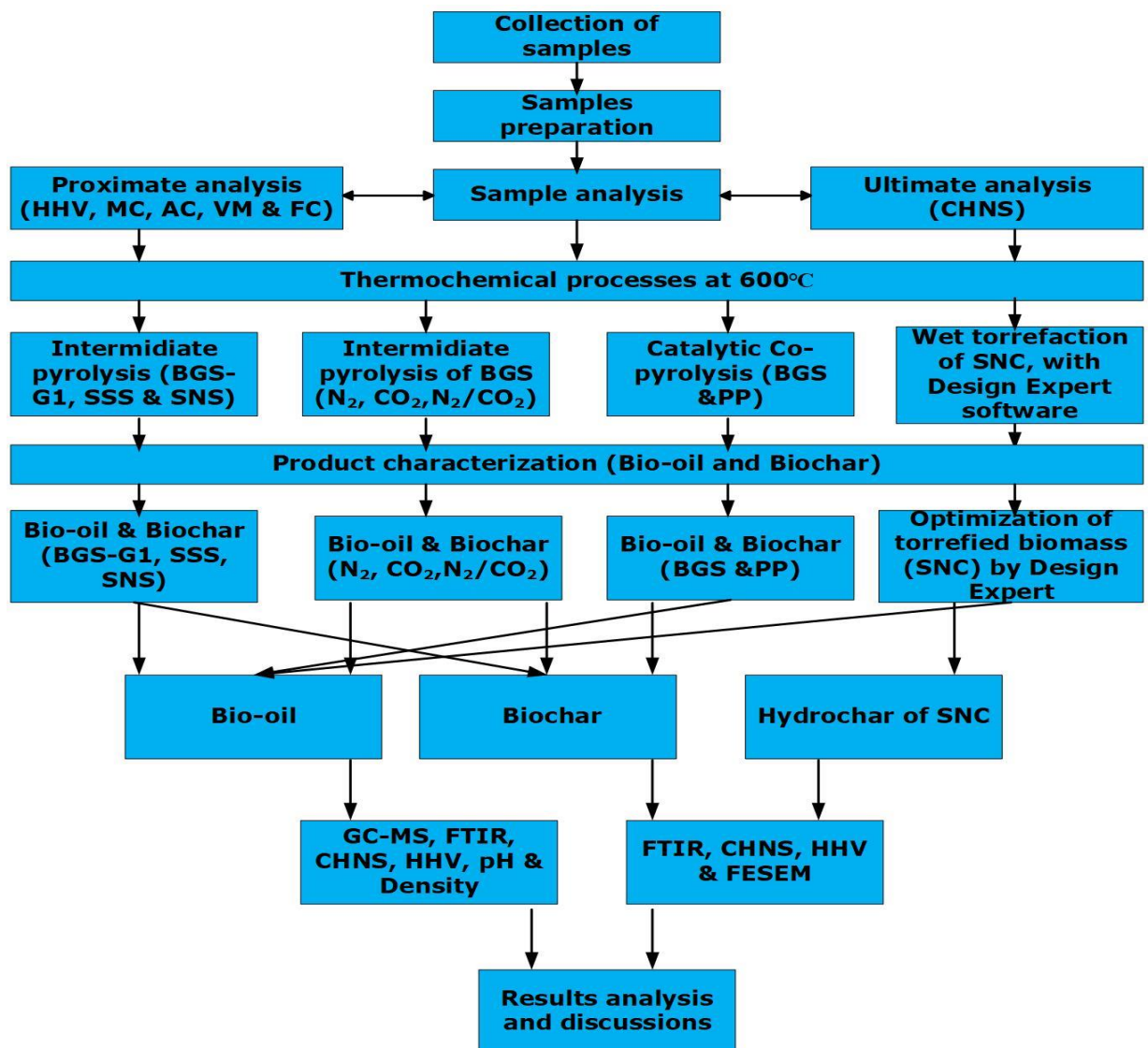


Figure 3.1: Flowchart for the research activities.

3.3 Methodology

The samples of biomasses were collected, and analysis was conducted to understand the physicochemical properties. Intermediate pyrolysis, catalytic co-pyrolysis and wet torrefaction processes of the biomass were studied to evaluate their bioenergy potentials. The investigation of intermediate and catalytic co-pyrolysis at 600 °C. The intermediate pyrolysis for BGS was conducted in presence of different inert gases (N₂, CO₂ and N₂/CO₂ (75:25) vol. %, while the mixture of SSS and PP was taken for intermediate co-pyrolysis and catalytic (Al₂O₃, 25wt.%Ni/Al₂O₃, ZSM-5, and 25wt.%Ni/ZSM-5) co-pyrolysis for optimum bio-oil yield. Lastly, the torrefaction of SNC under different temperatures (180 - 260 °C) and residence times (15 - 30), with deionized water as the medium of the experiment to improve its fuel properties was studied. The biochar, and bio-oil of products were analysed by FTIR, CHNS, GC-MS, HHV, pH, Density and FESEM equipment.

3.3.1 Biomass characterization

The physicochemical properties of biomass are pivotal in the efficiency of energy conversion technologies. Biomass fuel performance is affected by numerous properties, such as the higher heating value, moisture content, chemical composition, and particle

size. These properties vary from biomass to biomass, and natural variations of a given fuel type might be apparent [172]. The ultimate and proximate analyses were on a dry basis for the BGS, SSS, SNS, and SNC samples.

3.3.2 Ultimate analysis

CHNS analysis was carried out with an elemental analyzer (varioMacrocube SN20146077), 100 mg biomass sample was combusted in a controlled atmosphere and subsequently analysed. The amount of carbon, hydrogen, nitrogen, and sulphur calculations was done via the detection and quantification of the gases (CO_2 , H_2O , N_2 , and SO_2) released during the combustion. Products are flushed out of the chamber through the overheated high-purity copper, removing the oxygen and converting the NO_x to N_2 [173].

3.3.3 Proximate analyses

Proximate analysis determines the percentage of moisture content (MC), ash content (AC), volatile matter (VM), and fixed carbon (FC). The porcelain dishes were pre-dried in an oven at 105 ± 3 °C for 4 hours, dishes were re-weighed and recorded after being cooled in a desiccator. The measured MC was from the weight difference of the biomass sample after drying in an oven at 105 ± 3 °C for 16 h. The

1 g biomass was returned to the oven at 105 ± 3 °C for 4 hours for weight consistency and was removed and kept in a desiccator to cool to room temperature and then re-weighed to the nearest 0.1 mg (ASTM E 1755, E 1755-01, and E 1756-08).

The ash content calculation was based on the weight remaining after ashing and also considering the weight difference of the crucible used. One (1) g of the oven-dried sample was taken in a crucible and heated in a furnace at 575 ± 10 °C for 4 hours. The crucible was carefully removed into a desiccator and cooled down. The weighing of the crucible containing ash was to the nearest 0.1 mg. The evaluation of ash content was according to BS EN 14775:2009 & EN 14775:2009 (E) standards.

The VM determination was done by heating about 15 mg at a constant heating rate of 10 °C/min in a TGA/DSC unit. The analysis was performed under nitrogen at a 20 ml/min flow rate from room temperature to 110 °C and held for 10 min. The samples were then heated from 110 - 900 °C and held at 900 °C for 10 min. The volatile matter was calculated as the weight loss per cent occurred at 110 to 900 °C.

The FC content was calculated with the empirical formula as given below in Eqn. 3.1;

$$FC = 100 - (MC + VM + ASH)$$

Eqn. 3.1

where

FC= Fixed carbon (wt. %)

MC = Moisture content (wt. %)

VM = Volatile matter (wt. %)

ASH= Ash content (wt. %)

3.3.4 Thermogravimetric analysis (TGA)

TGA analysis was done via the thermogravimetric analyzer (TGA) (Perkin Elmer STA6000 TGA-DSC) to determine the Activation energy, pre-exponential factor, regression values, VM, and FC. TGA examine the decomposition behaviour of biomass. Then, the TGA study determines the pyrolytic behaviour of the BGS, SSS, SNS, and SNC. The co-pyrolysis behaviour of PP to SSS feedstocks was studied under different ratios such as SSS:PP in 0:1, 1:1, 1:3, 3:1, and 1:0. The volatile matter percentages of samples are the weight difference within 110 – 950 °C of the analysis. In comparison, the fixed carbon was determined from the non-pyrolyzed fuel using Eqn. 3.2.

3.3.5 The kinetics rate equation

The kinetic rate equation is started with the mass rate reaction equation from Eqn. 3.2.

$$\alpha = \frac{m_0 - m_t}{m_0 - m_\infty} \quad \text{Eqn. 3.2}$$

where,

m_0 = Initial mass,

m_t = Instantaneous mass at t, and

m_∞ = Final mass.

The kinetic function $f(\alpha)$ depends on the conditions and the stage of the reaction of the study, but it can usually be expressed as $(1 - \alpha)$ if the first reaction order is in consideration. According to Chong et al., (2017) the rate of reaction and Arrhenius equation as stated below Eqn. 3.3 and Eqn. 3.4 [174–176].

$$\frac{d\alpha}{dt} = kf(\alpha) \quad \text{Eqn. 3.3}$$

$$k = A \exp\left(-\frac{E}{RT}\right) \quad \text{Eqn. 3.4}$$

where,

A = pre-exponential factor (1/s),

E = activation energy (J/mol)

R = universal gas constant (8.3145 J/mol K), and

T = temperature (K).

By substituting the reaction rate Eqn. 3.3 into Eqn. 3.4 gives the following Eqn. 3.5:

$$\frac{d\alpha}{dt} = A \exp\left(-\frac{E}{RT}\right) f(\alpha) \quad \text{Eqn. 3.5}$$

For a constant heating rate, β (K/s) expression can be $\beta = dT/dt$ and included in the previous differential equation, obtaining a new expression is as follows in Eqn. 3.6 and 3.7.

$$\frac{d\alpha}{dt} = \beta \left(\frac{d\alpha}{dT} \right) = A \exp \left(-\frac{E}{RT} \right) f(\alpha) \quad \text{Eqn. 3.6}$$

Therefore:

$$\frac{d\alpha}{f(\alpha)} = \frac{k}{\beta} \cdot dT \rightarrow \frac{d\alpha}{f(\alpha)} = \frac{k_0}{\beta} e^{-Ea/RT} \cdot dT \quad \text{Eqn. 3.7}$$

The following integral in Eqn. 3.7, which is numerically solved, is obtained as in Eqn. 3.8 below:

$$g(\alpha) = \int_0^\alpha \frac{d\alpha}{f(\alpha)} = \frac{k}{\beta} \int_{T_0}^T e^{-Ea/RT} \cdot dT = \frac{k_0 E_a}{\beta R} P \left(\frac{E_a}{RT} \right) \quad \text{Eqn. 3.8}$$

The function $P \left(\frac{E_a}{RT} \right)$ has no exact solution but can be solved by numerical or approximation methods [177]. The Coats-Redfern method is among the most popular [178]. This method utilizes the asymptotic series expansion for approximating the exponential integral in Eqn. 3.8.

Doyle's approximation is expressed as

$$\ln[-\ln(1 - \alpha)] = \ln \left(\frac{AE_a}{\beta R} \right) - 5.33 - 1.052 \left(\frac{E_a}{RT} \right) \quad \text{Eqn. 3.9}$$

Where β is the heating rate ($^{\circ}\text{C}/\text{min}$), T is the absolute temperature (K), A is the pre-exponential factor ($\frac{1}{\text{s}}$), $(E)_a$ is the activation energy ($\frac{1}{\text{mol}}\text{K}$) and A can be related to specific heating rates $\ln[-\ln(1 - \alpha)]$ Vs. $1/T$.

Based on the model and mechanisms that gave the correlation coefficient (R^2) and the kinetic parameter in triplicates (E , A , and $f(x)$) were studied at TGA analysis temperatures ranging from 32 - 950 $^{\circ}\text{C}$

3.3.6 Higher heating value (HHV)

Higher heating value (HHV) is determined by an oxygen bomb calorimeter (Parr 6100_Calorimeter with a standard 1108 Oxygen Bomb, Parr Instruments, Molin, USA). The HHV is the amount of heat released per unit mass or volume of fuel after combustion, including the latent heat of vaporization of water.

The samples were weighed 1.0 g of liquid (bio-oil) or (bio-oil and cotton wool) or biochar into the sample holder in the bomb. Subsequently, a fuse wire was inserted according to the manual, the cylinder bomb lid was screwed firmly, oxygen connector was connected and filled up. Two litres of water were supplied in the

bucket inside the calorimeter and the lid was closed to determine the HHV.

3.3.7 Catalyst preparation.

The catalyst preparations were based on the impregnation of nickel on ZSM-5 and aluminium oxides (Al_2O_3).

3.3.7.1 *Nickel-ZSM-5 and Nickel- Al_2O_3 catalyst impregnation*

Aluminium oxide (Al_2O_3) was calcinated at 600 °C for 4 hours, and the Al_2O_3 catalyst was obtained and sealed in a plastic bag before determining the characterization. The nickel nitrate hexahydrate (purity > 98 %; Alfa Aesar) was used, as the Ni precursor was prepared for the impregnation method on the Al_2O_3 . The distilled water was titrated to know the amount needed for the catalyst support pore volume required to prepare the catalyst. The obtained aqueous solution was by mixing nickel nitrate hexahydrate, dissolved in 100 ml deionized water, and stirred while heated on a hot plate. The alumina (Al_2O_3) was added to the porcelain containing the amount of nickel solution for impregnation into the support to produce 50 g of 25 wt. %Ni- Al_2O_3 . The mixture was stirred continuously and heated to 90 °C at 700 rpm for 1 hour until a semi-solid slurry suspension turned into a transparent green solution. It

was dried in a rotary evaporator at 105 °C for about 2 hours and 4 hours at 600 °C for calcination. The catalyst was finely ground and sieved to a particle size of 50 - 212 µm; the powder Ni-based catalyst was obtained and sealed in a bottle before the characterization.

The Ni-modified ZSM-5 as described by Nishu et al., (2021) was prepared by 25 wt. % for this study of hydrated nickel nitrate ($\text{Ni}(\text{NO}_3)_2 \cdot 6\text{H}_2\text{O}$) using the wet impregnation method. An aqueous solution was prepared by titrating the deionized water to determine an exact quantity to impregnate the nickel nitrate in 100 mL of deionized water and stirred steadily till it dissolved completely. The 25 wt. % of ZSM-5 was mixed gently into the Nickel nitrate hexahydrate (purity > 98 %; Alfa Aesar) aqueous solution heated at 90 °C at 700rpm for 1 hour until the water evaporated in a hot plate magnetic stirrer. It was dried in a rotary evaporator at 105 °C for about 2 hr and further underwent calcination at 600 °C for 4 hours [179]. The preparation procedure for the Ni/ Al_2O_3 catalyst production was adopted from the Ni/ZSM-5 above. The alumina (Al_2O_3) added to the porcelain contained the amount of nickel solution for impregnation into the support at 25 wt. % Ni to produce 50 g of 25 wt. % Ni- Al_2O_3 . The catalyst was finely ground and sieved to a particle size of 50 - 212 µm; the powder Ni-based catalyst was obtained and sealed in a bottle before the characterization.

3.3.8 Characteristics of catalyst

The structures of samples were examined by powder X-ray diffraction (XRD) using a (Model X'pert Pro) instrument in reflection mode with Cu K α radiation and a power of 40 kV \times 40 mA ($\lambda = 1.542$ Å). Diffraction patterns performed were over $2\theta = 5\text{--}80^\circ$ with a step size of 0.02° . The morphology examinations of the samples were done by scanning electrons with an accelerating voltage of 200 kV. BET-specific surface area, pore volume, and pore size distribution of the samples were measured by N₂ sorption/desorption analyses (Builder, SSA-7000). The N₂ adsorption-desorption data determined the Brunauer-Emmett-Teller (BET) method and the specific surface areas of the catalysts, while the pore volumes were by the Barrett-Joyner-Halenda (BJH) method. The measurement of the surface acidity of the biochar was found by temperature-programmed desorption of ammonia (NH₃-TPD) 180. Nitrogen (N₂) adsorption was using an accelerated surface area porosimeter (ASAP) that was equipped with degassing ports (Micromeritics ASAP 2020, USA). The degassed catalyst samples were at 300 °C for 4h, and the N₂ isotherms measurement was at 77 K with the relative pressure $\left(\frac{P}{P_0}\right)$ ranging up to 0.99.

3.4 Experimental set-up

3.4.1 Intermediate pyrolysis

The intermediate pyrolysis of the biomass sample was under atmospheric pressure in a vertical fixed-bed reactor. During pyrolysis, the operating parameters contributed to the product quality and quantity of both bio-oil and biochar. The reaction temperature is essential in thermochemical process because it changes the biomass's volatile and condensable components [181]. Figure 3.2 represents the intermediate pyrolysis where all experiments use a weight mass of about 30 - 70 g in each set of samples. The samples were held on a stainless-steel mesh holder which was inserted into the reactor. The supported mesh/sieve was at 25 % of the 1.2 m height of the reactor from the bottom and screwed tight from the top.

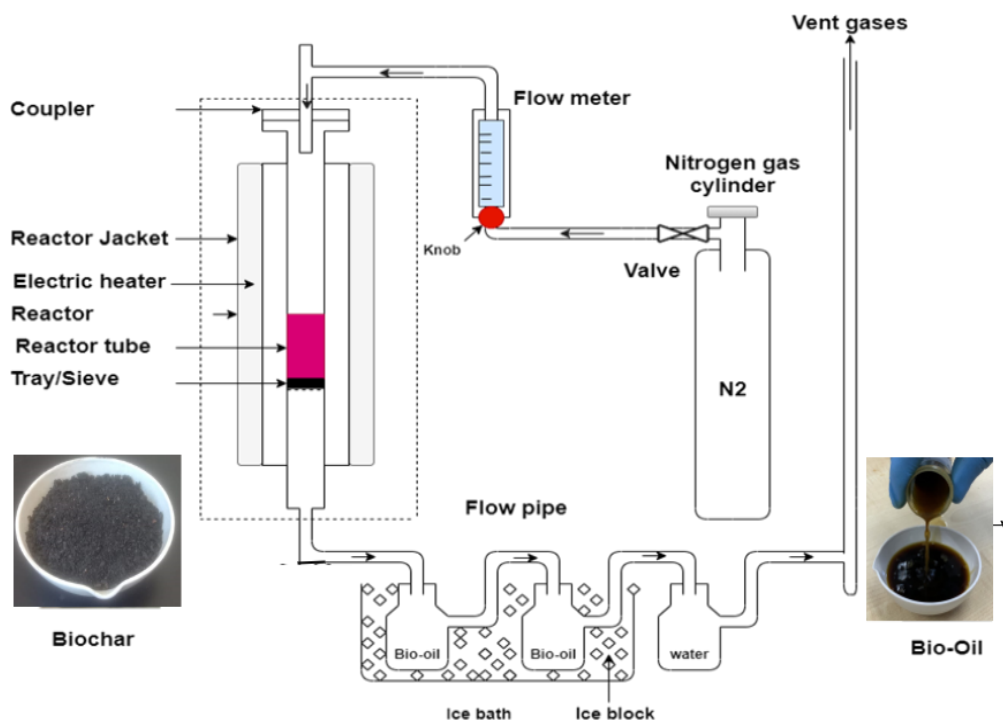


Figure 3.2: A vertical tubular reactor

A nitrogen (N_2) gas cylinder was connected to the reactor and initially used to purge the air, or other gases present in the reactor for about 180 s before operation at a flow rate of $30 \text{ cm}^3/\text{min}$. The flow rate adjustment made for the gas controller according to the experimental design was 5, 17.5 or $30 \text{ cm}^3/\text{min}$. The process operates at a rate of $50 \text{ }^\circ\text{C}/\text{min}$ to a reaction temperature of $600 \text{ }^\circ\text{C}$ and then held for 1 hour to the end of the experiment (reaction and cooling time). Mostly, pyrolysis temperatures are within $400 - 600 \text{ }^\circ\text{C}$ [124] $400 \text{ }^\circ\text{C}$ [182] $450 - 600 \text{ }^\circ\text{C}$ [143]. After some trial runs, $600 \text{ }^\circ\text{C}$ was selected as more suitable for the experiment. The appearance of fuming was observed within 15 minutes and disappeared after 30 minutes of operation. At the end, the experiment gas inflow of inert gas is intermittently increased to $30 \text{ }^\circ\text{C}/\text{min}$ for 3 minutes to purge

the reactor of all gas residues inside the reactor. The gas passed through a series of two condensers in an ice bath and finally into a water scrubber before being released or discharged through the laboratory exhaust. Biochar was collected from the reactor outlet after the unit cooled to less than 40 °C. The products (bio-oil and biochar) weights were recorded. The bio-oil was stored in a centrifuge tube and kept in a freezer at 4 °C, while the biochar was placed in a plastic bag for chemical and physical characterization without further treatment. The yield of the bio-oil, biochar and gas yield were determined by Eqn. 3.10, Eqn. 3.11 , and Eqn. 3.12 respectively.

$$\text{Bio - oil Yield (wt. \%)} = \frac{(\text{Bio-oil Weight (g)})}{(\text{Weight of BGS (g)})} \times 100 \quad \text{Eqn. 3.10}$$

$$\text{Biochar Yield (wt. \%)} = \frac{(\text{Bio-char Weight (g)})}{(\text{Weight of BGS (g)})} \times 100 \quad \text{Eqn. 3.11}$$

$$\text{Gas Yield (wt. \%)} = 100 - ((\text{Bio - oil}) + (\text{Biochar})(\text{wt. \%})) \quad \text{Eqn. 3.12}$$

3.4.2 Synergetic effect determination of biomass and PP

To investigate the synergetic effects in the co-pyrolysis of sweet sorghum stalks and polypropylene, the experimental weight loss ($W_{Exp.}$) of blend samples are compared with the theoretical weight loss ($W_{Cal.}$). The evaluation of the synergetic effect of co-pyrolysis of

sweet sorghum stalks and polypropylene can be from the difference (ΔW) between the calculated ($W_{Cal.}$) and experimental ($W_{Exp.}$) weight loss values. The difference between theoretical and experimental weight losses (ΔW) indicates the degree of synergism. If $\Delta W < 0$, it indicates a positive synergetic effect; if $\Delta W > 0$, it indicates a negative effect on the blend ratio [183]. According to Pattanayak et al., (2022), the expression of ΔW and $W_{calculated}$ can be as Eqn. 3.13 and Eqn. 3.14 respectively [183]

$$\Delta W = W_{Exp} - W_{Cal.} \quad \text{Eqn. 3.13}$$

$W_{Calculated}$ can be obtained by:

$$W_{Calculated} = X_1W_1 + X_2W_2 \quad \text{Eqn. 3.14}$$

where,

X_1 = mass fraction of SSS,

X_2 = mass fraction of PP in the mixtures,

W_1 = weight loss of SSS and,

W_2 = weight loss of PP.

3.4.3 Wet torrefaction experimental set-up (Objective 5).

The wet torrefaction (WT) process of Shea Nutshell (SNC) was conducted with the use of a 1 L high-pressure reactor autoclave (Model 2335, Amar Equipment Pvt. Ltd, India) [184]. It is made of a stainless-steel autoclave and designed to withstand pressure up to 350 bar and a temperature of 500 °C.

According to Soh et al., (2021), wet torrefaction operates within parameters (residence time 2 - 3 h), water-to-biomass ratio (20:1 - 1:1), and temperature (180 – 240 °C) but can go up to 260 °C [185]. The reactor was thoroughly cleaned with acetone, rinsed with distilled water, and then dried before the experiment. In the experiment, 20 g of biomass (dry weight) and 100 - 300 mL of deionized water were mixed in the reactor. The sealed coupler of the reactor uses vacuum grease, a high-temperature plastic gasket, and it is firmly tightened with a clamp bolt in a diagonal sequence to prevent leakage during the experiment. The K-type thermocouple was passed through the rear inlet and positioned in the middle of the heating zone to measure the reaction temperature. The water from the chiller at 20 °C was flowed around the bearing of the stirrer to avoid the stirrer damage. The agitated reactants were at a speed of 101 rotations per minute (rpm), and the experiment was then started by switching on the heater. During the investigation, the maximum pressure and temperature were 45 MPa, and 260 °C, respectively. The operating pressure during liquefaction was allowed to build up as the gas sampling and vent valves were securely tight to avoid leakage.

The SNC study was at three (3) temperatures, 200, 230, and 260 °C. The pressure and temperature in the reactor were recorded in 3-

minute intervals until the reactor temperature reached the targeted temperature. According to the experimental design, the reactor temperature residence time was 10 - 30 min. Immediately attaining the residence time allotted for each experiment run, the unit was shut down sequentially switching off the stirrer and then the heater. Afterwards, the reactor was allowed to cool down to room temperature, and the torrefied biomass was collected. The torrefied biomass was de-moisturized for 3 hours at 105 °C in an oven, then hydrochar was measured to determine the mass yield and collected in an air-tight plastic bag before further analyses. The mass, energy and filtrate yield calculations applied Eqn. 3.15, Eqn. 3.16, and Eqn. 3.17 respectively.

$$\text{Mass Yield , } MY = \frac{M_{\text{torrefied SNC}}}{M_{\text{raw SNC}}} * 100\% \quad \text{Eqn. 3.15}$$

where,

MY = Mass yield

$M_{\text{torrefied}}$ = Mass of torrefied SNC

M_{raw} = Mass of raw SNC

$$\text{Energy Yield , } EY (\%) = MY (\%) * \frac{HHV_{\text{torrefied SNC}}}{HHV_{\text{raw SNC}}} \quad \text{Eqn. 3.16}$$

where,

EY = Energy yield

$HHV_{\text{torrefied}}$ = Higher Heating Value of torrefied SNC

M_{raw} = Higher Heating Value of raw SNC

$$\text{Filtrate Yield , } FY = \frac{V_{\text{initial raw water}} - V_{\text{filtrate}}}{V_{\text{initial raw water}}} * 100\% \quad \text{Eqn. 3.17}$$

where,

FY = Filtrate yield

$V_{initial\ raw\ water}$ = Volume of initial raw water

$V_{filtrate}$ = Final filtrate of raw SNC

3.5 Product characterization

3.5.1 Bio-oil characterization

Proximate analysis, ultimate analysis, and heating value of bio-oil and bio-char samples were measured as discussed in Sections 3.3.2 - 3.3.3 and 3.3.6. The pH value of the bio-oil samples was measured using a digital handheld pH meter pre-calibrated with buffer solutions of pH 4.0, 7.0, and 10.0. The density of the bio-oil was measured using a density meter (DMA 4100 M, Anton Paar). Approximately 2 ml syringes were used to sample bio-oil and to avoid an air bubble. After operations, the samples were injected into the measuring cell, filled through the sample port, and readings were recorded [186].

3.5.2 GC- MS analysis

The bio-oil for this study was prepared at the ratio of bio-oil to methanol (1:10) in w/w %. Bio-oil methanol mixture was filled in a 1.5 μL vial container through a 0.45 μm polyethersulfone syringe filter. The composition analysis was using a GC-MS (Gas

Chromatography and Mass Spectrometry) analyzer (GC Clarus 680, Perkin Elmer) with the Elite - 5MS (Perkin Elmer) capillary column (30 m × 0.25 mm, film thickness 0.25 μm).

The sample volume of 1 μL was injected at 250 °C in split mode with a split ratio of 51:1. The temperature ramps of the GC oven were as follows: Initial heating at 40 °C, held for 2 min, increased by 10 °C/min to 300 °C, and sustained for 10 min. Gas was analysed and scanned at a source and transfer temperature of 250 °C using MS Clarus SQ 8 S (Perkin Elmer): 40 to 600Da. The carrier gas helium was at a gas flow rate of 1.0 mL/min, and the solvent delay for MS was 3 minutes. Electron ionization (EI) used was in MS, and standard mass spectra recorded were at an ionization energy of 70 eV. The identified chromatogram spectra were compared with the typical ranges of compounds from the NIST library.

3.5.3 Fourier transform infrared (FTIR)

The Fourier Transform Infra-Red (FTIR) characterization was determined for both the bio-oil and biochar and examine the chemical functional groups present with attenuated total reflectance (ATR) (Perkin Elmer Frontier MIR/FIR Spectrometer (Part Number: L1280044) with PIKE GladiATR). The bio-oil samples (1 - 2 drops) on the ATR node, while a few pinches of biochar were placed on the

ATR sample holder, and the node was also screwed on accordingly. The spectra record with scans 20 and a step size of 4 1/cm within 400 - 4000 1/cm wavenumbers.

3.5.4 Biochar characterization

The physicochemical analysis of biochar samples was analysed as discussed in Section 3.3.2 - 3.3.3.

3.5.5 Field emission scanning electron microscope/energy dispersive x-ray (FESEM/EDX)

FESEM and EDX analysis (FEI Quanta 400F model and INCA 400 Oxford instrument with X-Max Detector, USA) was to determine the morphology and elemental composition. Biochar was studied via the FESEM/EDX equipment with an accelerating voltage of 20 kV to verify the morphology.

3.6 Statistical experimental design and model development

The WT experiments at varying temperatures, residence times, and SNC/water ratios were designed in Design-Expert® software version 13.0.5.0 (www.statease.com) according to the central composite design (CCD). Twenty (20) experimental runs included three design factors and three levels and culminated from 14 non-centre and 6-

centre points. The investigated parameters of the coded levels are in Table 3.2 while the surface response was the mass yield. In addition, the corresponding energy yield and HHV for each experiment results are shown to illustrate the interaction between experimental factors and responses, statistical significance evaluation and analysis of variance (ANOVA), which included Fisher's F-test and p-values. ANOVA was used to determine the regression model fitness at a 95 % confidence level. Analyses such as correlation coefficient (R²), adjusted R², predicted R², adequate precision, 'lack-of-fit,' and standard deviation criterion were adopted to assess the validity and accuracy of the model. The investigated parameters of the coded levels are in Table 3.2 while the resulting design matrix of the mass yield, energy yield predicted, and responses are determined.

Table 3.2: Factors of boundary, constraints, levels, and SNC responses.

Name	Goal	Lower limit	Upper limit	Lower weight	Upper weight	Importance	Mean	Std. Dev.
A: Temperature	in range	200	260	1	1	3	230	25.3
B: H2O/Biomass	in range	5	15	1	1	3	10	4.15
C: Residence Time	in range	10	30	1	1	3	20	8.52

CHAPTER FOUR

4 Results and discussion

The results were arranged according to the research objectives sequentially. Results were presented and discussed as, the effect of particle size on physicochemical and kinetic analysis of BGS-G1. Physicochemical analysis and intermediate pyrolysis of BGS-G1, SSS, SNS. Evaluation of the impact of N₂, CO₂, and N₂/CO₂ (75:25) vol. % atmosphere, in an intermediate pyrolysis of BGS with varying flow rate. Examine the synergetic effects of SSS and PP in intermediate catalytic co-pyrolysis. Wet torrefaction of SNC using a Design-Expert® to improve its fuel properties with temperatures (180 - 260 °C), biomass-to-water (1:5 - 1:15) ratio and residence times (15-30) minutes. All the research objectives were to harness the biomass energy potential for bioenergy production.

4.1 Evaluate the effect of particle size on physicochemical and kinetic properties of BGS for biofuel.

Physicochemical analysis generally has three stages: proximate, ultimate, and thermogravimetry. Proximate analysis is the most important of the three, representing an essential initial step, and it involves determining the fixed carbon, volatile matter, moisture content, and ash content. The ultimate analysis is to evaluate the

composition of the fuel at the elemental level. The ultimate analysis focuses on the quantitative determination of carbon (C), oxygen (O), hydrogen (H), sulphur (S), and nitrogen (N) – the organic components. Ash analysis is associated with inorganic elements such as potassium (K), sodium (Na), silicon (Si), aluminium (Al), and iron (Fe) [187].

4.1.1 Proximate analysis for BGS-G1.

Biomass with high moisture content suits biochemical methods, including fermentation, anaerobic digestion, wet torrefaction, or hydrothermal carbonization [188]. Woody biomass has lower moisture than herbaceous biomass [189]. Most industrial biomass applications have thermochemical processes that utilize woody biomass and low-moisture varieties of herbaceous biomass [189]. Table 4.1 shows the BGS physicochemical analysis results for a thermochemical process as in section 3.3 and within the operating conditions for bioenergy (bio-oil and biochar) generation. The coded and investigated samples were untreated (UT1, UT2, and UT3) and pre-treated (PT1, PT2, and PT3), with particulate sizes as 1180, 600, and 300 μm , with additional two BG genotypes (BGS-G4 & BGS-G5).

Table 4.1: The BGS-G1, BGS-G4, and BGS-G5 proximate and ultimate analysis results.

Proximate Analysis										
S/No	Sample	Size (μm)	HHV (MJ/kg)	MC (wt. %)	AC (wt. %)	VM (wt. %)	FC (wt. %)	Ea (kJ/mol)	A	R²
1	BGS PT1	1180	17.3 \pm 0.4	5.4 \pm 0.3	5.6 \pm 0.3	74.7	9.9	19.4	31.60	0.96
2	BGS PT2	600	17.0 \pm 0.6	4.1 \pm 0.3	5.9 \pm 0.2	68.7	16.9	18.5	29.27	0.96
3	BGS PT 3	300	16.9 \pm 0.1	3.5 \pm 1.7	9.6 \pm 0.8	67.8	13.1	18.0	30.97	0.98
4	BGS UT1	1180	18.6 \pm 0.5	8.6 \pm 3.0	6.8 \pm 0.3	70.3	18.7	24.1	50.06	0.97
5	BGS UT2	600	18.3 \pm 0.6	7.4 \pm 2.3	7.0 \pm 0.1	69.2	20.8	24.9	58.95	0.96
6	BGS UT3	300	17.3 \pm 0.3	7.4 \pm 0.5	11.7 \pm 0.3	63	24	24.5	54.27	0.96
7	BGS G4	1180	16.0	11.7 \pm 0.5	9.1 \pm 0.1	62	17.2	18.8	28.39	0.94
8	BGS G5	1180	15.7	10.2 \pm 0.5	10.1 \pm 0.3	64.2	15.5	18.9	25.47	0.94

Ultimate Analysis								
S/No	Sample	C (wt. %)	H (wt. %)	S (wt. %)	N (wt. %)	O (wt. %)	H/C (wt. %)	O/C wt. %
1.	BGS-G1	43.9	6.1	0.1	1.3	41.8	1.6556	0.7148
2	BGS-G4	40.8	5.6	0.2	1.5	42.8	1.6353	0.7875
3	BGS-G5	39.0	6.1	0.2	2.1	42.5	1.8636	0.8180

At a relatively low heating rate, cellulose degrades to rather stable anhydrous cellulose resulting in charring of high char, but at a high heating rate rapid volatilization of cellulose produces volatile products. On heating biomass, volatile biomolecules of biomass are cleaved, producing the bio-oil after condensation [190]. Table 4.1 indicated that the BGS-G1 recorded the highest VM of 63.0 - 74.7 wt. %. The HHV is the heat released per unit of fuel mass after combustion, including the latent heat of vaporization. The HHV is related to high fixed carbon (FC) and carbon contents which are the primary heat source [191]. The BGS-G1 for the untreated led to the highest HHV of the samples. Table 4.1 shows the maximum HHV biomass of BGS-G1 (18.6 ± 0.5 MJ/kg) with the FC. Their HHV values were high and similar to those found in coals (16 – 34 MJ/kg) [192]. The HHV of the herbaceous biomass competed with the most agro-residues and woody plants. For example, a palm kernel shell recorded 18.82 MJ/kg HHV with a carbon content of 48.78 wt. % [193], whereas two perennial herbaceous crops (*Silphium perfoliatum* L. and *Helianthus salicifolius* A. Dietr.) had HHV of 17.72 and 18.44 MJ/kg respectively [194]. The HHV of samples can be determined using the modified Dulong's formula, as mentioned below in Eqn. 4.1.

$$HHV (MJ / kg) = [((33.5 (\%C) + (142.3) * (\%H) - (15.4) * (\%O)))/100]$$

Eqn. 4.1

where,
 C = carbon
 H = hydrogen
 O = oxygen and,
 N = nitrogen on a dry basis expressed in mass percentages.

The validation of the HHV using Eqn. 4.1 shows a confirmation of the experimental results BGS-G1, BGS-G4, and BGS-G5 as 16.88, 16.83, and 16.77 MJ/kg with a minimum error of about 10 %. Forest waste materials are high carbon (44 – 53 %) lignocellulosic materials with very little ash content (0.3 - 8 wt. %) [195]. High AC of biomass affects its potential fuel desirability, while high extractive content contributes to fuel desirability [196]. Ashes and inorganic elements are residues after biomass combustion and produce immense challenges in power plants, such as slagging, corrosion, and fouling [197]. The BGS-G1 had the lowest ash content among the three genotypes.

4.1.2 Ultimate analysis and Van Krevelen plot

High carbon content positively contributes to the fuels' high heating value (HHV). Hydrogen and oxygen contents of biomass sharply decrease due to dehydration reactions during pyrolysis. However, since the carbon content increases, higher heating values of products increase. The carbon conversion efficiency is about 60 % for the

biomass during pyrolysis. Forest waste materials have the highest in carbon (44 – 53 %) among lignocellulosic materials [195].

Table 4.2 shows the hydrogen of BGS-G1, BGS-G4, and BGS-G5 as 6.1, 5.6, and 6.1 wt. % respectively. The values recorded are similar to several biomass analyses of hydrogen where within the range of 4.5 – 7.0 wt. % in Table 4.2.

Table 4.2: Proximate analysis of some biomass.

Proximate Analysis							
S/No	Biomass	C	H	N	S	O	Ref.
1.	Sewage sludge	25.5	4.5	4.9	2.1	25.8	[198]
2.	Wood	47.5	5.3	0.4	<0.1	36.4	[199]
3.	Berley	44.2	6.1	0.4	0.6	30.4	[199]
4.	Pinewood sawdust	49.33	6.06	0.04	-	44.57	[200]
5.	Impereta cylindrical	50.035	5.923	1.145	-	42.897	[201]
6.	Eragrostis airoides	41.024	6.723	1.138	-	51.115	
7.	Oil palm trunk	45.79±0.07	6.15±0.02	1.47±0.01	1.47±0.01	46.33±0.07	[202]
8.	Rubberwood SD	47.55±0.23	6.22±0.02	0.32±0.01	0.03±0.01	45.91±0.26	
9.	Chesnut	45.5	5.7	0.2	0.0	48.2	
10.	Grape waste	50	6.0	2.0	0.1	34.4	[203]

Note "--": - Not detected

The BGS-G1, BGS-G4, and BGS-G5 samples had oxygen ranging between 41.8 - 42.5 wt. %, with only BGS-G1 oxygen lower than their carbon contents. The sulphur and nitrogen are relatively small as the minimum BGS-G1 (0.1 wt. %), and the maximum BGS-G5 (2.1 wt. %) require a more sophisticated process to mitigate the emissions for a scale-up plant. Low sulphur and nitrogen contents indicate their potential for thermochemical conversion due to low greenhouse gas emissions [191].

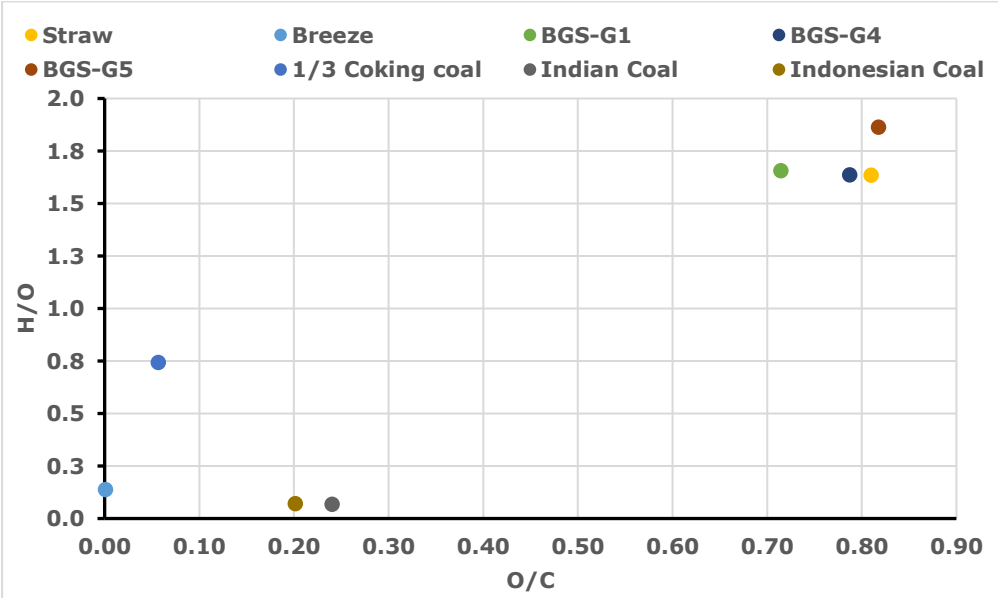


Figure 4.1: Van Krevelen Diagram of BGS-G1, G4 & G5.

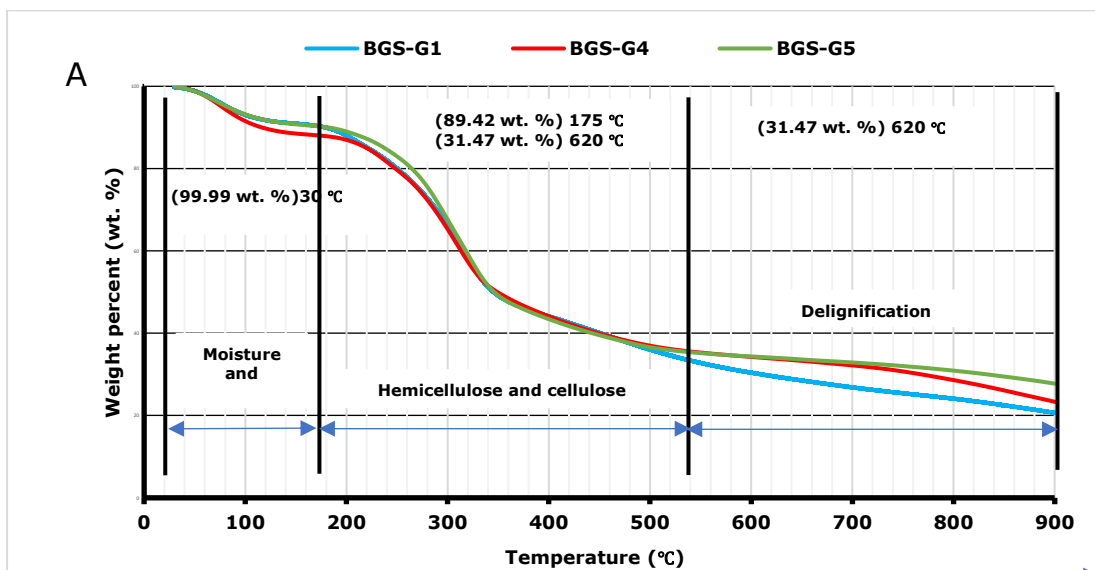
The Van Krevelen Diagram shows that BGS-G1 is a better biomass with the lowest O/C ratio, whereas BGS-G5 had both the highest H/C and O/C ratio. The BGS-G1 was best as compared to BGS-4 and BGS-G5 because it shows that its oxygen content is lower which allows for higher HHV. The high atomic ratio for BGS-G5 was due to

its low amount of C among the three genotypes (BGS-G1, BGS-G4 and BGS-G5) tested. While straw is a demonstration of having same O/C and O/C ratio for biomass like materials [171]. The BGS-G1 is tending towards the coal region in the Van Krevelen plot in Figure 4.1 and perhaps its biochar may demonstrate seem like properties of coal (Indian, Indonesian, coking coal and Breeze) [83] as compared to BGS-G4 and BGS-G5 samples above.

4.1.3 TGA analysis and kinetics

The thermal degradation profile of the selected BGS biomass samples is at the temperature ranges of 30 - 900 °C in Figure 4.2 (a & b). The TGA shows that stage I had a temperature range between 30 - 190 °C, showing the moisture and light volatiles removal by evaporation, with a weight loss for samples BGS-G1, BGS-G4, and BGS-G5 at an average of 10 wt. %. According to Singh et al., (2021) the temperature of 30 - 175 °C, and 50 - 160 °C, are attributed to moisture removal and light volatiles [204]. Stage II ranges between 190 - 620 °C, with weight loss for hemicellulose and cellulose devolatilization, this high volatility might result from the effect of smaller particle sizes. According to Singh et al., (2021), the temperature range (175 - 620 °C) at the second stage witnessed a weight loss of about 73 % and corresponded to the thermal degradation of hemicellulose and cellulose contents [204]. As the

BGS recorded about 57 wt. % weight loss for degradation of hemicellulose and cellulose in Figure 4.2 . The prominent peaks in the DTG plot attained in this region with the peak temperature at 320 °C were mainly because of cellulose decomposition [168]. An EFBF and POME sludge at 20 °C/min of nitrogen loss of 63.57 % of the cellulose and hemicellulose present in EFBF between 160 – 420 °C [206]. Stage III had a temperature range between 620 - 900 °C for recording a weight loss of about 10 wt. %. Lignin decomposition is slower due to a complex natural polymer of aromatic compounds to degrade with higher temperatures than cellulose and hemicellulose beyond 420 °C [206]. The third region had some mineral decomposition, and it could be advisable to undergo gasification of the samples studied above 700 °C for complete biomass utilization.



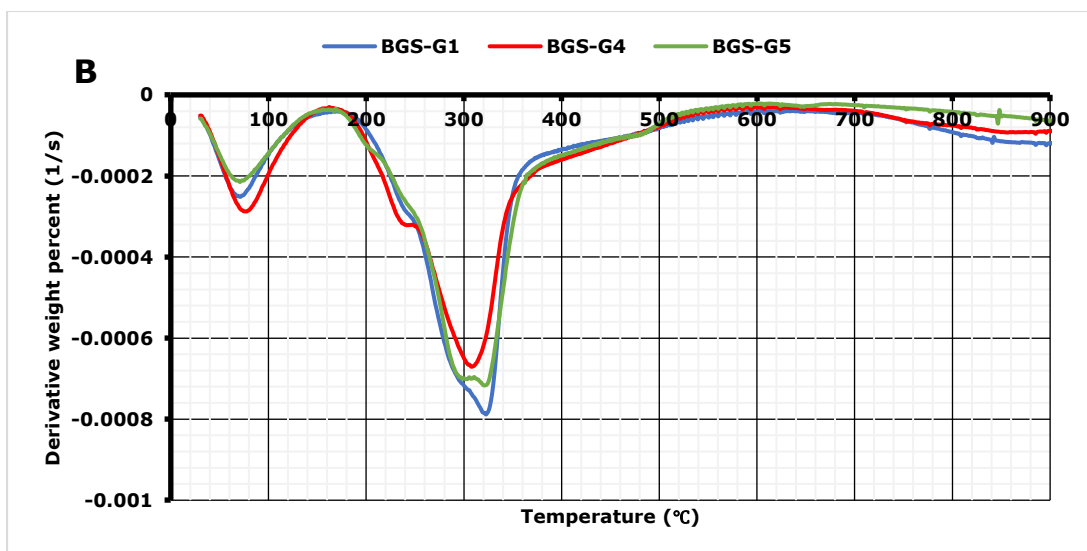


Figure 4.2: The (a) TGA and (b) DTG plots of BGS-G1, G4, & BGS-G5.

Thermogravimetric analysis of the DTG describes a suitable pyrolysis temperature range of 200 – 650 °C. The values of E_a and A can be related to specific heating rates by plotting $\ln [-\ln (1 - \alpha)]$ against $1/T$. In line with the weight loss analysis, the activation energy, Arrhenius factor, and coefficient of regression for the samples were determined by equations discussed earlier in Eqn. 3.2 - Eqn. 3.9.

4.2 The physicochemical analysis and intermediate pyrolysis of BGS-G1, SSS, & SNS.

This section studied the intermediate pyrolysis of three biomass types: BGS-G1, SSS and SNS to identify its energy potential for biofuel or bioenergy products. The analysis of raw BGS-G1, SSS and SNS biomass is shown in Figure 4.3 and the thermogravimetry analysis in Figure 4.2 and Figure 4.4. The intermediate pyrolysis

product yield and analysis are in Table 4.5, van Krevelen, FTIR, SEM and GCMS in. Figure 4.5-Figure 4.7 and Table 4.6.

Table 4.3: Ultimate, proximate, and EDX analysis of raw BGS-G1, SSS, and SNS.

Proximate Analysis			
Proximate parameters	BGS-G1	SSS	SNS
HHV(MJ/kg)	15.7	16.1	17.7
MC (wt. %)	10.7 ± 0.3	12.4 ± 0.3	12.3 ± 0.2
AC (wt. %)	10.0 ± 0.7	4.6 ± 0.3	2.0 ± 0.1
VM (wt. %)	67.3	73	61.2
FC (wt. %)	12	11	24.6
Ultimate parameters			
C (wt. %) *	39.7	34	45.2
H (wt. %) *	6.0	5.5	6.4
N (wt. %) *	1.2	0.7	0.4
S (wt. %) *	0.3	0.2	0.1
O (wt. %) *	32.1	42.6	33.6
EDX parameters			
C	50.0 ± 7.8	59.4 ± 4.28	46.7 ± 14.36
O	42.1 ± 4.1	39.8 ± 5.32	40.9 ± 7.32
Mg	0.1 ± 0.0	0.4 ± 0.30	0.1 ± 0.08
Al	2.9 ± 2.5	0.1 ± 0.00	0.9 ± 0.29
Si	2.5 ± 2.2	0.4 ± 0.00	10.0 ± 7.81
P	0.2 ± 0.0	0.6 ± 0.00	0.1 ± 0.01
S	0.1 ± 0.0	0.2 ± 0.00	0.13 ± 0.1
K	1.4 ± 0.4	0.2 ± 0.00	0.8 ± 0.51
Ca	0.2 ± 0.0	0.1 ± 0.00	0.2 ± 0.16
Fe	0.5 ± 0.3	0.1 ± 0.00	0.2 ± 0.03
Cl	0.1 ± 0.0	Nil	Nil

*Dry ash-free (daf) basis

4.2.1 Proximate analysis of BGS-G1, SSS and SNS

The ideal moisture content of feedstock for pyrolysis is ≤ 10 wt. % by weight [61]. Lower moisture content in biomass results in higher calorific value (HHV); BGS-G1, SSS, and SNS had MC values $\leq 12.4 \pm 0.3$ wt. % in Table 4.3, is the physicochemical analysis of the raw

biomass. Meanwhile, biomass with high volatile content produces high gas. In this study, the samples exhibited VM within (61.2 - 73.0 wt. %), which proves their decomposition potential. Less sulphur and higher VM content have an advantage in the gasification and pyrolysis processes in clean energy production. Fixed carbon serves as the primary heat generator during combustion, which estimates the total amount of char that can be produced. In Table 4.3 FC was ≤ 25 wt. %, however, the lower the FC, the higher the volatiles favour bio-oil production. The characteristics of an expected high value of FC are ≤ 25 wt. % for shell biomass, like those of wheat straw, miscanthus straw, bark, and sawdust [171]. The ash content of woody biomass is usually low, ≤ 2 wt. % in most species, while most biomass AC varies between 2.6 and 18.3 % [209]. The higher the AC, the more mineral and metallic compounds are present, affecting the product quality as fuel and decreasing the HHV. The alkali metals increase coke formation and fouling, interfering with the pyrolysis process and affecting bio-oil production [210]. The minimal mineral and ash content would lead to fewer challenges influencing energy/fuel production reactors. The HHV is the heat released per unit of fuel mass after combustion, including latent heat of vaporization. The results of the samples studied in Table 4.3 are relatively within the 15 - 18 MJ/kg, HHVs (Higher Heating Value) of the biomass.

4.2.2 Ultimate analysis of BGS-G1, SSS and SNS

Carbon is the most critical element in biomass which is crucial in determining its calorific value. The higher the carbon content in biomass, the higher its energy potential. The SSS biomass recorded the lowest carbon content of 34 wt. % and the highest SNS at 45.2 wt. % among the feedstocks analysed. Hydrogen contributes significantly to the overall value of heating, and the samples had hydrogen (H) content within 5.5 - 6.4 wt. % which is common for biomass. The current biomass samples studied had nitrogen content ≤ 1.2 wt. %, making them suitable for bioenergy conversion. In current samples, the sulphur content is within 0.1 - 0.3 wt. % (1000 - 3000 ppm), indicating a relatively lower proportion in the samples studied. The studied samples had their commonalities as the oxygen content was lower than the corresponding carbon content of the samples except for SSS having more oxygen than the carbon content in the biomass. Its nature of wide adaptability might characterize the oxygen level, productivity in marginal lands [211], drought resistance, waterlogging tolerance, and saline-alkali tolerance [27]. As investigated by Wright et al., (2017) the elemental analyses of sorghum biomass revealed carbon and oxygen at 43.72 and 49.91 wt. %, respectively [212]. The studied sample (SSS) in this

experiment recorded its oxygen and carbon as 42.6 and 34 wt. % respectively and constituting more oxygen in the raw sample.

4.2.3 Thermochemical analysis of BGS-G1, SSS and SNS.

The thermogravimetric analysis of BGS-G1 shows the TGA/DTG plot as the sample degrades in Figure 4.3 and Figure 4.4 respectively.

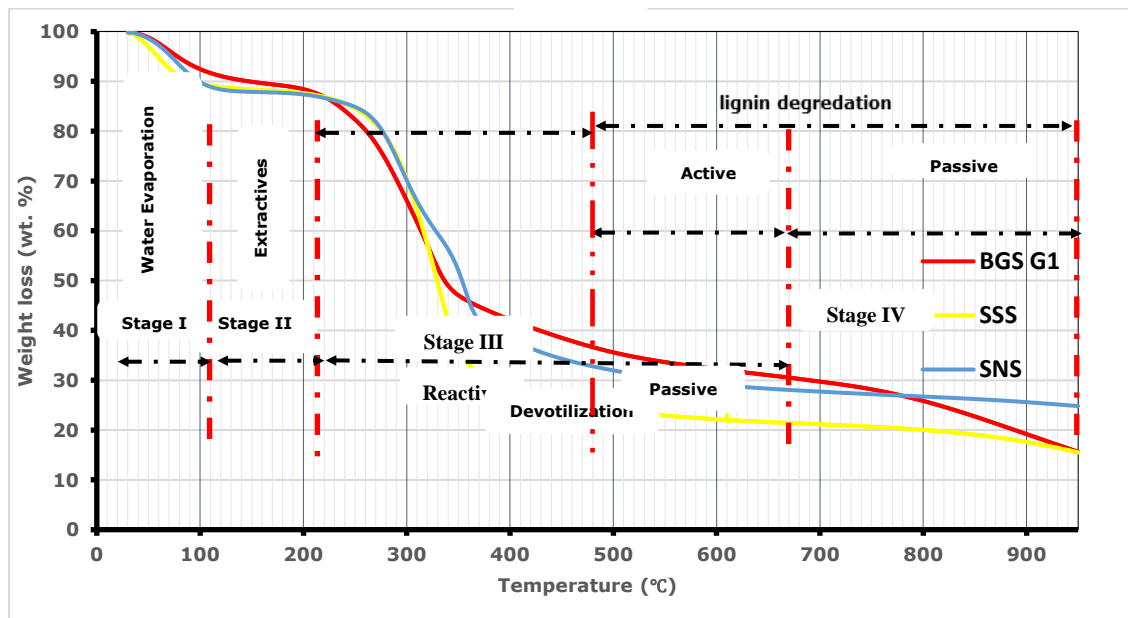


Figure 4.3: TGA plot of BGS-G1, SSS, & SNS.

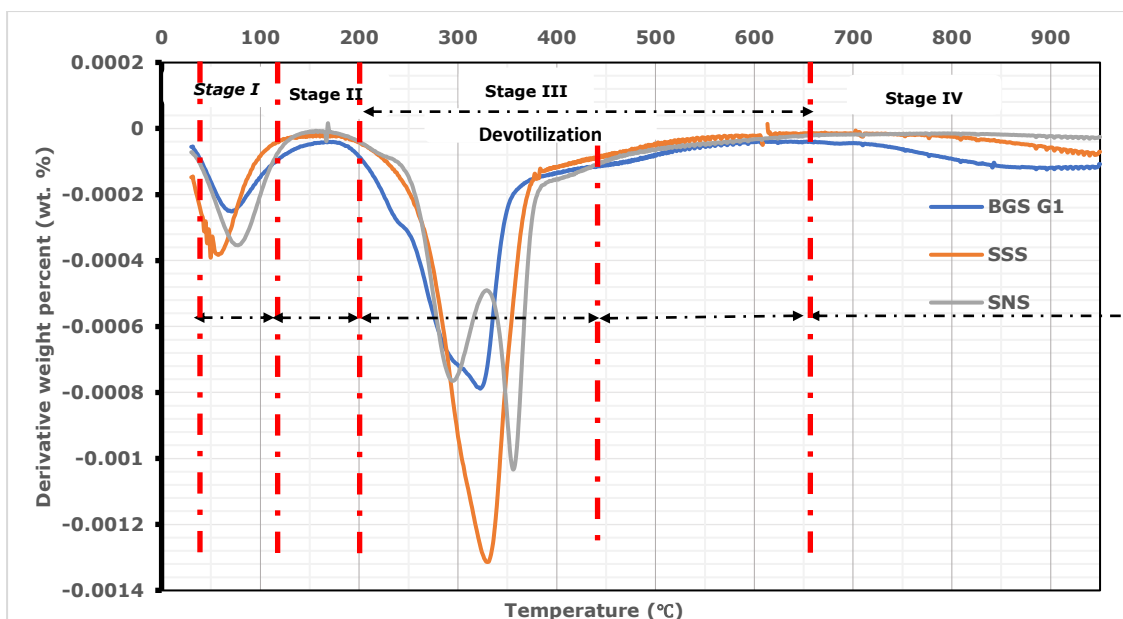


Figure 4.4: DTG plots of BGS-G 1, SSS, & SNS.

The TGA profile is divided into four stages in Figure 4.3. The first stage (moisture evaporation) is ≤ 110 °C, showing a rapid mass reduction as a result of the evaporation of moisture (water content). Stage II in Figure 4.3 ranges from 110 - 200 °C, and the thermal decomposition of extractives & hemicellulose results in weight loss at an average of 2.5 wt. % for all the samples. These samples (BGS 1, SSS, and SNS) contain nitrogenous compounds, contributing to weight loss at this stage [213]. Stage III in Figure 4.3 is in the temperature range of 200 - 450 °C and shows significant cellulose decomposition of weight loss on the TGA curve, accounting for 49.3 wt. %, 58.9 wt. %, and 49.8 wt. % for the samples BGS 1, SSS, and SNS respectively. The SSS had a higher devolatilization profile than the other samples, leading to more volatile compounds and bio-oil if adequately condensed. The devolatilization of hemicellulose and

cellulose occurs at about 150 - 430 °C [175]. The TGA stage IV showed gradual lignin decomposition and left both minerals and ash as the weight loss for SSS at around 24.8 wt. %, BGS-G1 and SNS were at an average of 15.7 wt. % at a temperature between 600 - 950 °C. As investigated by Mohammed et al., (2018) the TGA stage IV accounts for less than 5.50 wt. % weight loss, typical decomposition behaviour with a minimal carbohydrate in lignocellulosic materials. The DTG profile examination for the samples (BGS-G 1, SSS, and SNS) is shown in Figure 4.4 and data representation in Table 4.4. Due to its hardwood nature, two distinct peaks for SNS indicated the specific decomposition of hemicellulose and cellulose and a steep edge shoulder for BGS-G1 within the temperature range of 200 - 400 °C.

In Table 4.4 each of the kinetic triplets represents the physical concept of transition state theory, which links the activation energy (E_a) to the energy barrier and the pre-exponential factor (A) to the vibrational frequency of the activated complex. In this study, all samples had an activation energy of about 20.4 - 24.9 kJ/mol. Activation energy is the minimum energy required before molecules can initiate the reaction. The lower the activation energy, the faster the chemical reaction. Muhammed et al., (2015) observed that the lower activation energy may be attributed to effects of mass and heat transfer and the lower crystallinity index of the samples may

also facilitate cellulosic biomass degradation due to heat diffusion irresistibility [214]. The BGS-G1 activation energy is (20.43) lower compared to other samples (SSS and SNS) and therefore, BGS-G1 was more active in the reaction than the other samples in Table 4.4.

Table 4.4 showed the regression coefficient more converging at BGS-G1 as 0.9438 with a considerable exponential factor of 36.107. The moisture content (≤ 10.0 wt. %), extractives & cellulose devolatilization of all the samples were averagely equal except the hemicellulose & lignin decomposition of SSS stood at 83.7 wt. % higher the BGS-G1 and SNS, which is probably an indication of lower lignin present in the SSS sample.

Table 4.4: The Kinetic and TGA analysis

#No	Kinetic analysis and TGA	BGS-G1	SSS	SNS
1	E_a . (kJ/mol)	20.43	24.89	21.46
2	A	36.10739	94.32167	43.87463
3	R ²	0.9438	0.9196	0.9343
Stage (s)	TGA & DTG Stages of decomposition per temperature (°C) variation			
1	Moisture evaporation Weight loss (wt. %)	30 – 110 9.8	30 – 110 10.4	30 – 110 9.3
2	Extractives & cellulose devolatilization Temp. (°C) Weight loss (wt. %)	110-200 2.5	110-200 2.5	110-200 2.5
3	Hemicellulose & lignin decomposition Temp. (°C) Weight loss (wt. %)	150 – 650 49.3	149.2 - 652 58.9	125.3–479.3 & 479.3 – 674 49.8
4	Lignin decomposition Temp. (°C) Weight loss (wt. %)	620 – 950 15.7	652 - 950 24.8	674 – 950 15.7

4.2.4 Pyrolysis of BGS-G1, SSS and SNS product yield

The intermediate pyrolysis product yield results were determined using Eqn. 3.15 - Eqn. 3.17, as shown below. SSS had the highest bio-oil yield at 44.2 wt. %, which is significant compared to samples BGS-G1 and SNS at 38.0 and 39.6 wt. %, respectively. In one of the previous studies on pyrolysis of Bambara groundnut shells, process variables (temperature, heating, and nitrogen flow rate) were optimized using response surface methodology with a central composite design, and the optimum parameters at 600 °C, 50 °C/min, and 11 L/min yielded 36.49 wt. % bio-oil respectively 49. Their bio-oil yield was almost near to the current yield. However, a study by Mohammed et al., (2016) investigated the shells of two landraces (KARO and EX - Sokoto) in a vertical fixed bed pyrolysis reactor at a heating rate of 50 °C/min and nitrogen flow rate of 5 L/min. KARO shell produced more bio-oil and reached the maximum at 600 °C (37.21 wt. %) compared to EX - Sokoto with 32.79 wt. % under the same conditions. Nevertheless, the SSS in this present study recorded the highest yield in bio-oil of 44.2 wt. %, which seems comparable with the sweet sorghum bagasse study with the highest bio-oil outcome of 53.2 wt. % after treatment with 3 M NaOH [215]. The alkaline treatment affected the product distribution of, sweet sorghum bagasse, and more identified phenol derivatives were recorded compared to lower concentrations from the bio-oil.

Table 4.5: The bio-oil and bio-char proximate and ultimate analysis

PARAMETERS	BIO-OIL			BIO-CHAR		
	BGS-G1	SSS (N)	SNS	BGS-G1	SSS	SNS
Yield wt. %	38.0 ± 6.4	44.2 ± 6	39.7 ± 5.2	45.7 ± 4	27.1 ± 1.1	43.6 ± 6.0
HHV (MJ/kg)	23.7 ± 1.8	23.8 ± 1.8	26.5 ± 2.0	18.8 ± 1.2	22.5 ± 3.5	26.4 ± 1.8
Density (g/cm ³)	1.01 ± 0.0	1.04 ± 0.0	1.04 ± 0.0	-	-	-
pH	5.01	2.57	2.87	-	-	-
CHNS analysis						
C (wt. %)	52.9	56.3	63.3	48.4	74.9	61.3
H (wt. %)	00.8	07.5	08.3	04.0	02.9	04.7
N (wt. %)	00.9	01.5	01.6	01.2	00.5	00.7
S (wt. %)	00.4	00.2	00.2	00.5	00.7	01.0
O (wt. %)	45.1	34.5	26.6	45.9	21.00	32.3
O/C ratio	00.85	00.61	00.42	00.95	00.28	00.53
C wt. % Increase	24.95	39.60	28.59	17.97	54.6	26.26
EDX analysis wt. %						
C				49.96 ± 7.8	59.36 ± 4.28	46.74 ± 14.36
O				42.1 ± 4.1	39.83 ± 5.32	40.93 ± 7.32
Mg				0.07 ± 0.0	0.35 ± 0.30	0.14 ± 0.08
Al				2.99 ± 2.5	0.14 ± 0.00	0.90 ± 0.29
Si				2.45 ± 2.2	0.41 ± 0.00	10.01 ± 7.81
P				0.15 ± 0.0	0.6 ± 0.00	0.08 ± 0.01
S				0.13 ± 0.0	0.16 ± 0.00	0.13 ± 0.09
K				1.43 ± 0.4	0.16 ± 0.00	0.78 ± 0.51
Ca				0.20 ± 0.0	0.14 ± 0.00	0.23 ± 0.16
Fe				0.54 ± 0.3	0.12 ± 0.00	0.15 ± 0.03
Cl				0.06 ± 0.0		

The different agricultural residues used in pyrolysis studies resulted in similar bio-oil yields. An ablative pyrolysis laboratory reactor with rotating blades produced nearly 50 % (w/w) bio-oil from corncob pellets at optimum parametric temperature, inert gas flow rate, and fixed rotation speed of 550 °C, 5 L/min, and 6 Hz, respectively [216]. According to Kabir et al., (2017) the oil yield from oil palm mesocarp fibre and palm frond oil with a slow-heating fixed-bed reactor at 550 and 600 °C, had a maximum output of 48 wt. % and 47 wt. % bio-oil, respectively [219]. Salehi et al., (2009) studied the fast pyrolysis of sawdust in a fixed-bed system to produce biochar, biogas, and bio-oil between 20-27, 36-45, and 33-45 wt. %, respectively at a temperature of 500 °C [217]. Batch-scale slow pyrolysis of sawdust at a heating rate of 34 °C/min in a fixed-bed reactor yielded bio-oil (34.9 wt. %), biochar (38.6 wt. %), and pyro-gas (26.5 wt. %) at an optimum temperature of 500 °C [218]. Also, a study on sweet sorghum bagasse yielded a maximum of 15.94 wt. % bio-oil at 449.85 °C [27]. In the case of the SSS sample studied in this work, the yield (bio-oil and biochar) was high, 44.2 and 27.1 wt. %, respectively. According to Kabir et al., (2017), Higher bio-oil yield (48 wt. % and 47 wt. %) recorded [219] was resulted because the carbon is higher than the oxygen of OPMF (45.38 and 41.00 wt. %), while the PF (42.04 and 51.24 wt. %) compared to SSS carbon and oxygen content (34 and 42.6 wt. %) in terms of the weight percentage and percentage

composition might be responsible and not necessarily the process adopted. The higher carbon content would increase the bio-oil yield and the higher oxygen in SSS might facilitate the low bio-oil organic phase production. The fixed-bed reactor for OPMF and PF was (2.2 cm x 35 cm) compared to the reactor (Φ 25 x 120 cm) for the BGS-G1, SSS, and SNS experimental study. Modifying the reactor to confine the feeds avoids smearing the entire reactor and reduces the quantity of bio-oil produced.

4.2.5 Physicochemical analysis of BGS-G1, SSS, and SNS bio-oil and biochar

The HHV of bio-oils was higher than that of the biochar and biomass (BGS-G1, SSS, and SNS), as shown in Table 4.5 , respectively. Oil palm mesocarp fibre (OPMF) and palm frond (PF) oil studies revealed their HHV as 23 MJ/kg and 21 MJ/kg, respectively [219], which results are closely related to the current study. Nevertheless, the bio-oil and biochar from BGS-G1, SSS, and SNS showed their energy potential with comparatively high values of HHV for both the bio-oil and biochar than the raw biomass sample. According to Zhang et al. (2014), the pH of pyrolysis bio-oil is about 2.0 - 4.0 due to significant amounts of organic acids such as acetic acid, formic acid, etc [220]. The pH of BGS-G1 was 5.01, and not typical for bio-oils from lignocellulosic biomass. According to Jackson, (2011) the pH value of bio-oil increases while increasing the composition of the additive and

operating temperature [221]. However, in these situations, it might be due to the high amount of free fatty acid (carboxylic acid) compounds present in the GC-MS analysis of BGS-G1. The other two bio-oils have high acidity, which may lead to depletion of oil additives to reduce the wearing and tearing due to an increase in acid number or excessive oxidation of the oil, resulting in corrosion [220]. The acidity of the bio-oil could be reduced by forming an ester, thereby improving its pH value [222]. The intermediate pyrolysis product yield results were determined and show the bio-oil sample as their density in the range of 1.01 - 0.04 g/cm³, typical of bio-oil densities. The geological ageing of the fuel (biomass) lowers the atomic ratio of O to C, the older the fuel, the higher the energy content. The atomic ratio of biomass O/C and H/C classified for solid fuels is 0.4 - ≥ 1 and 1.0 - 1.8, respectively [223]. Different woods and bio-fibres contain different O/C ratios within 0.75 - 1.50, while the O/C ratio of fossil fuels (coal, charcoal, and tar) is 0 - 0.30 [224]. The higher H/C_{eff} ratio of biomass produces a higher content of saturated hydrocarbons in pyrolysis oil, while the lower H/C_{eff} ratio produces a higher range of ketones and phenolic compounds [225]. The energy source with a relatively lower O/C ratio has a high energy density and higher HHV because the chemical energy in C-C (carbon content) bonds is higher than in C-O bonds [226]. Figure 4.5 is the biochar and bio-oil Van Krevelen plot of BGS-G1, SSS, and SNS demonstrating H/C and O/C of a higher heating value and a promising biofuel for enriching energy

potential compared to the raw biomass samples. The EDX analysis of biomass in Table 4.5 shows relatively low amounts of Al, Si, and K (BGS-G 1), K, and Al, Si, and K (SNS) on their surface. BGS-G1, SSS, and SNS could have catalytic potential due to the content of metals such as Al, Si, and Fe.

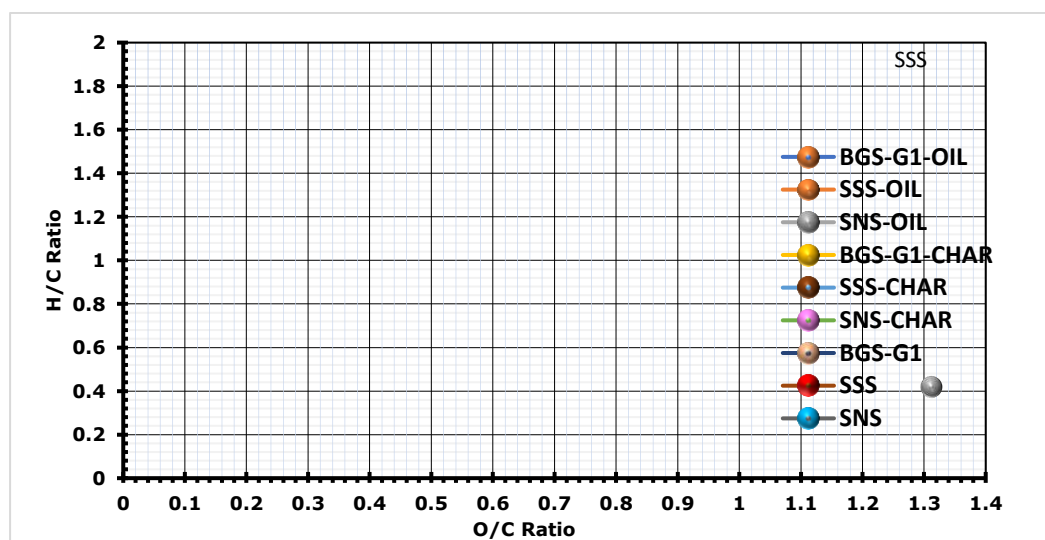


Figure 4.5: Van Krevelen plot of BGS, SSS, and SNS products.

Figure 4.5 shows the CHNS results, the carbon content in the biomass, bio-oils, and biochar in the BGS-G1, SSS and SNS, indicating improved and significant energy potential generation. The BGS-G1, SSS, and SNS carbon content of biomass from Table 4.3 is the physicochemical analysis of the raw biomasses. The oxygen content was within (34 - 45.2) wt. % rose by 24.95 - 39.60 % for bio-oil and 17.97 - 54.61 % for biochar in Table 4.5. The tested oxygen content in the bio-oil and biochar samples was lower than the carbon content in the corresponding biomass. The biofuels with higher oxygen

content are less suitable for energy production. Biomass with higher oxygen and hydrogen but less carbon reduces their HHV because energy contained in carbon-hydrogen and carbon-oxygen bonds are lesser than carbon-carbon bonds [203]. The oxygen content in the structure of phenolic compounds is very complex to be broken down (or removed) in the form of water to improve the heating values. The fuel efficiency depends on the proximate and ultimate analysis of biomass and the atomic ratio of H/C and O/C [201]. The elemental analysis of biomass recognizes that high hydrogen and nitrogen content in biomass inhibits energy generation and production.

4.2.6 Fourier transform infrared (FTIR) of BGS-G1, SSS and SNS

Figure 4.6(a) shows FTIR spectra of the BGS-G1 bio-oils, in the case of BGS-G1, the bands in the range 2922 - 2852 and 1520 - 1464 1/cm were alkane and alkene compounds, probably due to C-H stretching vibrations reported by Morali et al., (2016) [227]. Kotaiah et al., (2017) noticed bio-oil had peaks at wavelength 2850 - 3000 1/cm and 1400 - 1620 1/cm for Alkane (C-H stretch intense) and aromatic (C=C stretch medium-weak, multiple bands) functional groups [27]. Figure 4.6(a) shows the FTIR plot of the SSS and SNS samples had the bands of the functional groups at 3600 - 3200 1/cm, 1815 - 1628 1/cm, 1520 - 1464 1/cm, 1271 - 1206 1/cm, and 1109 - 755 1/cm representing the O-H, C=O, C-H, C-O, and C-H stretching,

respectively. A peak at 2922 – 2852 1/cm represents C-H stretching for alkene, ketone, and aldehyde compounds. Figure 4.6(a) depicts that the BGS-G1, SSS, and SNS bio-oil results had chemicals such as BGS-G1(alkanes & alkenes), SSS (phenols, alcohols, ketones, aldehydes, esters & alkenes), SNS (alkanes, ketones, aldehydes, alkenes & esters).

Figure 4.6(b) shows the biochar FTIR spectra had the functional group band for BGS-G1 at 1520 - 1464 1/cm indicating alkene compounds. The spectrum of the biochar functional groups of 1400 and 1600 1/cm is attributed to the O-H or C-O stretching vibration of phenol or the C=O stretching vibration of aromatic rings [228]. The FTIR spectra of SSS and SNS biochar confirmed the functional groups from stretching vibrations and wavelength at 1085, 1750, 2848 – 2933, and 3618 – 3858 1/cm as -C-O, -C=O, C-H, and O-H groups respectively [229]. The reported bands could correlate with phosphate (PO_4^{3-}), or Si-O-Si in-plane (unbalanced stretching) or C=O stretching vibrational structures observed between 1000 1/cm and 1100 1/cm [228]. These bands are absent in biochar samples pyrolyzed at 600 °C, as prevalent in BGS-G1 above, because cleavage of these organic groups contributes to higher mass loss during thermal decomposition and evolution of gases (e.g., CO₂). The peak around the wavelength of 900 1/cm is assigned to C - O - C of

glycosidic bond, while the peak at 1200 is C - O and C - H in polysaccharides and lignin. The wavelength of 1370 1/cm depicts O - H phenolic compounds, 1510 1/cm as C = C in lignin, and 1550 1/cm as C-O in aromatic rings [230]. The biochar contains chemicals such as BGS-G1 (alkenes), SSS (phenols, alcohols, ketones, aldehydes, esters & alkenes), SNS (phenols, alcohols, alkanes, ketones, aldehydes, alkenes & esters), respectively.

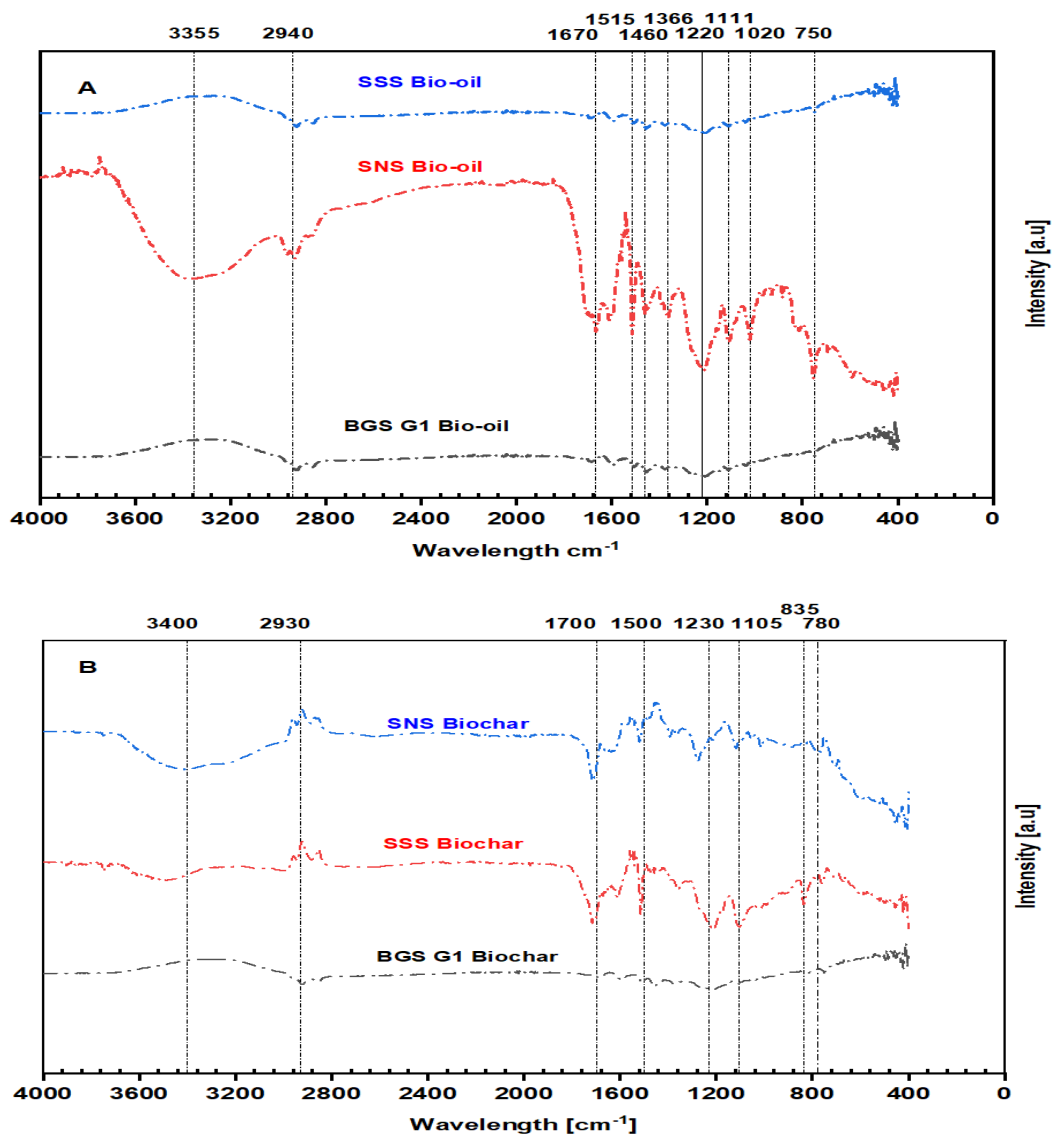


Figure 4.6: The BGS, SSS, & SNS FTIR analysis of (a) bio-oil and (b) biochar.

Table 4.8, shows the gas chromatography and mass spectrometry (GC-MS) analysis of BGS-G1, SSS, and SNS bio-oils. The compounds identified with high quality in MS spectra were grouped as major chemical groups such as ketones, aldehydes, phenols, fatty acids, and benzene, with 40, 46, and 24 compounds for BGS-G1, SSS, and SNS, respectively. As reported by Pittman et al. (2012) bio-oils contain aldehydes, carboxylic acids, hydroxy aldehydes, and ketones. It includes phenols, furan, levoglucosan, mono-, di- and higher saccharides. After pyrolysis, the aldehydes, carboxylic acids, hydroxyl aldehydes, and ketones are among the complex oxygenated products from biomass cellulose and lignin components [232]. Levoglucosan (1,6-anhydrous- β -D-glucopyranose) (LG) is an anhydrous sugar and the main product of cellulose from pyrolysis [233]. The anhydrous sugar is mainly cellulose, contributing to ~67 – 79 wt. % of total pyrolytic sugars in bio-oil, while the remaining are from hemicellulose. The pyrolytic sugars > 96% are in the H₂O-soluble fraction of bio-oil. They are mainly in cellulose-derived anhydrous sugars such as levoglucosan and cellobiose [234]. Furans, in bio-oil, are primarily from the decomposition of hemicellulose, while cellulose contributes minimally but produces more hydroxymethyl-furfural and 2-furyl methanol [235]. The fatty acids of BGS-G1, SSS, and SNS are at 11.4, 5.5, and 0.0 area % of this study. The main composition of the bio-oils (BGS-G1, SSS and SNS) was the phenolic compounds containing about 25.9, 30.9, and 15.6

area %, respectively. As reported by Fan, (2017) over 40 wt. % bio-oil and about 20 wt. % of it are phenolic compounds produced at optimum pyrolysis temperature [236]. Indeed, these phenolics are mainly compounds in bio-oil derived from lignin [237]. The phenols are weak acids found in high concentrations with an insignificant impact on storage facilities of the corrosion properties of the oil [238]. Phenols (phenol, phenol,3-ethyl-, p-cresol) in bio-oil were produced from the lignin component [239]. It generally increased with the high pyrolysis temperatures due to the breakage of various C-C and C-O-C ether bonds of lignin of the nitrogen-containing organics [240]. The high content of esters and phenols is more valuable as bioenergy than traditional fossil fuels [195]. These are the essential compounds in bio-oils and have diverse potential. Phenolic-rich extracted bio-oil obtained higher aromatic hydrocarbon yield (7.3 wt. % increased from 1.1 wt. %) and lower coke yield (1.42 wt. % decrease from 15.79 wt. %) than raw bio-oil [241]. It is upgradable to enhance more aromatic hydrocarbon via a suitable catalyst.

Table 4. 6: The GCMS classification according to the major chemicals area percentage.

S/NO	RT	KETONE COMPOUND	BGA-G1 Area %	SSS Area %	SNS Area %
1	3.043	Cyclopentanone	0.533	0.405	-
2	3.759	2-Cyclopenten-1-one	-	0.64	0.416
3	3.824	Cyclopentanone, 2-methyl-	0.435	-	-
4	4.949	2-Cyclopenten-1-one, 2-methyl	0.527	0.565	-
5	5.079	Ethanone, 1-(2-furanyl)-	-	0.473	-
6	5.139	Butyrolactone	-	0.455	-
7	6.075	2-Cyclopenten-1-one, 3-methyl-	0.539	-	-
8	6.51	2-Cyclopenten-1-one, 3,4-dimethyl-	0.451	-	-
9	6.985	Cyclohexene, 1-methyl-5-(1-methylethenyl)-, (R)-	-	-	0.484
10	7.145	2-Cyclopenten-1-one, 2-hydroxy-3-methyl-	-	1.11	-
11	7.185	2-Cyclopenten-1-one, 2,3-dimethyl	0.85	0.541	-
12	10.907	1H-I-en-1-one, 2,3-dihydro-4-Hydroxy-3-	-	0.407	-
13	11.237	methylacetophenone	1.086	-	-
14	14.443	3',5'-Dimethoxyacetophenone	-	0.592	-
15	16.699	2-Pentanone, 1-(2,4,6-trihydroxyphenyl)	-	0.48	-
TOTAL			4.421	5.688	0.9
ALDEHYDE COMPOUND					
16	3.689	Furfural	-	1.066	1.142

17	4.194	2-Furanmethanol	0.429	0.503	-
18	5.905	2-Furancarboxaldehyde, methyl-	-	-	-
TOTAL			0.429	1.569	1.142
PHENOLIC COMPOUNDS					
19	6.345	Phenol	3.15	2.865	0.862
20	7.5	Phenol, 2-methyl-	2.362	1.897	0.685
21	7.87	Phenol, 3-methyl-	3.113	2.288	-
22	7.925	p-Cresol	-	-	1.115
23	7.94	Phenol, 2-methoxy-	2.834	2.829	2.166
24	8.286	Phenol, 2,6-dimethyl-	0.46	-	-
25	8.781	Phenol, 2-ethyl-	0.63	0.309	-
26	8.946	Phenol, 2,4-dimethyl-	1.396	1.204	0.425
27	8.981	Phenol, 2-ethyl-	0.749	-	0.309
28	9.241	Phenol, 4-ethyl-	1.227	5.118	0.269
29	9.351	2-Methoxy-5-methylphenol	-	0.567	0.619
30	9.511	2-Methoxy-5-methylphenol	1.077	0.954	1.992
31	10.166	m-Guaiacol	0.587	-	-
32	11.247	2-Methoxy-4-vinylphenol	-	2.461	0.767
33	11.752	Phenol, 2,6-dimethoxy-	1.424	3.994	1.825
34	11.837	Phenol, 2-methoxy-4-(1-propenyl)-	-	-	0.617
35	11.917	Phenol, 2-methoxy-4-propyl-	1.094	0.58	0.863
36	12.472	Phenol, 2-methoxy-6-(1-propenyl)-	0.534	0.691	0.617
37	13.027	Phenol, 2-methoxy-4-(1-propenyl)-	1.324	0.88	-
38	10.236	Phenol, 4-ethyl-3-methyl-	0.629	0.407	-

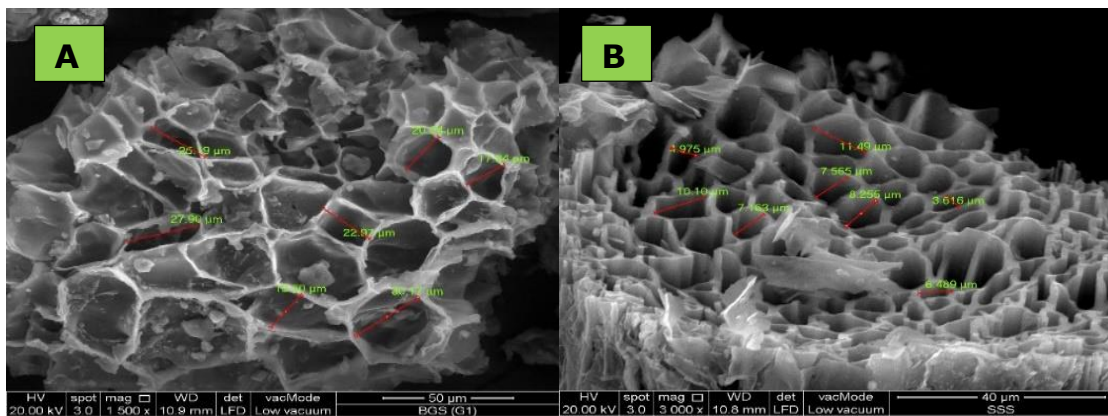
39	10.561	Phenol, 2-ethyl-4-methyl-	0.887	-	
40	10.721	Phenol, 4-ethyl-2-methoxy-	2.515	2.828	2.485
41	15.964	Phenol, 2,6-dimethoxy-4-(2-propenyl)-	-	1.012	-
TOTAL			25.992	30.884	15.616
FATTY ACID					
42	18.635	n-Hexadecanoic acid	3.601	2.208	-
43	20.195	9,12-Octadecadienoic acid (Z, Z)-	0.976	0.574	-
44	20.25	9-Octadecenoic acid, (E)-	3.021	1.894	-
45	20.46	Octadecanoic acid	2.35	0.801	-
46	22.131	9-Octadecenamide, (Z)-	0.506	-	-
47	23.417	Disooctyl phthalate	-	-	-
48	25.237	13-Docosenamide, (Z)-	0.914	-	-
49	25.253	13-Docosenamide, (Z)-	-	-	-
TOTAL			11.368	5.477	0
BENZENE COMPOUNDS					
50	9.796	Catechol	-	0.954	0.723
51	9.911	Benzofuran, 4,7-dimethyl-	-	0.46	-
52	10.041	Benzofuran, 2,3-dihydro	-	-	-
53	10.096	Benzaldehyde, 3-methyl-	-	6.045	-
54	10.552	1,2-Benzenediol, 3-methoxy-	-	0.875	0.409
55	10.712	1,2-Benzenediol, 3-methyl-	-	0.396	-
56	11.147	1,2-Benzenediol, 4-methyl-	-	0.384	0.643
57	11.462	Benzene, 1-methoxy-4-propyl-	0.523	-	-
58	12.327	4-Ethylcatechol	0.518	0.654	0.555
59	12.817	1,4-Benzenediol, 2,5-dimethyl	-	0.942	-
60	12.978	1,2,4-Trimethoxybenzene	0.825	-	-

61	13.913	Benzene, 1,2,3-trimethoxy-5-methyl-	0.477	1.525	-
62	11.147	1,2-Benzenediol, 4-methyl-	-	0.384	0.643
63	11.462	Benzene, 1-methoxy-4-propyl-	0.523	-	-
64	12.327	4-Ethylcatechol	0.518	0.654	0.555
65	12.817	1,4-Benzenediol, 2,5-dimethyl	-	0.942	-
66	12.978	1,2,4-Trimethoxybenzene	0.825	-	-
67	13.913	Benzene, 1,2,3-trimethoxy-5-methyl-	0.477	1.525	-
TOTAL			4.686	15.74	3.528
GRAND TOTAL			46.896	59.358	21.186

- Note: Indicates not detected (ND)

4.2.7 Field emission scanning electron microscopy-energy dispersive x-ray (FESEM/EDX).

Figure 4.7 illustrates the FESEM image in BGS-G1, SSS, and SNS biochar samples at 40 μm and shows a typical image of the metal-free amorphous carbon structure. The samples exhibited round-shaped silica bodies on the fibre, which were about $\geq 10 \mu\text{m}$ in size, and their matrix consisted of a lignin layer covering the entire surface strand. The BGS-G1, SSS, and SNS samples exhibited a rough dispersed surface and high porosity. The resulting biochar's porous structure showed various shapes in the macro-and-mesopores. According to Ghani et al., (2008), the enhanced properties of the pores are by the pyrolysis reaction in the presence of nitrogen/oxygen at high temperatures [201].



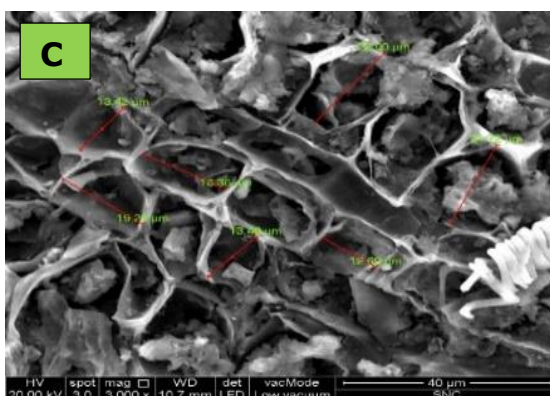


Figure 4.7: SEM-EDX (a) BGS-G1 (1,500X, 50 μm), (b) SSS (3000X, 40 μm) (c) SNS (3000X, 40 μm) image analyses.

The SSS sample has long passages of about 10.10 μm pore size and a smooth surface resembling a series of parallel lines. As reported by Ghani et al., (2008) the images of the aligned honeycomb-like groups recorded pores of about 10 μm in diameter on the surface of the biochar, most of which are composed of the carbon skeleton of the raw material biological capillary. The fibrous structure of the biochar indicated that the rubber wood is a softwood material and crystalline [243], which illustrates the same softwood for SSS images in Figure 4.7. The pores are cross-linked and categorized as hardwood material, unlike activated rubber wood. The rate of pore formation could exceed pore destruction as pores enlarge and collapse in the earlier or later stages of pyrolysis and vice versa. However, a 5 - 6 μm pore diameter with a membrane thickness of 2.3 - 2.66 μm tends to have water holding capacity [244]. Biomass physical and chemical activation produces biochar with high surface area and adjustable porosity [245]. High-temperature biomass processing produces

biochar and activated carbon of a significant porosity and surface area [246]. The capillary structure of biochar is affected by pyrolysis temperatures below 450 °C; it is less pronounced. At the same time, the temperature of 450 - 850 °C shows that the structure causes micropores at hexagonal planes and condensed volatiles. That leads to partial blocking of porosity of biochar production from waste rubber-wood-sawdust.

From Figure 4.7(a, c), it is evident that the porosity of BGS-G1 and SNS was in the range of 10 - 30 µm. Generally, the porosity of biochar with 30 µm holds H₂O in place. According to Zheng et al., (2022) the effect of pyrolysis temperature on the biochar nutrient and water retention capacity. Its pore diameter of 5 - 10 µm as the micropore area of green waste biochar pyrolyzed at 600 °C [102]. The surface area formed by biochar is its micropore area, which significantly affects its water adsorption capacity [243]. However, its use depends on the contact with the surface, whether for catalytic or adsorption activity. Due to SNS's porous nature, the FESEM images confirmed biochar's possible application for adsorption/desorption studies, water treatment, purification, soil enrichment, and carbon energy production.

The EDX spectrum of the biochar showed significant elements (e.g., carbon, oxygen, calcium, phosphorus, magnesium, and potassium).

The mineral elements are similar for almost all the biochar studied. The significant minerals for SSS and SNS are Si, Al, K, and Al, Si, respectively, elements on the k-shell of the sample atom after the gamma-ray bombardment are generated according to their weight composition. In addition, the biochar contained P, Ca, and Mg at a relatively high level compared to the mineral element analyses. The EDX spectra of biochar derived from manure confirmed N, P, Ca, Mg, and K are valuable soil nutrient enrichment [181], and the pore, surface, and chemical properties of SEM-EDX mesoporous biochar as excellent medium for soil enrichment [181].

4.3 The role of various inert gases (N₂, CO₂, and N₂/CO₂) in intermediate pyrolysis on BGS.

4.3.1 Feedstock properties

Due to the similarity in the physicochemical properties of SSS with BGS-G1, BGS-G1 was used for inert gas pyrolysis. The BGS feedstock proximate properties constitute HHV, MC, AC, VM, and FC as 15.7 MJ/kg, 10.7 ± 0.3 wt. %, 10.0 ± 0.7 wt. %, 67.3 wt. %, and 12 wt. %, respectively, while the CHNS analysis of BGS biomass resulted in 39.7, 6.0, 1.2, 0.3, and 42.8 wt. % for carbon, hydrogen, nitrogen, sulphur, and oxygen, respectively.

4.3.2 Product yields for different inert gases and flow rates.

Figure 4.8 shows the yields of intermediate pyrolysis products at 5, 17.5, and 30 mL/min flow rates for different inert gases (N_2 , CO_2 , and N_2/CO_2). In the pyrolysis of BGS, the resulting bio-oil, biochar and syngas generally maintained an average equal yield across the different inert gases at their respective flow rates. The bio-oil yields during the inert gases (N_2 , CO_2 , and N_2/CO_2) and their respective flow rates (5, 17.5, and 30) mL/min used, illustrate that the inert gases do not significantly affect the product yield examined in this study. In a similar study, there was little or no difference in product yield (bio-oil) in the various atmospheres (Ar , N_2 , and CO_2), ranging from 23.56 – 32.88 %, with CO_2 recording the most negligible yield of 25.25 % and Ar was 32.88 % of the initial mass of the Brewer's Spent Grain (BSG) at 600 °C [247].

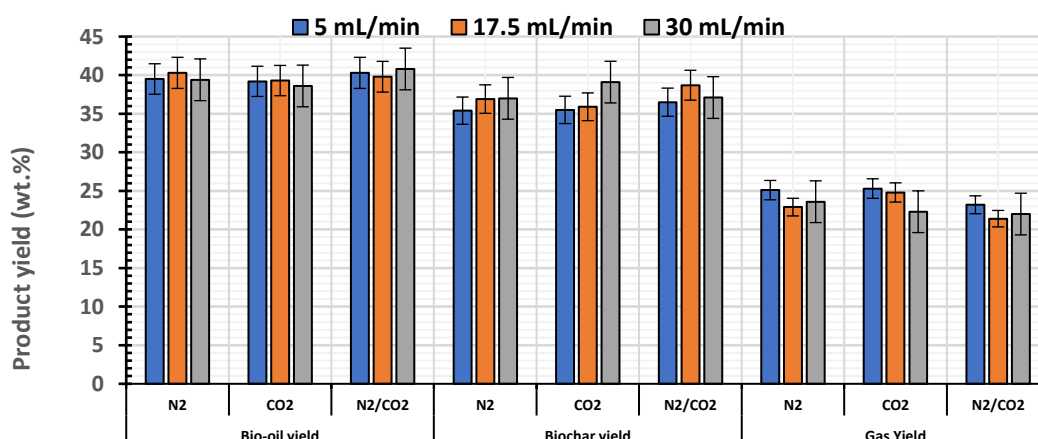


Figure 4.8: Intermediate pyrolysis products yield at 5, 17.5, and 30 mL/min flow rates for different inert gases (N_2 , CO_2 , and N_2/CO_2).

There was a slight increase in biochar when the flow rate of CO₂ increased from 17.5 to 30 mL/min, which might be a result of carbon capture from Ca or other alkaline metals in biomass. A modest degree of carbon capture can be expected at a higher flow rate of CO₂ at 30 mL/min. A relative increase in biochar was noticed for the increase in the flow rate of pyrolysis gases N₂ and CO₂. However, their combined effect declined biochar yield for the increase in N₂/CO₂ flow rate, from 17.5 to 30 mL/min. It can be deduced that, at a higher flow rate, carbon capture from CO₂ cannot occur. However, more heat distribution can happen due to the combined effect of a higher flow rate of N₂ and a lower heat capacity of CO₂. Therefore, a simultaneous increase was observed in both bio-oil and gas. The carbon content in the biochar of CO₂ was the highest from the CHNS in Table 4.7. According to Guizani et al., (2014), CO₂ had an impact on gas, biochar yield, and their respective properties [248]. Bieniek et al., (2022) investigated the effect that carrier gases (argon, nitrogen, and carbon dioxide), at 500, 600, and 700 °C, have on the quality and yield in a brewer's spent grain intermediate pyrolysis. When the temperature increased from 500–700 °C, the char yield decreased from 28 wt. % to 19 wt. %. However, the char obtained in the CO₂ atmosphere had approximately 2 % more carbon but did not affect the combustion properties (ignition and burnout temperatures) [247]. In addition, the acid concentration of the oil fraction depended on the order of the carrier gas, as Ar > N₂ > CO₂. [25]. CO₂, as a reaction

medium, provides thermal cracking of harmful organic compounds and significantly improves the thermal efficiency of biomass pyrolysis, yielding a more intense biomass decomposition than in an N₂ atmosphere, and improving biochar adsorption capacity [249].

Table 4.7: The CHNS of biomass, product yield and their EDX analysis for the inert gases at 17.5 mL/min.

S/No	Components	C	H	N	S						
1	#RAW-BGS	39.7	6	1.2	0.3						
#	Bio-oil										
1	BGS-N ₂	60.49	3.035	2.56	0.377						
2	BGS-CO ₂	53.57	2.631	1.66	0.257						
3	BGS-N ₂ /CO ₂	58.62	2.734	2.51	0.347						
#	Biochar										
1	BGS-N ₂	50.04	2.659	1.9	0.253						
2	BGS-CO ₂	58.13	2.718	1.38	0.157						
3	BGS-N ₂ /CO ₂	55.79	2.525	1.99	0.264						
#	EDX	C	O	K	Al	Si	S	Cl	Mg K	Fe K	P K
1	BGS-N ₂	68.7 ± 3.0	22.7 ± 4.6	10.5 ± 5.9	1.7 ± 1.6	2.2 ± 2.2	0.4 ± 0.1	10.4 ± 0.1	0.2 ± 0.0	0.9 ± 1.1	
2	BGS-CO ₂	50.1 ± 5.0	37.8 ± 3.8	9.1 ± 5.1	5.5 ± 3.9	5.1 ± 3.2	0.3 ± 0.2	20.2 ± 0.1	0.3 ± 0.1	11.3 ± 1.0	1.3
3	BGS-N ₂ /CO ₂	57.2 ± 8.6	27.0 ± 3.7	9.2 ± 3.7	2.2 ± 0.8	2.4 ± 1.0	0.2 ± 0.1	10.3 ± 0.0	0.3 ± 0.2	20.5 ± 0.2	1.0 ± 0.4

Note: RAW-BGS is raw biomass as received

4.3.3 Bio-oil energy and pH of bio-oil

Figure 4.9 shows the HHV of the bio-oil produced in the presence of carrier gases: nitrogen, carbon dioxide, and flue gas, at varying flow rates. During the investigation, the HHV for N₂ was lower in the pyrolysis products than its raw biomass and CO₂ or N₂/CO₂. There was no significant difference between the HHV of bio-oils produced in the presence of CO₂ or N₂/CO₂, as the standard deviation was approximately two (2.0), which was a trend in HHV for bio-oils across the flow rates. The reason for the high standard deviation for BGS-N₂ bio-oil could be the heterogeneous nature of bio-oil. In the presence of N₂/CO₂, the HHV of bio-oil was higher, at 17.5 mL/min, compared to other flow rates (5 and 30 mL/min). This suggests that CO₂ influences bio-oil HHV; however, as the flow rate increased, the HHV decreased, due to the high amount of N₂. These observations revealed that the high flow rate of N₂ promoted the decomposition of biomass, and many high calorific value components escaped as uncondensed gas. Similar results were noticed for yard waste torrefaction in inert gases (N₂, CO₂, and N₂/CO₂) environments. Carbon dioxide gave the best carrier gas for improved energy, in which HHV enhanced from 15.6–22.2 MJ/kg [250]. This depicts the significant impact of CO₂ as an inert gas. As reported by Jaideep et al., (2021) carbon dioxide was the best

carrier gas among N_2 , CO_2 , and flue gas in energy intensification, as it enhanced the HHV and the energy yield [250]. The torrefied yard waste study concluded that the lower heat capacity of CO_2 might be responsible for the improvement of the properties of the torrefied waste. According to Onsree et al., (2020), CO_2 in the reacting gas (0 – 18 % v/v balanced with N_2) concentration with higher torrefaction temperatures enhances solid yields, which enables overall higher thermal inertia as the specific heat of CO_2 is more significant than N_2 , and N_2 removes some heat in the process, and chemical reactions, as well as the catalytic reaction of CO_2 with the feed (biomass pellets) [251].

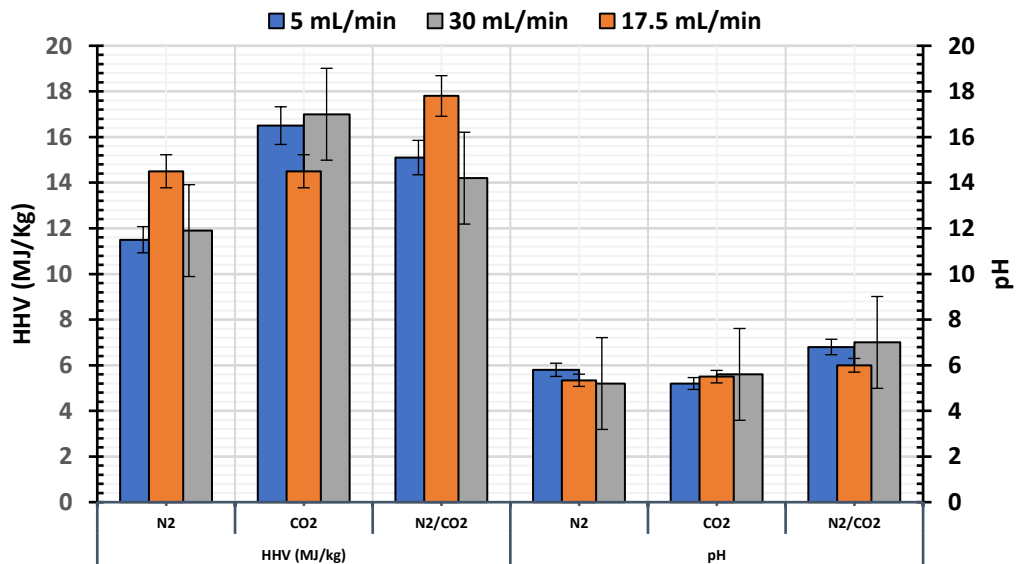


Figure 4.9: HHV (MJ/kg) and pH of bio-oils produced at 5, 17.5, and 30 mL/min flow rates for different inert gases (N_2 , CO_2 , and N_2/CO_2).

In Figure 4.9, the pH value of the bio-oil produced was 5.2 – 7, while bio-oil produced in the presence of N₂/CO₂ had an almost neutral pH and was in the range of some biomass pyrolysis in several studies. In GC-MS analysis results affirmed that this study recorded minimum acid in the pyrolysis bio-oil. Pyrolysis of agricultural and natural resources reported a bio-oil with a pH ranging between 2.8 – 4.0 [252]. According to Aziz et al., (2017), the esterification process has improved the pH value from 3.37 to 5.09 – 5.12 [253]. The tendency of the pH value of the produced bio-oil in this study towards neutrality may be due to esters present in the bio-oil BGS samples of the GC-MS analysis which is quite remarkable. The bio-oil could be useful in avoiding corrosion during application in industries, machinery, and the transportation sector as an energy source.

The CHNS analysis in Table 4.7 shows the raw biomass with 39.7 wt. %, compared with the bio-oil products with high carbon content within 53.6 – 60.5 wt. %, representing an improved carbon content. Similarly, the biochar carbon from CHNS analysis was at 50.0 – 58.1 wt. %, which, relatively, agreed with the EDX surface analysis at 50.1 – 68.7 wt. %. The carbon content of biochar for EDX analysis showed that BGS-N₂ had higher carbon than the other two biochar samples, which is in contrast to the CHNS results. One would expect

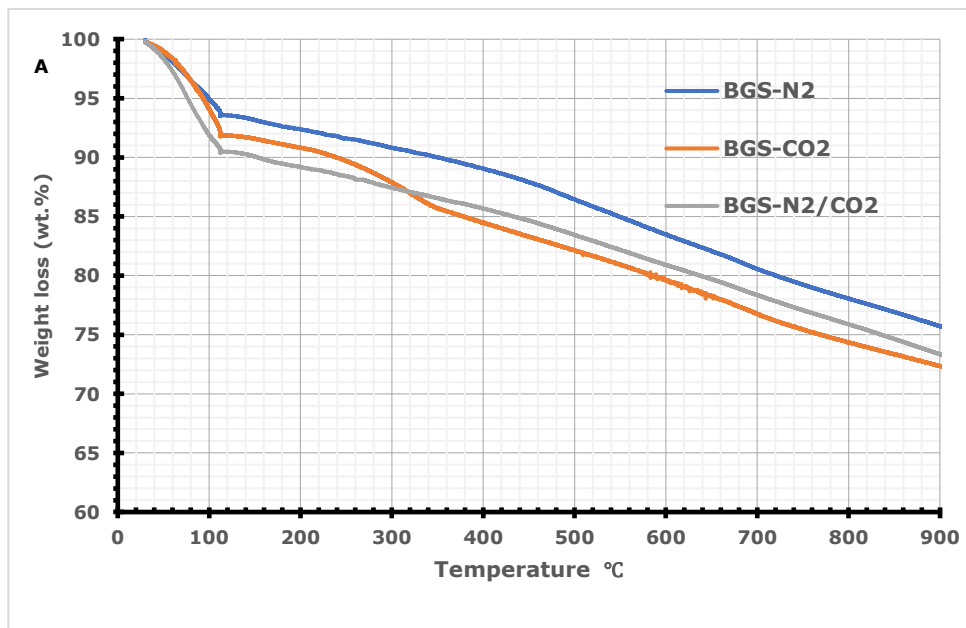
the presence of some carbon capture of CO₂ during pyrolysis, in the form of carbonates for the other two biochar samples. Therefore, BGS-CO₂ and BGS-N₂/CO₂ biochar have higher carbon content than BGS-N₂, however, EDX analysis cannot detect this carbon. In addition, EDX is a locally specialized analysis and, therefore, some surfaces can have higher amounts than other surfaces. The inert gas, N₂, showed the highest bio-oil carbon content, while CO₂ had the lowest amount of carbon. As mentioned earlier, N₂ promoted biomass decomposition, producing more carbon in bio-oil. The hydrogen contents of the bio-oils were ≤ 3.04 wt. %, while the hydrogen contents of all the biochar were ≤ 2.72 wt. %, which was relatively low for bio-oil compared to other studies. However, similar hydrogen contents for biochar were noted in the literature [202]. The nitrogen contents (N) for the bio-oils were ≤ 2.6 wt. %, whereas for biochar they were recorded as 2.0 ± 0.0 wt. %. The sulphur contents (S) in bio-oils were ≤ 0.377 wt. %, which were above the set standards of 0.05 mass % in ASTM (American Society for Testing Materials) D7544. The studied bio-oil H/C ratios were 0.58 – 0.6, which were lower than that of the raw BGS (1.8). The bio-oil H/C ratios tended toward the coal and anthracite. Alvarez et al., (2018) noted that H/C and O/C molar ratios of biomass are like or lower than certain coals, such as bituminous coal and anthracite [226], the atomic H/C and O/C values for lignite are 0.78 – 1.26

and 0.22 – 0.38, coal as 0.34 – 0.98 and 0.01 – 0.25, and anthracite as 0.02 – 0.37 and 0 – 0.03 [84]. Biomass generates lower smoke and steam during combustion, and thereby produces higher efficiency, with their HHV solid fuels values like lignite (28 MJ/kg) or coke (29 MJ/kg) [226].

4.3.4 Thermogravimetric analysis

The thermal degrading behaviour of BGS-N₂, BGS-CO₂, and BGS-N₂/CO₂ biochar samples were analysed. Figure 4.10(a) shows moisture content (MC) removal, within 30 – 120 °C, for BGS-N₂ (6.83 wt. %), BGS-CO₂ (8.84 wt. %), and BGS-N₂/CO₂ (9.52 wt. %). Sample weight loss and rate of weight loss under continuous dynamic conditions, as functions of time or temperature, in the range of 25–800 °C [308]. In addition, the devolatilization of some light bio-oil compounds adsorbed on biochar pores occurred at this stage. The temperature ranges from 120 – 900 °C and there was a continuous gentle slope, which may be due to the devolatilization of most of the VM that was left in the biochar. After the de-moisturization, the total weight percentage loss for BGS-N₂, BGS-CO₂, and BGS-N₂/CO₂ were 17.46, 18.75, and 16.96 wt. %, respectively. Biochar has higher thermal stability, up to 900 °C, as the overall mass loss ranges from 25 – 28 wt. %. Similar behaviour

for biochar samples was noticed with ice husk biochar (RHB), rice straw biochar (RSB), maize stover biochar (MSB), and sugarcane biochar (SCB) [254]. In the current study, biochar produced in the presence of a nitrogen atmosphere had higher stability than the biochar samples produced within the other two atmospheres.



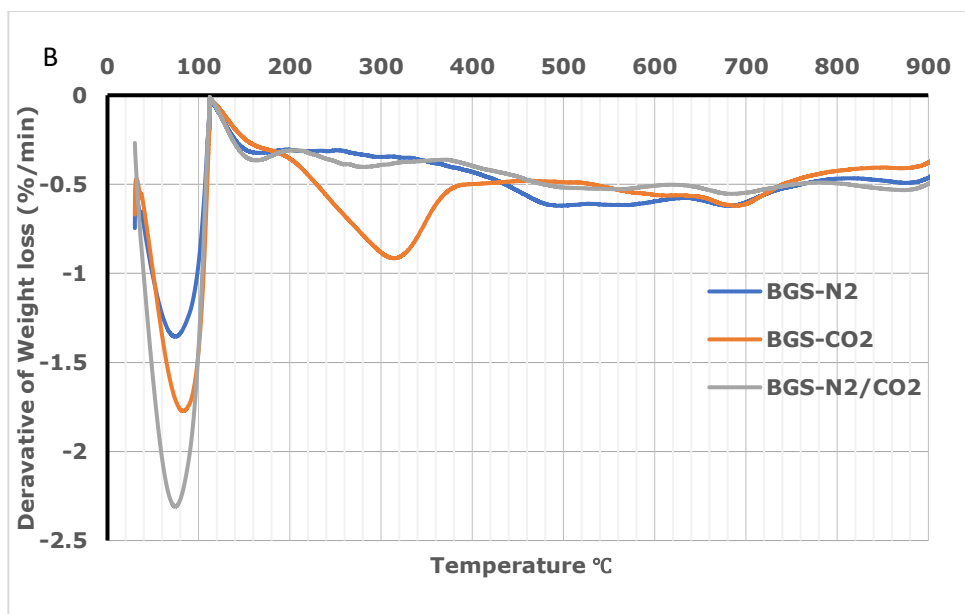


Figure 4.10: (a) TGA and (b) DTG graphs for biochar produced in N_2 , CO_2 , and N_2/CO_2 inert gases at 17.5 mL/s.

Figure 4.10(b) shows the DTG BGS- CO_2 degradation, which is different to the other two biochar degradations. At approximately 200 – 300 °C, an increasing weight loss for the BGS- CO_2 biochar occurred. Although there were no significant differences in bio-oil or biochar yields at different gases, the number of compounds identified in the GC-MS analysis of bio-oil for BGS- CO_2 was lower than that of the bio-oils from BGS- N_2 and BGS- N_2/CO_2 . Therefore, BGS- CO_2 had some unidentified molecular range compounds which could not be detected in the GC. The presence of similar compounds can be expected on biochar that has been devolatilized at this temperature.

4.3.5 Fourier transform infrared (FT-IR)

FT-IR spectra of the bio-oil and biochar (BGS-N₂, BGS-CO₂, and BGS- N₂/CO₂) are in Figure 4.11(a & b). The inert gases do not significantly affect the disparity among the products (bio-oil and biochar). The functional group, above the 1500 1/cm wavenumbers, most likely contains aliphatic (C-H), unsaturated alkene (C=C), alkyne (C≡C), and alcohol (O-H) compounds. The intensity at 3300 1/cm in the range of 3600 – 3000 1/cm is broad and short, indicating that H-bonding is very polar, and grouped as O-H stretching primarily contains alcohol (O-H) or carboxylic (C=O). In contrast, the wavenumber within 2950 – 2800 1/cm had a sharp and short intensity at 2920 which is non-polar and likely an alkane [255], with C-H stretching in the bio-oil and biochar.

In Figure 4.11(a), BGS-CO₂ and BGS-N₂/CO₂ had a medium peak, or less intensity, compared to the BGS-N₂ at 1695 1/cm, most likely as ketone group (C=O) is approximately at 1700 1/cm. No significant difference was observed in this peak intensity for bio-oils from the three different gases. Except on wavelength of 1620 1/cm with high intensity and 1220 1/cm with unblunt intensity compared to BGS-N₂/CO₂ and BGS-N₂ bio-oil FTIR. However, BGS-CO₂ and

BGS-N₂/CO₂ had more ketone presence in bio-oil for the GC-MS analysis compared to BGS-N₂. On the other hand, in Figure 4.11(b), the peak at 1600 1/cm (C=C) was more potent than that at 1695 1/cm, for BGS-N₂.

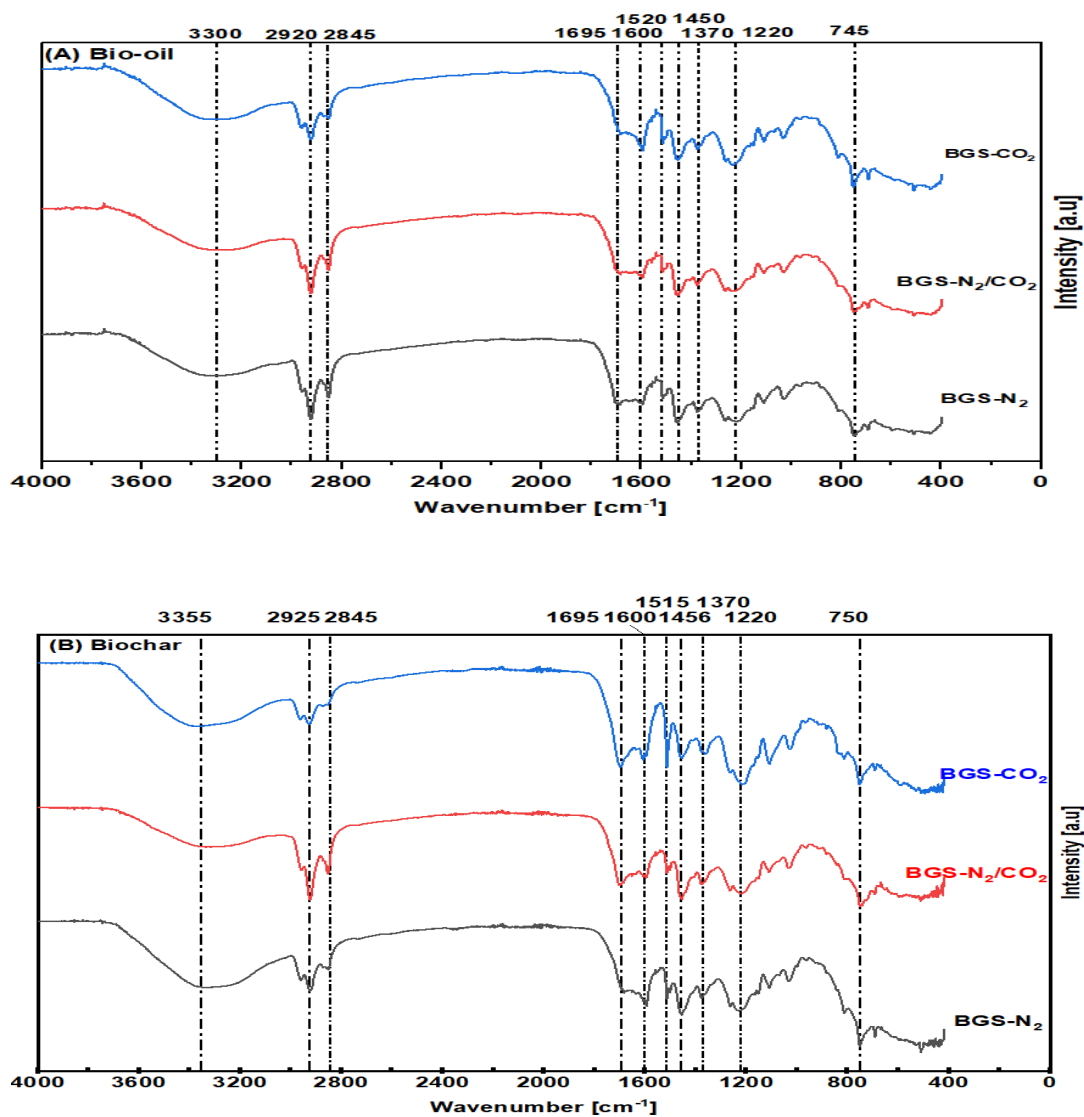


Figure 4.11: FTIR (a) Bio-oil and (b) biochar produced in N₂, CO₂, and N₂/CO₂ inert gases at 17.5 mL/s.

Figure 4.11(a), the fingerprint at 1660 1/cm frequency was a terminal alkene with small intensity but was more pronounced in BGS-CO₂ than BGS-N₂ and BGS-N₂/CO₂; while in Figure 4.11(b), BGS-N₂ was more pronounced than BGS-CO₂ and BGS-N₂/CO₂ for biochar. The ester (C-O), and possibly the carboxyl group (1220), lie at 1200 1/cm, with more intensity in BGS-CO₂ biochar than in bio-oil. Another interesting comparison occurred at 1100 1/cm, which was likely an alcohol or ester (C-O) band [256], with the C-O stretching vibration in both bio-oil and biochar. However, this was only evident in BGS CO₂ biochar. These C-O chemical bonds might result from phenols and partial lignin decomposition [257]. The fingerprint at 750 1/cm was identified as an aromatic (ortho) C-H stretching in bio-oil and biochar in Figure 4.11(a & b).

4.3.6 Field emission scanning electron microscopy - electron dispersive x-ray (FESEM-EDX)

Figure 4.12 illustrates that, compared to the raw BGS pore size of 17.24 – 30.17 μm, the biochar witnessed a honeycomb structure with an enlarging pore size in Figure 4.12(a). The best-recorded data, in descending order based on pore size, were: BGS-CO₂ (41.3 – 65.2 μm) ≥ BGS-N₂/CO₂ (21.3 – 54.7 μm) ≥ BGS-N₂ (45.02 –

52.26 μm). High porosity and carbon content suggested its effective use as an activated carbon adsorbent for environmental applications, after physical or chemical activation. The tendency of CO_2 to react with hydrogenated and oxygenated groups provided a higher surface area for biochar [249]. According to Guizani et al., (2014), biochar obtained in a CO_2 environment had an almost six times increase in surface area and had a different chemical composition compared to the N_2 environment [258]. The biomass pyrolysis of volatile organic carbon and thermal cracking from peat pyrolysis was enhanced in CO_2 , producing a larger biochar surface area in CO_2 than N_2 atmosphere [259]. It was evident that CO_2 and N_2/CO_2 produced an increase in the pore size, and a large surface area, of the biochar. However, CO_2 , as an inert gas in the pyrolysis of food waste, affected the composition of the vapours and probably inhibited cyclic component formation, which is hazardous to the environment and human health [21].

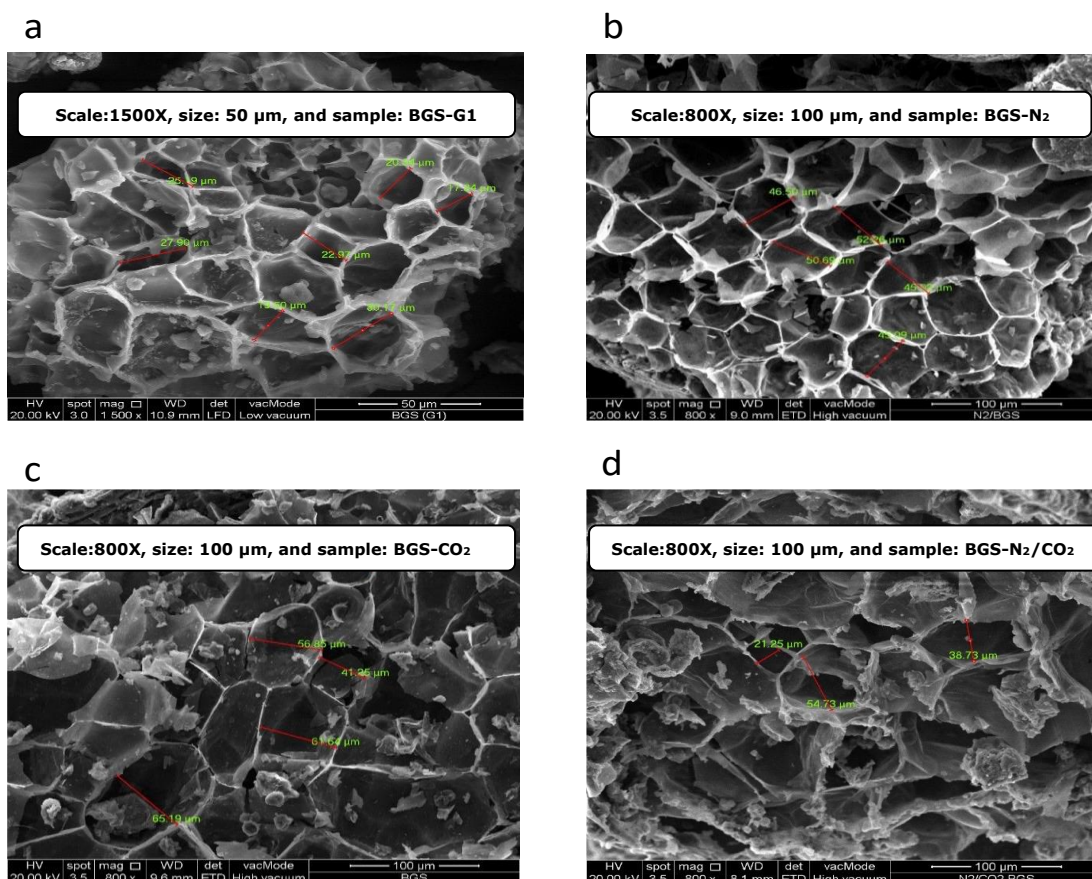


Figure 4.12: SEM images for (a) BGS-G1 (biomass) (b) biochar BGS-N₂ (c) biochar BGS-CO₂ (d) biochar BGS- N₂/CO₂.

4.3.7 Bio-oil chemical composition via GC-MS analysis

GC-MS analysis shows all the compounds that matched with the NIST library (R-match more than 700). Identified compounds accounted for the total area percentage of the bio-oils from BGS-N₂, BGS-CO₂, and BGS-N₂/CO₂, which were 34.5, 50.2, and 65.0, respectively. All the compounds were categorized as alkene, acid, benzenes, ketone, phenols, alcohol, aldehyde, alkyl, and ester. The GCMS chemical composition indicated many aromatic compounds

of tar formation, the most abundant compounds were ketone, phenol, and benzene. BGS-N₂/CO₂ showed the highest area percentage of the retrieved chemicals in the bio-oil products. A previous study mentioned that CO₂ in biomass pyrolysis provides thermal cracking of harmful organic compounds, enhances syngas generation, and suppresses benzene derivatives and polycyclic formation of aromatic hydrocarbons [249]. This study showed that benzene derivatives were more suppressed in N₂/CO₂ and CO₂ than in N₂. The BGS-CO₂ and BGS-N₂/CO₂ had the highest chemical composition yields, and phenol derivatives were present in relatively higher amounts for the N₂/CO₂ atmosphere, compared to the other two gas atmospheres, as presented in and Appendix 4.3.1 - Appendix 4.3.3.

The cellulose bio-oil pyrolysis yields: anhydrosugars, furans, ketones, acids, aldehydes, alcohols, phenols, and hydrocarbon compounds. Levoglucosan is the major product [260]. This study revealed the presence of all the compounds, except levoglucosan was undetected. The GCMS in Table 4.8 shows that BGS-CO₂ and N₂/CO₂ had similar compounds compared to BGS-N₂ for the ester and alcohol groups. However, most of these ketones and alcohols are higher molecular weight compounds. As discussed in section 4.3.3, more cracking occurs in the presence of nitrogen gas

compared to the other two gases. The Ketonization reaction converts carboxylic acids to ketones and releases CO₂ and H₂O, effectively reducing the acids' corrosiveness [260]. The number of ketones in BGS-N₂ was lower than the other two gases, which resulted in slightly high levels of acid for BGS-N₂ bio-oil. The acids reported were higher organic acids and therefore they do not significantly contribute to bio-oil pH. Lignin is composed of phenylpropane structural units and the main components in the lignin bio-oil are phenols and their derivatives. Further cracking of phenols provides benzene and its derivatives. The amount of benzene derivatives was higher for BGS-N₂ compared to the other two gases. In the case of phenol derivatives, BGS-N₂ had a lower amount. These results ensure further cracking in the presence of nitrogen gas.

The GC-MS results in and Appendix 4.3.1 - Appendix 4.3.3 deduce that the presence of three inert gases has similar mechanisms as those reported in the literature for cellulose, hemicellulose and levoglucosan [261]. Shen et al., (2017) demonstrated that the chromatograms of various biomasses subjected to slow pyrolysis and fast pyrolysis in N₂, and CO₂ environments are similar, indicating that the carrier gas and biomass pattern have no remarkable effects on the components in bio-oils produced from

pyrolysis at 450 °C. The mechanisms of hemicelluloses and cellulose are very similar, they start with the depolymerization of polysaccharide chains to form oligosaccharides, through cleavage of the xylan chain in the glycosidic linkage and re-organisation of the molecules produced to contain 1,4-anhydro-D-xylopyranose. The 1,4-anhydro-D-xylopyranose is further decomposed to form small-molecular-weight compounds (furfural and two- and three-carbon fragments) [249].

Table 4.8: GCMS bio-oil compound produced at 17.5 mL/s.

S/No	ALKANE	BGS-N ₂ Area %	BGS-CO ₂ Area %	BGS-N ₂ /CO ₂ Area %
1	(+)-2-Aminoheptane			1.737
2	Tridecane	0.274	0.502	
3	Heptadecane, 2,6,10,15-tetramethyl-		0.578	
4	Stigmastan-6,22-dien, 3,5-dedihydro-		0.527	
	Sub-Total	0.274	1.607	1.737
	ALKENE			
5	Cyclobutene, 2-propenylidene-		1.528	
6	Naphthalene, 2,2-dimethyl-1-oxa-2-sila-1,2-dihydro-	0.273		
	Sub-Total	0.273	1.528	0
	AMIDE			
7	Pyrimidine, 4,5-dimethyl-		0.687	
8	Nonadecanamide		0.541	
	Sub-Total	0	1.228	0
	ALDEHYDE			
9	Pentanal, 2,3-dimethyl-		0.969	
	Sub-Total	0	0.969	0
	ALCOHOL Derivatives			
10	1-Propanol, 2-amino-, (ñ)-			1.737
11	Oxiranemethanol, (R)-			0.859
12	Cyclobutanol			0.506
13	1,6-Heptadien-4-ol			0.383
14	Ethanol, 2-(9,12-octadecadienyloxy)-, (Z,Z)-		0.476	

Sub-Total		0	0.476	3.485
ESTER				
15	Nicotinic acid, 2-phenylethyl ester		0.637	
16	Formic acid, tetrahydrofurfuryl ester			0.354
17	Propanoic acid, 3-chloro-, 4-formylphenyl ester		1.004	
18	Oxalic acid, 2-isopropylphenyl pentyl ester			0.887
19	Hexadecanoic acid, methyl ester		0.678	
20	12,15-Octadecadienoic acid, methyl ester		0.528	
21	6-Octadecenoic acid, methyl ester, (Z)-		2.736	
Sub-Total		0	5.583	1.241
CARBOXYLIC ACID				
22	Butanoic acid, 4-hydroxy-		1.004	
23	Phosphonic acid, (p-hydroxyphenyl)-	3.125	0.463	
24	n-Hexadecanoic acid	0.357	3.991	0.463
25	trans-13-Octadecenoic acid		0.887	
Sub-Total		3.482	6.345	0.463
PHENOL Derivatives				
26	Phenol	3.125	4.696	9.849
27	Phenol, 2-methyl-	2.203		
28	Phenol, 3-methyl-	3.689	2.936	13.947
29	Phenol, 2-methoxy-	1.618		
30	Phenol, 3-methyl-		4.507	
31	Phenol, 2-methoxy-		3.557	4.165
32	Phenol, 2,6-dimethyl-	0.445	0.53	1.021
33	Phenol, 2,5-dimethyl-			

34	Phenol, 2-ethyl-	0.54		1.095
35	Phenol, 2,5-dimethyl-	1.667		2.359
36	Phenol, 4-ethyl-	1.268	1.477	3.599
37	Phenol, 2-ethyl-5-methyl-	0.371		0.763
38	2-Methoxy-5-methylphenol		1.054	0.642
39	Phenol, 3,4-dimethyl-		0.454	0.384
40	Phenol, 2,3,5-trimethyl-			0.407
41	Phenol, 2-ethyl-4-methyl-	1.233		1.279
42	Phenol, 3,4,5-trimethyl-		0.476	
43	Phenol, 4-ethyl-3-methyl-		0.849	1.141
44	Phenol, 3-propyl-	0.431	0.691	0.776
45	Phenol, 4-ethyl-2-methoxy			1.789
46	2,5-Diethylphenol	0.33		0.831
47	Phenol, 2-ethyl-4,5-dimethyl-		0.618	
48	2-Methoxy-4-vinylphenol			0.975
49	Phenol, 2,6-dimethoxy	0.321	0.761	0.748
50	Phenol, 2-methoxy-4-propyl-		0.736	0.562
51	Phenol, 2-methoxy-6-(2-propenyl)-	0.448	0.984	1.116
Sub-Total		17.689	24.326	47.448
KETONE				
52	3-Hexanone			0.552
53	Cyclopentanone		0.556	1.005
54	Cyclopentanone, 2-methyl-	0.229		
55	2-Cyclopenten-1-one			0.449
56	Cyclohexanone			0.933
57	Cyclopentanone, 2-methyl-		0.7	
58	2-Cyclopenten-1-one, 2-methyl-	0.319	0.753	0.874

59	2-Cyclopenten-1-one, 3,4-dimethyl-	0.323	1.678	2.11
Sub-Total		0.871	3.687	5.923
BENZENE Derivatives				
60	Benzene, 1,3-dimethyl-	0.309	0.619	0.816
61	Benzenepropanoyl bromide	0.236	0.637	0.452
62	Benzene, 1,2,3-trimethyl-	0.367		
63	Benzene, 1-ethyl-2-methyl-			0.358
64	3-Butynylbenzene			1.319
65	Benzene, pentyl-		1.052	
66	Benzene, 1-methoxy-4-methyl-	0.499		
67	Benzene, 1,4-dimethoxy-2-methyl-	0.921	2.138	
68	2,5,6-Trimethylbenzimidazole	0.241		0.464
69	1,2-Diethoxy-4-ethylbenzene			0.404
70	ndolizine, 1-methyl-			0.415
71	1,4-Benzenediol, 2,5-dimethyl-	0.278		
72	Benzene, 1,1'-(diazomethylene)bis-			0.439
73	Benzene, (nitromethyl)-	6.682		
75	Benzonitrile,2-(4-benzyloxybenzylidenamino)-	1.984		
77	Benzonitrile, m-phenethyl-	0.408		
Sub-Total		11.925	4.446	4.667
Total		34.514	50.195	64.964

Nevertheless, anhydrosugar compounds were not available from the cellulose pyrolysis of BGS. The intensity of cracking varies as nitrogen gas causes more intensified cracking than CO₂, whereas N₂/CO₂ gas had a combined effect of intensified cracking of N₂ and CO₂ having low heat capacity. According to Shen et al., (2017) enhanced thermal cracking by introducing CO₂ contribute less tar generated from woody biomass than N₂ pyrolysis at 650 °C [249].

4.4 Synergetic effects and intermediate catalytic co-pyrolysis of SSS with polypropylene (PP).

This section discusses the synergetic effects of SSS and PP in an intermediate catalytic co-pyrolysis. The SSS pyrolysis produced the highest bio-oil compared to BGS-G1, and SNS, therefore the use of the PP in SSS is to take its advantages to produce rich hydrocarbon product. Catalytic co-pyrolysis of the biomass and PP to improve the energy properties of pyrolysis oil which may reduce the impact of greenhouse gas emissions and proffering alternative energy sources. The biomass SSS and PP were selected because the combination of both biomass and PP waste will produce bioenergy with cost-effectiveness and minimal environmental effect as PP is a product from fossil, while biomass is eco-friendly.

4.4.1 Catalyst properties

4.4.1.1 *BET and XRD Analysis*

The ZSM-5 catalysts recorded the highest single point surface area of 377.39 m²/g, which avails material per unit mass (i.e. more surface contact) for catalyst modification or impregnation and catalytic reactions during pyrolysis among others tested (calcined Al₂O₃, 10wt.%Ni/Al₂O₃, and 15wt.%Ni/Al₂O₃) with an average adsorption pore size width, Å (209.2 and 333.9) of their adsorption capacity and their micropores at about 279.74 m²/g holding materials as lower of about 0.0074 and 0.0069 cm³/g. The microporous structure of the ZSM-5 catalyst had a reduced average adsorption pore size width of 25.27 Å. The surface area of calcined Al₂O₃, 10wt.%Ni/Al₂O₃, and 15wt.%Ni/Al₂O₃ demonstrated an increase in surface area from 0.5457 m²/g to 1.4099 m²/g for 10wt.%Ni/Al₂O₃, but the surface area decreased to 0.9078 m²/g for 15wt.%Ni/Al₂O₃. As the surface area was reduced with Ni loading, the pore size increased from 209.2 - 333.9 m²/g According to Li et al., (2018), the surface area change may result from the Ni content exceeding 10 %; overloaded may cover the surface on supportive Al₂O₃, leading to decreased pore volume and specific surface area [263]. According to Karimi et al., (2015), the % dispersion and crystallite sizes of cobalt particles determined pore volumes (single

point) m^2/g of the catalyst studied are $\leq 2.2 \text{ m}^2/\text{g}$ [3], and Al_2O_3 and $\text{Ni}/\text{Al}_2\text{O}_3$ catalyst studied at temperatures from 600 – 1200 °C and pore volume $\leq 0.442 \text{ m}^2/\text{g}$ [265].

ZSM-5 catalyst pore volume seems larger than the Al_2O_3 and $\text{Ni}/\text{Al}_2\text{O}_3$. from 1.4099 to 0.9078. The adsorption pore size increased as the Nickel loading increased (calcined Al_2O_3 , 10wt.% $\text{Ni}/\text{Al}_2\text{O}_3$, 15wt.% $\text{Ni}/\text{Al}_2\text{O}_3$) as 168.7, 209.2, and 333.9 Å. whereas, ZSM-5 had a lower adsorption pore size width of 25.27 Å. The Nickel loading of 25wt.% $\text{Ni}/\text{Al}_2\text{O}_3$ was more recommendable as it might further increase the pore size of the catalyst and perhaps facilitate a better yield for the catalytic co-pyrolysis. In the present study, the highest yield of bio-oil with a feed-to-catalyst ratio of $\text{Al}_2\text{O}_3(1:1/2)$ and 25wt.% $\text{Ni}/\text{Al}_2\text{O}_3(1:1/4)$, followed by ZSM-5(1:1/4) catalyst. It implies that the increased adsorption pore size resulted in better yield.

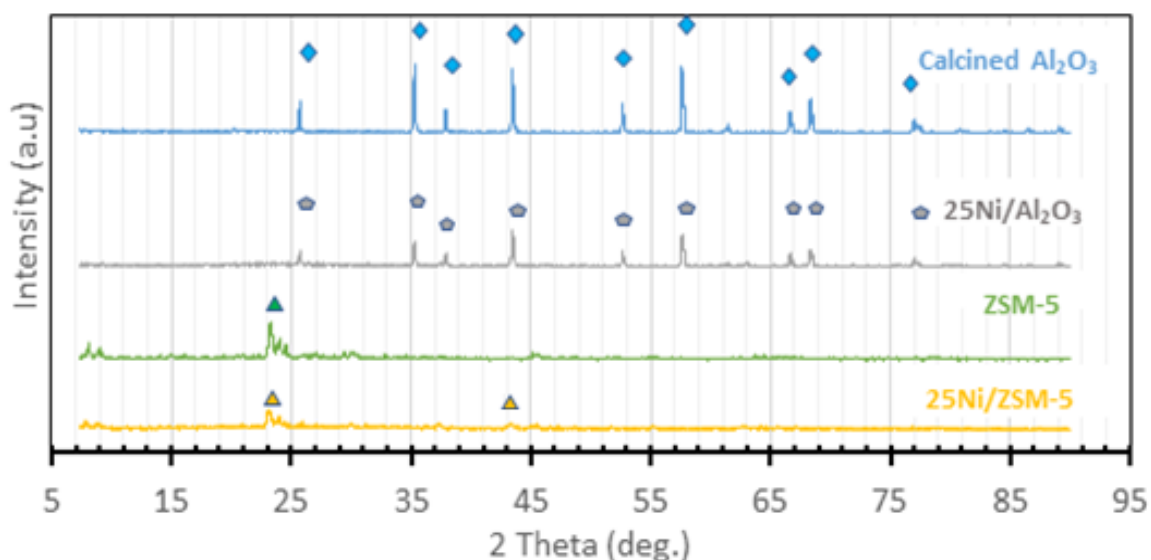


Figure 4.13: The XRD data for the catalyst analysis.

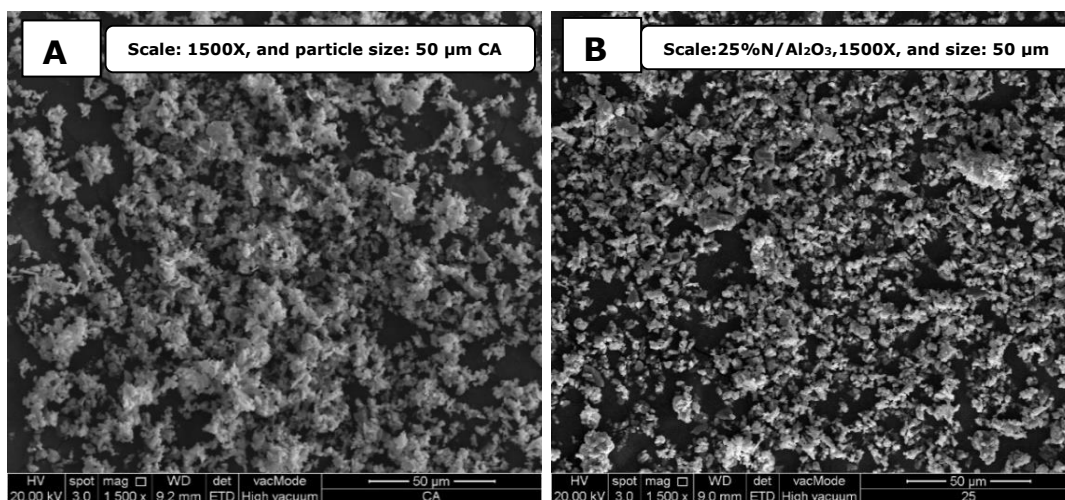
Figure 4.13 shows the XRD catalyst patterns of Al_2O_3 , 25wt.%Ni/ Al_2O_3 , ZSM-5 and 25wt.%Ni/ZSM-5. According to Sekyere et al., (2023), ZSM-5 and Ni/ZSM-5 catalysts showed the characteristic peak of MFI (Mobil-five type) zeolites structure is an aluminosilicate zeolite belonging to the pentasil family of zeolites with $7 - 9^\circ$ and $22.5 - 25^\circ$ [112]. The peak difference in ZSM-5 and 25wt.%Ni/ZSM-5 might be due to the saturation of the Nickel-ZSM-5 impregnation, which reduces major compositions and the crystalline structure with different XRD patterns from ZSM-5. The calcined Al_2O_3 and impregnated 25wt.%Ni/ Al_2O_3 had peaks of diffraction at $2\theta = 26^\circ, 35^\circ, 38^\circ, 44^\circ, 53^\circ, 58^\circ, 67^\circ, 69^\circ$ and 77° as successful migration and dispersion of the Nickel oxides. According to Khachatur et al., (2015) reveals that reduced Ni-

Al₂O₃-LDH catalyst exhibits highly dispersed Ni of 3 - 5 nm particle sizes spread on top, partially encapsulated nanoparticles, while some are embedded in the Al₂O₃ matrix [297]. The changes from Al₂O₃ to Ni/ Al₂O₃ peak led to its peak reduction due to the impregnation of Ni/ Al₂O₃ as Al₂O₃ support got saturated. Hameed et al., (2022) stated crystallite size reduction might be due to a successful migration and dispersion of NiO to the surface and channels in ZSM-5, as NiO crystallite peak formation at $2\theta = 43^\circ$ [266]. As the impregnation of 25wt.% Nickel on calcined Al₂O₃ the peaks decrease. The diminishing peaks are most likely due to the degree of the impregnation on the catalyst support (Al₂O₃), but no new diffraction peaks were observed. According to Hameed et al., (2022), the peak intensity of the NiO/ZSM-5 catalyst shifted and was lower than the calcined ZSM-5 catalyst, perhaps because of the transfer of NiO into ZSM-5 [266]. Also, Huang et al., (2018) revealed that XRD patterns of the prepared catalysts of activated alumina diffraction peaks of Al₂O₃, Ni/Al₂O₃ and Ni supportive material exhibited diffraction peaks of gamma alumina at 37.7° , 43.2° and 67.7° , as Ni species at 44.5° , 51.9° and 76.4° [267]. The successful distribution of metal oxide was apparent in the catalyst structure by BET analysis. In Figure 4.13, the XRD patterns of the impregnated/synthesized 25wt.%Ni/ZSM-5 and 25wt.%Ni/Al₂O₃ catalysts show similar peaks according to Sekyere et al., (2023) the

calcined ZSM-5, as no new diffraction peak appeared [112]. The diffraction peaks coincide with most peaks of Al_2O_3 , Ni/ Al_2O_3 in Figure 4.11. The remarkable Ni diffraction peak when NiO content exceeds 25 % in the sample catalyst indicates the formation of large Ni particles [267]. The XRD patterns in Figure 4.13 are consistent with BET results in Appendix 4.4.1.

4.4.1.2 *Field Emission Scanning Electron Microscopy - Electron Dispersive X-ray (FESEM-EDX).*

Figure 4.14, shows below the catalyst FESEM used in bio-oil production, and properties activity understudied.



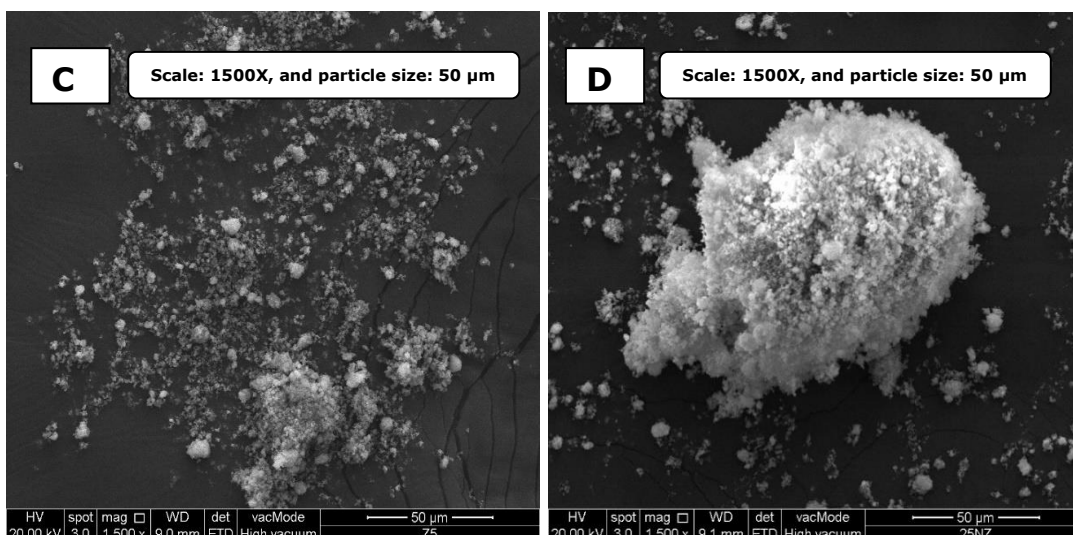


Figure 4.14: FESEM (a) Al_2O_3 (b) 25wt.%Ni/ Al_2O_3 (c) ZSM-5 (d) 25wt.%Ni/ZSM-5 catalyst.

The morphology and particle-size distributions are estimated by FESEM catalyst images. Figure 4.14(a) shows the calcined Al_2O_3 had even particle distribution, whereas the 25wt.%Ni/ Al_2O_3 with a textural outlook was finely arranged 50 μm particulate size in Figure 4.14(b). Particles look loosely dispersed perhaps due to 25 wt. % of nickel impregnations. Figure 4.14(c) is a representation of ZSM-5 images which are fine and looped particulate unevenly distributed with some crystals. Figure 4.14(d) FESEM image representation of the impregnated 25wt.%Ni/ZSM-5 appeared agglomerated whitish-like particulate structure. The morphology of the 25wt.%Ni/ Al_2O_3 and calcined Al_2O_3 might have more active sites to facilitate the reaction processes.

4.4.2 Thermogravimetry Analysis

Figure 4.15(a and b) show the thermal degradation curves and their derivative curves for different ratios of SSS biomass and PP plastic mixtures. The ratios were selected as SSS:PP (1:0), SSS:PP (3:1), SSS:PP (1:1), SSS:PP (1:3), and SSS:PP (0:1), which accounts for 0, 25, 50, 75, and 100 wt. % of PP in the mixture. The impact of the temperature within the 32 - 120 °C was mainly due to the biomass's moisture content. As the plastic blending ratio increased its moisture content weight decreased in descending order (SSS:PP (1:0), SSS:PP (3:1), SSS:PP (1:1), SSS:PP (1:3) and SSS:PP (0:1)). The thermogravimetric profiles for biomass (SSS:PP (1:0)) and plastic (SSS:PP (0:1)) became distinctive. The biomass (SSS:PP (1:0)) had major degradation within 250 - 400 °C in descending order (SSS:PP (1:0), SSS:PP (3:1), SSS:PP (1:1), SSS:PP (1:3) and SSS:PP (0:1)), which corresponds to the degradation of cellulose and hemicellulose. Meanwhile, the polypropylene (SSS:PP (0:1)) decomposition was in the range of 350 - 500 °C. This is an indication that biomass degrades earlier than the plastic feedstock. According to Zhang (2016), the thermal degradation of cellulose was within 300 - 400 °C, while the LDPE thermal decomposition was at 400 - 500 °C without solid residue formation [270]. As reported by Oyedun et al., (2014) maximum decomposition

happens for biomass (bamboo, empty fruit bunch and sawdust) - polystyrene (PS) blends at 399 – 424 °C and biomass - HDPE blends at 454 – 509 °C characteristics compared with plastics. Biomass decomposition mostly begins around 200 °C for cellulose and hemicellulose, while lignin is from 400 °C upward. The synergetic effect would be more with lignin fraction and plastic; the plastic and biomass (lignin) thermal degradation curves overlap at 470 °C with < 30 wt. % than the other biomass components because the lignin and plastics had similarities [271]. The temperature ranges from 600 – 900 °C in the TG curve depicts that the more SSS ratio in the SSS:PP ratio, the higher the amount of residue after pyrolysis. Therefore, it is postulated that the higher biomass ratio provides a higher yield of biochar. This is confirmed by the study of Oyedun et al., (2014), where the biochar increased with increased biomass ratio in the co-feed of plastic (polystyrene and high-density polyethylene) and biomass (bamboo, empty fruit bunch and sawdust) [271]. While the plastic degradation (SSS:PP (0:1)) witnessed very low or no weight remained after 500 °C.

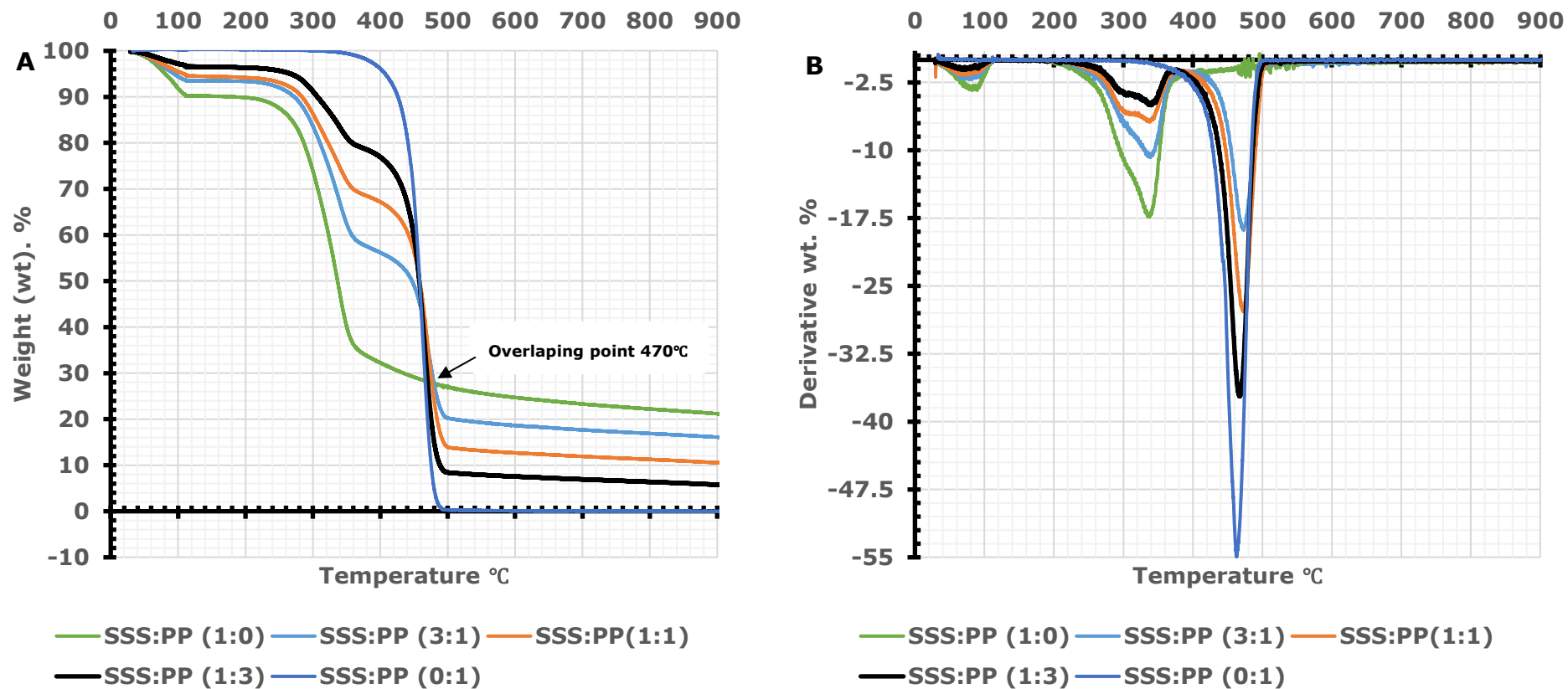


Figure 4.15: The (a) TGA and (b) DTG graph for PP: SSS and SSS: PP (1:3 to 3:1) ratio.

Biomass co-pyrolysis is one of the potential options to improve the quality of bio-oil. The differences in chemical and physical properties of different feedstocks lead to different thermal reactivities for the kinetics and mechanisms of EFBF with POME sludge during co-pyrolysis [272].

A positive or negative synergic effect relies on the type and contact between the components, temperature and heating rate, removal or equilibrium of volatiles formed, and the addition of solvents, catalysts, and hydrogen donors. The synergetic behaviour was positive for the SSS:PP (1:1) as it maintained a medium degradation between all the SSS:PP samples, which was averagely consistent from the initial 30 °C to the final stage at 900 °C in Figure 4.16(a) as compared to the other ratios.

4.4.2.1 Synergistic effect evaluation

To determine the existence of synergistic effects in the co-pyrolysis of plastic and biomass and to illustrate the interaction mechanism, the experimental and theoretical product yields of co-pyrolysis were compared. Theoretical results are calculated by Eqn. 4.2, according

to the proportionally weighted average of the results measured from the thermogravimetry analysis.

$$Y_{theoretical} = \omega \times Y_{biomass} + (1 - \omega) \times Y_{plastic} \dots\dots\dots Eqn. 4.2$$

In the equation above,

- $Y_{theoretical}$ = The weight-averaging theoretical value,
- ω = the plastic mixing percentage, (wt. %),
- $Y_{plastic}$ = The experimental value of plastic pyrolysis, and
- $Y_{biomass}$ = The experimental value of biomass pyrolysis.

Figure 4.16 (a and b) show the TGA and DTG curves of SSS:PP blends heated at 10 °C/min in the presence of N₂. The peak of the profile of both the DTG varies according to the blending ratios or percentages, the higher the SSS percentage ratio the more the mass of residue recorded.

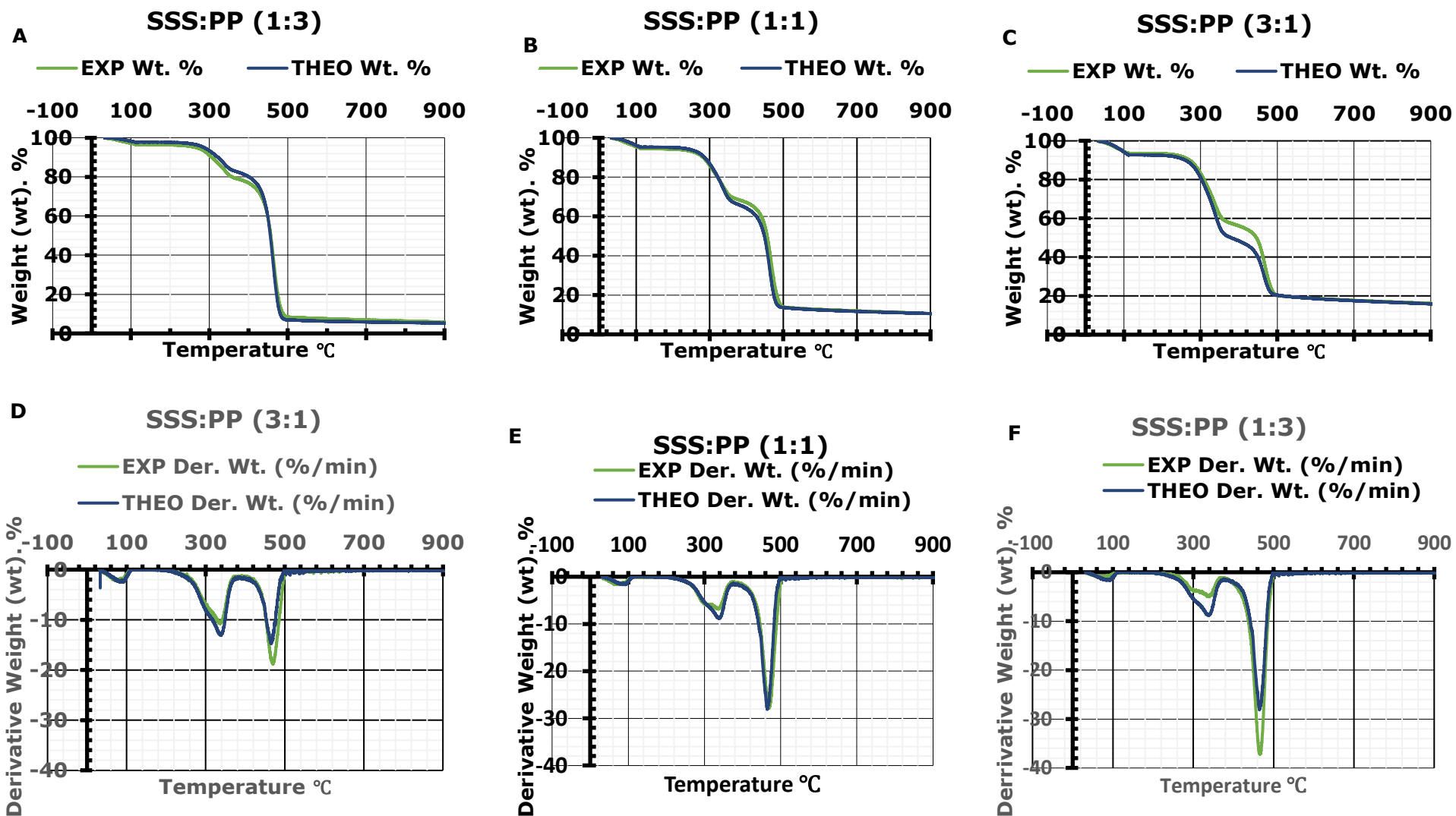


Figure 4.16: The TGA SSS:PP (a) (1:3), (b) (1:1), and (c) (3:1) and DTG SSS:PP (d) (3:1), (e) (1:1), and (f) (1:3) synergetic experimental and theoretical plots.

The TGA in Figure 4.16 (a, b and c) shows the degradation trend of the SSS:PP for all the samples. The first peak had smaller experimental curves for all the blends in Figure 4.16 (d, e and f). The initial temperature at around 70 °C for the DTG showed that the experimental plots had lower peaks in Figure 4.16(d, e and f). Meanwhile, the second stage peaks at 340 °C were due to the biomass degradation and volatility of experimental losses. However, the degradation in Figure 4.16(d, and f) at around 465 °C where the theoretical had a lower peak as compared to their corresponding experimental plots except SSS:PP is 1:1 where both the experimental and theoretical plots are aligned or almost identical demonstrating some positive synergetic effect. The higher peak for the experimental plot SSS:PP (1:3) might be due to the heavy hydrocarbon in PP as compared to SSS. Therefore, a negative synergistic effect can be expected for biomass degradation. The negative synergetic effects on major pyrolysis products blending ratio were demonstrated on the co-pyrolysis of coal and oil palm biomass [273], while co-pyrolysis of sewage sludge and pine sawdust blends behave independently, which neither increase nor decrease of volatile happened [274], Also, an inhibitive effect in co-pyrolysis of petrochemical wastewater sludge with lignite blending ratio synergetic effects promoted gas as against less liquid and solid products [275].

4.4.3 Intermediate co-pyrolysis

The co-pyrolysis of the SSS:PP (1:1) mixture provided a liquid yield of 47.8 ± 0.2 wt. % as demonstrated in Figure 4.17 compared to the low bio-oil yield of 42.9 ± 0.1 wt. % for (SSS:PP (1:0)), while the theoretical yield is 47.6 wt. % which is almost equal to the experimental liquid oil yield. In this case, the theoretical yield for the co-pyrolysis of SSS:PP (1:1) mixture is 47.6 wt. %, which is very close to the experimental liquid yield obtained (47.8 ± 0.2 wt. %). According to Ashish et al., (2016), the optimum liquid yield for sugarcane bagasse (SCB)/LDPE co-pyrolysis was 52.75 % at 500 °C with a 1:1 blend ratio [298]. In another study by Gitanjali et al., (2023) in a study of Plastic Waste (PW) and Melia Dubia (MD) (50:50) ratio yielded 68.3 % liquid oil [299]. An increase in liquid products with a decrease in both char and gas yields a positive synergetic effect in co-pyrolysis studies if liquid fuel production is the main focus.

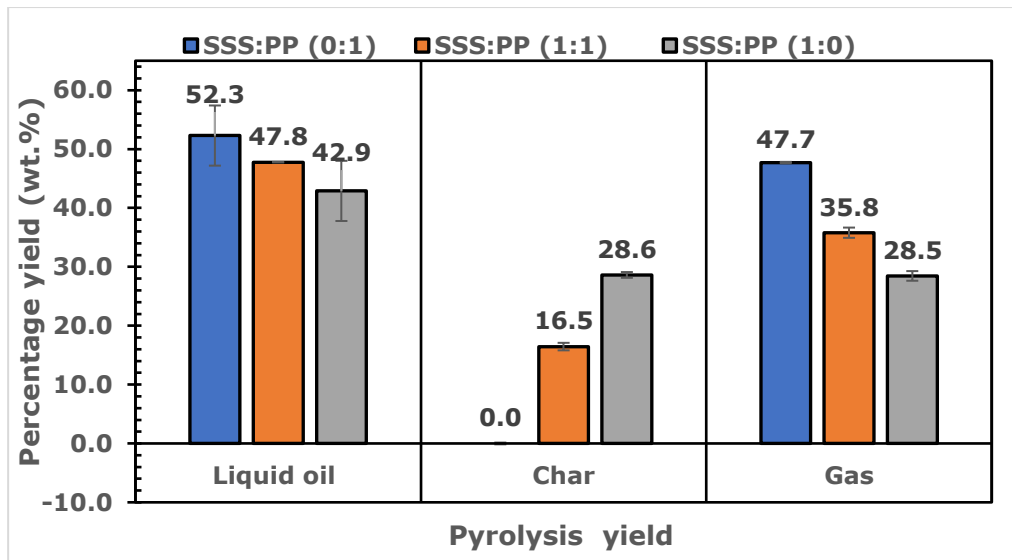


Figure 4.17: The co-pyrolysis oil, char, and gas yields.

A previous study on thermal co-pyrolysis focused on cellulose biomass (groundnut shells) and plastic mixtures provided a liquid yield of around 50 wt. % at an LB:PP ratio of 0.5 and ~32 wt. % at a ratio of 2 [285]. As reported by Farah et al., (2022), the char yields are predominantly at about an average of ~25 wt. % for largely biomass materials [300]. In this study, the residual char yield of SSS:PP (1:1) was 16.5 ± 0.6 wt. %.

According to Praveen et al., (2020), the influence of LB on PP decomposition degrades at a lower temperature than plastic [277]. The thermal breakdown of plastic proceeds as a radical chain process that includes steps of radical initiation, chain propagation, and radical termination. During the initial stage of co-pyrolysis, radicals

from the LB components initiate the chain scission of the plastic polymer chain [277]. A higher plastic ratio led to higher wax production, while lower plastic might demonstrate higher petrochemicals and the least amount of wax formation [111]. The negative synergetic effects on major pyrolysis products blending ratio were demonstrated on the co-pyrolysis of coal and oil palm biomass [273], while co-pyrolysis of sewage sludge and pine sawdust blends behave independently, which neither increase nor decrease of volatile happened [274]. Also, an inhibitive effect in co-pyrolysis of petrochemical wastewater sludge with lignite blending ratio synergetic effects promoted gas as against less liquid and solid products [275].

4.4.4 Intermediate catalytic co-pyrolysis.

Catalytic co-pyrolysis of sweet sorghum stalk and polypropylene in a 1:1 ratio holds promise as a sustainable approach for bioenergy production and waste management, offering opportunities to generate value from renewable resources and waste materials. Figure 4.13 XRD analysis demonstrated that the developed catalyst 25wt.%Ni/Al₂O₃ was promising on catalytic co-pyrolysis of (SSS:PP 1:1) and, revealed that the SSS:PP (1:1) in Figure 4.17, and Figure 4.18.

Figure 4.18 had a positive synergetic effect on liquid oil yield due to contact between the SSS feed particulate size and the PP. It, therefore, results in hydrogen transfer (more alkane and alkene) in the GCMS analysis and yields an optimum liquid oil, and gas. The liquid oil yield was considerably high but could be improved by condensing more of the gas yield for more liquid oil production as in Figure 4.18. Plastics, tyres and lubricant oil act as hydrogen donors, aiding coal hydrogenation and inducing positive synergistic interaction with biomass pyrolysis with positive synergies [276].

Figure 4.18 shows that catalytic co-pyrolysis SSS:PP (1:1) with bio-oil yield increased within $46.2 \pm 2.0 - 51.5 \pm 0.7$ wt. %, with a subsequent slight increment in gas yield. In another work, biomass co-pyrolysis with waste plastics produced a high bio-oil of 52.3 wt. %, while a study on co-pyrolysis with ZSM-5 catalyst yield dropped to 49.3 wt. % with gas yield further increased due to the pyrolysis volatiles cracking [278]. According to Yunwu et al., (2020), a study of enhancing the aromatic hydrocarbon yield from the catalytic co-pyrolysis of xylan and LDPE with a dual-catalytic-stage combined CaO/HZSM-5 catalyst the energy yield and chemical modification point of view of a xylan-to-LDPE ratio of 1:1 was optimal [301]. According to Hong et al., (2017), polypropylene and cellulose

catalytic co-pyrolysis demonstrates an enhanced yield of aromatic hydrocarbons over desilicated ZSM-5 because of the synergistic effects between cellulose and polypropylene [302]. As reported by Zhang et al., (2014) the catalytic co-pyrolysis of polystyrene and pine sawdust produced the highest and lowest yields of aromatics (47 %) and olefins (11.4 %) [303].

The catalyst and catalyst ratio effect in Figure 4.18 shows that the feed-catalyst (Feed: Al_2O_3) ratio of (1:1/2) yields the highest liquid. The catalytic effect seems to be active in Al_2O_3 (1:1/2) with the least biochar at 9.9 wt. %, which indicates that a high amount of Al_2O_3 cracked more biochar particles into liquid compounds. The best bio-oil HHV of (Feed: Ni/ Al_2O_3) ratio of (1:1/4). The biochar yield was slightly higher with Al_2O_3 as compared to the presence of ZSM-5. Yu et al., (2020) illustrated those insufficient active sites (Lewis's acidity) could be the limiting factor of Al_2O_3 shifting of porosity or acidity [279]. However, Ni impregnation on these supports helped to reduce the biochar yield slightly as compared to their supports alone.

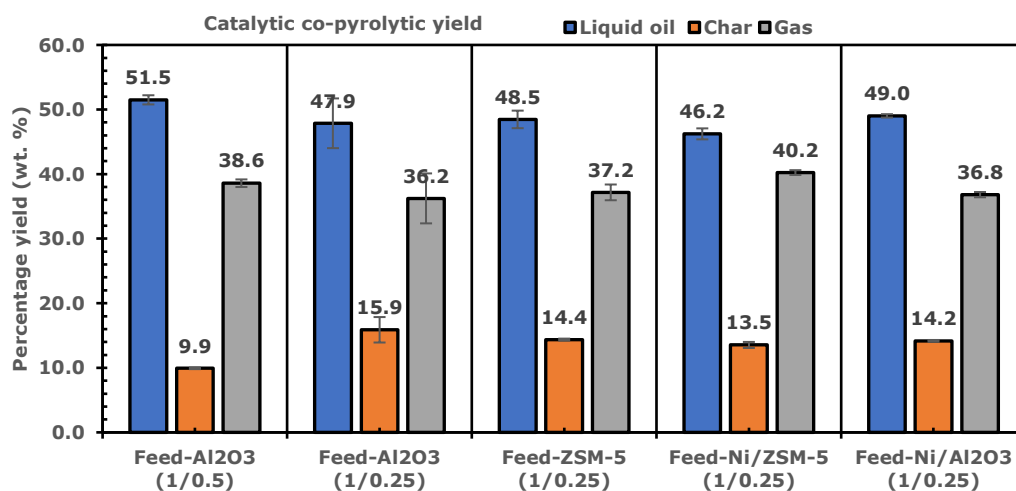


Figure 4.18: The catalytic co-pyrolysis product (bio-oil, biochar, and biogas) products.

According to Dyer et al., (2021) co-pyrolyzed biomass/plastic (the poly-alkene waste plastics (HDPE, LDPE, and PP)) mixtures (1:1) ratio with ZSM-5 catalysis, yielded similar results with char yield ranging from 13.1 – 15.1 wt. % and oil yield was within 51.6 – 56.0 wt. % [278]. From Table 4.9 and Figure 4.18, the optimum bio-oil and biochar yield with their respective HHV are Feed: Ni/Al₂O₃ ratio of (1:1/4) as the best bio-oil yield of 49.07 wt. % with HHV of 41.1 ± 0.7 MJ/kg, and a biochar yield of 14.17 wt. % and HHV of 10.3 MJ/kg respectively. The biomass SSS:PP (0:1 to 1:1) in Figure 4.18 blend of biomass and PP waste will minimize the ecological destruction and cost-effectiveness as compared to fossil fuel. The uncondensed gas is measured by the difference of biochar and bio-oil from biomass.

4.4.5 Physicochemical (ultimate, proximate, and EDX) analysis of SSS/PP products.

Table 4.9 illustrates the HHV and pH values for the co-pyrolysis SSS:PP (1:0), SSS:PP (1:1), and SSS:PP (0:1). The HHV of pyrolysis oil for the SSS:PP (1:1) was closer towards PP pyrolysis oil. At SSS:PP (1:1) the pH value increased toward alkalinity from 2.99 for SSS:PP (1:0) to 3.30 for SSS:PP (1:1). The HHV of co-pyrolysis char remained almost equal as that of the SSS:PP (0:1) sample indicating the char was mainly from lignin present in the biomass. The Feed-catalyst ratio bio-oil had HHV for all the samples at an average of 41 MJ/kg, but the Ni/Al₂O₃ (1:1/4) pH value tilting towards neutrality as compared to the other samples with the char at a maximum of 10 MJ/kg. According to Qiu et al, 2020) catalytic co-pyrolysis of sewage sludge and rice husk over biochar catalyst studied recorded a 4.06 pH value after catalysts application it rose to between 5.01–5.48 pH value due to acids and phenols compound reductions [293]. Microwave-induced in-situ catalytic co-pyrolysis of empty fruit bunches with a waste truck tyre demonstrated the ability to reduce pH acidic values from 4.0 to approximately 5.0 [294].

Table 4.9: The intermediate catalytic co-pyrolysis products, HHV and ultimate analysis

PARAMETERS	BIO-OIL			BIOCHAR					
Feed Pyrolysis ratio	HHV (MJ/kg)	pH		HHV (MJ/kg)					
SSS:PP (0:1)	44.3 ± 0.43	3.8		-					
SSS:PP (1:1)	40.3 ± 0.05	3.3		22.4 ± 0.34					
SSS:PP (1:0)	16.3 ± 0.55	3.0		22.9 ± 0.10					
Feed-Catalyst ratio	HHV (MJ/kg)	pH		HHV (MJ/kg)					
Feed- Al ₂ O ₃ (1:1/2)	41.5 ± 0.5	3.4		5.4 ± 0.11					
Feed-Al ₂ O ₃ (1:1/4)	41.0 ± 0.9	3.4		8.7 ± 0.05					
Feed-ZSM-5 (1:1/4)	41.8 ± 2.4	3.6		9.8 ± 0.03					
Feed-Ni/ZSM-5 (1:1/4)	ND	3.0		10.4 ± 0.15					
Feed-Ni/Al ₂ O ₃ (1:1/4)	41.1 ± 0.7	3.5		10.3 ± 0.06					
Bio-oil CHNS analysis	C wt. %	H wt. %	N wt. %	S wt. %	O wt. %	H/C ratio	O/C ratio		
SSS:PP (0:1)	75.8 ± 4.9	12.7 ± 0.9	0.8 ± 0.1	0.1 ± 0.0	10.7 ± 5.6	0.17 ± 0.0	0.14 ± 0.8		
SSS:PP (1:1)	78.2 ± 0.0	13.1 ± 0.0	0.1 ± 0.0	0.1 ± 0.0	7.7 ± 0.0	0.2 ± 0.0	0.1 ± 0.0		
SSS:PP (1:0)	53.6 ± 0.8	7.8 ± 0.1	1.5 ± 0.0	0.1 ± 0.0	37 ± 0.7	0.14 ± 0.0	0.69 ± 0.2		
Bio-oil (1:1)-Cat-CHNS analysis	C wt. %	H wt. %	N wt. %	S wt. %	O wt. %	O/C ratio	H/C ratio		
Feed-Al ₂ O ₃ (1:1/2)	78.9 ± 0.1	13.0 ± 0.0	1.0 ± 0.0	0.1 ± 0.0	7.1 ± 0.1	0.16 ± 1.7	0.09 ± 0.0		
Feed-Al ₂ O ₃ (1:1/4)	77.6 ± 0.7	12.9 ± 0.2	1.0 ± 0.2	0.1 ± 0.1	8.4 ± 1.1	0.16 ± 0.0	0.11 ± 0.2		
Feed-ZSM-5 (1:1/4)	79.6 ± 0.1	13.0 ± 0.2	0.9 ± 0.1	0.3 ± 0.3	6.3 ± 0.5	0.16 ± 0.0	0.08 ± 0.1		
Feed-Ni/ZSM-5 (1:1/4)	80.9 ± 0.5	12.8 ± 0.2	0.9 ± 0.1	0.1 ± 0.0	5.7 ± 0.8	0.16 ± 0.0	0.07 ± 0.1		
Feed-Ni/Al ₂ O ₃ (1:1/4)	78.6 ± 0.0	13.2 ± 0.0	0.1 ± 0.0	0.9 ± 0.0	7.1 ± 0.0	0.2 ± 0.0	0.10 ± 0.0		
EDX Biochar analysis	C	O	Mg	Al	Si	K	Ca	Cl	Fe
SSS:PP (1:1)	68.9 ± 20.5	22.5±13.2	0.3 ± 0.2	0.45 ± 0.1	4.6 ± 7.5	2.8 ± 2.1	1.0 ± 1,2		

SSS:PP (1:1)	76.5 ± 6.2	18.2 ± 4.6	0.3 ± 0.0	0.1 ± 0.0	1.9 ± 1.1	2.5 ± 0.5	0.44 ± 0.2	0.3	0.2±0.1
EDX Bio-oil co- pyrolysis analysis	C	O	Mg	Al	Si	K	Ca	Cl	Fe
Feed-Al ₂ O ₃ (1:1/2)	48.9 ± 7.1	34.8 ± 3.4	0.2 ± 0.0	14.4 ± 4.1	0.7 ± 0.4	0.6 ± 0.3	0.4 ± 0.2	0.1±0.0	
Feed-Al ₂ O ₃ (1:1/4)	32.4 ± 8.2	41.9 ± 4.8		16.5 ± 6.5	6.1 ± 4.4	2.5 ± 0.9		0.2±0.0	0.4±0.2
Feed-ZSM-5 (1:1/4)	55.4 ± 6.5	28.9 ± 2.0	0.4 ± 0.1	9.6 ± 3.5	1.1 ± 0.3	1.7 ± 0.4	0.8 ± 0.1	0.3±0.1	
Feed-Ni/ZSM-5 (1:1/4)	40.7 ± 18.9	41.2 ± 10		1.3 ± 0.7	15.7 ± 8.7	1.0 ± 0.3	0.2 ± 0.2		
Feed-Ni/Al ₂ O ₃ (1:1/4)	31.7 ± 2.6	39.8 ± 1.0	0.4 ± 0.0	1.8 ± 1.0	18'6 ± 6.2	1.6 ± 0.2	0.67 ± 0.1		

Note: ND_ Not Determined

The CHNS of the SSS:PP (1:1) showed high carbon and hydrogen content as compared to SSS:PP (0:1 and 1:0), while nitrogen, sulphur and oxygen had the least content, which could facilitate a high conversion process easily for the desired clean energy products. In the catalytic co-pyrolysis, the CHNS are aligned as in Table 4.9. The results are averagely the same except for Feed-Ni/Al₂O₃ (1:1/4), with the least nitrogen content of 0.1 ± 0.0 wt. % but sulphur content of 0.9 ± 0.0 wt. %. However, the presence of Ni on supports demonstrated a slightly higher C yield as compared to the other samples. The inorganic material in the feedstock (biomass) may influence the co-pyrolysis catalytic process of volatile metals, such as alkali and alkaline earth metals (AAEM) can deactivate the ZSM-5 catalyst and poison the catalyst's active sites. The volatile metals in the ash may also initiate a positive effect that AAEM can catalyse and thermolysis reactions in the pyrolysis vapour phase and change the liquid product composition 280. The EDX for SSS:PP (1:1) co-pyrolysis is richer in carbon and lower in oxygen and other metal compounds as compared to SSS:PP (1:0). The EDX catalytic co-pyrolysis analysis of Feed-ZSM-5 (1:1/4) had the optimum carbon and oxygen which corroborate the CHNS analysis results.

4.4.6 Van Krevelen analysis

The atomic ratio of the hydrogen-carbon and oxygen-carbon ratio for the SSS:PP catalytic co-pyrolysis bio-oil demonstrates a lower H/C and O/C ratio in Figure 4.19, which eminently shows a higher potential of HHV. The SSS reveals that the O/C ratio was within 0.50 - 0.55 as the H/C ratio lies at 1.75 - 1.8. The SSS:PP (0:1) shows a similar lower O/C with SSS:PP (1:1). According to William et al., (2022) the Co-pyrolysis of beech wood (BW) and polyamide-6: Impact of plastic concentration and wood/plastic synergistic effects, the van Krevelen of BW and polyamide-6 (5 %), polyamide-6 (10 %) and polyamide-6 (20 %) had reaffirmed the $H/C > 1.0 - 1.3$ and $O/C \leq 0.3$ [295]. As reported by Sakulkit et al., (2020) study of characteristics of pyrolysis products from pyrolysis and co-pyrolysis of rubber wood and oil palm trunk biomass for biofuel and value-added applications, the H/C of crude oil and heavy fuel oil were ≥ 1.5 while the O/C were ≤ 0.1 [296]. The higher the H/O the tendency to record a high value for the HHV which is commendable.

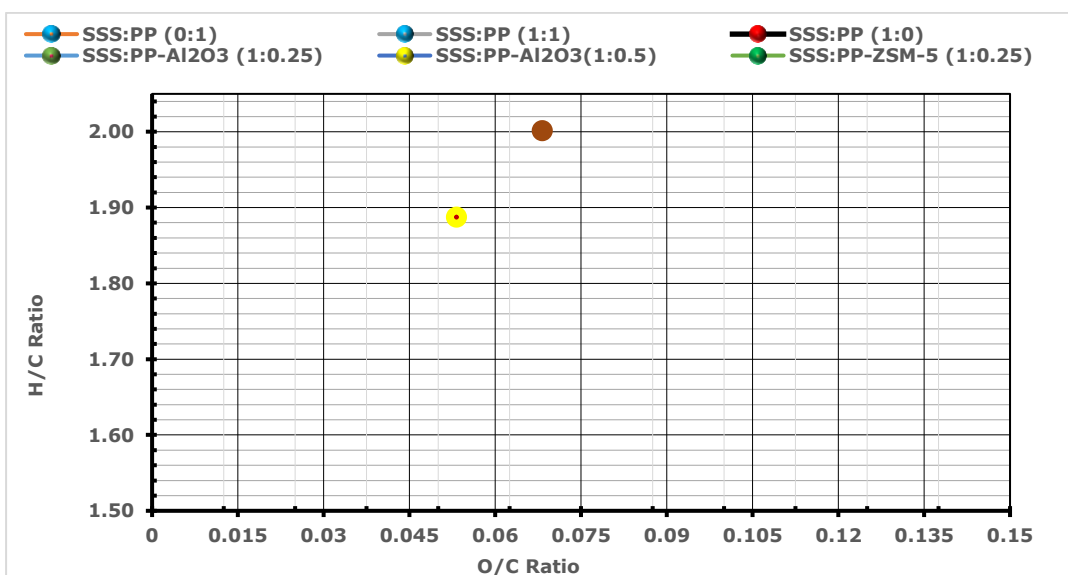
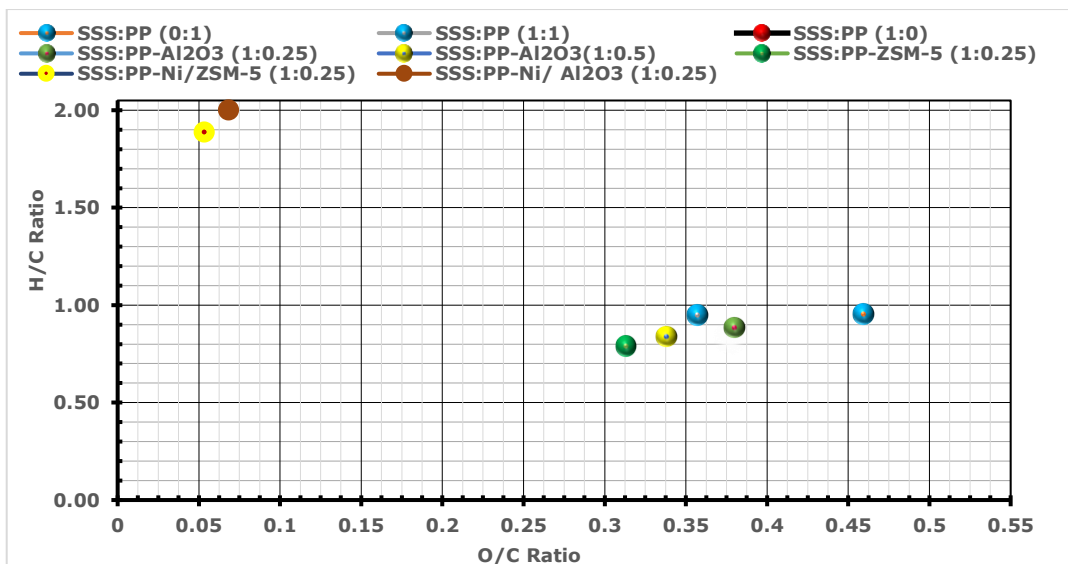


Figure 4.19: Van Krevelen of SSS:PP (0:1), SSS:PP (1:1), SSS:PP (1:0), SSS:PP-Al₂O₃ (1:1/4), SSS:PP-Al₂O₃ (1:1/2), SSS:PP-ZSM-5 (1:1/4), SSS:PP-Ni/ZSM-5 (1:1/4), SSS:PP-Ni/Al₂O₃ (1:1/4) samples.

4.4.7 Fourier transform infra-red (FTIR) SSS:PP pyrolysis products.

Figure 4.20(a and b) represents the FTIR of all the studied samples displayed 6 identified compounds, The SSS:PP (0:1), SSS:PP (1:1), SSS:PP (1:0), Feed-Al₂O₃ (1:1/4), Feed- Al₂O₃ (1:1/2), Feed-ZSM-

5 (1:1/4), Feed-Ni/ZSM-5 (1:1/4), Feed-Ni/Al₂O₃ (1:1/4). The wavenumbers above 1500 1/cm functional group are most likely aliphatic (C-H), unsaturated alkene (C=C), alkyne (C≡C), and alcohol (O-H) compounds.

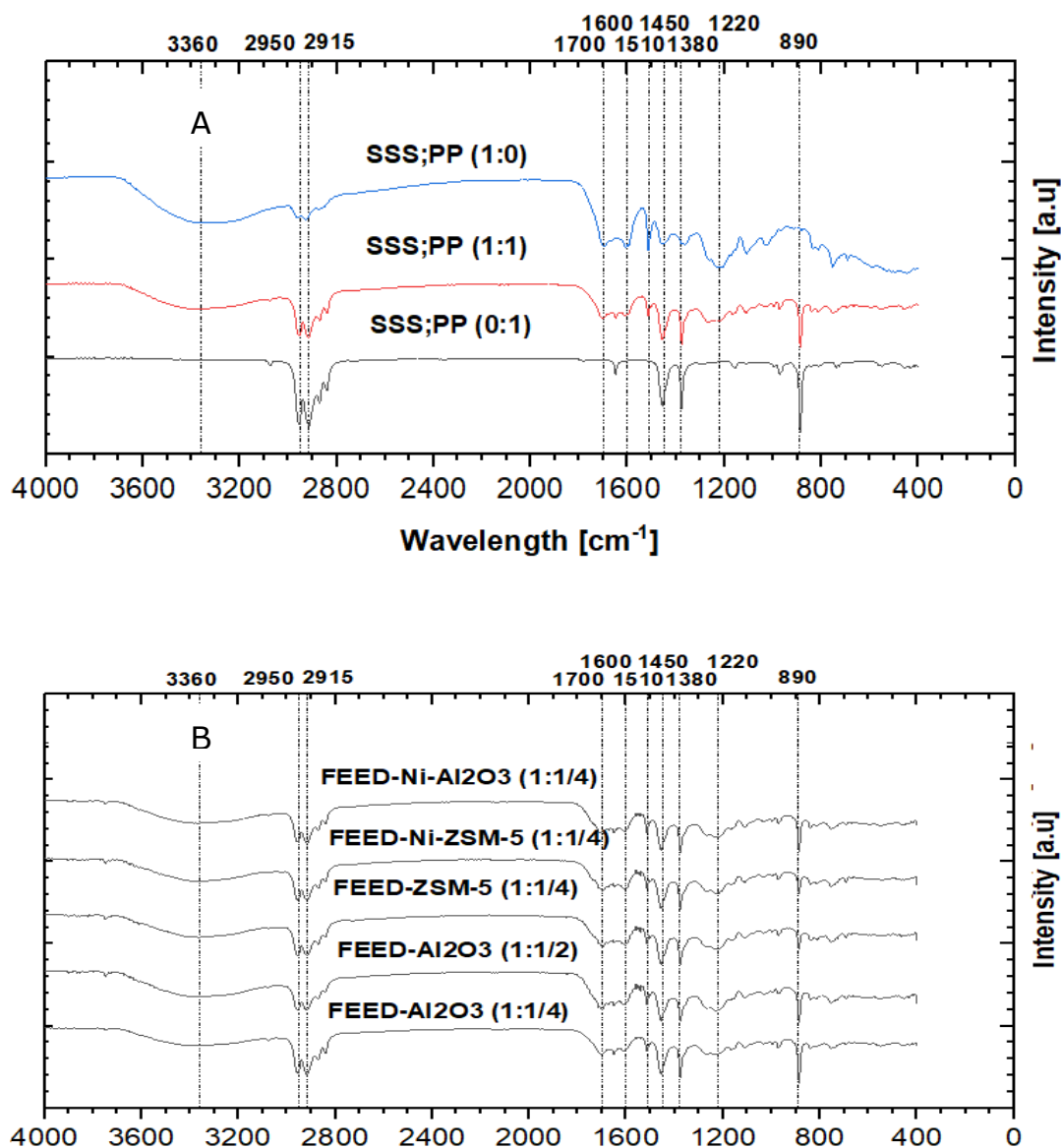


Figure 4.20: FTIR for pyrolysis oil (a) SSS:PP (0:1), SSS:PP (1:1), SSS:PP (1:0) and (b) Feed-Al₂O₃ (1:1/4), Feed-Al₂O₃ (1:1/2), Feed-ZSM-5 (1:1/4), Feed-Ni/ZSM-5 (1:1/4), Feed-Ni/Al₂O₃ (1:1/4).

The prominent adsorption intensity at 3360 1/cm is in the range of 3600 – 3200 1/cm short and broad corresponds to stretching vibrations of O-H bonds, typically associated with hydroxyl (-OH) groups in Figure 4.20(a) SSS:PP (1:1), and evidently in SSS:PP (1:0), but completely absent in the SSS:PP (0:1) sample. According to Ibrahim et al., (2022), the presence is an H-bonding (O-H stretching contains alcohol (O-H) and is very polar [281]. The peaks at around 3318 1/cm were attributed to -OH groups [282] and relatively obvious and orderly as SSS:PP (1:0) > SSS:PP (1:1) > FEED-Al₂O₃ (1:1/2) > FEED-Ni/Al₂O₃ (1:1/4) and almost diminishing in the FEED-ZSM-5 (1/1/4) bio-oil samples, because ZSM-5 as higher limiting factor for OH as compared to Al₂O₃ [293]. The presence of hydroxyl groups in SSS may influence the interactions between sweet sorghum stalk and polypropylene in the SSS:PP (1:1) mixture. It's possible that hydrogen bonding or other interactions occur between the hydroxyl groups of SSS and the polymer chains of PP, resulting in changes in the intensity or shape of the absorption band at 3360 1/cm.

In contrast, the wavenumber within 3000 – 2900 1/cm had the sharp and short intensity observed at wavenumbers 2950 and 2915 1/cm in the FTIR spectrum of SSS:PP (1:1) indicates the presence

of aliphatic hydrocarbons, likely arising from the alkyl chains of both sweet sorghum stalk and polypropylene. The preservation of distinct peaks with high intensity suggests minimal alteration of the chemical molecular structures of the individual components in the mixture, which is non-polar and likely an alkane [281], with C-H stretching in the bio-oil. The absorption peak at 2870 - 2970 $1/\text{cm}$ for CH, and CH₂, is an aliphatic hydrocarbon product [284]

Figure 4.20 shows the wavenumber of 1700 and 1500 $1/\text{cm}$ with an intensity broad spectrum between the two associates within 1900 - 1600 $1/\text{cm}$ (C=O, aldehydes and organic acids, ketones and esters) [283], and collaborated with the peaks at 1702 $1/\text{cm}$ also attributed to C=O stretching [282]. The absorption band at 1700 $1/\text{cm}$ likely arises from carbonyl stretching vibrations in components of sweet sorghum stalk, such as ester groups in hemicellulose or potential carbonyl-containing compounds resulting from thermal degradation during pyrolysis. The band at 1500 $1/\text{cm}$ may arise from aromatic stretching vibrations in lignin or other aromatic compounds present in SSS. The peak at about 1600 $1/\text{cm}$ is more pointed in SSS:PP (1:0) as compared to SSS:PP (0:1). Polypropylene, SSS:PP (0:1) being a synthetic polymer, doesn't contain aromatic structures in its chemical composition. Therefore, its presence in the SSS:PP (1:0) mixture would dilute the intensity of the peak at 1600 $1/\text{cm}$

associated with aromatic compounds, resulting in a less pronounced or broadened peak compared to samples without PP, which corresponds to the C=C groups stretching in aromatic rings [282].

The peaks at 1510 and 1200 1/cm were present in all the samples in Figure 4.20. Figure 4.20 (a and b) except the SSS:PP (1:0) bio-oil. The peaks at 1510 1/cm typically correspond to stretching vibrations of aromatic carbon-carbon (C=C) bonds, indicating the presence of aromatic compounds, while 1200 1/cm could be attributed to various functional groups, including stretching vibrations of C-O bonds in esters or ethers, or vibrations of C-C bonds in aliphatic structures. As reported by Liu et al., (2022) the peak at 1509 and 1200 1/cm are aromatic compounds and: alcohols and acids (C-O-H), respectively [283]. Moreover, between 1100 - 1200 1/cm was assigned to C-O [282]. The 1450 and 1373 1/cm are C-H stretching and an alkene peak representation, which was pointed but broad only in the SSS:PP (1:0), perhaps because of the liquid phase in the bio-oil sample from biomass pyrolysis. As reported by Hou et al., (2022) the peaks at 1365 - 1490 1/cm are absorption for CH, and CH₂, showing aliphatic hydrocarbon skeletons' presence in the yielded samples [284]. The peak at 890 1/cm for SSS:PP (0:1) is broad but in the opposite direction

compared to SSS:PP (1:1) oil samples, because it undergoes immense intermolecular hydrogen bonding.

Figure 4.20(b) FTIR analysis of the samples is largely hydrocarbon with biofuel prospects for energy generation. Overall, the FTIR results demonstrated that the catalytic co-pyrolysis had more excellent C-H-containing functional groups and aliphatic hydrocarbon. The wavelength of the catalytic co-pyrolysis bio-oil is consistent all through in terms of their FTIR. The FTIR analysis in characterizing the chemical composition, properties, intensity, and broadness of bio-oils produced through catalytic co-pyrolysis processes, suggests that the observed consistency is a desirable attribute in such products. Moreover, suggests the likely enhancement ability of biomass-plastic co-pyrolysis to sorb a wide range of organic contaminants or impurities such as methylene blue [282].

4.4.8 GC- MS (Gas chromatography-mass spectrometry)

In Figure 4.21 the GC-MS analysis result shows a total of seven (7) (a) two non-catalysts, and (b) five catalysts -oil samples: The SSS:PP (1:1), SSS:PP (0:1), SSS:PP-(Al₂O₃) (1:1/2), SSS:PP-

(25wt.%Al₂O₃) (1:1/4), SSS:PP-(25wt.%Ni/Al₂O₃) (1:1/4), SSS:PP-(ZSM-5) (1:1/4), and SSS:PP (25wt.%ZSM-5) (1:1/4).

The SSS:PP (0:1), SSS:PP (Al₂O₃) (1:1/2), Al₂O₃ (1:1/4), and Ni/Al₂O₃ (1:1/4) results had more hydrocarbon, with fractions of acetic acid and alcohols. The SSS:PP (1:1) co-pyrolysis has relatively more acetic acid than the catalysed SSS:PP (1:1), except for the ZSM-5 catalyst. The non-catalyst SSS:PP (1:1) samples constituted a high percentage of alkane, while ZSM-5 (1:1/4) produced other compounds such as benzene and acetic acid. Contrarily, the 25wt.%Ni/ZSM-5 (1:1/4) results indicate more alkene produced than alkane and alcohol produced in addition to acetic acids and benzene. Praveen et al., (2020), stated that the primary pyrolysis products of PP are mainly branched olefins and alkanes, resulting from the haphazard scission of the parent polymer chain [285]. Generally, the 25wt.%Ni/Al₂O₃ catalyst would be the optimum to produce higher hydrocarbon with the least acids. However, if more alkane is required, a non-catalyst of SSS:PP (1:1) would be more appropriate. The 25wt.%Ni/ZSM-5 (1:1/4) is favourable if benzene generation is also of preference in the product.

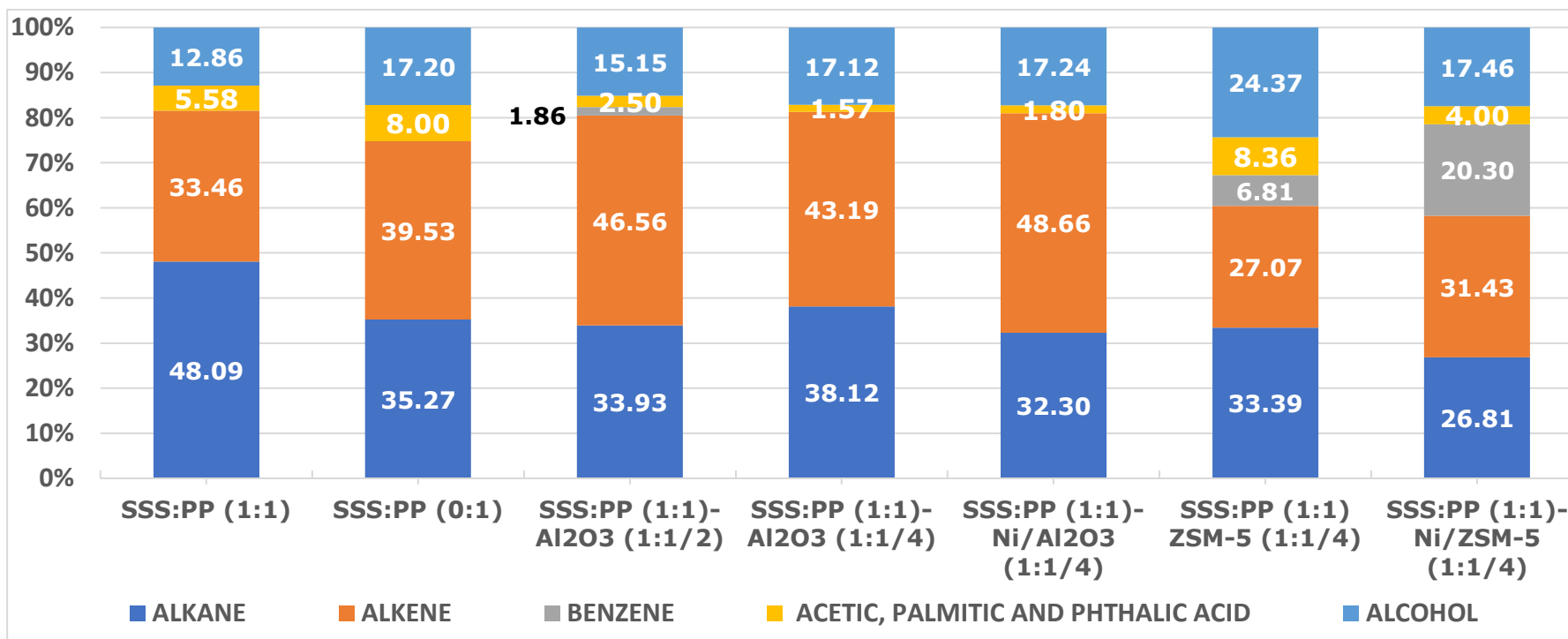


Figure 4.21: The GCMS classification according to the significant chemicals and area percentage.

Mostly, the hydrogen transfer occurs from the PP chain to the SSS-derived radicals, stabilizing SSS degradation products. This mechanism helps improve the hydrocarbon yield and restricts char formation. The PP-rich hydrogen polymer provides large hydrogen to the SSS and increases the hydrocarbon yield. As a result, the pyrolysis oil projected yield is to increase a high PP proportion, as shown in Figure 4.18. According to Li et al., (2018), the selectivity of this hydrogenation reaction showed the same trend mainly because NiO can produce a more active centre on the catalyst surface, catalytic performance of Ni/Al₂O₃ catalyst for hydrogenation of 2-methylfuran to 2-methyltetrahydrofuran which facilitates the hydrogenation reaction [286]. The final bio-oil in all co-pyrolysis experiments contained rich hydrocarbons and less oxygenate phase.

Figure 4.21 shows the product distribution of SSS and PP mixtures. The feed mixture formed useful hydrocarbons (aliphatic and aromatics) and had a combined yield between ~49.63 for the ZSM-5 (1:1/4) catalyst and ~76.3 for Al₂O₃ (1:1/4), while the non-catalyst SSS:PP (1:1) had 89.7 area %. Yellow poplar and HDPE were co-pyrolyzed using mesoporous Al-MCM-41 and HZSM-5 catalysts to study the catalytic effects. The HZSM-5 catalyst quickly converted HDPE into higher aromatic and gas yields with long-chain

hydrocarbon products [287]. The catalyst effect on SSS:PP (1:1) also contributed to char reduction ($\sim 16.45 \pm 0.63$ wt. %) as against $\sim 28.62 \pm 0.86$ wt. % to (see Figure 4.21). The aromatics deoxygenation was an additional reaction mechanism for producing hydrocarbons [288]. According to Praveen et al., (2020) maintaining a hydrogen-rich environment during catalytic co-pyrolysis has contributed to the conversion of biomass to useful hydrocarbons and lowered char formation [285].

4.4.9 Comparison of the Intermediate and catalytic co-pyrolysis.

The intermediate pyrolysis heating rate of the experiments was recorded as 33 °C/min, at 600 °C. The SSS bio-oil yield was 44.2 ± 6 , and the catalytic co-pyrolysis of SSS:PP 25 %Ni/Al₂O₃ (1:0.25) bio-oil yielded 49.02 ± 0.26 wt. %. According to Wenfei., (2024), in catalytic pyrolysis of biomass waste using montmorillonite-supported ultrafine iron nanoparticles for enhanced bio-oil optimum yield was 56.9 % during the catalytic pyrolysis of corncob and was suitable to produce bio-oil [311]. As reported by Abrar et al., (2022) as co-pyrolysis for bio-oil production via fixed bed reactor using date seeds and plastic waste as biomass, recorded better option for a higher bio-oil yield (59.16 %) [2022]. According to Obie et al., (2024) co-pyrolysis of plastic waste and macroalgae *Ulva Lactuca*,

a sustainable valorisation approach towards the production of bio-oil and biochar produced the highest bio-oil yield of 37.91 % of hydrocarbon content attaining 57.16 % was achieved under optimal conditions at 500 °C with a feedstock mixture consisting of 40 % *U. lactuca* and 60 % PET. As co-pyrolysis of polyethylene and black liquor using Mo-Ni/HZSM-5 for preparing high-quality bio-oil for an increased hydrocarbon from 14.92 % to 42.03 % [312], the addition of plastics can significantly improve the hydrocarbons yield of black liquor [314]. In this circumstance of SSS:PP (1:1) feed ratio of the catalytic co-pyrolysis of SSS:PP 25 %Ni/Al₂O₃ (1:0.25) yielded bio-oil of 49.02 ± 0.26 wt. % as the most optimum but lower biochar yield.

The SSS bio-oil and biochar HHV were within 23.8 ± 1.8 and 22.5 ± 3.5 MJ/kg, while the catalytic co-pyrolysis of SSS:PP 25 % Ni/Al₂O₃ (1:0.25) bio-oil and biochar recorded at 41.1 ± 0.7 and 10.3 MJ/kg respectively. According to Obie et al., (2024) a co-pyrolysis of plastic waste and macroalgae *Ulva Lactuca*, a sustainable valorisation approach towards the biochar production with HHV of 16.03 MJ/kg [314]. As reported Chiun et al., (2023), co-pyrolyzed palm shell and PS with 40:60 ratio at 600 °C and 45 min reaction time, produced bio-oil with HHV of 40.34 MJ/kg [310]. The co-pyrolysis of plastic and biomass bio-oil HHV are within 30 –

40 MJ/kg, while the catalytic co-pyrolysis of SSS:PP 25% Ni/Al₂O₃ (1:0.25) bio-oil as 41.1 ± 0.7 which is quite impressive in line with related works and supersedes in most cases and biochar recorded 10.3 MJ/kg respectively. According to Nabeel et al., (2024), catalytic co-pyrolysis of *Vachellia Farnesiana* with polypropylene plastic to produce bio-oil with an improved gross calorific value from 37.82 to 40.44 MJ/kg to the fuel standard within 42 - 46 MJ/kg [313]. The intermediate catalytic co-pyrolysis of SSS:PP 25% Ni/Al₂O₃ (1:0.25) is more promising in increasing HHV of the bio-oil produced in comparison to SSS pyrolysis. The catalytic co-pyrolysis bio-oil of SSS:PP 25 %Ni/Al₂O₃ (1:0.25) adjudged best yield with excellent C-H- functional groups, and aliphatic hydrocarbon corroborated by GCMS analysis of about 38 % (alkane), 43 % (alkene), while about 17 % (alcohol).

4.5 Wet torrefaction of SNC under different temperatures and residence times to improve its fuel properties.

4.5.1 Hydrothermal process water phase diagram

Hydrothermal process, hydrolysis and degradation of cellulose and hemicellulose will occur close to the critical point [283]. A detailed view of the physicochemical properties of subcritical water is presented in Figure 4.22. The physicochemical properties of hot

compressed water (HCW) play a significant role in the chemical reactions occurring in a hydrothermal operation. At elevated temperatures, the HCW has lower density and viscosity, which leads to an increased diffusion rate compared to standard water conditions. The reduction in the mass transfer resistances facilitates the diffusion rate and mobility of chemical compounds, which quickens the reactions [283]. When the water reaches the critical point, water has other distinctive characteristics such as high solubility for organic compounds and low viscosity [284]. These few prominent properties constitute subcritical water as a unique reaction environment. Water demonstrates a good, harmless, cost-effective reaction environment in WT processes. In Figure 4.22, hydrothermal carbonization (HTC), hydrothermal liquefaction (HTL) and hydrothermal gasification (HTG) reactions start before the critical point. As the HCW reactions approach the critical point ($T_{cr} = 374^{\circ}\text{C}$, $P_{cr} = 22.1 \text{ MPa}$, $\rho_c = 320 \text{ kg/m}^3$), the properties of the phase become identical. The ionic product (K_w) at the critical point drastically reduces to 1.86×10^{-16} [283].

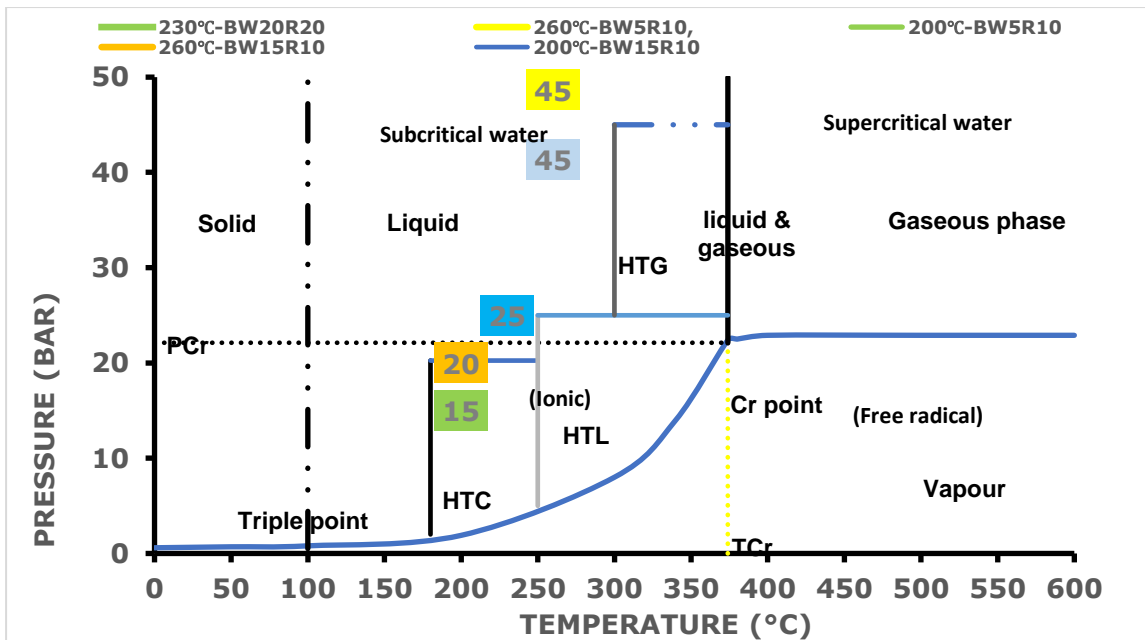


Figure 4.22: Water phase diagram for a hydrothermal process.

At this point, ionization products of water (H_3O^+ and OH^-) may act as a natural acid and base to catalyse many chemical reactions. The WT for an HCW reaction temperature of ≤ 300 °C is more befitting for the highest ionic product to enhance biomass decomposition. In this study, the pressure increased twice from 20 to 45 bar as the reaction temperature increased from 200 to 260 °C as pressure attained at 260 °C (45 bar) was higher than the saturated vapour pressure of water at the corresponding temperature.

4.5.2 ANOVA statistical model analysis.

The ANOVA for the model (2FI model) and their parameters are given in Table 4.10, with an F-value of 36.73 and a p-value of <0.0001, which implies that the model is significant. The model terms with a p-value of <0.05 indicated that the parameters have a significant effect on the yield. In this case, the effects of temperature (A), water/biomass (B), and their interactive effect (AB) are significant. In addition, the overall predictive capacity of the model was quantified via the R² terms: adjusted R² and predicted R². The model will be reliable if R² > 0.7. On the other hand, a predicted R² value with a maximum deviation of 0.2 is desired to ensure good agreement between actual and predicted values. The adequate precision of the model that represents the signal-to-noise ratio was 21.6757, ensuring its suitability to navigate the design space. The final equation in coded factors determining the mass yield (MY) which enables predictions of the response for given levels of each factor is shown in Eqn. 4.3.

$$\text{Exp. Yield} = 59.40 - 4.88A - 2.82B + 0.3414C + 3.49AB - 0.0962AC + 1.12B \quad \text{Eqn. 4.3}$$

where,

Exp. Yield = Experimental yield
A = Temperature (°C)

B = H₂O/Biomass ratio (g/g)
C = Residence time (min)

There is a 0.5771 possibility that a Lack of Fit F-value this large could occur due to noise and a standard deviation of 1.56, with a regression coefficient of 0.9443; the non-significant lack of fit is good, so it is a successful model applicable for related experiments. The final equation for coded factors determining the mass yield (MY) was to make predictions about the response for given levels of each factor using Eqn. 4.3 from the Design-Expert® software.

As the coefficients of A and B indicate, the mass yield decreased as the temperature and W/B ratio increased. Reductions in yield for the increase in temperature were reported in the literature [283], [79]. The mass yield and HHV led to a high energy yield of ~75 % and a maximum of ~90 % for 260°C-W/B5R10. Barskov et al. reported that the energy yield for WT of agricultural waste ranges from 5.0 % to 101.5 %, equivalent to an average of 71.9 % energy. In this study, the average energy yield was 82.9 %, a 15.3 % increase more than the agricultural waste energy 285. The HHV of torrefied SNC waste ranged within 12.21 – 15.81 MJ/kg, with an average of 13.6 MJ/kg higher than that of raw SNC by 72.9 %. The higher the torrefaction temperature, the higher the HHV value and the lower the mass yield. HHV increased with increased process

temperature and decreased mass yield [82]. As the W/B ratio increased from 5 to 15 at 260 °C, the HHV was reduced. However, there was no significant reduction in HHV when the W/B ratio increased from 5 to 15 at 200 °C. This could be due to the ionic effect of water at high temperatures, which improves reactions.

Table 4.10: ANOVA for 2FI model, yield, fit & model summary statistics.

Source	Sum squares	of Df	Mean square	F-value	P-value	Adeq. Precision	
Model	536.11	6	89.35	36.73	< 0.0001	21.6757	significant
A-Temperature	322.77	1	322.77	132.69	< 0.0001		
B-Water /Biomass	104.18	1	104.18	42.83	< 0.0001		
C-Residence Time	1.61	1	1.61	0.6604	0.431		
AB	97.51	1	97.51	40.09	< 0.0001		
AC	0.0741	1	0.0741	0.0305	0.8641		
BC	9.97	1	9.97	4.1	0.064		
Residual	31.62	13	2.43				
Lack of Fit	18.63	8	2.33	0.8962	0.5771		Not Significant
Pure Error	12.99	5	2.6				
Cor Total	567.73	19					
Source	Sequential P-value	Lack of fit P-value	Adjusted R ²	Predicted r ²	STD. Dev.	R ²	Press
2FI	0.0002	0.5771	0.9186	0.8517	1.56	0.9443	84.19 Suggested

Table 4.11: Design of Experiment, report on the actual and predicted responses product yields for SNC

Run	A: Temp. (°C)	B:H ₂ O/Biomass ratio (g/g)	C: Residence time (min)	Hydrochar Yield (wt. %)	Predicted Yield (wt. %)	HHV (MJ/kg)	Energy yield (%)	Pressure (bar)
1	200	5	30	69.65	69.91	11.54	82.76	14
2	230	10	20	56.75	59.40	14.31	83.62	25
3	230	10	37	61.70	59.98	13.09	83.16	22
4	260	5	10	55.00	54.72	15.81	89.54	45
5	260	15	30	57.00	56.56	13.98	82.05	42
6	200	15	30	60.65	59.53	13.16	82.19	22
7	230	10	20	59.10	59.40	13.45	81.85	25
8	230	18	20	53.50	54.90	13.05	71.89	27
9	230	2	20	64.40	63.91	11.51	76.33	28
10	230	10	20	60.20	59.40	11.22	69.55	25
11	230	10	30	59.15	58.82	12.22	74.43	26
12	200	5	10	72.23	71.27	12.95	96.32	15
13	230	10	20	56.00	59.40	12.19	70.29	26
14	260	5	30	53.30	52.98	13.96	76.62	48
15	180	10	20	67.30	67.54	10.29	71.31	9
16	230	10	20	59.20	59.40	9.77	59.56	28
17	260	15	10	55.50	53.84	12.21	69.78	45
18	230	10	20	58.80	59.40	13.98	84.64	28
19	280	10	20	51.15	51.27	13.86	73.00	60
20	200	15	10	57.50	56.42	12.79	75.73	20

Table 4.10 shows the design of the experiment for 20 runs, with both the experimental and predicted yields of the hydrochar, its energy percentage and HHV. The experimental yield ranges attained were within 51.15 - 72.23 wt. % as shown in Table 4.10


There would be cellulose degradation in addition to hemicellulose and lignin. In the literature, the influence of the W/B ratio was not relatively significant but showed an improvement in fuel properties (grindability and lowered AC); the low ratio allowed the highest energy yield to be achieved [184],[79]. Low-oxygenated compounds increase the hydrophobicity of torrefied biomass, thus enhancing combustion between 200 °C and 300 °C [149].

The 3-D interaction plot with the parameters (temperature, and water-to-biomass ratio) in Figure 4.23(a) at 260 °C and 15 minutes of the residence time, translating to an HHV of about 15 MJ/kg. It depicts the optimum temperatures and biomass-to-water ratio from 230 – 260 °C, and within 10 - 15 ratio anchoring its standard error of design at 0.6. Figure 4.23(b) consolidates and confirms the interaction of the temperature and biomass-to-water ratio as 230 °C and +15 respectively as optimum parameters. However, the biomass-to-water ratio could best interact at 254.39 °C in agreement with 260°C-W/B5R10 used in the experiment.

Factor Coding: Actual

Std Error of Design

● Design Points

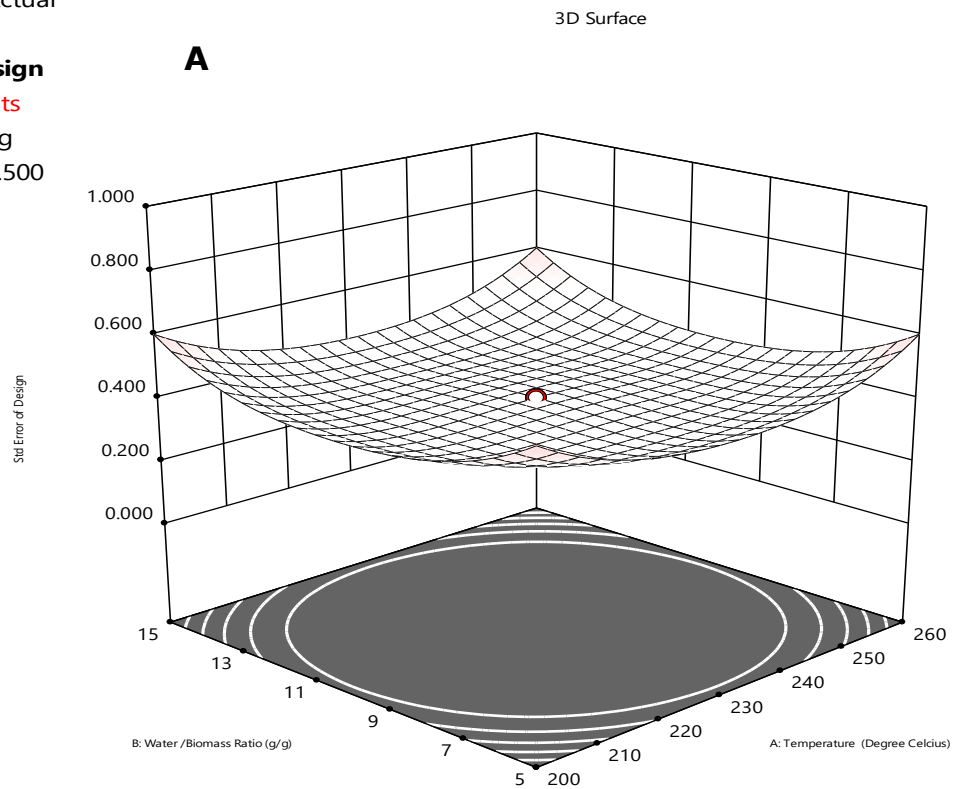
Std Error Shading
0.500  1.500

X1 = A

X2 = B

Actual Factor

C = 20



Factor Coding: Actual

Exp. Yield (%)

● Design Points

⋯ 95% CI Bands

⋯ 95% PI Bands

⋯ 95% TI Bands (p=99%)

X1 = A

X2 = B

Actual Factor

C = 20

■ B- 5

▲ B+ 15

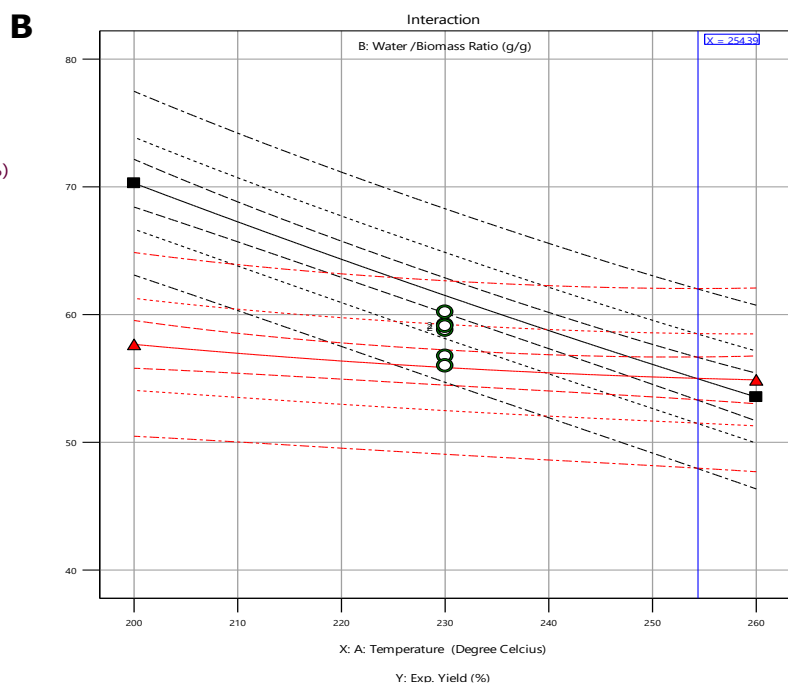


Figure 4.23: (a) The 3-D surface standard error of design and (b) model graph parameter interactions for the experimental yield %.

4.5.3 Proximate analysis of raw and torrefied SNC biomass.

Proximate analyses of the raw and torrefied SNC are shown in Table 4.12 below. The raw SNC's moisture content (MC) was 47.03 ± 1.18 wt. %. therefore, the SNC was highly suitable for hydrothermal pre-treatment. The MC significantly improved between the raw and the torrefied SNC, which was likely due to moisture re-adsorption at slightly different atmospheric conditions. As expected, the samples torrefied at 260°C-W/B15R10 and had lower moisture content than those torrefied at 200°C-W/B5R10.

Table 4.12: Proximate analysis raw and torrefied SNC result.

Proximate analysis		HHV	MC	AC	VM	FC
S/NO	Hydrochar	(MJ/kg)	(wt. %)			
1	Raw SNC received	7.87	47.0 ± 1.18	20.6 ± 0.28	27.5	4.9
2	Raw SNC for WT	9.712	16 ± 0.0	37.92 ± 3.6	ND	ND
3	200°C-W/B5R10	12.95	10.5 ± 0.1	45.433 ± 1.6	15.68	27.19
4	200°C-W/B15R10	12.79	05.1 ± 0.0	47.36 ± 1.3	27.24	20.3
5	230°C-W/B10R20	14.31	07.0 ± 0.0	51.09 ± 0.01	25.11	16.8
6	260°C-W/B5R10	15.81	11.0 ± 1.4	50.99 ± 1.01	10	28.01
7	260°C-W/B15R10	12.21	03.1 ± 3.1	53.85 ± 3.83	23.39	19.26

Note: ND- not determined

The raw sample had a low VM of about 27.5 wt. % as a by-product of the shea butter extraction, which may not favour pyrolysis potential. There was a reduction in the VM of torrefied samples. However, at the same temperature as the W/B ratio increased, the VM of the torrefied sample increased. This could be due to the presence of severe reactions at higher amounts of water (therefore higher pressure) which led to easily volatile compounds from FC, and the corresponding reduction in FC was observed. The samples studied had FC < 25 wt. %, except for 200°C- W/B5R10 and 260°C- W/B5R10, which recorded higher values due to the low W/B ratio. As stated, the low amount of water brought more polymerization and C-C formation. A significant increase in FC was noticed after torrefaction [80], and FC is linked directly with biomass energy potential. The relatively high AC of raw SNC might have resulted from the initial heat treatment undergone during the extraction of shea butter. The AC increased as the torrefaction temperature increased [82]. According to Jaideep et al., (2021) an increase in AC results from the breakdown of carbon-hydrogen bonds and loss of volatile content [250]. However, the ash content of the biomass was not washed away with the filtrate, which likely affect the torrefied biomass in energy and environmental applications. A study by Monti et al., (2008) revealed that a 0.2 MJ/kg decrease in HHV resulted from a 1 % ash content increase for six energy crops [197]. In

addition, the higher ash content was directly proportional to lower heating values. Usually, HTC hydrochar results in low ash content due to the formation of acetic acid that solubilizes and leaches out inorganics from the solid fraction [286]. However, the current study had a slight difference as AC was increasing. The filtrate collected in this study had a pH of 5, which shows the absence of acidic or hemicellulose-derived components. Therefore, acid was not present during WT for the removal of minerals, and it is recommended to use acid catalysts to reduce as content of torrefied biomass.

4.5.4 Atomic ratio (AR).

The torrefied biomass at 260°C-W/B5R10 demonstrated a 25.6 % decrease in oxygen and a 53.0 % carbon content increase as compared to the raw SNC. Meanwhile, 260°C-W/B15R10 demonstrated only a 19.3 % decrease in oxygen and a 20.0 % increase in carbon content. These results showed that the W/B ratio increases the amount of oxygenated compound in torrefied biomass and might result in a high amount of VM. As shown in Figure 4.24, the atomic ratios of torrefied biomass H/C and O/C are between 1.0 and 1.5 and less than or equal to 0.5, respectively. Many kinds of wood and bio-fibre contain varied oxygen (O/C ratio) within 0.75 – 1.50, while fossil fuels (coals, char, and tar) have an oxygen content of O/C ranging from 0 to 0.30 [224]. The results from the current

study were compared to wetland biomass such as *H. verticillata*, *M. spicatum*, and *C. indica* [76]. Cui et al.'s study showed that hydrochar produced at 200 °C had an O/C ratio near to 0.5 and hydrochar produced at 260°C had an O/C ratio near to 0.2. As compared to their study, SNC torrefaction resulted from lower oxygen content, which varied from 0.01 to 0.2 as temperature increased [76].

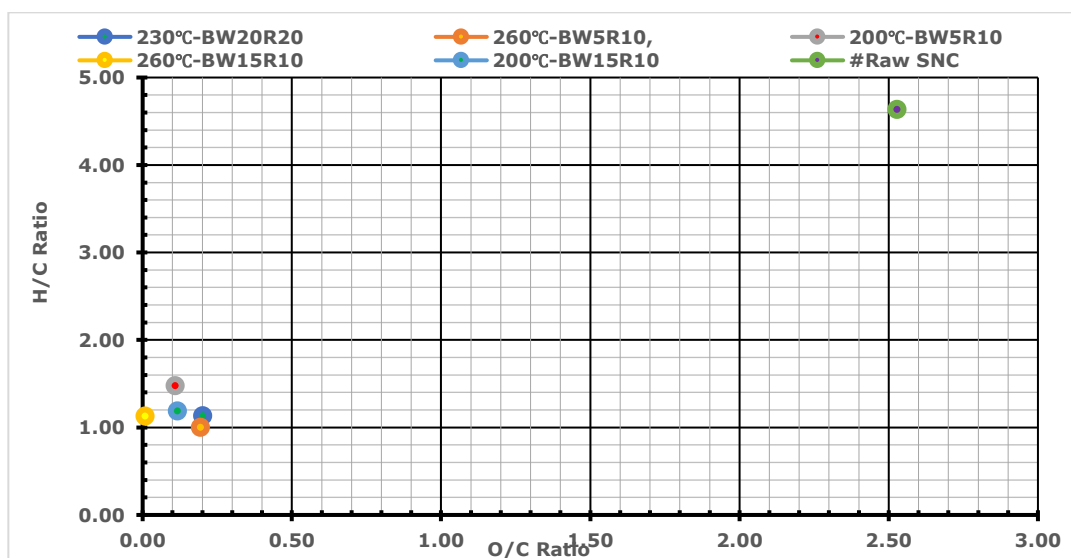


Figure 4.24: Van Krevelen diagram for hydrochar 230°C-W/B10R20, 260°C-W/B5R10, 200°C-W/B5R10, 260°C-W/B15R10, 200°C-W/B15R10, and Raw SNC.

The torrefaction process reduces the oxygen-to-carbon (O/C) and hydrogen-to-carbon (H/C) ratios, making biomass more compatible with coal [287]. The reduction of oxygenated compounds increased hydrophobicity and minimized water adsorption from the atmosphere by the torrefied biomass, thereby facilitating combustion [150]. Normally, the coal H/C ratio varies from 0.5 to

1, whereas the O/C ratio varies from 0.02 to 0.2 from anthracite to lignite. Though lignite has a high hydrogen content, it has lower HHV due to the high amount of oxygen as compared to anthracite coal.

4.5.5 Thermal analysis of SNC

The thermal degradation properties of SNC samples were analysed and presented in Table 4.13; thermal degradation can be subdivided into three characteristic phases, namely moisture evaporation and light components (32 – 115 °C), devolatilization of cellulose, and hemicellulose (115 – 400 °C), followed by lignin decomposition (400 – 900 °C).

Table 4.13: Electron-dispersive X-ray (EDX) analysis composition.

Element (s)	Raw SNC	200°C- W/B5R10	200°C- W/B15R10	230°C- W/B10R20	260°C- W/B5R10	260°C- W/B15R10
C	57.0±8.9	66.1±0.4	51.2±2.7	54.2±8.2	69.3±6.9	72.8±1.6
O	35.9±5.5	27.7±1.1	39.4±18.	23.6±3.4	25.1±4.3	24.0±1.7
N	1.2±1.6	3.9±0.6	Nil	17.5±0.5	4.1±0.0	4.2±0.0
Mg	0.3±0.1	0.2±0.0	0.1±0.1	0.3±0.2	0.2±0.1	0.3±0.1
Al	1.23±0.5	0.62±0.1	0.21±0.1	0.84±0.7	0.56±0.6	0.35±0.2
Si	3.92±3.7	2.3±0.4	8.85±8.9	1.82±1.8	2.13±3.0	0.60±0.4
S	0.2±0.1	0.25±0.0	0.11±0.0	0.34±0.3	0.20±0.0	0.21±0.0
K	0.84±0.3	0.22±0.0	0.06±0.0	0.84±1.0	0.09±0.0	0.14±0.0
Ca	0.29±0.1	0.28±0.0	0.16±0.1	3.58±5.3	0.26±0.1	0.43±0.2
Fe	0.17±0.1	0.3±0.0	0.08±0.0	0.09±0.0	0.10±0.0	0.11±0.1
Ti	0.20 ± 0.1	0.21 ± 0.0	Nil	10.7 ± 1.6	0.22 ± 0.0	0.03 ± 0.0
Pore size (µm)	1.614-4.598	1.464-4.941	2.353-4.666	1.173-2.685	1.680-3.034	0.797-3.831

4.6 Summary of products analysis of the objectives.

This section contains the product yield and result analysis in Table 4.1 and Table 4.14 for physicochemical analysis, intermediate pyrolysis of BGS-G1, SSS and SNS, intermediate pyrolysis of BGS-G1 with different inert gases, catalytic co-pyrolysis of SSS and PP, and wet torrefaction of SNC.

In objective one smaller particle sizes favour complete pyrolysis in bio-oil production. The BGS-UT1 had the maximum HHV of 18.6 ± 0.5 MJ/kg, with MC $\leq 8.6 \pm 3.0$ wt. %, and a minimum AC of 6.8 ± 0.5 wt. %. The lower MC of PT1 and UT1 are 5.4 ± 0.3 and 8.6 ± 3.0 wt. %, in their category, recorded the highest VM of 74.7 and 70.3 wt. % of 1180 μm particle size respectively. The proximate analysis reflects BGS carbon-hydrogen, oxygen, nitrogen, and sulphur content as 43.9, 6.1, 41.7, 1.3, and 0.1 wt. %. It has a high carbon, low nitrogen, and sulphur content valuable for bioenergy compared to BGS-G4 and BGS-G5. The Van Krevelen diagram shows a low O/C and H/C ratio for BGS-G1 (0.9507), which also depicts HHV convergence in Table 4.1. The kinetics study with the best regression coefficient of 0.9717 had an activation energy of 21.00 KJ/mol and a pre-exponential factor of 43.3. The dry BGS has an average total weight loss of 61.47 wt. % within the temperature

range of 184 – 620 °C, and the solid product was ≤ 38.53 wt. %, reflecting its potential as a renewable energy source because of its high volatile content and low ash and mineral (10.35 wt. %) content.

The analysis performed for the three samples (BGS-G1, SSS, and SNS), which are readily available wastes from industrial and agricultural activities, was fruitful. The fixed carbon for all the samples was less than 25 wt. % and the VM was above 69 wt. %. The H/C and O/C ratios of the BGS-G1 and SNS (bio-oil and biochar) are close within the Van Krevelen diagram except for the SSS (biomass) only. Intermediate pyrolysis of BGS-G1, SSS, and SNS operated at 600 °C, which recorded an average heating rate ≥ 33.0 °C/min yielded bio-oil of 38.0 ± 6.4 , 44.2 ± 6 , 39.7 ± 5.2 wt. % respectively. The high quantity of phenols and ketone present in all the samples of the GC-MS result studied was due to the lower H/C ratio. The oxygenates in the bio-oil should be removed to increase the high content of esters and phenols as they are more valuable as bioenergy than traditional fossil fuels. The HHV recorded for the BGS-G1, SSS, and SNS for both bio-oil and biochar were 23 - 26 and 18-26 MJ/kg, respectively. The HHV percentage increase of bio-oil is 33.75, 31.1, 33.21 % and biochar is 16.49, 28.40, and 32.95 %. The overall physicochemical analysis and products (bio-oil and biochar) acknowledged, that SNS among the three samples has the best biofuel potential.

The intermediate pyrolysis heating rate of BGS-G1, SSS, and SNS was recorded as 33 °C/min, at a temperature of 600 °C with the best bio-oil yield (SSS) of 44.2 ± 6 wt. %. The BGS-G1, SSS, and SNS bio-oil and biochar HHV were within 23 - 26 and 18-26 MJ/kg, respectively, but the SNS biochar and bio-oil yielded the highest HHV with around 26.5 MJ/kg. The BGS intermediate pyrolysis oil yield at different flow rates in the presence of N₂, CO₂ or N₂/CO₂ did not change significantly (39 - 40 wt. %). The pH values tend towards neutrality ($5.2 \pm 0.1 - 5.8 \pm 0.9$), because of low acids compounds in bio-oil, while the presence of CO₂ influenced the HHV positively.

Table 4.14: Summary of products analysis for objectives 2, 3, 4 and 5.

PARAMETERS	BIO-OIL			BIOCHAR		
Intermediate pyrolysis	BGS-G1	SSS (N)	SNS	BGS-G1	SSS	SNS
Yield wt. %	38.0 ± 6.4	44.2 ± 6	39.7 ± 5.2	45.7 ± 4	27.1 ± 1.1	43.6 ± 6.0
HHV (MJ/kg)	23.7 ± 1.8	23.8 ± 1.8	26.5 ± 2.0	18.8 ± 1.2	22.5 ± 3.5	26.4 ± 1.8
Density (g/cm ³)	1.01 ± 0.0	1.04 ± 0.0	1.04 ± 0.0	-	-	-
pH	5.01	2.57	2.87	-	-	-
Intermediate pyrolysis	Bio-oil	Bio-oil	Bio-oil	Biochar	Biochar	Biochar
BGS-G1	(5 mL/min)	(17.5 mL/min)	(30 mL/min)	(5 mL/min)	(17.5 mL/min)	(30 mL/min)
Yield wt. % (N ₂)	39.5	40.3	39.4	35.4	35.5	36.5
Yield wt. % (CO ₂)	39.2	39.3	38.6	36.9	35.9	38.7
Yield wt. % (N ₂ / CO ₂)	40.3	39.8	40.8	37.0	39.1	37.1
HHV (MJ/kg) (N ₂)	11.5	14.5	11.9	-	-	-
HHV (MJ/kg) (CO ₂)	16.5	14.5	17.0	-	-	-
HHV (MJ/kg) (N ₂ / CO ₂)	15.1	17.8	14.2	-	-	-
PARAMETERS	Bio-oil	Bio-oil	Bio-oil	Biochar	Biochar	
Feed Pyrolysis ratio	HHV (MJ/kg)	pH	Uncertainty	HHV (MJ/kg)	Uncertainty	
SSS:PP (0:1)	44.3 ± 0.43	3.8-4.3	2.95	0.00 ± 0.00	0	
SSS: PP (1:1)	40.3 ± 0.05	3.30	0.09	22.4 ± 0.34	0.37	
SSS:PP (1:0)	16.3 ± 0.55	2.99	0.07	22.9 ± 0.10	0.5	
Feed-Catalyst ratio	BIO-OIL	BIO-OIL	BIO-OIL	BIOCHAR	BIOCHAR	
Feed-Al ₂ O ₃ (1:1/2)	41.5 ± 0.5	3.36	0.50	5.4 ± 0.11	0.09	
Feed-Al ₂ O ₃ (1:1/4)	41.0 ± 0.9	3.37- 3.43	2.23	8.7 ± 0.05	1.14	
Feed-ZSM-5 (1:1/4)	41.8 ± 2.4	3.56	0.97	9.8 ± 0.03	0.11	
Feed-Ni/ZSM-5 (1:1/4)	38.4 ± 0.4	2.99	0.60	10.4 ± 0.15	0.34	
Feed-Ni/Al ₂ O ₃ (1:1/4)	41.1 ± 0.7	3.48	0.19	10.3 ± 0.06	0.10	

Hydrochar (SNC) (wt. %)	HHV (MJ/kg)	Filtrate yield	Filtrate pH	Hydrochar	Energy yield
200°C-W/B5R10	12.95	60.0	4.96	72.23	96.32
200°C-WB15R10	12.79	80.7	5.30	57.50	95.73
230°C-W/B10R20	14.31	67.5	5.24	56.75	83.62
260°C-W/B5R10	15.81	55.0	6.37	55.00	89.54
260°C-W/B15R10	12.21	66.7	6.95	55.50	69.78

The intermediate catalytic co-pyrolysis of SSS and PP feeds was studied over Al_2O_3 , and 25wt. %Ni/ Al_2O_3 catalysts, acidic catalysts (ZSM-5) and 25wt. %Ni/ZSM-5. The 25wt. %Ni/ Al_2O_3 catalyst had the optimum bio-oil and HHV at 49.02 ± 0.26 wt. % and 41.1 ± 0.7 MJ/kg respectively. It is adjudged the best yield with high excellent C-H- functional groups, and aliphatic hydrocarbon corroborated by the GCMS analysis, with more alkene formation perhaps because of the catalyst effect and temperature absorption capacity with low heat rate release of polymeric materials in the pyrolysis, as compared with the co-pyrolysis of SSS:PP (1:1) with an improved pH value. It has the potential to substitute conventional fuels after being subjected to further treatments.

This study focused on investigating the mass and energy potential of the SNC via WT. The MC of the raw SNC was 47.03 ± 1.18 wt. %, which was suitable for a hydrothermal process. The torrefied SNC mass yield was 55.0 wt. % at 260 °C, W/B ratio of 5 and residence time of 10 min, and 45 bar. The mass yield of torrefaction was highly influenced by temperature and W/B ratio. The torrefied samples with relatively high AC, as a negative attribute for energy. The utilization of an acid catalyst for WT was suggested to remove the acid content of torrefied biomass. The highest HHV of 15.8 MJ/kg was reported for torrefied SNC in this study. However, the HHV of torrefied SNC were relatively high compared to the raw SNC.

The optimum energy yield and HHV of 89.5 % and 15.81 MJ/kg, accounting for 75 % and 90 % increment for 260°C-W/B5R10 as compared to the raw SNC. The torrefied samples had a unique surface morphology with a consistent porous structure compared to the raw SNC. In conclusion, SNC has high potential as an energy component using the WT process; however, the removal of AC was required to utilize it in the energy field.

CHAPTER FIVE

5 Conclusion and recommendation (Future work)

5.1 Research summary.

The bio-oil production from Bambara Groundnut Shells (BGS-G1), Sweet Sorghum Stalk (SSS), and Shea Nutshells (SNS) via pyrolysis and wet torrefaction have limited or no classical study. This research study included the intermediate pyrolysis of BGS, SSS, SNS, and wet torrefaction of SNC to produce high-energy products such as bio-oil and biochar. Objective 4 biomass (SSS) was adopted for the catalytic co-pyrolysis because it yields more pyrolysis oil, more sustainable for energy, while SNC was used in a hydrothermal process because of its high moisture content. The results of the experimental studies and analysis were discussed, and the following conclusions were deduced, with some future recommendations.

5.2 Conclusion

The three BGS genotypes; BGS-G1, BGS-G4, and BGS-G5 physicochemical analysis were studied. BGS-G1 recorded the highest carbon content of 43.9, wt. % and lower O/C ratio with a DTG/TGA pyrolysis temperature within 190 - 650 °C suitable for bioenergy than BGS (G4 and G5) samples. The intermediate pyrolysis heating rate of BGS-G1, SSS, and SNS was recorded as 33 °C/min, at 600 °C with the best bio-oil yield (SSS) of 44.2 ± 6

wt. %. The BGS-G1, SSS, and SNS bio-oil and biochar HHV were within 23 - 26 and 18-26 MJ/kg, respectively, but the SNS biochar and bio-oil yielded the highest HHV with around 26.5 MJ/kg. The BGS intermediate pyrolysis oil yield at different flow rates in the presence of N₂, CO₂ or N₂/CO₂ did not change significantly (39 - 40 wt. %). The pH values tend towards neutrality (5.2 ± 0.1 – 5.8 ± 0.9), because of low acids compounds in bio-oil, while the presence of CO₂ influenced the HHV positively. The intermediate catalytic co-pyrolysis of SSS and PP were studied over amphoteric catalysts (Al₂O₃, and 25 %Ni/Al₂O₃) and acidic catalysts (ZSM-5 and 25 %Ni/ZSM-5). The 25 %Ni/Al₂O₃ (1:0.25) had the optimum bio-oil and HHV at 49.02 ± 0.26 wt. % and 41.1 ± 0.7 MJ/kg and adjudged the best yield with excellent C-H- functional groups, and aliphatic hydrocarbon corroborated by GCMS analysis of about 38 % (alkane), 43 % (alkene), while about 17 % (alcohol). It has the potential to substitute conventional fuels after being subjected to further treatments. The MC of the raw SNC was 47.03 ± 1.18 wt. %, which is suitable for HTC due to the high moisture level. The optimum torrefied SNC (260°C-W/B5R10) yielded 55.0 wt. % hydrochar, with a pressure of ≤ 4.5 MP. The hydrochar mass reduction yield resulted in the optimum energy yield and higher heating value (HHV) of 89.54 % and 15.81 MJ/kg, accounting for ~ 75 % and ~ 90 % increments compared to the raw SNC.

The findings suggested that BGS, SSS, and SNS produced better bio-oil and char and processed in their uniqueness as underutilized crop biomass, as well as polypropylene which improved their biofuel properties. However, SSS was an outstanding biomass for bio-oil yield (44.2 wt. %), while the SNS bio-oil and biochar yielded the highest HHV with around 26.5 MJ/kg for bioenergy in comparison to all three samples.

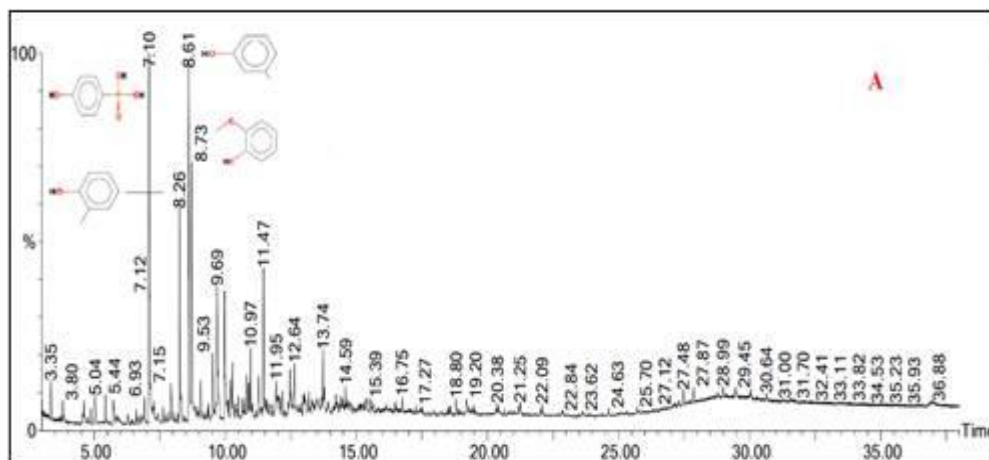
5.3 Recommendation (Future work)

The intermediate and catalytic co-pyrolysis of SSS to bio-oil and wet torrefaction of SNC to hydrochar of high-grade fuel presented a high prospect for conventional fuel. This research was carried out in a fixed bed reactor and a high-pressure batch wet torrefaction reactor, recommendations, and future work on these studies are to be engaged upon in furtherance of this research.

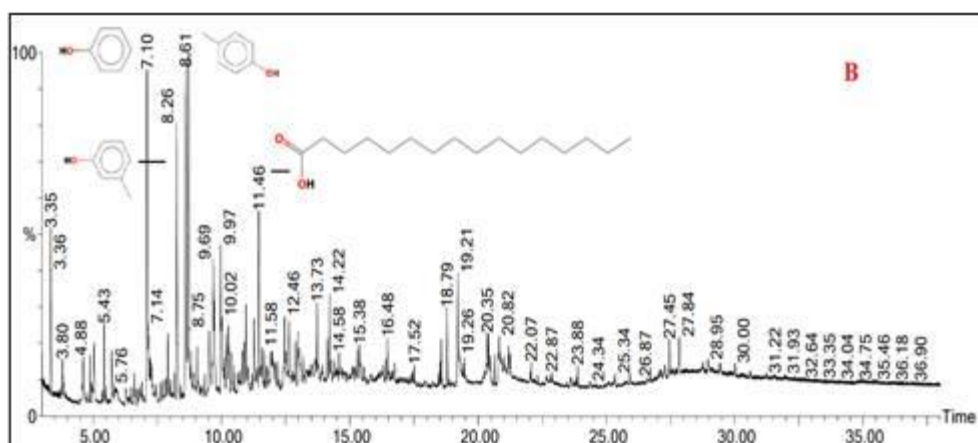
- 1) Continuous intermediate pyrolysis and co-pyrolysis of SSS, SNS and wet torrefaction of SNC with improved process parameters.
- 2) The internal combustion engine test, parameter evaluation and valuable green chemical extraction from the aqueous phase of bio-oil from the SSS, SNS and SNC.
- 3) Intermediate pyrolysis of SSS, SNS, and catalytic co-pyrolysis of SSS and PP liquid-oil and biochar.

4) The economic evaluation of the process or Techno-economic analysis for the continuous intermediate catalytic co-pyrolysis of SSS, SNS, and SNC and product upgrades to meet the environmental protection agency.

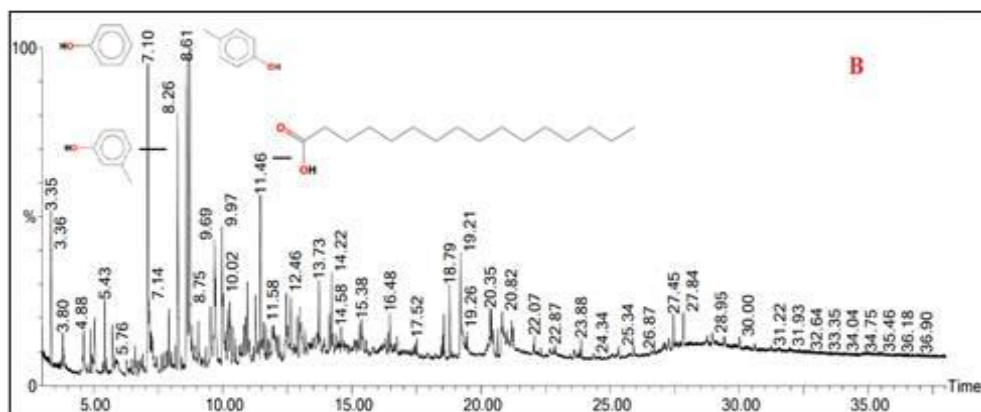
Appendices



Appendix 4.3.1: The GC-MS chromatogram for bio-oil produced during the pyrolysis in the presence of N_2 inert gas at 17.5 mL/min.



Appendix 4.3.2: The GC-MS chromatogram for bio-oil produced during the pyrolysis in the presence of CO_2 inert gas at 17.5 mL/min.



Appendix 4.3.3: The GC-MS chromatogram for bio-oil produced during the pyrolysis in the presence of N_2/CO_2 inert gas at 17.5 mL/min.

Appendix 4.4.1: BET analysis of calcined Al₂O₃ catalysts

S/No	Catalyst wt. %	Average Adsorption pore size width, Å	Total Single point adsorption pore volume cm ³ /g	Single point surface area m ² /g
1	Al ₂ O ₃	168.7	0.0022	0.5457
2	10Ni/ Al ₂ O ₃	209.2	0.0074	1.4099
3	15Ni/ Al ₂ O ₃	333.9	0.0069	0.9078
4	ZSM-5	25.27	0.2321	377.39

Note: Prepared activated alumina is used as a carrier by calcination of activated alumina at 600°C

References

- [1] A. Williams, J. M. Jones, L. Ma, and M. Pourkashanian, *Pollutants from the combustion of solid biomass fuels*, vol. 38, no. 2. 2012, pp. 113–137. doi: 10.1016/j.pecs.2011.10.001.
- [2] M. P. González-Vázquez, R. García, M. V. Gil, C. Pevida, and F. Rubiera, "Comparison of the gasification performance of multiple biomass types in a bubbling fluidized bed," *Energy Convers Manag*, vol. 176, no. July, pp. 309–323, 2018, doi: 10.1016/j.enconman.2018.09.020.
- [3] M. Auersvald *et al.*, "Hydrotreatment of straw bio-oil from ablative fast pyrolysis to produce suitable refinery intermediates," *Fuel*, vol. 238, no. October 2018, pp. 98–110, 2019, doi: <https://doi.org/10.1016/j.fuel.2018.10.090>.
- [4] M. Verma, S. Godbout, S. K. Brar, O. Solomatnikova, S. P. Lemay, and J. P. Larouche, "Biofuels production from biomass by thermochemical conversion technologies," *International Journal of Chemical Engineering*, vol. 2012, 2012, doi: 10.1155/2012/542426.
- [5] C. U. Jensen, J. K. R. Guerrero, S. Karatzos, G. Olofsson, and S. B. Iversen, "Hydrofaction™ of forestry residues to drop-in renewable transportation fuels," *Direct Thermochemical Liquefaction for Energy Applications*, pp. 319–345, Jan. 2018, doi: 10.1016/B978-0-08-101029-7.00009-6.
- [6] J. Baruah *et al.*, "Recent trends in the pretreatment of lignocellulosic biomass for value-added products," *Front Energy Res*, vol. 6, no. DEC, pp. 1–19, 2018, doi: 10.3389/fenrg.2018.00141.
- [7] A. T. Hoang *et al.*, "Progress on the lignocellulosic biomass pyrolysis for biofuel production toward environmental sustainability," *Fuel Processing Technology*, vol. 223, no. July, p. 106997, 2021, doi: 10.1016/j.fuproc.2021.106997.
- [8] A. K. Azad, M. G. Rasul, M. M. K. Khan, S. C. Sharma, and R. Islam, "Prospect of Moringa seed oil as a sustainable biodiesel fuel in Australia: A review," *Procedia Eng*, vol. 105, no. Ictc 2014, pp. 601–606, 2015, doi: 10.1016/j.proeng.2015.05.037.
- [9] R. Singh and S. Kumar, "Green technologies and environmental sustainability," *Green Technologies and Environmental Sustainability*, pp. 1–492, 2017, doi: 10.1007/978-3-319-50654-8.
- [10] D. Gielen, F. Boshell, D. Saygin, M. D. Bazilian, N. Wagner, and R. Gorini, "The role of renewable energy in the global energy transformation," *Energy Strategy Reviews*, vol. 24, no. January, pp. 38–50, 2019, doi: 10.1016/j.esr.2019.01.006.
- [11] N. A. Rashidi, Y. H. Chai, and S. Yusup, "Biomass Energy in Malaysia: Current Scenario, Policies, and Implementation Challenges," *Bioenergy Res*, no. 0123456789, 2022, doi: 10.1007/s12155-022-10392-7.
- [12] H. Bhakta, A. K. Sarmah, and B. Dubey, "Hydrothermal carbonization of renewable waste biomass for solid biofuel production : A discussion on process mechanism , the influence of process parameters ,

- environmental performance and fuel properties of hydrochar," *Renewable and Sustainable Energy Reviews*, vol. 123, no. May 2019, p. 109761, 2020, doi: 10.1016/j.rser.2020.109761.
- [13] A. Garba, "Biomass Conversion Technologies for Bioenergy Generation: An Introduction," in *Biotechnological Applications of Biomass*, T. P. Basso, T. O. Basso, and L. C. Basso, Eds., Rijeka: IntechOpen, 2020. doi: 10.5772/intechopen.93669.
- [14] W. A. Kenney, L. Sennerby-Forsse, and P. Layton, "A review of biomass quality research relevant to the use of poplar and willow for energy conversion," *Biomass*, vol. 21, no. 3, pp. 163–188, 1990, doi: 10.1016/0144-4565(90)90063-P.
- [15] M. Bošnjaković, "INFLUENCE OF MOISTURE CONTENT IN WOOD CHIPS ON THE BOILER OPERATION Heat exchanger with finned tubes View project Renewable Energy Sources View project INFLUENCE OF MOISTURE CONTENT IN WOOD CHIPS ON THE BOILER OPERATION," no. September 2020.
- [16] O. D. Mante and F. A. Agblevor, "Catalytic pyrolysis for the production of refinery-ready biocrude oils from six different biomass sources," *Green Chemistry*, vol. 16, no. 6, pp. 3364–3377, 2014, doi: 10.1039/c4gc00555d.
- [17] Z. I. Y, T. B. I, and G. N. N, "Investigation on biomass briquettes as energy source in relation to their calorific values and measurement of their total carbon and elemental contents for efficient biofuel utilization," *Pelagia Research Library Advances in Applied Science Research*, vol. 4, no. 4, pp. 303–309, 2013.
- [18] T. A. Volk, L. P. Abrahamson, and D. J. Aneshansley, "Developing a Willow Biomass Crop Enterprise for," *Willow Biomass in the United States*, no. January 2000.
- [19] A. Sridevi, G. Narasimha, G. Ramanjaneyulu, K. Dileepkumar, B. R. Reddy, and P. S. Devi, "Saccharification of pretreated sawdust by *Aspergillus niger* cellulase," *3 Biotech*, vol. 5, no. 6, pp. 883–892, 2015, doi: 10.1007/s13205-015-0284-7.
- [20] D. Aboagye, N. Banadda, N. Kiggundu, and I. Kabenge, "Assessment of orange peel waste availability in ghana and potential bio-oil yield using fast pyrolysis," *Renewable and Sustainable Energy Reviews*, vol. 70, no. December 2016, pp. 814–821, 2017, doi: 10.1016/j.rser.2016.11.262.
- [21] Y. Lee, S. Kim, E. E. Kwon, and J. Lee, "Effect of carbon dioxide on thermal treatment of food waste as a sustainable disposal method," *Journal of CO2 Utilization*, vol. 36, no. November 2019, pp. 76–81, 2020, doi: 10.1016/j.jcou.2019.11.004.
- [22] P. Roy, A. Dutta, and J. Gallant, "Evaluation of the life cycle of hydrothermally carbonized biomass for energy and horticulture application," *Renewable and Sustainable Energy Reviews*, vol. 132, no. July, p. 110046, 2020, doi: 10.1016/j.rser.2020.110046.

- [23] A. A. Id, P. Coelho, and J. Garc, "applied sciences An Experimental Technology of Drying and Clean Combustion of Biomass Residues", doi: 10.3390/app8060905.
- [24] S. Matali, N. A. Rahman, S. S. Idris, N. Yaacob, and A. B. Alias, "Lignocellulosic Biomass Solid Fuel Properties Enhancement via Torrefaction," *Procedia Eng*, vol. 148, pp. 671–678, 2016, doi: 10.1016/j.proeng.2016.06.550.
- [25] M. Morin, S. Pécate, M. Hémati, and Y. Kara, "Pyrolysis of biomass in a batch fluidized bed reactor: Effect of the pyrolysis conditions and the nature of the biomass on the physicochemical properties and the reactivity of char," *J Anal Appl Pyrolysis*, vol. 122, pp. 511–523, 2016, doi: 10.1016/j.jaap.2016.10.002.
- [26] D. V. Suriapparao and R. Vinu, "Effects of Biomass Particle Size on Slow Pyrolysis Kinetics and Fast Pyrolysis Product Distribution," *Waste Biomass Valorization*, vol. 9, no. 3, pp. 465–477, 2018, doi: 10.1007/s12649-016-9815-7.
- [27] D. Kotaiah Naik, K. Monika, S. Prabhakar, R. Parthasarathy, and B. Satyavathi, "Pyrolysis of sorghum bagasse biomass into biochar and bio-oil products: A thorough physicochemical characterization," *J Therm Anal Calorim*, vol. 127, no. 2, pp. 1277–1289, 2017, doi: 10.1007/s10973-016-6061-y.
- [28] M. A. Salam, K. Ahmed, N. Akter, T. Hossain, and B. Abdullah, "A review of hydrogen production via biomass gasification and its prospect in Bangladesh," *Int J Hydrogen Energy*, vol. 43, no. 32, pp. 14944–14973, 2018, doi: 10.1016/j.ijhydene.2018.06.043.
- [29] V. S. Sikarwar, M. Zhao, P. S. Fennell, N. Shah, and E. J. Anthony, "Progress in biofuel production from gasification," *Prog Energy Combust Sci*, vol. 61, pp. 189–248, 2017, doi: 10.1016/j.pecs.2017.04.001.
- [30] C. U. Pittman *et al.*, "Characterization of bio-oils produced from fast pyrolysis of corn stalks in an auger reactor," *Energy and Fuels*, vol. 26, no. 6, pp. 3816–3825, 2012, doi: 10.1021/ef3003922.
- [31] K. M. Qureshi, A. N. Kay Lup, S. Khan, F. Abnisa, and W. M. A. Wan Daud, "A technical review on semi-continuous and continuous pyrolysis process of biomass to bio-oil," *J Anal Appl Pyrolysis*, vol. 131, no. December 2017, pp. 52–75, 2018, doi: 10.1016/j.jaap.2018.02.010.
- [32] A. Pandey, T. Bhaskar, M. Stocker, and R. Sukumaran, *Recent Advances in Thermo-Chemical Conversion of Biomass*. 2015. doi: 10.1016/B978-0-444-63289-0.10000-6.
- [33] T. Gebgeegziabher, A. O. Oyedun, Y. Zhang, and C. W. Hui, *Effective optimization model for biomass drying*, vol. 32. Elsevier B.V., 2013. doi: 10.1016/B978-0-444-63234-0.50017-8.
- [34] E. T. Kostas, D. Beneroso, and J. P. Robinson, "The application of microwave heating in bioenergy: A review on the microwave pre-treatment and upgrading technologies for biomass," *Renewable and*

- Sustainable Energy Reviews*, vol. 77, no. November 2016, pp. 12–27, 2017, doi: 10.1016/j.rser.2017.03.135.
- [35] V. B. Agbor, N. Cicek, R. Sparling, A. Berlin, and D. B. Levin, "Biomass pretreatment: Fundamentals toward application," *Biotechnol Adv*, vol. 29, no. 6, pp. 675–685, 2011, doi: 10.1016/j.biotechadv.2011.05.005.
- [36] X. Hu and M. Gholizadeh, "Biomass pyrolysis: A review of the process development and challenges from initial researches up to the commercialisation stage," *Journal of Energy Chemistry*, vol. 39, no. x, pp. 109–143, 2019, doi: 10.1016/j.jechem.2019.01.024.
- [37] H. B. Goyal, D. Seal, and R. C. Saxena, "Bio-fuels from thermochemical conversion of renewable resources: A review," *Renewable and Sustainable Energy Reviews*. 2008. doi: 10.1016/j.rser.2006.07.014.
- [38] I. I. Enagi, K. A. Al-attab, and Z. A. Zainal, "Liquid biofuels utilization for gas turbines: A review," *Renewable and Sustainable Energy Reviews*. 2018. doi: 10.1016/j.rser.2018.03.006.
- [39] I. I. Enagi, K. A. Al-attab, and Z. A. Zainal, "Liquid biofuels utilization for gas turbines: A review," *Renewable and Sustainable Energy Reviews*, vol. 90, no. April 2017, pp. 43–55, 2018, doi: 10.1016/j.rser.2018.03.006.
- [40] L. D. M. Torquato, P. M. Crnkovic, C. A. Ribeiro, and M. S. Crespi, "New approach for proximate analysis by thermogravimetry using CO₂ atmosphere: Validation and application to different biomasses," *J Therm Anal Calorim*, vol. 128, no. 1, pp. 1–14, 2017, doi: 10.1007/s10973-016-5882-z.
- [41] R. García, C. Pizarro, A. G. Lavín, and J. L. Bueno, "Biomass proximate analysis using thermogravimetry," *Bioresour Technol*, vol. 139, pp. 1–4, 2013, doi: 10.1016/j.biortech.2013.03.197.
- [42] J. D. Morris, S. S. Daood, S. Chilton, and W. Nimmo, "Mechanisms and mitigation of agglomeration during fluidized bed combustion of biomass: A review," *Fuel*, 2018, doi: 10.1016/j.fuel.2018.04.098.
- [43] A. A. Atiku, N. A. Aviara, and M. A. Haque, "Performance Evaluation of a Bambara Ground Nut Sheller," *Agricultural Engineering International: CIGR Journal*, vol. VI, pp. 1–18, 2004.
- [44] X. L. Tan *et al.*, "Bambara Groundnut: An Underutilized Leguminous Crop for Global Food Security and Nutrition," *Front Nutr*, vol. 7, no. December, pp. 1–16, 2020, doi: 10.3389/fnut.2020.601496.
- [45] S. S. Mwale, S. N. Azam-Ali, and F. J. Massawe, "Growth and development of bambara groundnut (*Vigna subterranea*) in response to soil moisture. 1. Dry matter and yield," *European Journal of Agronomy*, vol. 26, no. 4, pp. 345–353, 2007, doi: 10.1016/j.eja.2006.09.007.
- [46] M. Musa and A. Singh, "Performance of Bambara groundnut (*Vigna subterranea* L. Verdc.) with rice husk biochar and Christmas Island Rock Phosphate application," *International Journal of Recycling of Organic Waste in Agriculture*, vol. 8, no. s1, pp. 93–101, 2019, doi: 10.1007/s40093-019-0278-2.

- [47] C. Mathews, "Food and Agricultural Organisation of the United Nation." Accessed: Sep. 19, 2019. [Online]. Available: <http://www.fao.org/traditional-crops/bambaragroundnut/en/>
- [48] I. Y. Mohammed, Y. A. Abakr, M. Musa, S. Yusup, A. Singh, and F. K. Kazi, "Valorization of Bambara groundnut shell via intermediate pyrolysis: Products distribution and characterization," *J Clean Prod*, vol. 139, pp. 717–728, 2016, doi: 10.1016/j.jclepro.2016.08.090.
- [49] I. Y. Mohammed, Y. A. Abakr, J. N. Xing Hui, P. A. Alaba, K. I. Morris, and M. D. Ibrahim, "Recovery of clean energy precursors from Bambara groundnut waste via pyrolysis: Kinetics, products distribution and optimisation using response surface methodology," *J Clean Prod*, vol. 164, pp. 1430–1445, 2017, doi: 10.1016/j.jclepro.2017.07.068.
- [50] G. Stevens and R. A. Y. Holou, "Sweet sorghum as a biofuel crop," *Issues in Environmental Science and Technology*, no. January, pp. 56–76, 2010, doi: 10.1039/9781849732048-00056.
- [51] D. Jiang *et al.*, "Mapping global environmental suitability for sorghum bicolor (L.) Moench," *Energies (Basel)*, vol. 12, no. 10, 2019, doi: 10.3390/en12101928.
- [52] M. Wang, Y. Chen, X. Xia, J. Li, and J. Liu, "Energy efficiency and environmental performance of bioethanol production from sweet sorghum stem based on life cycle analysis," *Bioresour Technol*, vol. 163, pp. 74–81, 2014, doi: 10.1016/j.biortech.2014.04.014.
- [53] A. Almodares and M. R. Hadi, "Production of bioethanol from sweet sorghum: A review." 2010.
- [54] A. A. Warra, "Cosmetics Potential Ofshea Butter.Pdf," *Knowledge review, Malaysia*, vol. Current re. pp. 80–86, 2011. doi: 10.3923/crc.2011.8.86.
- [55] I. Abdul-Mumeen, H. D. Zakpaa, C. M.-R. Felix, and S. T. Lowor, "Vitellaria paradoxa fruit pulp bioethanol production potential: A review," *African Journal of Biochemistry Research*, vol. 14, no. 2, pp. 33–45, 2020, doi: 10.5897/ajbr2019.1070.
- [56] N. A. Aviara, M. A. Haque, and I. A. Izge, "Physical and Frictional Properties of Sheanut," *Agro-Science*, vol. 1, no. 2. 2000. doi: 10.4314/as.v1i2.1452.
- [57] A. U. Itodo, F. W. Abdulrahman, L. G. Hassan, S. A. Maigandi, and U. O. Happiness, "Chemistry of pyrolysis and kinetic studies of shea nut (Vitellaria paradoxa) shells activated carbon for textile wastewater treatment," *Iranian Journal of Chemistry and Chemical Engineering*, vol. 30, no. 2, pp. 51–57, 2011.
- [58] C. M. Igwebuike, S. Awad, Y. A. Olanrewaju, and Y. Andrès, "The prospect of electricity generation from biomass in the developing countries," *International Journal of Smart Grid and Clean Energy*, no. May, pp. 150–156, 2021, doi: 10.12720/sgce.10.2.150-156.
- [59] A. Tagade, N. Kirti, and A. N. Sawarkar, "Pyrolysis of agricultural crop residues: An overview of researches by Indian scientific community," *Bioresour Technol Rep*, vol. 15, no. May, p. 100761, 2021, doi: 10.1016/j.biteb.2021.100761.

- [60] P. Das, C. V.P., T. Mathimani, and A. Pugazhendhi, "Recent advances in thermochemical methods for the conversion of algal biomass to energy," *Science of the Total Environment*, vol. 766, p. 144608, 2021, doi: 10.1016/j.scitotenv.2020.144608.
- [61] A. Sarvaramini, G. P. Assima, and F. Larachi, "Dry torrefaction of biomass - Torrefied products and torrefaction kinetics using the distributed activation energy model," *Chemical Engineering Journal*, vol. 229, pp. 498–507, 2013, doi: 10.1016/j.cej.2013.06.056.
- [62] Z. Z. Chowdhury, K. Pal, R. Bin Johan, W. A. Y. Dabdawb, M. E. Ali, and R. F. Rafique, "Comparative evaluation of physiochemical properties of a solid fuel derived from *adansonia digitata* trunk using torrefaction," *Bioresources*, vol. 12, no. 2, pp. 3816–3833, 2017, doi: 10.15376/biores.12.2.3816-3833.
- [63] I. L. Motta, N. T. Miranda, R. Maciel Filho, and M. R. Wolf Maciel, "Biomass gasification in fluidized beds: A review of biomass moisture content and operating pressure effects," *Renewable and Sustainable Energy Reviews*, vol. 94, no. May, pp. 998–1023, 2018, doi: 10.1016/j.rser.2018.06.042.
- [64] K. A. Babatunde, O. O. Agbede, I. I. Olateju, S. D. Bamidele, O. M. Osulale, and F. N. Osulale, "Biomass Gasification Potential in Nigeria: A Review," *LAUTECH Journal of Civil and Environmental Studies*, vol. 3, no. Issue 1, 2019, doi: 10.36108/laujoces/9102/20(0280).
- [65] M. Larsson, *Global energy transformation: Four necessary steps to make clean energy the next success story*. 2009. doi: 10.1057/9780230244092.
- [66] D. Meier, B. Van De Beld, A. V. Bridgwater, D. C. Elliott, A. Oasmaa, and F. Preto, "State-of-the-art of fast pyrolysis in IEA bioenergy member countries," *Renewable and Sustainable Energy Reviews*. 2013. doi: 10.1016/j.rser.2012.11.061.
- [67] I. L. Motta, N. T. Miranda, R. Maciel Filho, and M. R. Wolf Maciel, "Biomass gasification in fluidized beds: A review of biomass moisture content and operating pressure effects," *Renewable and Sustainable Energy Reviews*. 2018. doi: 10.1016/j.rser.2018.06.042.
- [68] A. R. K. Gollakota, N. Kishore, and S. Gu, "A review on hydrothermal liquefaction of biomass," *Renewable and Sustainable Energy Reviews*, vol. 81, no. August 2016, pp. 1378–1392, 2018, doi: 10.1016/j.rser.2017.05.178.
- [69] A. T. Sipra, N. Gao, and H. Sarwar, "Municipal solid waste (MSW) pyrolysis for bio-fuel production: A review of effects of MSW components and catalysts," *Fuel Processing Technology*, vol. 175, no. November 2017, pp. 131–147, 2018, doi: 10.1016/j.fuproc.2018.02.012.
- [70] D. Shen, W. Jin, J. Hu, R. Xiao, and K. Luo, "An overview on fast pyrolysis of the main constituents in lignocellulosic biomass to valued-added chemicals: Structures, pathways and interactions," *Renewable*

- and Sustainable Energy Reviews*, vol. 51, pp. 761–774, 2015, doi: 10.1016/j.rser.2015.06.054.
- [71] T. Shan Ahamed, S. Anto, T. Mathimani, K. Brindhadevi, and A. Pugazhendhi, "Upgrading of bio-oil from thermochemical conversion of various biomass – Mechanism, challenges and opportunities," *Fuel*, vol. 287, no. August, p. 119329, 2021, doi: 10.1016/j.fuel.2020.119329.
- [72] Z. Yao, S. You, T. Ge, and C. H. Wang, "Biomass gasification for syngas and biochar co-production: Energy application and economic evaluation," *Appl Energy*, vol. 209, no. July 2017, pp. 43–55, 2018, doi: 10.1016/j.apenergy.2017.10.077.
- [73] R. V. P. Antero, A. C. F. Alves, S. B. de Oliveira, S. A. Ojala, and S. S. Brum, "Challenges and alternatives for the adequacy of hydrothermal carbonization of lignocellulosic biomass in cleaner production systems: A review," *J Clean Prod*, vol. 252, p. 119899, 2020, doi: 10.1016/j.jclepro.2019.119899.
- [74] OECD/FAO, "Chapter 9. Biofuels," *OECD-FAO Agricultural Outlook 2018-2027*, pp. 191–206, 2018.
- [75] S. S. Ail and S. Dasappa, "Biomass to liquid transportation fuel via Fischer Tropsch synthesis - Technology review and current scenario," *Renewable and Sustainable Energy Reviews*, vol. 58, pp. 267–286, 2016, doi: 10.1016/j.rser.2015.12.143.
- [76] X. Cui *et al.*, "Hydrothermal carbonization of different wetland biomass wastes: Phosphorus reclamation and hydrochar production," *Waste Management*, vol. 102, pp. 106–113, 2020, doi: 10.1016/j.wasman.2019.10.034.
- [77] X. Zhuang, Y. Song, H. Zhan, X. Yin, and C. Wu, "Gasification performance of biowaste-derived hydrochar: The properties of products and the conversion processes," vol. 260, no. October 2019, 2020, doi: 10.1016/j.fuel.2019.116320.
- [78] C. Lin *et al.*, "Thermochemical Gasification of real MSW-derived hydrochar under various atmosphere and temperature," *Thermochim Acta*, vol. 683, no. November 2019, p. 178470, 2020, doi: 10.1016/j.tca.2019.178470.
- [79] M. Wnukowski, P. Owczarek, and Ł. Niedźwiecki, "WET torrefaction of miscanthus - characterization of hydrochars in view of handling, storage and combustion properties," *Journal of Ecological Engineering*, vol. 16, no. 3, pp. 161–167, 2015, doi: 10.12911/22998993/2950.
- [80] S. Nizamuddin, N. S. Jayakumar, J. N. Sahu, P. Ganesan, A. W. Bhutto, and N. M. Mubarak, "Hydrothermal carbonization of oil palm shell," *Korean Journal of Chemical Engineering*, vol. 32, no. 9, pp. 1789–1797, 2015, doi: 10.1007/s11814-014-0376-9.
- [81] P. Biller and A. B. Ross, *Production of biofuels via hydrothermal conversion*. Elsevier Ltd, 2016. doi: 10.1016/B978-0-08-100455-5.00017-5.
- [82] W. A. Oyebode and H. O. Ogunsuyi, "Impact of torrefaction process temperature on the energy content and chemical composition of stool tree (*Alstonia congenisis* Engl) woody biomass," *Current Research in*

- Green and Sustainable Chemistry*, vol. 4, no. May, p. 100115, 2021, doi: 10.1016/j.crgsc.2021.100115.
- [83] A. Williams, M. Pourkashanian, J. M. Jones, and N. Skorupska, "Properties of Coal," *Combustion and Gasification of Coal*, pp. 21–54, 2019, doi: 10.1201/9781315139746-2.
- [84] Y. Y. Gan *et al.*, "Torrefaction of microalgal biochar as potential coal fuel and application as bio-adsorbent," *Energy Convers Manag*, vol. 165, no. January, pp. 152–162, 2018, doi: 10.1016/j.enconman.2018.03.046.
- [85] C. He *et al.*, "Wet torrefaction of biomass for high quality solid fuel production: A review," *Renewable and Sustainable Energy Reviews*, vol. 91, no. April, pp. 259–271, 2018, doi: 10.1016/j.rser.2018.03.097.
- [86] W. H. Chen, J. Peng, and X. T. Bi, "A state-of-the-art review of biomass torrefaction, densification and applications," *Renewable and Sustainable Energy Reviews*. 2015. doi: 10.1016/j.rser.2014.12.039.
- [87] C. M. S. da Silva *et al.*, "Biomass torrefaction for energy purposes – Definitions and an overview of challenges and opportunities in Brazil," *Renewable and Sustainable Energy Reviews*, vol. 82, no. July 2017, pp. 2426–2432, 2018, doi: 10.1016/j.rser.2017.08.095.
- [88] M. Grigiante, M. Brighenti, and D. Antolini, "A generalized activation energy equation for torrefaction of hardwood biomasses based on isoconversional methods," *Renewable Energy*. 2016. doi: 10.1016/j.renene.2016.07.054.
- [89] E. T. Kostas, D. Beneroso, and J. P. Robinson, "The application of microwave heating in bioenergy: A review on the microwave pre-treatment and upgrading technologies for biomass," *Renewable and Sustainable Energy Reviews*, vol. 77, no. April, pp. 12–27, 2017, doi: 10.1016/j.rser.2017.03.135.
- [90] H. Khodaei, Y. M. Al-Abdeli, F. Guzzomi, and G. H. Yeoh, "An overview of processes and considerations in the modelling of fixed-bed biomass combustion," *Energy*. 2015. doi: 10.1016/j.energy.2015.05.099.
- [91] E. R. Widjaya, G. Chen, L. Bowtell, and C. Hills, "Gasification of non-woody biomass: A literature review," *Renewable and Sustainable Energy Reviews*, vol. 89, no. September 2016, pp. 184–193, 2018, doi: 10.1016/j.rser.2018.03.023.
- [92] L. J. R. Nunes, J. C. O. Matias, and J. P. S. Catalão, "Biomass combustion systems: A review on the physical and chemical properties of the ashes," *Renewable and Sustainable Energy Reviews*, 2016, doi: 10.1016/j.rser.2015.08.053.
- [93] A. A. A. Abuelnuor *et al.*, "Characteristics of biomass in flameless combustion: A review," *Renewable and Sustainable Energy Reviews*. 2014. doi: 10.1016/j.rser.2014.01.079.
- [94] A. Morato-Godino, S. Sánchez-Delgado, N. García-Hernando, and A. Soria-Verdugo, "Pyrolysis of *Cynara cardunculus* L. samples – Effect of operating conditions and bed stage on the evolution of the conversion," *Chemical Engineering Journal*, vol. 351, no. April, pp. 371–381, 2018, doi: 10.1016/j.cej.2018.06.114.

- [95] L. E. Hernandez-Mena, A. A. B. Pecora, and A. L. Beraldo, "Slow pyrolysis of bamboo biomass: Analysis of biochar properties," *Chem Eng Trans*, vol. 37, no. May, pp. 115–120, 2014, doi: 10.3303/CET1437020.
- [96] Q. Yang, F. Han, Y. Chen, H. Yang, and H. Chen, "Greenhouse gas emissions of a biomass-based pyrolysis plant in China," *Renewable and Sustainable Energy Reviews*, vol. 53, pp. 1580–1590, 2016, doi: <https://doi.org/10.1016/j.rser.2015.09.049>.
- [97] W. Cai, R. Liu, Y. He, M. Chai, and J. Cai, "Bio-oil production from fast pyrolysis of rice husk in a commercial-scale plant with a downdraft circulating fluidized bed reactor," *Fuel Processing Technology*, vol. 171, no. November 2017, pp. 308–317, 2018, doi: 10.1016/j.fuproc.2017.12.001.
- [98] X. Gong, Y. Yu, X. Gao, Y. Qiao, M. Xu, and H. Wu, "Formation of anhydro-sugars in the primary volatiles and solid residues from cellulose fast pyrolysis in a wire-mesh reactor," *Energy and Fuels*, vol. 28, no. 8, pp. 5204–5211, 2014, doi: 10.1021/ef501112q.
- [99] Y. Elkasabi, C. A. Mullen, A. L. M. T. Pighinelli, and A. A. Boateng, "Hydrodeoxygenation of fast-pyrolysis bio-oils from various feedstocks using carbon-supported catalysts," *Fuel Processing Technology*, vol. 123, pp. 11–18, 2014, doi: 10.1016/j.fuproc.2014.01.039.
- [100] P. Roy and G. Dias, "Prospects for pyrolysis technologies in the bioenergy sector: A review," *Renewable and Sustainable Energy Reviews*, vol. 77, no. February, pp. 59–69, 2017, doi: 10.1016/j.rser.2017.03.136.
- [101] H. Bouaik, A. Tabal, A. Barakat, K. El Harfi, and A. Aboulkas, "Optimal parameters and structural composition of bio-oil and biochar from intermediate pyrolysis of red algal biomass," *Comptes Rendus Chimie*, vol. 24, no. 31, pp. 1–15, 2021, doi: 10.5802/CRCHIM.90.
- [102] Y. Zheng, J. Wang, D. Wang, and Z. Zheng, "Advanced catalytic upgrading of biomass pyrolysis vapor to bio-aromatics hydrocarbon: A review," *Applications in Energy and Combustion Science*, vol. 10, no. February, p. 100061, 2022, doi: 10.1016/j.jaecs.2022.100061.
- [103] L. K. Ncube, A. U. Ude, E. N. Ogunmuyiwa, R. Zulkifli, and I. N. Beas, "An overview of plastic waste generation and management in food packaging industries," *Recycling*, vol. 6, no. 1, pp. 1–25, 2021, doi: 10.3390/recycling6010012.
- [104] K. Praveen Kumar and S. Srinivas, "Catalytic Co-pyrolysis of Biomass and Plastics (Polypropylene and Polystyrene) Using Spent FCC Catalyst," *Energy and Fuels*, vol. 34, no. 1, pp. 460–473, 2020, doi: 10.1021/acs.energyfuels.9b03135.
- [105] Q. Xie *et al.*, "Fast microwave-assisted catalytic co-pyrolysis of microalgae and scum for bio-oil production," *Fuel*, vol. 160, pp. 577–582, 2015, doi: 10.1016/j.fuel.2015.08.020.
- [106] D. V. Suriapparao *et al.*, "Role of ZSM5 catalyst and char susceptor on the synthesis of chemicals and hydrocarbons from microwave-assisted

- in-situ catalytic co-pyrolysis of algae and plastic wastes," *Renew Energy*, vol. 181, pp. 990–999, 2022, doi: 10.1016/j.renene.2021.09.084.
- [107] Z. Tang *et al.*, "Co-pyrolysis of microalgae with low-density polyethylene (LDPE) for deoxygenation and denitrification," *Bioresour Technol*, vol. 311, no. March, p. 123502, 2020, doi: 10.1016/j.biortech.2020.123502.
- [108] J. Liu, Q. Hou, M. Ju, P. Ji, Q. Sun, and W. Li, "Biomass pyrolysis technology by catalytic fast pyrolysis, catalytic co-pyrolysis and microwave-assisted pyrolysis: A review," *Catalysts*, vol. 10, no. 7, pp. 1–26, 2020, doi: 10.3390/catal10070742.
- [109] W. Luo *et al.*, "Catalytic co-pyrolysis of herb residue and polypropylene for pyrolysis products upgrading and diversification using nickel-X/biochar and ZSM-5 (X = iron, cobalt, copper)," *Bioresour Technol*, vol. 349, no. February, p. 126845, 2022, doi: 10.1016/j.biortech.2022.126845.
- [110] P. Parthasarathy, S. Zuhara, T. Al-Ansari, and G. McKay, "A review on catalytic CO₂ pyrolysis of organic wastes to high-value products," *Fuel*, vol. 335, no. November 2022, p. 127073, 2023, doi: 10.1016/j.fuel.2022.127073.
- [111] X. Jin, J. H. Lee, and J. W. Choi, "Catalytic co-pyrolysis of woody biomass with waste plastics: Effects of HZSM-5 and pyrolysis temperature on producing high-value pyrolytic products and reducing wax formation," *Energy*, vol. 239, p. 121739, 2022, doi: 10.1016/j.energy.2021.121739.
- [112] D. T. Sekyere *et al.*, "Production of light olefins and aromatics via catalytic co-pyrolysis of biomass and plastic," *Fuel*, vol. 333, no. P2, p. 126339, 2023, doi: 10.1016/j.fuel.2022.126339.
- [113] H. Zhang, Y. T. Cheng, T. P. Vispute, R. Xiao, and G. W. Huber, "Catalytic conversion of biomass-derived feedstocks into olefins and aromatics with ZSM-5: The hydrogen to carbon effective ratio," *Energy Environ Sci*, vol. 4, no. 6, pp. 2297–2307, 2011, doi: 10.1039/c1ee01230d.
- [114] A. Gambarotta, M. Morini, and A. Zubani, "A non-stoichiometric equilibrium model for the simulation of the biomass gasification process," *Appl Energy*, vol. 227, pp. 119–127, Oct. 2018, doi: 10.1016/j.apenergy.2017.07.135.
- [115] I. L. Motta, N. T. Miranda, R. Maciel Filho, and M. R. Wolf Maciel, "Biomass gasification in fluidized beds: A review of biomass moisture content and operating pressure effects," *Renewable and Sustainable Energy Reviews*. 2018. doi: 10.1016/j.rser.2018.06.042.
- [116] S. Heidenreich and P. U. Foscolo, "New concepts in biomass gasification," *Prog Energy Combust Sci*, vol. 46, pp. 72–95, 2015, doi: 10.1016/j.peccs.2014.06.002.
- [117] K. A. Al-attab and Z. A. Zainal, "Syngas production and combustion characteristics in a biomass fixed bed gasifier with cyclone combustor," *Appl Therm Eng*, 2017, doi: 10.1016/j.applthermaleng.2016.11.084.

- [118] J. G. Speight and H. Processes, "Fischer-Tropsch Reactor Learn more about Fischer-Tropsch Reactor Hydrocarbons from Synthesis Gas," 2011.
- [119] P. Mponzi, "Production of Biofuels by Fischer Tropsch," p. 1, 2011.
- [120] T. Anttinen, "Numerical Modelling of Combustion and Emission Formation in a Diesel Engine with Different Fuel Injection Characteristics," 2005.
- [121] M. Dudyński, J. C. Van Dyk, K. Kwiatkowski, and M. Sosnowska, "Biomass gasification: Influence of torrefaction on syngas production and tar formation," *Fuel Processing Technology*, 2015, doi: 10.1016/j.fuproc.2014.11.018.
- [122] K. M. Qureshi, A. N. Kay Lup, S. Khan, F. Abnisa, and W. M. A. Wan Daud, "A technical review on semi-continuous and continuous pyrolysis process of biomass to bio-oil," *J Anal Appl Pyrolysis*, vol. 131, no. February, pp. 52–75, 2018, doi: 10.1016/j.jaap.2018.02.010.
- [123] G. Perkins, T. Bhaskar, and M. Konarova, "Process development status of fast pyrolysis technologies for the manufacture of renewable transport fuels from biomass," *Renewable and Sustainable Energy Reviews*. 2018. doi: 10.1016/j.rser.2018.03.048.
- [124] S. Du, Y. Sun, D. P. Gamliel, J. A. Valla, and G. M. Bollas, "Catalytic pyrolysis of miscanthus×giganteus in a spouted bed reactor," *Bioresour Technol*, vol. 169, pp. 188–197, 2014, doi: 10.1016/j.biortech.2014.06.104.
- [125] T. J. Dugaard, D. L. Dalluge, R. C. Brown, and M. M. Wright, "Effect of thermophysical properties of heat carriers on performance of a laboratory-scale auger pyrolyzer," *Fuel Processing Technology*, vol. 176, no. March, pp. 182–189, 2018, doi: 10.1016/j.fuproc.2018.03.024.
- [126] W. Treedet and R. Suntivarakorn, "Design and operation of a low-cost bio-oil fast pyrolysis from sugarcane bagasse on circulating fluidized bed reactor in a pilot plant," *Fuel Processing Technology*, vol. 179, no. May, pp. 17–31, 2018, doi: 10.1016/j.fuproc.2018.06.006.
- [127] M. D. Ibrahim, S. T. Gopakumar, Y. A. Abakr, M. I. Yakub, and S. J. Zwalnan, "Technological Challenges & Environmental Mitigation via Bio-oil Production from Biomass Resources," *IOP Conf Ser Earth Environ Sci*, vol. 489, no. 1, 2020, doi: 10.1088/1755-1315/489/1/012008.
- [128] R. Suntivarakorn, W. Treedet, P. Singbua, and N. Teeramaetawat, "Fast pyrolysis from Napier grass for pyrolysis oil production by using circulating Fluidized Bed Reactor: Improvement of pyrolysis system and production cost," *Energy Reports*, vol. 4, pp. 565–575, 2018, doi: 10.1016/j.egyr.2018.08.004.
- [129] Y. Song, J. Zhu, C. Zhang, Z. Sun, and X. Lu, "Comparison of liquid-solid flow characteristics in upward and downward circulating fluidized beds by CFD approach," *Chem Eng Sci*, no. xxxx, 2018, doi: 10.1016/j.ces.2018.11.022.
- [130] M. E. E. Abashar, "Investigation of the efficiency of sorption-enhanced methanol synthesis process in circulating fast fluidized bed reactors,"

- Fuel Processing Technology*, vol. 179, no. July, pp. 387–398, 2018, doi: 10.1016/j.fuproc.2018.07.028.
- [131] P. Salatino and R. Solimene, "Mixing and segregation in fluidized bed thermochemical conversion of biomass," *Powder Technol*, vol. 316, pp. 29–40, 2017, doi: 10.1016/j.powtec.2016.11.058.
- [132] M. Amutio, G. Lopez, J. Alvarez, M. Olazar, and J. Bilbao, "Fast pyrolysis of eucalyptus waste in a conical spouted bed reactor," *Bioresour Technol*, vol. 194, pp. 225–232, 2015, doi: 10.1016/j.biortech.2015.07.030.
- [133] J. Alvarez, M. Amutio, G. Lopez, J. Bilbao, and M. Olazar, "Fast co-pyrolysis of sewage sludge and lignocellulosic biomass in a conical spouted bed reactor," *Fuel*, vol. 159, no. x, pp. 810–818, 2015, doi: 10.1016/j.fuel.2015.07.039.
- [134] J. Alvarez, G. Lopez, M. Amutio, J. Bilbao, and M. Olazar, "Bio-oil production from rice husk fast pyrolysis in a conical spouted bed reactor," *Fuel*, vol. 128, pp. 162–169, 2014, doi: 10.1016/j.fuel.2014.02.074.
- [135] J. Alvarez *et al.*, "Characterization of the bio-oil obtained by fast pyrolysis of sewage sludge in a conical spouted bed reactor," *Fuel Processing Technology*, vol. 149, pp. 169–175, 2016, doi: 10.1016/j.fuproc.2016.04.015.
- [136] A. R. Fernandez-Akarregi, J. Makibar, G. Lopez, M. Amutio, and M. Olazar, "Design and operation of a conical spouted bed reactor pilot plant (25 kg/h) for biomass fast pyrolysis," *Fuel Processing Technology*, vol. 112, pp. 48–56, 2013, doi: 10.1016/j.fuproc.2013.02.022.
- [137] B. M. Wagenaar, W. Prins, and W. P. M. van Swaij, "Pyrolysis of biomass in the rotating cone reactor: modelling and experimental justification," *Chem Eng Sci*, vol. 49, pp. 5109–5126, 1994.
- [138] B. Wagenaar, H. A. M. Kuipers, T. U. Eindhoven, W. Prins, and W. Van Swaij, "The Rotating Cone Flash Pyrolysis Reactor," no. February 2014, 1993, doi: 10.1007/978-94-011-1336-6.
- [139] M. I. Jahirul, M. G. Rasul, A. A. Chowdhury, and N. Ashwath, "Biofuels production through biomass pyrolysis- A technological review," *Energies (Basel)*, vol. 5, no. 12, pp. 4952–5001, 2012, doi: 10.3390/en5124952.
- [140] P. Fu, X. Bai, W. Yi, Z. Li, and Y. Li, "Fast pyrolysis of wheat straw in a dual concentric rotary cylinder reactor with ceramic balls as recirculated heat carrier," *Energy Convers Manag*, vol. 171, no. April, pp. 855–862, 2018, doi: 10.1016/j.enconman.2018.06.035.
- [141] B. M. Wagenaar, W. Prins, and W. P. M. van Swaij, "Pyrolysis of biomass in the rotating cone reactor: modelling and experimental justification," *Chem Eng Sci*, vol. 49, no. 24, pp. 5109–5126, 1994, doi: 10.1016/0009-2509(94)00392-0.
- [142] P. Singbua, W. Treedet, P. Duangthong, V. Seithtanabutara, and R. Suntivarakorn, "Bio-Oil Production of Napier Grass by Using Rotating Cylindrical Reactor," *Energy Procedia*, vol. 138, pp. 641–645, 2017, doi: 10.1016/j.egypro.2017.10.180.

- [143] P. Fu, X. Bai, Z. Li, W. Yi, Y. Li, and Y. Zhang, "Fast pyrolysis of corn stovers with ceramic ball heat carriers in a novel dual concentric rotary cylinder reactor," *Bioresour Technol*, vol. 263, no. March, pp. 467–474, 2018, doi: 10.1016/j.biortech.2018.05.033.
- [144] M. Mathew and L. Muruganandam, "Pyrolysis of Agricultural Biomass using an Auger Reactor: A Parametric Optimization," *International Journal of Chemical Reactor Engineering*, vol. 15, no. 3, 2017, doi: 10.1515/ijcre-2016-0133.
- [145] J. N. Brown, "Development of a lab-scale auger reactor for biomass fast pyrolysis and process optimization using response surface methodology," p. 249, 2009.
- [146] L. Ingram *et al.*, "Pyrolysis of wood and bark in an auger reactor: Physical properties and chemical analysis of the produced bio-oils," *Energy and Fuels*, vol. 22, no. 1, pp. 614–625, 2008, doi: 10.1021/ef700335k.
- [147] G. Luo, D. S. Chandler, L. C. A. Anjos, R. J. Eng, P. Jia, and F. L. P. Resende, "Pyrolysis of whole wood chips and rods in a novel ablative reactor," *Fuel*, vol. 194, pp. 229–238, 2017, doi: 10.1016/j.fuel.2017.01.010.
- [148] A. V. Bridgwater, "A Guide to Fast Pyrolysis of Biomass for Fuels," *PyNe Guide*, no. March 1999.
- [149] D. Reißmann, D. Thrän, and A. Bezama, "Hydrothermal processes as treatment paths for biogenic residues in Germany: A review of the technology, sustainability and legal aspects," *Journal of Cleaner Production*. 2018. doi: 10.1016/j.jclepro.2017.10.151.
- [150] J. Fang, L. Zhan, Y. S. Ok, and B. Gao, "Minireview of potential applications of hydrochar derived from hydrothermal carbonization of biomass," *Journal of Industrial and Engineering Chemistry*, vol. 57, pp. 15–21, 2018, doi: 10.1016/j.jiec.2017.08.026.
- [151] T. Wang, Y. Zhai, Y. Zhu, C. Li, and G. Zeng, "A review of the hydrothermal carbonization of biomass waste for hydrochar formation: Process conditions, fundamentals, and physicochemical properties," *Renewable and Sustainable Energy Reviews*, vol. 90, no. February, pp. 223–247, 2018, doi: 10.1016/j.rser.2018.03.071.
- [152] S. Nizamuddin *et al.*, "An overview of effect of process parameters on hydrothermal carbonization of biomass," *Renewable and Sustainable Energy Reviews*, vol. 73, no. December 2015, pp. 1289–1299, 2017, doi: 10.1016/j.rser.2016.12.122.
- [153] J. Fang, L. Zhan, Y. S. Ok, and B. Gao, "Minireview of potential applications of hydrochar derived from hydrothermal carbonization of biomass," *Journal of Industrial and Engineering Chemistry*, vol. 57, pp. 15–21, 2018, doi: 10.1016/j.jiec.2017.08.026.
- [154] A. Gallifuoco, L. Taglieri, and A. A. Papa, "Hydrothermal carbonization of waste biomass to fuel : A novel technique for analyzing experimental data," *Renew Energy*, vol. 149, pp. 1254–1260, 2020, doi: 10.1016/j.renene.2019.10.121.

- [155] G. Wang, J. Zhang, J. Lee, X. Mao, L. Ye, and W. Xu, "Hydrothermal carbonization of maize straw for hydrochar production and its injection for blast furnace ☆," *Appl Energy*, vol. 266, no. December 2019, p. 114818, 2020, doi: 10.1016/j.apenergy.2020.114818.
- [156] S. K. Hoekman, A. Broch, and C. Robbins, "Hydrothermal Carbonization (HTC) of Lignocellulosic Biomass," pp. 1802–1810, 2011, doi: 10.1021/ef101745n.
- [157] J. Xu, J. Zhang, J. Huang, W. He, and G. Li, "Conversion of phoenix tree leaves into hydro-char by microwave-assisted hydrothermal carbonization," *Bioresour Technol Rep*, vol. 9, no. November 2019, p. 100353, 2020, doi: 10.1016/j.biteb.2019.100353.
- [158] P. Zhao, Y. Shen, S. Ge, and K. Yoshikawa, "Energy recycling from sewage sludge by producing solid biofuel with hydrothermal carbonization," *Energy Convers Manag*, vol. 78, pp. 815–821, 2014, doi: 10.1016/j.enconman.2013.11.026.
- [159] T. Wang, Y. Zhai, Y. Zhu, C. Li, and G. Zeng, "A review of the hydrothermal carbonization of biomass waste for hydrochar formation: Process conditions, fundamentals, and physicochemical properties," *Renewable and Sustainable Energy Reviews*, vol. 90, no. December 2016, pp. 223–247, 2018, doi: 10.1016/j.rser.2018.03.071.
- [160] A. R. K. Gollakota, M. Reddy, M. D. Subramanyam, and N. Kishore, "A review on the upgradation techniques of pyrolysis oil," *Renewable and Sustainable Energy Reviews*, vol. 58, pp. 1543–1568, 2016, doi: 10.1016/j.rser.2015.12.180.
- [161] F. Li, A. R. Zimmerman, X. Hu, Z. Yu, J. Huang, and B. Gao, "One-pot synthesis and characterization of engineered hydrochar by hydrothermal carbonization of biomass with ZnCl₂," *Chemosphere*, vol. 254, p. 126866, 2020, doi: 10.1016/j.chemosphere.2020.126866.
- [162] M. Volpe *et al.*, "Reactivity of cellulose during hydrothermal carbonization of lignocellulosic biomass," *Fuel Processing Technology*, vol. 206, no. February, p. 106456, 2020, doi: 10.1016/j.fuproc.2020.106456.
- [163] G. Wang *et al.*, "Hydrothermal carbonization of maize straw for hydrochar production and its injection for blast furnace," *Appl Energy*, vol. 266, no. March, p. 114818, 2020, doi: 10.1016/j.apenergy.2020.114818.
- [164] Y. Chen, L. Guo, W. Cao, H. Jin, S. Guo, and X. Zhang, "Hydrogen production by sewage sludge gasification in supercritical water with a fluidized bed reactor," *Int J Hydrogen Energy*, vol. 38, no. 29, pp. 12991–12999, 2013, doi: 10.1016/j.ijhydene.2013.03.165.
- [165] S. Seif, S. Fatemi, O. Tavakoli, and H. Bahmanyar, "Hydrogen production through hydrothermal gasification of industrial wastewaters using transition metal oxide catalysts," *Journal of Supercritical Fluids*, vol. 114, pp. 32–45, 2016, doi: 10.1016/j.supflu.2016.03.028.
- [166] J. A. Onwudili, A. R. Lea-Langton, A. B. Ross, and P. T. Williams, "Catalytic hydrothermal gasification of algae for hydrogen production: Composition of reaction products and potential for nutrient recycling,"

- Bioresour Technol*, vol. 127, pp. 72–80, 2013, doi: 10.1016/j.biortech.2012.10.020.
- [167] A. Seçer, E. Faki, Ş. Türker Üzden, and A. Hasanoğlu, "Hydrothermal co-gasification of sorghum biomass and çan lignite in mild conditions: An optimization study for high yield hydrogen production," *Int J Hydrogen Energy*, vol. 45, no. 4, pp. 2668–2680, 2020, doi: 10.1016/j.ijhydene.2019.11.196.
- [168] Y. W. Huang, M. Q. Chen, Q. H. Li, and W. Xing, "Hydrogen-rich syngas produced from co-gasification of wet sewage sludge and torrefied biomass in self-generated steam agent," *Energy*, 2018, doi: 10.1016/j.energy.2018.07.097.
- [169] J. A. Okolie, S. Nanda, A. K. Dalai, and J. A. Kozinski, "Hydrothermal gasification of soybean straw and flax straw for hydrogen-rich syngas production: Experimental and thermodynamic modelling," *Energy Convers Manag*, vol. 208, no. February, p. 112545, 2020, doi: 10.1016/j.enconman.2020.112545.
- [170] D. S. Gökkaya, M. Sert, M. Sağlam, M. Yüksel, and L. Ballice, "Hydrothermal Gasification of the Isolated Hemicellulose and Sawdust of the White Poplar (*Populus alba* L.)," *J Supercrit Fluids*, p. 104846, 2020, doi: 10.1016/j.supflu.2020.104846.
- [171] J. A. Okolie, S. Nanda, A. K. Dalai, and J. A. Kozinski, "Hydrothermal gasification of soybean straw and flax straw for hydrogen-rich syngas production: Experimental and thermodynamic modeling," *Energy Convers Manag*, vol. 208, no. November 2019, p. 112545, 2020, doi: 10.1016/j.enconman.2020.112545.
- [172] D. Ciolkosz, "Characteristics of biomass as a heating fuel," *Renewable and Alternative Energy Fact Sheet*, vol. 5, pp. 1–2, 2010.
- [173] J. Cai *et al.*, "Review of physicochemical properties and analytical characterization of lignocellulosic biomass," *Renewable and Sustainable Energy Reviews*. 2017. doi: 10.1016/j.rser.2017.03.072.
- [174] Y. Y. Chong, S. Thangalazhy Gopakumar, S. Gan, H. Kiat Ng, and L. Yee Lee, "Synergic Effect and Kinetic Mechanisms for Co-Pyrolysis of Empty Fruit Bunch and Palm Oil Sludge," *The Institution of Engineers, Malaysia*, vol. Vol. 78, no. No. 1, pp. 1–5, 2017.
- [175] L. Wang and J. L. and Q. B. Hanwu Lei, "Thermal decomposition behavior and kinetics for pyrolysis and catalytic pyrolysis of Douglas fir," *RSC Adv*, vol. 10, no. 8, pp. 2196–2202, 2018, doi: 10.1039/c7ra12187c.
- [176] D. Trache, A. Abdelaziz, and B. Siouani, "A simple and linear isoconversional method to determine the pre-exponential factors and the mathematical reaction mechanism functions," *J Therm Anal Calorim*, vol. 128, no. 1, pp. 335–348, 2017, doi: 10.1007/s10973-016-5962-0.
- [177] A. Álvarez, C. Pizarro, R. García, J. L. Bueno, and A. G. Lavín, "Determination of kinetic parameters for biomass combustion," *Bioresour Technol*, vol. 216, pp. 36–43, 2016, doi: 10.1016/j.biortech.2016.05.039.

- [178] S. L. Wonga, N. Ngadia, and T. A. T. Abdullahb, "Kinetic modeling of LDPE Pyrolysis Using Coats-Redfern Method," *International Conference of Fuel Cell and Hydrogen Technology (ICFCHT2015)*. Kuala Lumpur, Malaysia, 2015.
- [179] Nishu *et al.*, "Performance of alkali and Ni-modified ZSM-5 during catalytic pyrolysis of extracted hemicellulose from rice straw for the production of aromatic hydrocarbons," *Renew Energy*, vol. 175, pp. 936–951, 2021, doi: 10.1016/j.renene.2021.05.005.
- [180] Y. Wang, L. Huang, T. Zhang, and Q. Wang, "Hydrogen-rich syngas production from biomass pyrolysis and catalytic reforming using biochar-based catalysts," *Fuel*, vol. 313, no. December 2021, p. 123006, 2022, doi: 10.1016/j.fuel.2021.123006.
- [181] W. T. Tsai, S. C. Liu, H. R. Chen, Y. M. Chang, and Y. L. Tsai, "Textural and chemical properties of swine-manure-derived biochar pertinent to its potential use as a soil amendment," *Chemosphere*, vol. 89, no. 2, pp. 198–203, 2012, doi: 10.1016/j.chemosphere.2012.05.085.
- [182] I. Y. Mohammed, Y. A. Abakr, M. Musa, S. Yusup, A. Singh, and F. K. Kazi, "Valorization of Bambara groundnut shell via intermediate pyrolysis: Products distribution and characterization," *J Clean Prod*, vol. 139, pp. 717–728, 2016, doi: 10.1016/j.jclepro.2016.08.090.
- [183] S. Pattanayak, L. Hauchhum, C. Loha, L. Sailo, and D. Saha, "Thermal performance and synergetic behaviour of co-pyrolysis of Northeast Indian bamboo biomass with coal using thermogravimetric analysis," *Biomass Conversion and Biorefinery*. 2022. doi: 10.1007/s13399-021-02196-0.
- [184] Y. W. Phuang *et al.*, "Wet torrefaction pre-treatment of yard waste to improve the fuel properties," *Mater Sci Energy Technol*, vol. 4, pp. 211–223, 2021, doi: 10.1016/j.mset.2021.06.005.
- [185] M. Soh, D. S. Khaerudini, J. J. Chew, and J. Sunarso, "Wet torrefaction of empty fruit bunches (EFB) and oil palm trunks (OPT): Effects of process parameters on their physicochemical and structural properties," *S Afr J Chem Eng*, vol. 35, no. June, pp. 126–136, 2021, doi: 10.1016/j.sajce.2020.09.004.
- [186] A. Paar, "Instruction Manual DMA 4100 M DMA 4500 M DMA 5000 M," p. 152, 2012.
- [187] B. N. Madanayake, S. Gan, C. Eastwick, and H. K. Ng, "Biomass as an energy source in coal co-firing and its feasibility enhancement via pre-treatment techniques," *Fuel Processing Technology*, vol. 159, pp. 287–305, 2017, doi: 10.1016/j.fuproc.2017.01.029.
- [188] A. Missaoui, S. Bostyn, V. Belandria, B. Cagnon, B. Sarh, and I. Gökalp, "Hydrothermal carbonization of dried olive pomace: Energy potential and process performances," *J Anal Appl Pyrolysis*, vol. 128, no. September, pp. 281–290, 2017, doi: 10.1016/j.jaap.2017.09.022.
- [189] A. Tomczyk, Z. Sokołowska, and P. Boguta, "Biochar physicochemical properties: pyrolysis temperature and feedstock kind effects," *Rev Environ Sci Biotechnol*, vol. 19, no. 1, pp. 191–215, 2020, doi: 10.1007/s11157-020-09523-3.

- [190] M. Tripathi, J. N. Sahu, and P. Ganesan, "Effect of process parameters on production of biochar from biomass waste through pyrolysis: A review," *Renewable and Sustainable Energy Reviews*. 2016. doi: 10.1016/j.rser.2015.10.122.
- [191] A. O. Onokwai, E. S. A. Ajisegiri, I. P. Okokpujie, R. A. Ibikunle, M. Oki, and J. O. Dirisu, "Characterization of lignocellulose biomass based on proximate, ultimate, structural composition, and thermal analysis," *Mater Today Proc*, no. xxxx, 2022, doi: 10.1016/j.matpr.2022.05.313.
- [192] T. R. Pacioni, D. Soares, M. Di Domenico, M. F. Rosa, R. de F. P. M. Moreira, and H. J. José, "Bio-syngas production from agro-industrial biomass residues by steam gasification," *Waste Management*, vol. 58, pp. 221–229, 2016, doi: 10.1016/j.wasman.2016.08.021.
- [193] M. Shahbaz, S. Yusup, A. Inayat, D. O. Patrick, A. Pratama, and M. Ammar, "Optimization of hydrogen and syngas production from PKS gasification by using coal bottom ash," *Bioresour Technol*, 2017, doi: 10.1016/j.biortech.2017.05.119.
- [194] D. Peni, M. J. Stolarski, and M. Dębowski, "Green biomass quality of perennial herbaceous crops depending on the species, type and level of fertilization," *Ind Crops Prod*, vol. 184, no. February 2022, doi: 10.1016/j.indcrop.2022.115026.
- [195] M. Raza *et al.*, "Progress of the Pyrolyzer Reactors and Advanced Technologies for Biomass Pyrolysis Processing," pp. 1–42, 2021.
- [196] A. Demirbas, "Relationships between heating value and lignin, moisture, ash and extractive contents of biomass fuels," *Energy Exploration and Exploitation*, vol. 20, no. 1, pp. 105–111, Feb. 2002, doi: 10.1260/014459802760170420.
- [197] A. Monti, N. Di Virgilio, and G. Venturi, "Mineral composition and ash content of six major energy crops," *Biomass Bioenergy*, vol. 32, no. 3, pp. 216–223, 2008, doi: 10.1016/j.biombioe.2007.09.012.
- [198] J. Alvarez, M. Amutio, G. Lopez, I. Barbarias, J. Bilbao, and M. Olazar, "Sewage sludge Valorization by flash pyrolysis in a conical spouted bed reactor," *Chemical Engineering Journal*, vol. 273, pp. 173–183, 2015, doi: 10.1016/j.cej.2015.03.047.
- [199] Y. Yang, J. G. Brammer, A. S. N. Mahmood, and A. Hornung, "Intermediate pyrolysis of biomass energy pellets for producing sustainable liquid, gaseous and solid fuels," *Bioresour Technol*, vol. 169, pp. 794–799, 2014, doi: 10.1016/j.biortech.2014.07.044.
- [200] M. Amutio, G. Lopez, M. Artetxe, G. Elordi, M. Olazar, and J. Bilbao, "Influence of temperature on biomass pyrolysis in a conical spouted bed reactor," *Resour Conserv Recycl*, vol. 59, pp. 23–31, 2012, doi: 10.1016/j.resconrec.2011.04.002.
- [201] Y. D. Singh, P. Mahanta, and U. Bora, "Comprehensive characterization of lignocellulosic biomass through proximate, ultimate and compositional analysis for bioenergy production," *Renew Energy*, vol. 103, pp. 490–500, 2017, doi: 10.1016/j.renene.2016.11.039.

- [202] P. Shrivastava, A. Kumar, P. Tekasakul, S. S. Lam, and A. Palamanit, "Comparative investigation of yield and quality of bio-oil and biochar from pyrolysis of woody and non-woody biomasses," *Energies (Basel)*, vol. 14, no. 4, pp. 1–23, 2021, doi: 10.3390/en14041092.
- [203] M. V. Gil, P. Oulego, M. D. Casal, C. Pevida, J. J. Pis, and F. Rubiera, "Mechanical durability and combustion characteristics of pellets from biomass blends," *Bioresour Technol*, vol. 101, no. 22, pp. 8859–8867, 2010, doi: 10.1016/j.biortech.2010.06.062.
- [204] S. Singh, T. Patil, S. P. Tekade, M. B. Gawande, and A. N. Sawarkar, "Studies on individual pyrolysis and co-pyrolysis of corn cob and polyethylene: Thermal degradation behavior, possible synergism, kinetics, and thermodynamic analysis," *Science of the Total Environment*, vol. 783, p. 147004, 2021, doi: 10.1016/j.scitotenv.2021.147004.
- [205] M. G. Grønli, G. Várhegyi, and C. D. Blasi, "Thermogravimetric analysis and devolatilization kinetics of wood," *Ind Eng Chem Res*, vol. 41, no. 17, pp. 4201–4208, 2002, doi: 10.1021/ie0201157.
- [206] Y. Y. Chong, S. Thangalazhy-Gopakumar, S. Gan, H. K. Ng, L. Y. Lee, and S. Adhikari, "Kinetics and Mechanisms for Copyrolysis of Palm Empty Fruit Bunch Fiber (EFBF) with Palm Oil Mill Effluent (POME) Sludge," *Energy and Fuels*, vol. 31, no. 8, pp. 8217–8227, 2017, doi: 10.1021/acs.energyfuels.7b00877.
- [207] T. Wigley, A. C. K. Yip, and S. Pang, "A detailed product analysis of bio-oil from fast pyrolysis of demineralised and torrefied biomass," *J Anal Appl Pyrolysis*, vol. 123, pp. 194–203, 2017, doi: 10.1016/j.jaap.2016.12.006.
- [208] M. Mierzwa-Hersztek, K. Gondek, M. Jewiarz, and K. Dziejcz, "Assessment of energy parameters of biomass and biochars, leachability of heavy metals and phytotoxicity of their ashes," *J Mater Cycles Waste Manag*, vol. 21, no. 4, pp. 786–800, 2019, doi: 10.1007/s10163-019-00832-6.
- [209] D. Smółka-Danielowska and M. Jabłońska, "Chemical and mineral composition of ashes from wood biomass combustion in domestic wood-fired furnaces," *International Journal of Environmental Science and Technology*, vol. 19, no. 6, pp. 5359–5372, 2022, doi: 10.1007/s13762-021-03506-9.
- [210] H. Suopajarvi, E. Pongrácz, and T. Fabritius, "The potential of using biomass-based reducing agents in the blast furnace: A review of thermochemical conversion technologies and assessments related to sustainability," *Renewable and Sustainable Energy Reviews*. 2013. doi: 10.1016/j.rser.2013.05.005.
- [211] S. Mathur, A. V. Umakanth, V. A. Tonapi, R. Sharma, and M. K. Sharma, "Sweet sorghum as biofuel feedstock: Recent advances and available resources," *Biotechnol Biofuels*, vol. 10, no. 1, pp. 1–19, 2017, doi: 10.1186/s13068-017-0834-9.

- [212] M. Wright, I. Lima, and R. Bigner, "Stability and Use of Sweet Sorghum Bagasse," *Sugar Tech*, vol. 19, no. 5, pp. 451–457, 2017, doi: 10.1007/s12355-016-0503-5.
- [213] I. Y. Mohammed, Z. Abba, H. M. Matias-peralta, and Y. A. Abakr, "Thermogravimetric study and evolved gas analysis of new microalga using TGA-GC-MS," pp. 669–678, 2018.
- [214] I. Y. Mohammed, Y. A. Abakr, F. K. Kazi, S. Yusup, I. Alshareef, and S. A. Chin, "Comprehensive characterization of Napier grass as a feedstock for thermochemical conversion," *Energies (Basel)*, vol. 8, no. 5, pp. 3403–3417, 2015, doi: 10.3390/en8053403.
- [215] T. Z. Sehume, C. A. Strydom, J. R. Bunt, and H. H. Schobert, "Bio-oil Production from Sweet Sorghum Bagasse Via Liquefaction Using Alkaline Solutions and Identification of Phenolic Products," *Waste Biomass Valorization*, vol. 11, no. 7, pp. 3593–3607, 2020, doi: 10.1007/s12649-019-00893-6.
- [216] N. Khuenkao and N. Tippayawong, "Bio-oil Production from Ablative Pyrolysis of Corncob Pellets in a Rotating Blade Reactor," *IOP Conf Ser Earth Environ Sci*, vol. 159, no. 1, 2018, doi: 10.1088/1755-1315/159/1/012037.
- [217] E. Salehi, J. Abedi, and T. Harding, "Bio-oil from sawdust: Pyrolysis of sawdust in a fixed-bed system," *Energy and Fuels*, vol. 23, no. 7, pp. 3767–3772, 2009, doi: 10.1021/ef900112b.
- [218] B. Soni and S. K. Karmee, "Towards a continuous pilot scale pyrolysis based biorefinery for production of biooil and biochar from sawdust," *Fuel*, vol. 271, no. March, p. 117570, 2020, doi: 10.1016/j.fuel.2020.117570.
- [219] G. Kabir, A. T. Mohd Din, and B. H. Hameed, "Pyrolysis of oil palm mesocarp fiber and palm frond in a slow-heating fixed-bed reactor: A comparative study," *Bioresour Technol*, vol. 241, pp. 563–572, 2017, doi: 10.1016/j.biortech.2017.05.180.
- [220] L. Zhang, C. Shen, and R. Liu, "GC – MS and FT-IR analysis of the bio-oil with addition of ethyl acetate during storage," vol. 2, no. January, pp. 1–6, 2014, doi: 10.3389/fenrg.2014.00003.
- [221] R. L. Jackson, "Production of High pH Value Bio-oil from Woody Biomass and Poultry litter," 2011.
- [222] S. Omar, S. Alsamaq, Y. Yang, and J. Wang, "Production of renewable fuels by blending bio-oil with alcohols and upgrading under supercritical conditions," *Front Chem Sci Eng*, vol. 13, no. 4, pp. 702–717, 2019, doi: 10.1007/s11705-019-1861-9.
- [223] P. Basu, *Biomass gasification, pyrolysis and torrefaction*, Second Edi. London: Academic Press is an imprint of Elsevier, 2013.
- [224] M. Ahmad and H. Subawi, "New Van Krevelen diagram and its correlation with the heating value of biomass," *Apex Journal*, vol. 2, no. 10, pp. 295–301, 2013.
- [225] M. Wang, S.-L. Zhang, and P.-G. Duan, "Slow pyrolysis of biomass: effects of effective hydrogen-to-carbon atomic ratio of biomass and reaction atmospheres," *Energy Sources, Part A: Recovery, Utilization,*

- and Environmental Effects*, vol. 0, no. 0, pp. 1–14, 2019, doi: 10.1080/15567036.2019.1665150.
- [226] J. Alvarez *et al.*, "Valorization of citrus wastes by fast pyrolysis in a conical spouted bed reactor," *Fuel*, vol. 224, no. July 2017, pp. 111–120, 2018, doi: 10.1016/j.fuel.2018.03.028.
- [227] U. Morali, N. Yavuzel, and S. Şensöz, "Pyrolysis of hornbeam (*Carpinus betulus* L.) sawdust: Characterization of bio-oil and bio-char," *Bioresour Technol*, vol. 221, pp. 682–685, 2016, doi: 10.1016/j.biortech.2016.09.081.
- [228] W. T. Tsai, S. C. Liu, H. R. Chen, Y. M. Chang, and Y. L. Tsai, "Textural and chemical properties of swine-manure-derived biochar pertinent to its potential use as a soil amendment," *Chemosphere*, vol. 89, no. 2, pp. 198–203, 2012, doi: 10.1016/j.chemosphere.2012.05.085.
- [229] P. A. Alaba *et al.*, "Investigating the electrocatalytic oxidation of glycerol on simultaneous nitrogen- and fluorine-doped on activated carbon black composite," *Diam Relat Mater*, vol. 101, no. November 2019, p. 107626, 2020, doi: 10.1016/j.diamond.2019.107626.
- [230] M. Brienzo, S. Fikizolo, Y. Benjamin, and L. Tyhoda, "In fl uence of pretreatment severity on structural changes , lignin content and enzymatic hydrolysis of sugarcane bagasse samples," vol. 104, pp. 271–280, 2017, doi: 10.1016/j.renene.2016.12.037.
- [231] C. U. Pittman *et al.*, "Characterization of bio-oils produced from fast pyrolysis of corn stalks in an auger reactor," in *Energy and Fuels*, American Chemical Society, Jun. 2012, pp. 3816–3825. doi: 10.1021/ef3003922.
- [232] S. A. Lewis, R. M. Connatser, M. V. Olarte, and J. R. Keiser, "Determining aromatic and aliphatic carboxylic acids in biomass-derived oil samples using 2,4-dinitrophenylhydrazine and liquid chromatography-electrospray injection-mass spectrometry/mass spectrometry," *Biomass Bioenergy*, vol. 108, no. July 2017, pp. 198–206, 2018, doi: 10.1016/j.biombioe.2017.10.043.
- [233] I. Itabaiana Junior, M. Avelar Do Nascimento, R. O. M. A. De Souza, A. Dufour, and R. Wojcieszak, "Levogluconan: A promising platform molecule," *Green Chemistry*, vol. 22, no. 18, pp. 5859–5880, 2020, doi: 10.1039/d0gc01490g.
- [234] Y. Yu, Y. W. Chua, and H. Wu, "Characterization of Pyrolytic Sugars in Bio-Oil Produced from Biomass Fast Pyrolysis," *Energy and Fuels*, vol. 30, no. 5, pp. 4145–4149, 2016, doi: 10.1021/acs.energyfuels.6b00464.
- [235] G. Lyu, S. Wu, and H. Zhang, "Estimation and comparison of bio-oil components from different pyrolysis conditions," *Front Energy Res*, vol. 3, no. JUN, pp. 1–11, 2015, doi: 10.3389/fenrg.2015.00028.
- [236] L. Fan, "Bio-oil from fast pyrolysis of lignin: Effects of process and upgrading parameters," *Bioresour Technol*, no. 241, pp. 1118–1126, 2017, doi: 10.1016/j.biortech.2017.05.129.

- [237] Y. Wei *et al.*, "Hydrocarbon produced from upgrading rich phenolic compound bio-oil with low catalyst coking," *Fuel*, vol. 178, pp. 77–84, 2016, doi: 10.1016/j.fuel.2016.03.039.
- [238] A. Oasmaa, D. C. Elliott, and J. Korhonen, "Acidity of biomass fast pyrolysis bio-oils," *Energy and Fuels*, vol. 24, no. 12, pp. 6548–6554, 2010, doi: 10.1021/ef100935r.
- [239] Y. Sun *et al.*, "Pyrolysis of flaxseed residue: Exploration of characteristics of the biochar and bio-oil products," *Journal of the Energy Institute*, vol. 97, pp. 1–12, 2021, doi: 10.1016/j.joei.2021.03.020.
- [240] Y. Sun *et al.*, "Pyrolysis of flaxseed residue: Exploration of characteristics of the biochar and bio-oil products," *Journal of the Energy Institute*, vol. 97, pp. 1–12, 2021, doi: 10.1016/j.joei.2021.03.020.
- [241] Y. Wei *et al.*, "Hydrocarbon produced from upgrading rich phenolic compound bio-oil with low catalyst coking," *Fuel*, vol. 178, pp. 77–84, 2016, doi: 10.1016/j.fuel.2016.03.039.
- [242] W. A. W. A. K. Ghani *et al.*, "Biochar production from waste rubber-wood-sawdust and its potential use in C sequestration: Chemical and physical characterization," *Ind Crops Prod*, vol. 44, pp. 18–24, 2013, doi: 10.1016/j.indcrop.2012.10.017.
- [243] W. A. W. A. K. Ghani *et al.*, "Biochar production from waste rubber-wood-sawdust and its potential use in C sequestration: Chemical and physical characterization," *Ind Crops Prod*, vol. 44, pp. 18–24, 2013, doi: 10.1016/j.indcrop.2012.10.017.
- [244] W. A. W. A. K. Ghani *et al.*, "Biochar production from waste rubber-wood-sawdust and its potential use in C sequestration: Chemical and physical characterization," *Ind Crops Prod*, vol. 44, pp. 18–24, 2013, doi: 10.1016/j.indcrop.2012.10.017.
- [245] M. Erfani Jazi *et al.*, "Structure, chemistry and physicochemistry of lignin for material functionalization," *SN Appl Sci*, vol. 1, no. 9, pp. 1–19, 2019, doi: 10.1007/s42452-019-1126-8.
- [246] S. Jiang *et al.*, "Characterization of hard- and softwood biochars pyrolyzed at high temperature," *Environ Geochem Health*, vol. 39, no. 2, pp. 403–415, 2017, doi: 10.1007/s10653-016-9873-6.
- [247] A. Bieniek, W. Jerzak, M. Sieradzka, Ł. Mika, K. Sztekler, and A. Magdziarz, "Intermediate Pyrolysis of Brewer's Spent Grain: Impact of Gas Atmosphere," *Energies (Basel)*, vol. 15, no. 7, p. 2491, 2022, doi: 10.3390/en15072491.
- [248] C. Guizani, F. J. Escudero Sanz, and S. Salvador, "Effects of CO₂ on biomass fast pyrolysis: Reaction rate, gas yields and char reactive properties," *Fuel*, vol. 116, no. August, pp. 310–320, 2014, doi: 10.1016/j.fuel.2013.07.101.
- [249] Y. Shen, D. Ma, and X. Ge, "CO₂-looping in biomass pyrolysis or gasification," *Sustain Energy Fuels*, vol. 1, no. 8, pp. 1700–1729, 2017, doi: 10.1039/c7se00279c.

- [250] R. Jaideep *et al.*, "Enhancement of fuel properties of yard waste through dry torrefaction," *Mater Sci Energy Technol*, vol. 4, pp. 156–165, 2021, doi: 10.1016/j.mset.2021.04.001.
- [251] T. Onsree and N. Tippayawong, "Torrefaction of Maize Residue Pellets with Dry Flue Gas," *Bioenergy Res*, vol. 13, no. 1, pp. 358–368, 2020, doi: 10.1007/s12155-019-10058-x.
- [252] S. Sadaka and A. A. Boateng, "Pyrolysis and Bio Oil," *Agriculture and Natural Resources*, vol. 1, no. FSA1052, pp. 1–6, 2017.
- [253] S. M. A. Aziz, R. Wahi, Z. Ngaini, S. Hamdan, and S. A. Yahaya, "Esterification of Microwave Pyrolytic Oil from Palm Oil Kernel Shell," *J Chem*, vol. 2017, 2017, doi: 10.1155/2017/8359238.
- [254] S. Chaturvedi, S. V. Singh, V. C. Dhyani, K. Govindaraju, R. Vinu, and S. Mandal, "Characterization, bioenergy value, and thermal stability of biochars derived from diverse agriculture and forestry lignocellulosic wastes," *Biomass Convers Biorefin*, 2021, doi: 10.1007/s13399-020-01239-2.
- [255] J. L. Chukwunke, M. C. Ewulonu, I. C. Chukwujike, and P. C. Okolie, "Physico-chemical analysis of pyrolyzed bio-oil from swietenia macrophylla (mahogany) wood," *Heliyon*, vol. 5, no. 6, pp. 0–6, 2019, doi: 10.1016/j.heliyon.2019.e01790.
- [256] S. B. Singh and M. De, "Thermally exfoliated graphene oxide for hydrogen storage," *Mater Chem Phys*, vol. 239, no. April 2019, p. 122102, 2020, doi: 10.1016/j.matchemphys.2019.122102.
- [257] X. Yang, H. Lyu, K. Chen, X. Zhu, S. Zhang, and J. Chen, "Selective Extraction of Bio-oil from Hydrothermal Liquefaction of *Salix psammophila* by Organic Solvents with Different Polarities through Multistep Extraction Separation," *Bioresources*, vol. 9, no. 3, pp. 5219–5233, 2014, doi: 10.15376/biores.9.3.5219-5233.
- [258] C. Guizani, F. J. Escudero Sanz, and S. Salvador, "Effects of CO₂ on biomass fast pyrolysis: Reaction rate, gas yields and char reactive properties," *Fuel*, vol. 116, pp. 310–320, 2014, doi: <https://doi.org/10.1016/j.fuel.2013.07.101>.
- [259] J. Lee, X. Yang, H. Song, Y. S. Ok, and E. E. Kwon, "Effects of carbon dioxide on pyrolysis of peat," *Energy*, vol. 120, pp. 929–936, 2017, doi: 10.1016/j.energy.2016.11.143.
- [260] Z. Yang *et al.*, "Effect of postsynthesis preparation methods on catalytic performance of Ti-Beta zeolite in ketonization of propionic acid," *Microporous and Mesoporous Materials*, vol. 330, no. November 2021, p. 111625, 2022, doi: 10.1016/j.micromeso.2021.111625.
- [261] P. R. Patwardhan, R. C. Brown, and B. H. Shanks, "Product Distribution from the Fast Pyrolysis of Hemicellulose," *ChemSusChem*, vol. 4, no. 5, p. 636, 2011.
- [262] I. Barbarias, G. Lopez, M. Artetxe, A. Arregi, J. Bilbao, and M. Olazar, "Valorisation of different waste plastics by pyrolysis and in-line catalytic steam reforming for hydrogen production," *Energy Convers Manag*, vol. 156, 2018, doi: 10.1016/j.enconman.2017.11.048.

- [263] Z. J. Li, Y. H. Huang, M. Zhu, X. R. Chen, and H. Mei, "Catalytic performance of Ni/ Al₂O₃ catalyst for hydrogenation of 2-methylfuran to 2-methyltetrahydrofuran," *Ranliao Huaxue Xuebao/Journal of Fuel Chemistry and Technology*, vol. 46, no. 1, 2018, doi: 10.1016/s1872-5813(18)30003-3.
- [264] S. Karimi, A. Tavasoli, Y. Mortazavi, and A. Karimi, "Enhancement of cobalt catalyst stability in Fischer-Tropsch synthesis using graphene nanosheets as catalyst support," *Chemical Engineering Research and Design*, vol. 104, pp. 713–722, 2015, doi: 10.1016/j.cherd.2015.10.016.
- [265] J. Gao *et al.*, "Ni/ Al₂O₃ catalysts for CO methanation: Effect of Al₂O₃ supports calcined at different temperatures," *Journal of Energy Chemistry*, vol. 22, no. 6, pp. 919–927, 2013, doi: 10.1016/S2095-4956(14)60273-4.
- [266] H. N. Hameed, raja mohamad hafriz raja shahruzzaman, N. A. Arifin, E. S. Tan, S. B. ALI, and A. H. Shamsuddin, "Catalytic Co-Pyrolysis of Blended Biomass - Plastic Mixture Using Synthesized Metal Oxide(Mo)-Dolomite Based Catalyst," *SSRN Electronic Journal*, vol. 168, no. October 2022, doi: 10.2139/ssrn.4137898.
- [267] Z. J. Li, Y. H. Huang, M. Zhu, X. R. Chen, and H. Mei, "Catalytic performance of Ni/ Al₂O₃ catalyst for hydrogenation of 2-methylfuran to 2-methyltetrahydrofuran," *Ranliao Huaxue Xuebao/Journal of Fuel Chemistry and Technology*, vol. 46, no. 1, pp. 54–58, 2018, doi: 10.1016/s1872-5813(18)30003-3.
- [268] I. Barbarias, G. Lopez, M. Artetxe, A. Arregi, J. Bilbao, and M. Olazar, "Valorisation of different waste plastics by pyrolysis and in-line catalytic steam reforming for hydrogen production," *Energy Convers Manag*, vol. 156, no. November 2017, pp. 575–584, 2018, doi: 10.1016/j.enconman.2017.11.048.
- [269] I. Kazemnejad, A. Feizbakhsh, A. Niazi, and A. Tavasoli, "Highly dispersed cobalt Fischer–Tropsch synthesis catalysts supported on γ -Al₂O₃, CNTs, and graphene nanosheet using chemical vapor deposition," *International Journal of Industrial Chemistry*, vol. 10, no. 4, pp. 321–333, 2019, doi: 10.1007/s40090-019-00195-9.
- [270] X. Zhang *et al.*, "Thermal behavior and kinetic study for catalytic co-pyrolysis of biomass with plastics," *Bioresour Technol*, vol. 220, pp. 233–238, Nov. 2016, doi: 10.1016/j.biortech.2016.08.068.
- [271] A. O. Oyedun, C. Z. Tee, S. Hanson, and C. W. Hui, "Thermogravimetric analysis of the pyrolysis characteristics and kinetics of plastics and biomass blends," *Fuel Processing Technology*, vol. 128, pp. 471–481, 2014, doi: 10.1016/j.fuproc.2014.08.010.
- [272] Y. Y. Chong, S. Thangalazhy-Gopakumar, S. Gan, H. K. Ng, L. Y. Lee, and S. Adhikari, "Kinetics and Mechanisms for Copyrolysis of Palm Empty Fruit Bunch Fiber (EFBF) with Palm Oil Mill Effluent (POME) Sludge," *Energy and Fuels*, vol. 31, no. 8, pp. 8217–8227, Aug. 2017, doi: 10.1021/acs.energyfuels.7b00877.
- [273] S. S. Idris, N. A. Rahman, K. Ismail, A. B. Alias, Z. A. Rashid, and M. J. Aris, "Investigation on thermochemical behaviour of low rank Malaysian

- coal, oil palm biomass and their blends during pyrolysis via thermogravimetric analysis (TGA)," *Bioresour Technol*, vol. 101, no. 12, pp. 4584–4592, Jun. 2010, doi: 10.1016/j.biortech.2010.01.059.
- [274] X. Zhu *et al.*, "Co-pyrolysis behaviors and kinetics of sewage sludge and pine sawdust blends under non-isothermal conditions," *J Therm Anal Calorim*, vol. 119, no. 3, pp. 2269–2279, 2015, doi: 10.1007/s10973-014-4321-2.
- [275] L. Mu, J. Chen, P. Yao, D. Zhou, L. Zhao, and H. Yin, "Evaluation of co-pyrolysis petrochemical wastewater sludge with lignite in a thermogravimetric analyzer and a packed-bed reactor: Pyrolysis characteristics, kinetics, and products analysis," *Bioresour Technol*, vol. 221, pp. 147–156, Dec. 2016, doi: 10.1016/j.biortech.2016.09.011.
- [276] L. Wang, H. Lei, J. Liu, and Q. Bu, "Thermal decomposition behavior and kinetics for pyrolysis and catalytic pyrolysis of Douglas fir," *RSC Adv*, vol. 8, no. 4, pp. 2196–2202, 2018, doi: 10.1039/c7ra12187c.
- [277] K. Praveen Kumar and S. Srinivas, "Catalytic Co-pyrolysis of Biomass and Plastics (Polypropylene and Polystyrene) Using Spent FCC Catalyst," *Energy and Fuels*, vol. 34, no. 1, 2020, doi: 10.1021/acs.energyfuels.9b03135.
- [278] A. C. Dyer, M. A. Nahil, and P. T. Williams, "Catalytic co-pyrolysis of biomass and waste plastics as a route to upgraded bio-oil," *Journal of the Energy Institute*, vol. 97, 2021, doi: 10.1016/j.joei.2021.03.022.
- [279] I. K. M. Yu *et al.*, "Tailoring acidity and porosity of alumina catalysts via transition metal doping for glucose conversion in biorefinery," *Science of the Total Environment*, vol. 704, 2020, doi: 10.1016/j.scitotenv.2019.135414.
- [280] J. Liu, Q. Hou, M. Ju, P. Ji, Q. Sun, and W. Li, "Biomass pyrolysis technology by catalytic fast pyrolysis, catalytic co-pyrolysis and microwave-assisted pyrolysis: A review," *Catalysts*, vol. 10, no. 7. 2020. doi: 10.3390/catal10070742.
- [281] C. Guizani, F. J. Escudero Sanz, and S. Salvador, "Effects of CO₂ on biomass fast pyrolysis: Reaction rate, gas yields and char reactive properties," *Fuel*, vol. 116, pp. 310–320, 2014, doi: 10.1016/j.fuel.2013.07.101.
- [282] F. Li, A. R. Zimmerman, X. Hu, Z. Yu, J. Huang, and B. Gao, "One-pot synthesis and characterization of engineered hydrochar by hydrothermal carbonization of biomass with ZnCl₂," *Chemosphere*, vol. 254, 2020, doi: 10.1016/j.chemosphere.2020.126866.
- [283] R. Liu, G. Liu, B. Yousaf, Z. Niu, and Q. Abbas, "Novel investigation of pyrolysis mechanisms and kinetics for functional groups in biomass matrix," *Renewable and Sustainable Energy Reviews*, vol. 153, Jan. 2022, doi: 10.1016/j.rser.2021.111761.
- [284] J. Hou, D. Zhong, and W. Liu, "Catalytic co-pyrolysis of oil sludge and biomass over ZSM-5 for production of aromatic platform chemicals," *Chemosphere*, vol. 291, 2022, doi: 10.1016/j.chemosphere.2021.132912.

- [285] K. Praveen Kumar and S. Srinivas, "Catalytic Co-pyrolysis of Biomass and Plastics (Polypropylene and Polystyrene) Using Spent FCC Catalyst," *Energy and Fuels*, vol. 34, no. 1, pp. 460–473, Jan. 2020, doi: 10.1021/acs.energyfuels.9b03135.
- [286] L. Zeng-jie, Z. Ming, C. Xiao-rong, and M. Hua, "Catalytic performance of Ni/Al₂O₃ catalyst for hydrogenation of 2-methylfuran to 2-methyltetrahydrofuran," 2018.
- [287] J. Liu, Q. Hou, M. Ju, P. Ji, Q. Sun, and W. Li, "Biomass pyrolysis technology by catalytic fast pyrolysis, catalytic co-pyrolysis and microwave-assisted pyrolysis: A review," *Catalysts*, vol. 10, no. 7. 2020. doi: 10.3390/catal10070742.
- [288] D. V. Suriapparao, R. Gautam, and L. Rao Jeeru, "Analysis of pyrolysis index and reaction mechanism in microwave-assisted ex-situ catalytic co-pyrolysis of agro-residual and plastic wastes," *Bioresour Technol*, vol. 357, Aug. 2022, doi: 10.1016/j.biortech.2022.127357.
- [289] M. J. Gan *et al.*, (2019). "Enhancement of Palm Kernel Shell Fuel Properties via Wet Torrefaction: Response Surface, Optimization, and Combustion Studies," *Energy and Fuels*, 2019, doi: 10.1021/acs.energyfuels.9b02229.
- [290] A. Kruse and E. Dinjus, (2007). "Hot compressed water as reaction medium and reactant. Properties and synthesis reactions," *Journal of Supercritical Fluids*, vol. 39, no. 3, pp. 362–380, 2007, doi: 10.1016/j.supflu.2006.03.016.
- [291] S. Barskov *et al.*, (2019). "Torrefaction of biomass: A review of production methods for biocoal from cultured and waste lignocellulosic feedstocks," *Renew Energy*, vol. 142, pp. 624–642, 2019, doi: 10.1016/j.renene.2019.04.068.
- [292] F. Codignole Luz, S. Cordiner, A. Manni, V. Mulone, and V. Rocco, (2018). "Biochar characteristics and early applications in anaerobic digestion-a review," *J Environ Chem Eng*, vol. 6, no. 2, pp. 2892–2909, 2018, doi: 10.1016/j.jece.2018.04.015.
- [293] D. R. Nhuchhen and M. T. Afzal, "HHV predicting correlations for torrefied biomass using proximate and ultimate analyses," *Bioengineering*, vol. 4, no. 1, 2017, doi: 10.3390/bioengineering4010007.
- [293] Zhenzi Qiu, Yunbo Zhai, Shanhong Li, Xiangmin Liu, Xiaoping Liu, Bei Wang, Yali Liu, Caiting Li, Yanjun Hu c, "Catalytic co-pyrolysis of sewage sludge and rice husk over biochar catalyst: Bio-oil upgrading and catalytic mechanism". *Waste Management* 114 (2020) 225–233. <https://doi.org/10.1016/j.wasman.2020.07.013>.
- [294] Rubia Idris, William Woei Fong Chong, Atikah Ali, Sidah Idris, Wei Hsiang Tan, Rafidah Md Salim, Guo Ren Mong, Cheng Tung Chong, "Pyrolytic oil with aromatic-rich hydrocarbons via microwave-induced in-situ catalytic co-pyrolysis of empty fruit bunches with a waste truck tyre". *Energy Conversion and Management* Vol. 244, 2021, ,10.1016/j.enconman.2021.114502.

- [295] William de Rezende Locatel, Chetna Mohabeer, Dorothee Laurenti, Yves Schuurman, Nolven Guillaume,(2022) "Co-pyrolysis of beech wood and polyamide-6: Impact of plastic concentration and wood/plastic synergistic effects". *Journal of Analytical and Applied Pyrolysis* Vol. 168, Nov 2022, 105779. <https://doi.org/10.1016/j.jaap.2022.105779>.
- [296] Patipan Sakulkit,, Arkom Palamanit, Racha Dejchanchaiwong, Prasert Reubroycharoen,(2022) "Characteristics of pyrolysis products from pyrolysis and co-pyrolysis of rubber wood and oil palm trunk biomass for biofuel and value-added applications" *Journal of Environmental Chemical Engineering* (8) 2022, 104561, <https://doi.org/10.1016/j.jece.2020.104561>.
- [297] Khachatur V. Manukyan, Allison J. Cross, Armenuhi V. Yeghishyan, Sergei Rouvimov, Jeffrey J. Miller, Alexander S. Mukasyan, E.E. Wolf, (2015)."Highly stable Ni- Al₂O₃ catalyst prepared from a Ni-Al layered double hydroxide for ethanol decomposition toward hydrogen". *Applied Catalysis A: General* 508 (2015) 37-44. <http://dx.doi.org/10.1016/j.apcata.2015.10.007>
- [298] Ashish Dewangan, Debalaxmi Pradhan, R.K. Singh, (2016)."Co-pyrolysis of sugarcane bagasse and low-density polyethylene: Influence of plastic on pyrolysis product yield". *Fuel*, vol. 185, 1 December 2016, Pages 508-516 <https://doi.org/10.1016/j.fuel.2016.08.011>.
- [299] J Gitanjali, S Karthikeyan, S Sriramajayam, P Vijayakumary, K Chandrakumar, and D Ramesh,(2023) "Co-pyrolysis of Plastic Waste and Lignocellulosic Biomass for High-Recovery Fuel Oil". *The International Conference on Science, Engineering and Technology Practices for Sustainable Development (ICSETPSD-23)*. DOI 10.4108/eai.17-11-2023.2342866.
- [300] Farah Amalina , Abdul Syukor Abd Razak , Santhana Krishnan , Haspin Sulaiman , A.W. Zularisam , Mohd Nasrullah ,(2022). "Biochar production techniques utilizing biomass waste-derived materials and environmental applications – A review" *Journal of Hazardous Materials Advances* 7 (2022) 100134. <https://doi.org/10.1016/j.hazadv.2022.100134>.
- [301] Yunwu Zheng, Jida Wang, Can Liu, Xu Lin, Yi Lu, Wenbin Li, and Zhifeng Zheng, (2020) "Enhancing the aromatic hydrocarbon yield from the catalytic copyrolysis of xylan and LDPE with a dual-catalytic-stage combined CaO/HZSM-5 catalyst". *Journal of the Energy Institute* 93 (2020) 1833-1847. <https://doi.org/10.1016/j.joei.2020.03.014>.
- [302] Yeojin Hong, Yejin Lee, Pouya Sirous Rezaei, Beom Sik Kim, Jong-Ki Jeon, Jungho Jae, Sang-Chul Jung, Sang Chai Kim, Young-Kwon Park,(2016), "In-situ catalytic co-pyrolysis of cellulose and polypropylene over desilicated ZSM-5". *Catalysis Today*, Vol. 293-294, 2017, Pages 151-158. <https://doi.org/10.1016/j.cattod.2016.11.045>.
- [303] Huiyan Zhang, Jianlong Nie, Rui Xiao, Baosheng Jin, Changqing Dong, and Guomin Xiao., (2014). "Catalytic Co-pyrolysis of Biomass and Different Plastics (Polyethylene, Polypropylene, and Polystyrene) To

- Improve Hydrocarbon Yield in a Fluidized-Bed Reactor” *Energy Fuels* 2014, 28, 3, 1940–1947. <https://doi.org/10.1021/ef4019299>.
- [304] Ibrahim, M.D.; Abakr, Y.A.; Gan, S.; Lee, L.Y.; Thangalazhy-Gopakumar, S.,(2022). Intermediate Pyrolysis of Bambara Groundnut Shell (BGS) in Various Inert Gases (N₂, CO₂, and N₂/CO₂). *Energies* 2022, 15, 8421. <https://doi.org/10.3390/en15228421>
- [305] Mohammed, Isah Yakub (2017) Pyrolysis of Napier grass to bio-oil and catalytic upgrading to high grade bio-fuel. PhD thesis, University of Nottingham.
- [306] Rudyka V.I., Soloviov M.A., Malyna V.P., Kurylko S.Yu., Abdullin S.Yu., (2019). Actual Problems of Gasification of Fossil Raw Materials, Biomass and Waste with the Receipt of Fuels and Chemical Products (Analytical review of conference materials “GASIFICATION INDIA 2019”, “FROM WASTE TO ENERGY 2019”), DOI: 10.33070/etars.1.2021.03
- [307] J.A. Oyebanji, P.O. Okekunle, O.E. Itabiyi., (2023). Box Behnken design application for optimization of bio-oil yield from catalytic pyrolysis of agro-residue. *Fuel Communications* 16 (2023) 100091. <https://doi.org/10.1016/j.jfueco.2023.100091>.
- [308] Khairuddin Md Isa, Suhardy Daud, Nasrul Hamidin, Khudzir Ismail, Saiful Azhar Saad, Farizul Hafiz Kasim., (2011). Thermogravimetric analysis and the optimisation of bio-oil yield from fixed-bed pyrolysis of rice husk using response surface methodology (RSM). *Industrial Crops and Products*. doi:10.1016/j.indcrop.2010.10.024.
- [309] Witchakorn Charusiri., (2015). Fast Pyrolysis of Residues from Paper Mill Industry to Bio-oil and Value Chemicals: Optimization Studies International Conference on Technologies and Materials for Renewable Energy, Environment and Sustainability, TMREES15. *Energy Procedia* 74 (2015) 933 – 941.
- [310] Chiun Chao Seah, Chung Hong Tan , N.A. Arifin, R.S.R.M. Hafriz, A. Salmiaton , Saifuddin Nomanbhay a , A.H. Shamsuddin, 2023)., Co-pyrolysis of biomass and plastic: Circularity of wastes and comprehensive review of synergistic mechanism, “Results in Engineering 17 (2023) 100989”, <https://doi.org/10.1016/j.rineng.2023.100989>.
- [311] Wenfei Cai, Xiefei Zhu, Reeti Kumar, Zhi Zhu, Jian Ye , Jun Zhao, (2024), Catalytic pyrolysis of biomass waste using montmorillonite-supported ultrafine iron nanoparticles for enhanced bio-oil yield and quality, *Green Energy and Resources* 2 (2024) 100085”, <https://doi.org/10.1016/j.gerr.2024.100085>.
- [312] Yanlong Jia, Mengyan Wang, Bolun Li, Jiang Liu, Xueping Song, Min Wu, Yongjun Yin, (2024), Co-pyrolysis of waste plastics and black liquor catalyzed by Mo-Ni/HZSM-5 for preparing high-quality bio-oil, “*Journal of Analytical and Applied Pyrolysis* 180 (2024) 106540” <https://doi.org/10.1016/j.jaap.2024.106540>.
- [313] Nabeel Ahmad, Mujtaba Imtiaz, Murid Hussain, Um-e-Salma Amjad, Ibrahim M. Maafa, Usama Ahmed, Abdul Gani Abdul Jameel, Abdullah

Bafaqeer, (2024). Catalytic co-pyrolysis of *Vachellia Farnesiana* with polypropylene plastic to produce bio-oil: Parameter optimization study, "Fuel 367 (2024) 131495", <https://doi.org/10.1016/j.fuel.2024.131495>.

- [314] Obie Farobie, Apip Amrullah, Widya Fatriasari, Asep Bayu Dani Nandiyanto, Lusi Ernawati, Surachai Karnjanakom, Seng Hua Lee, Rangabhashiyam Selvasembian, Nur Izyan Wan Azelee, Muhammad Aziz, (2024), Co-pyrolysis of plastic waste and macroalgae *Ulva lactuca*, a sustainable valorization approach towards the production of bio-oil and biochar, Results in Engineering, Volume 24, 2024, 103098, ISSN 2590-1230, <https://doi.org/10.1016/j.rineng.2024.103098>.